

Copyright

by

Yue Zhang

2018

**The Dissertation Committee for Yue Zhang Certifies that this is the approved
version of the following dissertation:**

**Absorber and Aerosol Modeling in Amine Scrubbing for Carbon
Capture**

Committee:

Gary T. Rochelle, Supervisor

Lea Hildebrandt Ruiz

Roger T. Bonnecaze

Hallvard Fjøsne Svendsen

**Absorber and Aerosol Modeling in Amine Scrubbing for Carbon
Capture**

by

Yue Zhang

Dissertation

Presented to the Faculty of the Graduate School of

The University of Texas at Austin

in Partial Fulfillment

of the Requirements

for the Degree of

Doctor of Philosophy

The University of Texas at Austin

August 2018

Dedication

To my family

致我的家人

Acknowledgements

First and foremost, I would like to thank my advisor, Dr. Gary Rochelle. Working with him was the best learning experience in my life. I greatly appreciate his knowledge and creativity in our research discussions, his guidance and patience in our weekly meetings and practice presentations, and his trust and confidence in my abilities. Besides the scientific part, I also treasure the memories of playing board games, the long backpacking trips, and our adventures in Norway, England, Switzerland, Canada, and some other foreign countries. I was deeply impressed and inspired by his passion for life and the love he put into his family and us as well as his hobbies – he taught me how to find my passion for life and how to enjoy it. Special thanks to our administrative assistant, Maeve Cooney, for her tremendous help of editing my quarterly reports and papers. I also really enjoyed our random morning chats from blogs, dogs, to photography.

I would like to thank Dr. Lea Hildebrandt Ruiz, Dr. Roger Bonnezeze, and Dr. Hallvard Svendsen for serving on my dissertation committee. They brought meaningful and different angles to my research projects, and I could not have gone this far without them. I also would like to thank the faculty and staff in our department. I want to thank Dr. Michael Baldea, Dr. Benny Freeman, Dr. Venkat Ganesan, and Dr. David DiCarlo for offering the challenging and interesting graduate courses. I am thankful to our graduate advisor Dr. Hal Alper and program coordinators, Kate Baird, Laura Mondino, and Eloise Boisjoli for guiding me through the orientation, seminars, oral exams, as well as degree requirements and paperwork. Also, I'd like to thank Randy Rife, Jason Barborka, and Shallaco McDonald for providing technical support and managing our building.

I was fortunate to meet great colleagues in Rochelle group, and it's been a pleasure working with them. First, I would like to thank Dr. Darshan Sachde for being a perfect mentor who guided me through absorber modeling and set a great example for me. I also want to thank Dr. Steven Fulk, Dr. Jia-lin Kang, and Dr. Matt Beaudry for bringing their knowledge into the challenging aerosol project. Special thanks to Dr. Eric Chen for teaching me hands-on skills in the Separations Research Program (SRP) pilot plant and all SRP staffs for offering me the great opportunity of working on pilot plant design, control, and operation. Dr. Thomas Edgar and Dr. Matt Walters were also great resources to me when I was learning advanced process control. Also, I would like to thank my officemates, Dr. Darshan Sachde, Dr. Brent Sherman, Dr. Peter Frailie, Dr. Steven Fulk, Dr. Paul Nielsen, Kent Fischer, Ye Yuan, and Tianyu Gao for the incredibly enjoyable work environment and our great conversations. I'd like to thank the many other group members: Dr. Le Li, Dr. Omkar Namjoshi, Dr. Nathan Fine, Dr. Chao Wang, Dr. Yu-Jeng Lin, Dr. Di Song, Dr. Yang Du, Dr. Nathan Fine, Junyuan Ding, Korede Akinpelumi, Joe Selinger, Yuying Wu, and Ching-Ting Liu. I enjoyed our group meetings, group lunches, and the hikes to coffee, milk tea, and food trucks. I was so lucky to have them in my time at UT.

I gratefully acknowledge financial support from the Texas Carbon Management Program, the CO₂ Capture Pilot Plant Project, the U.S. Department of Energy through the CCS² project, Membrane Technology and Research, Inc. (MTR), the George Heuer Endowed Graduate Fellowship, the Agnes and Charles Wiebusch Fellowship, and the Howard Halff Endowed Graduate Fellowship.

I am especially thankful for the great summer internship experience at MTR, where I learned how to conduct research from an industrial perspective and how to accelerate technology from R&D to commercialization. Special thanks to my supervisor Brice

Freeman and dear colleagues at MTR: Dr. Richard Baker, Dr. Tim Merkel, Dr. Hans Wijmans, Jenny He, Dr. Pingjiao Hao, Dr. Ivy Huang, and Karl Amo. Brice, Richard, and Tim offered me great insights inside the membrane industry; Jenny and Pingjiao offered me a huge help to settle down in California; Karl taught me a lot in film photography. I also enjoyed our Friday beers, birthday parties, the MTR musical band, and the California summer. This internship was an unforgettable experience that I will treasure forever.

Finally, I would like to thank my parents for their endless love and support. I am also thankful to my grandparents, uncles, aunts, and cousins. Words simply cannot tell how much I love you. Thank you for encouraging me to work hard and do what I want. Thank you for giving me such a sweet home, and I see love everywhere. Thank you for teaching me how to enjoy life and become an interesting person. You are the number one reason I am where I am today, and I could never have accomplished so much without you. I also want to thank my best friend, and now my fiancé, Yifei. I am amazed at how we can be so different but feel so much alike - in our passion for Ph.D., photography, travel, food, and home decoration. The past five years could not have been more enjoyable without you. Life is a journey - I look forward to sharing my journey with you.

Abstract

Absorber and Aerosol Modeling in Amine Scrubbing for Carbon Capture

Yue Zhang, Ph.D.

The University of Texas at Austin, 2018

Supervisor: Gary T. Rochelle

A rate-based PZ aerosol growth model was developed in gPROMS[®] ModelBuilder. Amine Aerosol growth was simulated at the unique conditions of piperazine (PZ) and the pilot plant absorber configurations at the National Carbon Capture Center. Amine aerosol growth is driven by amine-limited diffusion. As aerosol concentration increases, aerosol growth decreases due to the depletion of the amine driving force in the gas phase. Aerosol growth can be increased by enhancing the gas-film mass transfer coefficient of packing. A solvent with moderate volatility, like PZ, will produce aerosol that grows to larger size and is easier to collect. Solvents with low volatility should be avoided as they produce aerosol that is hard to collect. Process configurations that provide greater water partial pressure in the water wash, such as higher operating temperature and pre-humidified empty space, will help aerosol grow.

Two pilot plant campaigns were designed and conducted in this work. 5 molal (m) PZ was operated for the first time and provided significant absorber performance benefits over 8 m PZ due to enhanced mass transfer rates from lower solvent viscosity.

Parametric tests were performed with a wide range of absorber operating conditions. With the existing model correction, the pilot plant absorber model could reasonably capture the measured absorber performance. For future campaigns, this work recommended that the pilot plant absorber should be operated at both pinched and not pinched conditions. Both equilibrium correction (correct for errors in solvent loading measurements and effects of degradation) and packing correction (correct for effects of rivulets and drop and additional mass transfer caused by distributors and chimney trays) should be utilized in the data reconciliation process.

A membrane-amine hybrid carbon capture system for natural gas combined cycle (NGCC) power plants was proposed and evaluated. When the inlet CO₂ increases from 4% to 18%, the total absorption costs decrease by 60% and the total regeneration costs remain the same. Amine scrubbing without the direct contact cooler was found to be a superior design for NGCC carbon capture. The absorber gas inlet must be designed to avoid excessive localized temperature and solvent evaporation.

Table of Contents

List of Tables	xvi
List of Figures	xx
Chapter 1 : Introduction	1
1.1 Amine Scrubbing Carbon Capture.....	1
1.2 Research Objectives for Aerosol Modeling.....	3
1.3 Research Objectives for Absorber Modeling.....	6
1.3.1 Predicting Pilot Plant Absorber Performance	6
1.3.2 Absorber Optimization with A Wide Range of CO ₂	8
Chapter 2 : Limiting Mechanisms and Mitigation of Amine Aerosol Growth in Scrubbing for Carbon Capture	10
2.1 Introduction.....	12
2.2 Modeling Methods.....	16
2.2.1 Rate-based Absorber Modeling	16
2.2.2 Aerosol Modeling	16
2.2.2.1 Aerosol Phase Material and Energy Balance	17
2.2.2.2 Bulk Gas Phase Material and Energy Balance.....	21
2.3 Amine Aerosol Growth Modeling Results	22
2.3.1 Modeling Conditions – NCCC Pilot Plant.....	22
2.3.2 Amine Aerosol Growth Profiles	24
2.3.3 Limiting Mechanisms for Aerosol Growth.....	32
2.4 Conclusions and Recommendations for Emissions Control.....	38
2.5 Acknowledgements.....	40

Chapter 3 : Modeling Absorber Performance at March 2015 UT-SRP Pilot Plant Campaign with 5 m PZ	41
3.1 Introduction.....	42
3.2 March 2015 Pilot Plant Campaign Overview	45
3.3 Material Balance Closure.....	47
3.4 Performance Results	54
3.4.1 Absorber Intercooling.....	55
3.4.2 Absorber Performance: 5 m vs. 8 m PZ.....	57
3.5 Model Details.....	59
3.5.1 Modeling Methods	59
3.5.2 Spray Nozzle Impact.....	60
3.5.3 Model Correction	61
3.6 Model Validation	64
3.6.1 Model-predicted Absorber Outlet CO ₂	64
3.6.2 Model-predicted Absorber Temperature Profiles	68
3.7 Conclusions.....	74
3.8 Acknowledgements.....	75
Chapter 4 : Absorber Data Reconciliation for April 2017 UT-SRP Pilot Plant Campaign	76
4.1 April 2017 Pilot Plant Campaign Overview	76
4.2 Material Balance Closure.....	79
4.2.1 Overall CO ₂ Material Balance	83
4.2.2 Mid CO ₂ Material Balance.....	96
4.3 Performance Results	100

4.3.1	Pilot Plant Absorber Performance Results.....	100
4.3.2	Absorber Intercooling	103
4.4	Model-predicted Absorber Performance	103
4.4.1	Model-predicted NTU with and without Interfacial Area Correction	104
4.4.2	Model-predicted NTU in Absorber Top and Bottom	110
4.5	Conclusions and Recommendations	114
4.5.1	Conclusions.....	114
4.5.2	Recommendations for Future Campaigns.....	115
4.6	Acknowledgements.....	115
Chapter 5 : Absorber Modeling for Carbon Capture from Natural Gas Applications.....		117
5.1	Introduction.....	118
5.2	Modeling Methods.....	122
5.3	Simple NGCC, Scrubbing with 5 m PZ.....	123
5.3.1	Absorber Configurations and Design Conditions	123
5.3.2	Absorber Performance	127
5.4	NGCC with 35% EGR, Scrubbing with 5 m PZ	130
5.4.1	Absorber Configurations and Design Conditions.....	130
5.4.2	Absorber Performance	132
5.5	NGCC Hybrid Capture with 5 m PZ	133
5.5.1	Absorber Configurations and Design Conditions.....	133
5.5.2	Absorber Performance with Gas Concentrated by Membrane	137
5.5.2.1	With DCC and IC (Cases 1, 3, & 4).....	137
5.5.2.2	With IC and no DCC (Case 2)	139

5.6 Economics Analysis of NGCC Capture with 5 m PZ.....	141
5.6.1 Absorber Economics with 5 m PZ.....	141
5.6.2 Total capture costs	144
5.7 NGCC Hybrid Capture with 2 m PZ/3 m HMPD Blend.....	146
5.7.1 Vapor-liquid-equilibrium Comparison of 5 m PZ and 2 m PZ/3 m HMPD.....	146
5.7.2 Absorber Configurations.....	147
5.7.3 Absorber Performance with 2 m PZ/3 m HMPD.....	148
5.7.3.1 Absorber design with DCC and IC (Case 3).....	148
5.7.3.2 Absorber design without DCC and with IC (Case 2).....	150
5.7.4 Absorber Economics.....	152
5.8 Conclusions.....	153
5.9 Acknowledgements.....	153
Chapter 6 : Absorber Test Plan Development for 2018 National Carbon Capture Center Pilot Plant Campaign.....	155
6.1 NCCC Pilot Plant Absorber Overview	155
6.2 NCCC Pilot Plant Absorber Modeling Activities.....	157
6.2.1 Pre-campaign Absorber Modeling Activities	157
6.2.2 In-campaign and Post-campaign Absorber Modeling Activities.....	157
6.3 Pre-campaign Absorber Test Plan Development for 2018 NCCC Campaign..	158
6.4 Loading Prediction Using Online Density Measurements	165
6.5 Conclusions.....	167
Chapter 7 : Conclusions and Recommendations	169
7.1 Summary.....	169

7.2	Conclusions and Recommendations for Aerosol Growth Modeling	170
7.2.1	Mechanisms and Mitigation of Amine Aerosol Growth.....	170
7.2.2	Recommendations for Aerosol Growth Model Development	171
7.3	Conclusions and Recommendations for Pilot Plant Absorber Data Reconciliation	171
7.3.1	Conclusions of the March 2015 Campaign with 5 m PZ.....	171
7.3.2	Conclusions of the April 2017 Campaign with 5 m PZ.....	172
7.3.3	Recommendations for Future Campaigns.....	173
7.4	Conclusions and Recommendations for Absorber Design	174
Appendix A: Amine Aerosol Growth Model Code		176
A.1	Aerosol Integration	176
A.2	Physical Properties	188
Appendix B: Development of DeltaV Graphical Operator Interface for the April 2017 UT-SRP Pilot Plant Campaign.....		195
B.1	Operator Interface Graphics	195
B.2	FTIR Auto Sampling System	197
B.3	Advanced Control for the Advanced Flash Stripper	199
B.1.1	Cold Rich Solvent Bypass Control	199
B.1.2	AFS Level Control	201
B.1.3	Rich Solvent Density Control	202
B.1.4	AFS Sump Temperature Control	203
B.4	One-click Data Spreadsheet	204
B.5	Acknowledgement.....	207

References.....	208
Vita.....	216

List of Tables

Table 2.1:	NCCC absorber inlet flue gas specifications.	23
Table 2.2:	Average relative driving force of PZ (Avg ϕ_{PZ}) and H ₂ O (Avg ϕ_{H2O}) in the absorber at 1–10 ⁸ drops/cm ³	36
Table 3.1:	Previous piperazine pilot plant absorber specifications.	45
Table 3.2:	Summary of pilot plant operating conditions.	47
Table 3.3:	Flow and analytical measurements available for absorber mass balance.	49
Table 3.4:	Titration-measured LLDGs and density-predicted LLDGs.	51
Table 3.5:	Summary of pilot plant absorber performance results for March 2015 Campaign. Parametric testing of absorber operating or equipment conditions is outlined in the table.	55
Table 3.6:	Effect of solvent concentration on absorber performance – results of parametric testing at pilot plant. All cases with intercooling with spray.	58
Table 3.7:	Independent global parameter sensitivity analysis with 95% confidence intervals for 2011 October pilot plant campaign (Sachde et al., 2013).	62
Table 3.8:	Model corrections required for November 2013 and October 2011 PZ pilot plant campaigns.	63
Table 3.9:	Model-predicted NTU and pilot plant-measured NTU in the March 2015 campaign.	65
Table 3.10:	Average Error (K) and Mean Absolute Percentage Error (%) of temperature measurements for each run.	73
Table 4.1:	Summary of pilot plant operating conditions.	78
Table 4.2:	Previous piperazine pilot plant absorber specifications.	79
Table 4.3:	Flow and analytical measurements available for absorber mass balance.	81

Table 4.4:	Titration-measured lean loadings with two density-predicted lean loadings (FT403 and FT201 at Point 5 in Figure 4.2).	84
Table 4.5:	Titration-measured rich loadings with four density-predicted rich loadings (DT200 and DT520 at Point 6, FT515 at Point 7a, and FT518 at 7b in Figure 4.2).	85
Table 4.6:	Titration-measured lean/rich loadings and titration-corrected density-predicted lean loadings (FT403 corrected by 5%) and rich loadings (DT520 corrected by 3%). These loadings are used in the following model analysis.	87
Table 4.7:	Measured absorber inlet and outlet CO ₂ by NDIR continuous inline CO ₂ measurements and FTIR discrete online sampling.	89
Table 4.8:	Comparison between CO ₂ removed calculated by absorber gas-side measurements, CO ₂ captured by absorber liquid-side measurements, and stripper overhead CO ₂ flow.	92
Table 4.9:	TIC-measured mid loadings and density-predicted mid loadings (DT430 at Point 9 in Figure 4.2).	97
Table 4.10:	Comparison between measured gas-side CO ₂ removed and measured liquid-side CO ₂ captured in absorber top.	98
Table 4.11:	Summary of pilot plant absorber performance results for April 2017 pilot plant campaign.	102
Table 4.12:	Comparison between measured NTU and predicted NTU using pilot plant absorber model with and without interfacial area correction.	105
Table 4.13:	Predicted NTU for runs with solvent rate greater than 15 GPM and calculated percentage change of predicted NTU.	109

Table 4.14: Comparison of measured and predicted NTU of absorber top and absorber bottom with 0.6 interfacial area correction in April 2017 pilot plant campaign.....	112
Table 5.1: Flue gas information for NGCC.....	123
Table 5.2: Absorber performance with/without DCC and with/without IC at intermediate LLDG = 0.182 (mol CO ₂ /mol alk) for simple NGCC with 5 m PZ.....	128
Table 5.3: Flue gas information for NGCC with 35% EGR.....	131
Table 5.4: Absorber performance with and without DCC at intermediate LLDG = 0.210 (mol CO ₂ /mol alk) with 5 m PZ.....	132
Table 5.5: Absorber inlet flue gas for NGCC hybrid capture.....	135
Table 5.6: The most cost-effective LLDGs with 5 m PZ.....	137
Table 5.7: Absorber performance with DCC and IC for Case 1, 3, & 4 at over-stripping LLDGs with 5 m PZ.....	138
Table 5.8: Absorber performance with IC and no DCC for Case 2 at intermediate LLDGs with 5 m PZ.....	139
Table 5.9: Absorber PEC (in Million USD) and CAPEX (in \$/TONNE CO ₂) with and without DCC for amine scrubbing with 5 m PZ from simple NGCC and NGCC with 35% EGR.....	142
Table 5.10: Absorber PEC in Million USD (\$M) of NGCC hybrid carbon capture with 5 m PZ.....	143
Table 5.11: Total capture costs (\$/TONNE CO ₂) comparison of NGCC carbon capture with 5 m PZ.....	145
Table 5.12: LLDGs used for Cases 2 and 3. Intermediate LLDG and over-stripping LLDG are defined by $P^*_{CO_2}/P_{CO_2,out}$	148

Table 5.13: Absorber performance of 5 m PZ and 2 m PZ/3 m HMPD at over-stripping LLDGs.	149
Table 5.14: Absorber performance of 5 m PZ and 2 m PZ/3 m HMPD at intermediate LLDGs.	150
Table 5.15: Absorber PEC (in Million USD) and CAPEX (in \$/TONNE CO ₂) of 5 m PZ and 2 m PZ/3 m HMPD for NGCC hybrid capture.	152
Table 6.1: NCCC absorber inlet flue gas specifications.	156
Table 6.2: Absorber test plan for 2018 NCCC pilot plant campaign.	159
Table 6.3: Predicted solvent densities as a function of loadings in 2018 NCCC pilot plant campaign.	166

List of Figures

Figure 1.1: Global greenhouse gas emissions in 2014 (EPA, 2014).	1
Figure 1.2: A typical process flow diagram for an amine scrubbing system (Lin, 2016).	2
Figure 1.3: Large plumes of PZ aerosol observed after 52 ppm SO ₃ injection at the April 2017 UT-SRP pilot plant campaign. Photos by Beaudry (Beaudry, 2017).	4
Figure 2.1: Comparison of amine driving forces for aerosol growth between 30 wt % PZ and MEA at 40 °C. Curves predicted from data by Nguyen (Nguyen, 2013). The PZ curve is used in this work. MEA volatility is a linear function of loading. PZ volatility is a non-linear function of loading. The CO ₂ partial pressure in the gas phase is assumed to be 1 kPa at the absorber top and 12 kPa at the absorber bottom.	15
Figure 2.2: NCCC absorber column configuration (40' absorber, 30' dry bed, 10' water wash, 0.22 lean loading, 90% CO ₂ removal, water wash at 40 °C, lean solvent at 40 °C, intercooling at 40 °C).	24
Figure 2.3: Aerosol growth profiles in the column at 1–10 ⁸ drops/cm ³ (40' absorber, 30' dry bed, 10' water wash, 0.22 lean loading, 90% CO ₂ removal, water wash at 40 °C, lean solvent at 40 °C, intercooling at 40 °C). High aerosol concentration reduces growth.	26
Figure 2.4: Column temperature profiles at 10 ⁷ drops/cm ³ (40' absorber, 30' dry bed, 10' water wash, 0.22 lean loading, 0.36 rich loading, 90% CO ₂ removal, water wash at 40 °C, lean solvent at 40 °C, intercooling at 40 °C).	27

Figure 2.5: The moles of PZ, H ₂ O, and CO ₂ per drop at 10 ⁷ drops/cm ³ (40' absorber, 30' dry bed, 10' water wash, 0.22 lean loading, 0.36 rich loading, 90% CO ₂ removal, water wash at 40 °C, lean solvent at 40 °C, intercooling at 40 °C).	28
Figure 2.6: Aerosol growth profile without intercooling (10 ⁷ drops/cm ³ , 40' absorber, 30' dry bed, 10' water wash, same lean solvent rate, 0.22 lean loading, 0.367 rich loading, 87% CO ₂ removal, water wash at 40 °C, lean solvent at 40 °C). Intercooling slows down aerosol growth.	29
Figure 2.7: Aerosol growth profiles in the absorber column with aerosol initial composition at 5 m PZ and 0.5 m PZ (10 ⁷ drops/cm ³ , 40' absorber, 30' dry bed, 10' water wash, 0.22 lean loading, 0.36 rich loading, 90% CO ₂ removal, water wash at 40 °C, lean solvent at 40 °C, intercooling at 40 °C).	30
Figure 2.8: PZ concentration in aerosol with initial composition at 5 m PZ and 0.5 m PZ (10 ⁷ drops/cm ³ , 40' absorber, 30' dry bed, 10' water wash, 0.22 lean loading, 0.36 rich loading, 90% CO ₂ removal, water wash at 40 °C, lean solvent at 40 °C, intercooling at 40 °C).	31
Figure 2.9: The moles of PZ, H ₂ O, and CO ₂ per drop with aerosol initial composition at 5 m PZ and 0.5 m PZ (10 ⁷ drops/cm ³ , 40' absorber, 30' dry bed, 10' water wash, 0.22 lean loading, 0.36 rich loading, 90% CO ₂ removal, water wash at 40 °C, lean solvent at 40 °C, intercooling at 40 °C).	32

Figure 2.10: PZ partial pressures in the gas phase, over the liquid phase, and over the aerosol phase at $1-10^8$ drops/cm ³ (40' absorber, 30' dry bed, 10' water wash, 0.22 lean loading, 0.36 rich loading, 90% CO ₂ removal, water wash at 40 °C, lean solvent at 40 °C, intercooling at 40 °C). As aerosol concentration increases, aerosol growth decreases due to depletion of the gas phase amine driving force.....	34
Figure 2.11: \emptyset PZ in the absorber at $1-10^8$ drops/cm ³ (40' absorber, 30' dry bed, 10' water wash, 0.22 lean loading, 0.36 rich loading, 90% CO ₂ removal, water wash at 40 °C, lean solvent at 40 °C, intercooling at 40 °C). Gas phase amine driving force decreases as aerosol concentration increases.	36
Figure 2.12: Aerosol growth with different amine volatility at 10^7 drops/cm ³ (40' absorber, 30' dry bed, 10' water wash, 0.22 lean loading, 0.36 rich loading, 90% CO ₂ removal, water wash at 40 °C, lean solvent at 40 °C, intercooling at 40 °C). Greater amine volatility increases aerosol growth with the caveat about high gas phase amine emissions.	37
Figure 2.13: Aerosol growth along the column with greater absorber top temperature (10^7 drops/cm ³ , 40' absorber, 30' dry bed, 10' water wash, 0.22 lean loading, 90% CO ₂ removal, lean solvent at 60 °C and water wash at 60 °C, intercooling at 40 °C). Greater absorber top temperature gives higher PZ driving force, resulting in faster aerosol growth.	38
Figure 3.1: Pilot plant absorber configuration in March 2015 (Lin et al., 2016).	46
Figure 3.2: Simplified absorber PFD with indications for sampling and measurement points used in the mass balance in this paper. Points 1 through 5 are summarized with corresponding descriptions in Table 3.3.	48

Figure 3.3: Pilot plant inlet CO ₂ measurements (Point 3 in Figure 3.2). NDIR measurements not depicted due to large offset from other measurements. ...	52
Figure 3.4: Pilot plant outlet CO ₂ measurements. FTIR (KO), NDIR located at Point 1b in Figure 3.2. Material balance from CO ₂ make-up (CO ₂ from bulk in Figure 3.2).....	53
Figure 3.5: CO ₂ Material balance around the absorber. Density-predicted loading and FTIR/CO ₂ flow data used for liquid and gas composition, respectively.	54
Figure 3.6: Stripper energy performance analysis for March 2015 pilot plant campaign (Lin et al., 2016).....	57
Figure 3.7: Spray nozzle equivalent interfacial area model used in March 2015 pilot plant campaign analysis (Sachde et al., 2013).	61
Figure 3.8: Ratio of model-predicted NTU to pilot plant-measured NTU for each run by applying interfacial area correction and CO ₂ correction (no data for Run 4).....	66
Figure 3.9: Ratio of model-predicted NTU to pilot plant-measured NTU by applying CO ₂ correction.	67
Figure 3.10: Absorber RTD elevations in March 2015 pilot plant campaign.	69
Figure 3.11: Model-predicted temperature profile compared with pilot plant-measured temperature profile for Case 7 (LLDG = 0.246, No IC No Spray, Removal = 80%).....	70
Figure 3.12: Model-predicted temperature profile compared with pilot plant-measured temperature profile for Case 13 (LLDG = 0.243, No IC With Spray, Removal = 68%).....	70

Figure 3.13: Model-predicted temperature profile compared with pilot plant-measured temperature profile for Case 5 (LLDG = 0.214, In-and-out IC, Removal = 94%).	71
Figure 3.14: Model-predicted temperature profile compared with pilot plant-measured temperature profile for Case 6 (LLDG = 0.255, Full Spray IC, Removal = 89%).	71
Figure 4.1: Pilot plant absorber configuration in April 2017.	77
Figure 4.2: Simplified absorber PFD with indications for sampling and measurement points used in the mass balance in this paper. Points 1 through 9 are summarized with corresponding descriptions in Table 4.3.	80
Figure 4.3: Measured absorber inlet CO ₂ by NDIR continuous inline CO ₂ measurements and FTIR discrete online sampling.	90
Figure 4.4: Measured absorber outlet CO ₂ by NDIR continuous inline CO ₂ measurements and FTIR discrete online sampling.	90
Figure 4.5: Ratios of absorber gas-side CO ₂ removed to stripper overhead CO ₂ plotted against run number. Absorber inlet and outlet CO ₂ measured by NDIR and FTIR.	93
Figure 4.6: Ratios of absorber gas-side CO ₂ removed to stripper overhead CO ₂ plotted against NDIR inlet CO ₂ . Absorber inlet and outlet CO ₂ measured by NDIR and FTIR.	94
Figure 4.7: Ratios of absorber gas-side CO ₂ removed to stripper overhead CO ₂ . Absorber inlet and outlet CO ₂ calculated from NDIR and FTIR averages.	95
Figure 4.8: Ratios of absorber liquid-side CO ₂ captured to stripper overhead CO ₂ . Titration loadings and titration-corrected density-predicted loadings are compared.	95

Figure 4.9: The CO ₂ material balance closure around absorber. Absorber CO ₂ material balance closes within +/- 20% when using titration-corrected density-predicted loadings on the liquid side and NDIR and FTIR average data on the gas side.....	96
Figure 4.10: Comparison between measured gas-side CO ₂ removed and measured liquid-side CO ₂ captured in the absorber top (top 10-ft section for 20-ft absorber or top 10-ft section for 30-ft absorber). Liquid-side CO ₂ captured is calculated from density-predicted lean and mid loadings as well as density-predicted lean loadings and TIC-measured mid loadings..	100
Figure 4.11: Comparison between measured NTU and predicted NTU using pilot plant absorber model with interfacial area correction.....	106
Figure 4.12: Comparison between measured NTU and predicted NTU using pilot plant absorber model without interfacial area correction.	107
Figure 4.13: Comparison between measured NTU and predicted NTU using pilot plant absorber model with interfacial area correction. The model with interfacial area correction systematically under-predicts NTU except for Runs 7 and 8.....	109
Figure 4.14: Comparison between measured NTU and predicted NTU using pilot plant absorber model without interfacial area correction. At 3.5-12% CO ₂ , the model without interfacial area correction can capture the measured absorber NTU within 20% error. At 20% CO ₂ , the model is able to capture the measured absorber NTU within 50% error.	110

Figure 4.15: Comparison between measured absorber top NTU and predicted absorber top NTU using pilot plant absorber model with interfacial area correction. The model with interfacial area correction systematically under-predicts measured absorber top NTU for all runs. This exhibits similar trend as absorber overall NTU prediction in Figure 4.13.	113
Figure 4.16: Comparison between measured absorber bottom NTU and predicted absorber bottom NTU using pilot plant absorber model with interfacial area correction. The model can capture the measured absorber bottom NTU for most runs within 50% error.	113
Figure 5.1: Process flow diagram of a simple natural gas combined cycle (NGCC) plant with amine scrubbing.	119
Figure 5.2: Process flow diagram of an NGCC plant with 35% exhaust gas recycle (EGR) with amine scrubbing.	120
Figure 5.3: Process flow diagram of an NGCC plant with membrane-amine hybrid carbon capture.	120
Figure 5.4: Solid solubility of 5 m PZ (Chen et al., 2014).	121
Figure 5.5: Absorber configuration with IC and no DCC.	125
Figure 5.6: Absorber configuration with DCC and IC.	125
Figure 5.7: Absorber configuration with DCC and no IC.	126
Figure 5.8: Temperature and flux profiles with IC and no DCC with 5 m PZ. Inlet CO ₂ at 4%; Water wash at 48 °C; Mid PA IC and Bot PA IC at 40 °C; L _R /G = 5; Intermediate LLDG = 0.182 (mol CO ₂ /mol alk); L = 1.2*L _{min}	128
Figure 5.9: Temperature and flux profiles with DCC and IC with 5 m PZ. Inlet CO ₂ at 4%; Mid Advanced PA IC at 40 °C; L _R /G = 3; Intermediate LLDG = 0.182 (mol CO ₂ /mol alk); L = 1.2*L _{min}	129

Figure 5.10: Temperature and flux profiles with DCC and no IC with 5 m PZ. Inlet CO ₂ at 4%; Intermediate LLDG = 0.182 (mol CO ₂ /mol alk); L = 1.2*L _{min}	129
Figure 5.11: Temperature and flux profiles with IC and no DCC with 5 m PZ. Inlet CO ₂ at 6.3%; Water wash at 48 °C; Mid PA IC and Bot PA IC at 40 °C; L _R /G = 5; Intermediate LLDG = 0.21 (mol CO ₂ /mol alk); L = 1.2*L _{min}	132
Figure 5.12: Temperature and flux profiles with DCC and IC with 5 m PZ. Inlet CO ₂ at 6.3%; Mid Advanced PA IC at 40 °C; L _R /G = 3; Intermediate LLDG = 0.21 (mol CO ₂ /mol alk); L = 1.2*L _{min}	133
Figure 5.13: NGCC hybrid capture. Amine scrubbing with DCC.	134
Figure 5.14: NGCC hybrid capture. Amine scrubbing without DCC.	134
Figure 5.15: Absorber with DCC and IC. Flue gas concentrated by membrane. In-and-out intercooling at 25 °C.....	136
Figure 5.16: Absorber with IC and no DCC. Flue gas concentrated by membrane. Bot PA IC at 25 °C (parallel cooling) or 50 °C (dry cooling).	136
Figure 5.17: Temperature and flux profiles with DCC and IC (Case 3) with 5 m PZ. Inlet CO ₂ at 18%; In-and-out IC at 25 °C; Over-stripping LLDG = 0.268 (mol CO ₂ /mol alk); L = 1.2*L _{min}	138
Figure 5.18: Temperature and flux profiles with IC and no DCC (Case 2) with 5 m PZ. Inlet CO ₂ at 14%; Dry Cooling, Bot PA IC at 50 °C; L _R /G = 5; Intermediate LLDG = 0.159 (mol CO ₂ /mol alk); L = 1.2*L _{min}	140
Figure 5.19: Temperature and flux profiles with IC and no DCC (Case 2) with 5 m PZ. Inlet CO ₂ at 14%; Parallel Cooling, Bot PA IC at 25 °C; L _R /G = 5; Intermediate LLDG = 0.159 (mol CO ₂ /mol alk); L = 1.2*L _{min}	140

Figure 5.20: Absorber CAPEX (in \$/TONNE CO ₂) with and without DCC for simple NGCC amine scrubbing capture, NGCC with EGR amine scrubbing capture, and NGCC hybrid capture with 5 m PZ.....	143
Figure 5.21: Total capture costs (\$/TONNE CO ₂) comparison of NGCC carbon capture with 5 m PZ.....	145
Figure 5.22: CO ₂ vapor-liquid-equilibrium (VLE) Comparison between 5 m PZ and 2 m PZ/3 m HMPD. PZ model was developed by Frailie (Frailie, 2014) and PZ/HMPD model was developed by Sherman (Sherman, 2016).....	147
Figure 5.23: Temperature and flux profiles with DCC and IC (Case 3) with 2 m PZ/3 m HMPD. In-and-out IC at 25 °C; Over-stripping LLDG = 0.191 (mol CO ₂ /mol alk); L = 1.2*L _{min}	149
Figure 5.24: Temperature and flux profiles without DCC (Case 2) with 2 m PZ/3 m HMPD. Bot PA IC at 50 °C; L _R /G = 5; Intermediate LLDG = 0.115 (mol CO ₂ /mol alk); L = 1.2*L _{min}	151
Figure 5.25: Temperature and flux profiles without DCC (Case 2) with 2 m PZ/3 m HMPD. Bot PA IC at 25 °C; L _R /G = 5; Intermediate LLDG = 0.115 (mol CO ₂ /mol alk); L = 1.2*L _{min}	151
Figure 6.1: NCCC absorber column configuration.	156
Figure 6.2: Model-predicted NCCC absorber temperature and flux profiles for Run 1.....	160
Figure 6.3: Model-predicted NCCC absorber temperature and flux profiles for Run 1 with 80-ft packing (at L _{min}).....	161
Figure 6.4: Model-predicted NCCC absorber temperature and flux profiles for Run 11.....	162

Figure 6.5: Model-predicted NCCC absorber temperature and flux profiles for Run 5.....	163
Figure 6.6: Model-predicted NCCC absorber temperature and flux profiles for Run 6.....	164
Figure 6.7: Solid solubility of 5 m PZ (Chen et al., 2014).....	164
Figure 6.8: Predicted solvent densities as a function of loadings in 2018 NCCC pilot plant campaign.....	167
Figure B.1: DeltaV user interface for absorber gas.....	195
Figure B.2: DeltaV user interface for absorber.....	196
Figure B.3: DeltaV user interface for the advanced flash stripper.....	196
Figure B.4: DeltaV user interface for the FTIR auto sampling switch control (Manual Mode)	198
Figure B.5: DeltaV user interface for the FTIR auto sampling switch control (Auto Mode).....	198
Figure B.6: DeltaV user interface for the FTIR heated lines control.....	199
Figure B.7: DeltaV Control Studio screenshots for the cold rich solvent bypass control.....	200
Figure B.8: DeltaV Control Studio screenshots for the AFS level control.....	202
Figure B.9: DeltaV Control Studio screenshots for the rich solvent density control.....	203
Figure B.10: DeltaV Control Studio screenshots for the AFS sump temperature control.....	204
Figure B.11: User interface of “one-click” time-based data log built using Microsoft Visual Basic.....	205

Chapter 1 : Introduction

1.1 AMINE SCRUBBING CARBON CAPTURE

Greenhouse gas emissions result in global climate change. Figure 1.1 shows the global greenhouse gas emissions in 2014 (EPA, 2014). At the global scale, the key greenhouse gases emitted by human activities are: CO₂, CH₄, N₂O, and F-gases. CO₂ from fossil fuels and industrial processes is the largest source of greenhouse gas emissions. Currently, the fossil fuels cannot be replaced and they should be burned in a cleaner and more environmentally responsible way. Carbon capture and storage enables industry processes to continue to operate while emitting fewer greenhouse gases.

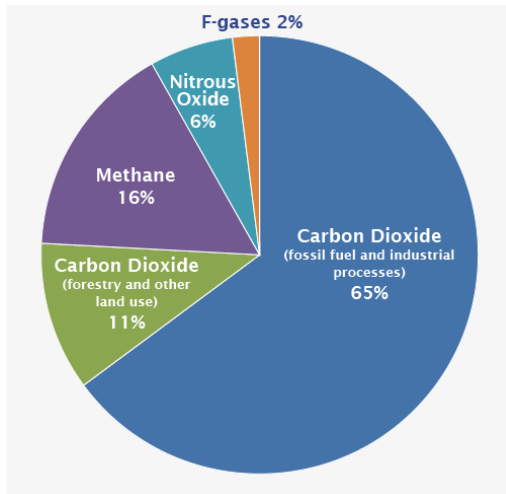


Figure 1.1: Global greenhouse gas emissions in 2014 (EPA, 2014).

This work is on the capture portion of carbon capture and storage. Amine scrubbing is a robust, energy-efficient, and flexible approach for post-combustion carbon capture (Rochelle, 2009). Figure 1.2 shows a typical process flow diagram for an amine scrubbing system (Lin, 2016). After pre-treatment, the flue gas, containing 4-20% inlet CO₂,

is fed into the bottom of the absorber. The absorber is usually operated at 40-60 °C, where the flue gas is in counter-current contact with the solvent. The lean solvent is fed to the top of the absorber; the rich solvent leaves the bottom of the absorber and is pumped through a cross exchanger to the stripper. In the stripper, the rich solvent counter-currently contacts hot vapor and the lean solvent is circulated back to the absorber. CO₂ is stripped out from the rich solvent and is sent to compressors for transport and storage. The scrubbed flue gas leaves the absorber and is fed to a water wash. The water wash is a packed column with water recycle, used to recover amine in the scrubbed gas and maintain the water balance of the system. Most solvents used for amine scrubbing are volatile. SO₃ or fine fly ash in flue gas serves as nuclei for amine aerosol, which will grow in the amine scrubbers. This work focuses on amine aerosol growth modeling and absorber design and development.

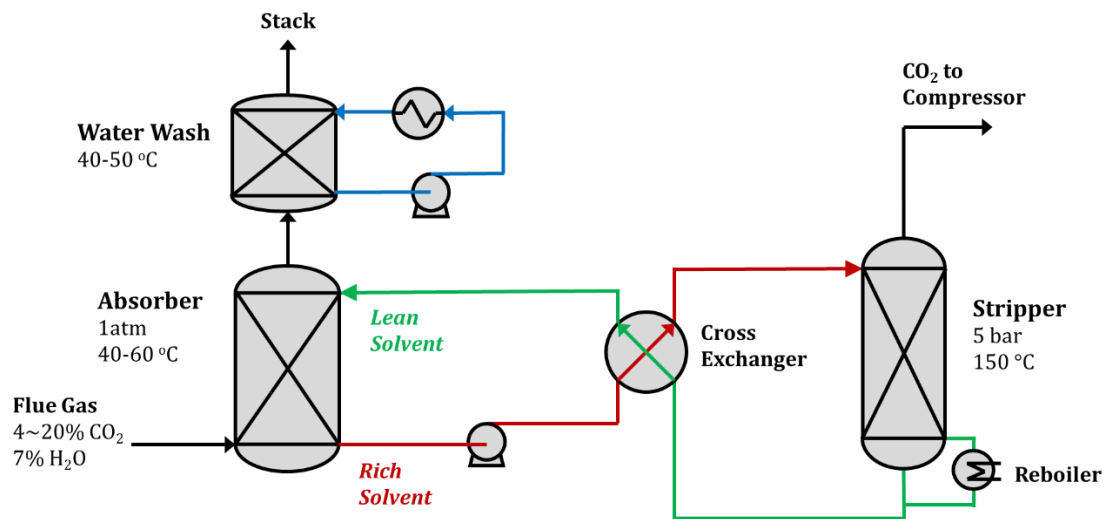


Figure 1.2: A typical process flow diagram for an amine scrubbing system (Lin, 2016).

1.2 RESEARCH OBJECTIVES FOR AEROSOL MODELING

Most amine solvents are volatile and will produce aerosols. Figure 1.3 shows one of the piperazine (PZ) aerosol tests in the April 2017 pilot plant campaign at The University of Texas Separations Research Program (UT-SRP). After SO₃ was injected, large plumes of PZ aerosol were observed at the absorber outlet. The amine emissions from scrubbers include gas phase emissions due to volatility, entrainment carryover, and amine carried in aerosol. The first two emission mechanisms have been widely studied, but amine aerosol growth mechanisms are not well understood. Reasonable environmental impact limits total amine emissions to less than 1 ppm, but amine carried in aerosol may increase emissions to more than 100 ppm. If aerosol is not captured, aerosol emissions will cause amine loss and environmental harm.

Several process configurations have been tested in the field for emission control. Acid wash was successfully demonstrated by Aker Solutions for reducing amine emissions (Bade et al., 2014; Knudsen et al., 2013). Linde-BASF successfully tested a two-stage water wash advanced emission control system (Stoffregen et al., 2014). A “dry bed” concept was demonstrated to reduce aerosol emissions by an order of magnitude at the post-combustion capture pilot plant in Niederaussem by BASF, Linde, and RWE Power (Moser et al., 2014, 2013). To define the most effective emissions control techniques, it is important to understand the limiting process of aerosol growth in the amine scrubbing process, which requires quantitative and accurate modeling work.



Figure 1.3: Large plumes of PZ aerosol observed after 52 ppm SO₃ injection at the April 2017 UT-SRP pilot plant campaign. Photos by Beaudry (Beaudry, 2017).

The first-generation amine solvent for carbon capture, monoethanolamine (MEA), is relatively volatile (Nguyen et al., 2011). Khakharia et al. used a simplified modeling approach in Aspen Plus[®] to simulate aerosol formation in MEA. He divided the absorber into ten small sections with counter-current contact between the liquid and gas phases as well as co-current contact of aerosol with the resulting gas phase (Khakharia et al., 2014). The model predicted that, with increasing temperature of the lean solvent, MEA emissions in the aerosol phase decreased while emissions in the gas phase increased. At high lean solvent temperature (70–80 °C), MEA emissions were caused mainly by volatile MEA in the gas phase (Khakharia et al., 2015).

Majeed et al. simulated MEA aerosol growth using a rate-based aerosol model in MATLAB[®] and found that both volatility and initial composition affected final droplet size: decreased volatility led to smaller droplets (Majeed et al., 2017a). Majeed had the limitation that MEA mass transfer from gas phase to aerosol phase was not included in the overall MEA mass balance. Majeed developed an improved MEA aerosol model in MATLAB[®], which accounted for the mass and heat transfer between gas and aerosol

phases (Majeed et al., 2017b). With this model, Majeed studied the effect of gas phase component depletion on the drop growth and predicted concentration profiles in the drop. He concluded that gas phase MEA depletion occurred with greater than 10^5 drops/cm³ with 1.5 μ m drops and 5 m MEA (Majeed et al., 2017b). These studies did not identify the limiting process for aerosol mass transfer.

Aqueous piperazine (PZ) has been developed as a superior solvent to MEA and is a well-defined second-generation solvent for amine scrubbing (Chen et al., 2014; Freeman et al., 2010; Rochelle et al., 2011). With a fast absorption rate, relatively wide solubility window, and good energy performance (Chen et al., 2014; Li, 2015; Rochelle et al., 2011), 5 molal (m) PZ (30 wt %) has been widely evaluated and tested in pilot plant campaigns (Chen et al., 2017; Lin et al., 2016; Sachde et al., 2013; Zhang et al., 2017b). PZ is less volatile than MEA but depends in a more nonlinear way on loading - the difference between PZ and MEA could make a significant difference in aerosol growth. It is important to understand how PZ aerosol grows in the scrubbers and how it can be captured. Fulk et al. developed a PZ aerosol growth model in MATLAB[®] but were not able to simulate aerosol smaller than 1 μ m and the aerosol mass was not included in the overall mass balance (Fulk, 2016).

This work has developed a rate-based PZ aerosol model with complete overall mass balance in gPROMS[®] ModelBuilder and simulated aerosol growth at the unique conditions of PZ and the pilot plant absorber configurations at the National Carbon Capture Center (NCCC) conditions. This work differs from previous aerosol modeling activities in that it adds to the previous PZ model the simulation of amine driving force depletion in the bulk gas phase. Compared to the previous work on MEA, this work focuses on understanding the limiting mechanisms of mass transfer on aerosol growth and how aerosol can be

captured. This work also simulates integrated absorber configurations and operating conditions that have been proposed to mitigate amine emissions, and gives recommendations for emissions control.

To summarize, the objectives of this work are to:

- Develop a rate-based aerosol growth model;
- Investigate aerosol growth mechanisms and identify the limiting mass transfer process;
- Predict aerosol growth at realistic plant conditions with PZ;
- Evaluate industrial emission control techniques and give recommendations.

1.3 RESEARCH OBJECTIVES FOR ABSORBER MODELING

1.3.1 Predicting Pilot Plant Absorber Performance

The CO₂ absorption process involves complicated rate and thermodynamic behaviors. Mass transfer is not in equilibrium; the liquid phase is highly non-ideal and involves multiple equilibrium reactions. As a result of heat of absorption, temperature bulge makes it even harder to predict absorber performance. A PZ model (“Independence”) was developed in Aspen Plus® RateSep™ with a rigorous e-NRTL thermodynamic framework and rigorous kinetics with reactions in the boundary layer by Frailie (Frailie, 2014), where the kinetics were regressed from bench-scale wetted wall column measurements and the packing parameters were regressed from pilot-scale measurements. However, the packing measurements were conducted independently in pilot columns with different solvent systems (Song, 2017; Tsai, 2010; Wang, 2015). They may not represent real packing performance due to effects of rivulets and drop and additional mass transfer caused by distributors and chimney trays. It is important to

improve our understanding and the existing packing model for scale-up by with pilot plant campaigns.

In previous work, pilot plant campaigns were designed and carried out with 30 wt % monoethanolamine (MEA) and 8 m (40 wt %) PZ (Kay et al., 2014; Knudsen et al., 2011; Rezazadeh et al., 2016; Sachde et al., 2013; Tait et al., 2016; von Harbou et al., 2014) to improve the existing packing model. With fast absorption rate, relatively wide solubility window, and good energy performance (Chen et al., 2014; Li, 2015; Rochelle et al., 2011), 5 m PZ (30 wt %) has become a new standard solvent for amine scrubbing carbon capture. In this work, the UT-SRP pilot plant is operated with 5 m PZ for the first time, and two pilot plant campaigns have been designed and conducted. Furthermore, the previous UT-SRP pilot plant campaigns only tested absorber performance with different column internals and intercooling configurations, but a parametric test of conditions relevant to absorber performance was not performed. To evaluate the absorber performance within a wider range of operating conditions, this work has designed test plans with systematically varied PZ concentration, inlet CO₂, gas rate, lean loading, solvent to gas ratio, and intercooling methods.

A rigorous data reconciliation method with the Independence PZ model was developed over a limited range of conditions by Plaza and Sachde during previous campaigns (Plaza, 2011; Sachde et al., 2013). Plaza developed pilot plant data collection methods and improved the PZ model (Plaza, 2011). Sachde developed a consistent method for absorber model validation and correction by utilizing a rigorous data reconciliation method using the October 2011 and November 2013 campaigns (Sachde et al., 2013). This work focuses more on the evaluation of the existing model correction method developed in previous campaigns using the newly collected absorber data.

To summarize, the objectives of this work are to:

- Predict pilot plant absorber performance over a wider range of operating conditions with aqueous PZ;
- Evaluate pilot plant absorber performance with 5 m PZ;
- Develop pilot plant test plans to maximize value of data for model development and improvement;
- Evaluate the existing packing model and correction method using the newly collected data.

1.3.2 Absorber Optimization with A Wide Range of CO₂

Amine scrubbing system optimization usually concerns the trade-off between capital expenses (CAPEX) and operating expenses (OPEX). CAPEX can be approximated as absorber packing costs and OPEX can be approximated as stripper energy costs (Frailie, 2014). The absorber is an expensive process unit. With a typical amine scrubbing plant to capture 90 % of the CO₂ from a 593 MWe coal-fired power plant, the absorber costs are 30% of the costs of the entire amine scrubbing plant (Frailie, 2014). Membrane Technology and Research (MTR) previously proposed a hybrid system combining amine scrubbing with membrane technology for carbon capture from coal-fired power plants (Freeman et al., 2014; Merkel et al., 2013; Johannes G Wijnmans et al., 2011). Maintaining the same overall CO₂ removal rate, flue gas CO₂ could be enriched by the membrane from 12% to 23%, and the flue gas volume entering the amine scrubbing system could be reduced by 47% (Freeman et al., 2014). As a result, absorber costs can be greatly reduced while stripper energy costs still remain the same.

Compared with applications with high CO₂, amine scrubbing is less attractive for natural gas combined cycle (NGCC) plants with 4% CO₂ (Rochelle, 2009). In this work, a membrane-amine hybrid carbon capture system for the NGCC power plants has been proposed and evaluated, and the CO₂ in the flue gas can be enriched from 4% to 18%. Previous study on NGCC capture mainly utilized 30 wt% MEA and 8 m PZ (Berstad et al., 2011; Gaspar et al., 2016; Rongrong et al., 2008; Sachde and Rochelle, 2014; Sipöcz and Tobiesen, 2012; Ystad et al., 2012). Different from previous work, 5 m PZ is evaluated in this study. Previous absorber modeling work for NGCC amine scrubbing carbon capture mainly focused on absorbers without intercooling or with simple intercooling, and none of them have utilized optimal cooling options or evaluated absorber with a wide range of operating conditions (Berstad et al., 2011; Gaspar et al., 2016; Plaza, 2011; Sachde and Rochelle, 2014; Sachde, 2016; Sipöcz and Tobiesen, 2012; Ystad et al., 2012). This work optimizes the absorber with different direct contact cooler options, multiple intercooling designs, different cooling options, and a wide range of lean loadings at 4% to 18% inlet CO₂. Technical economic analysis has been performed for the hybrid membrane-amine scrubbing system to evaluate the economic feasibility.

To summarize, the objectives of this work are to:

- Design and optimize absorber process configurations with a wide range of CO₂ with 5 m PZ;
- Perform technical economic analysis and conclude with cost-effective absorber designs and operating conditions.

Chapter 2 : Limiting Mechanisms and Mitigation of Amine Aerosol Growth in Scrubbing for Carbon Capture¹

SO₃ or fine fly ash in flue gas serves as nuclei for amine aerosol, which will grow in the amine scrubber. If the aerosol is not captured, aerosol emissions will cause amine loss and environmental harm. Aerosol emissions will be avoided if the aerosol grows large enough to be captured by impaction. Amine aerosol management requires accurate modeling of aerosol growth in the absorber and water wash. This work models aerosol growth at the unique conditions of piperazine (PZ) and the pilot plant absorber configurations of the National Carbon Capture Center (NCCC). It adds to the previous PZ model the simulation of amine driving force depletion in the bulk gas phase. Compared with the previous work on monoethanolamine (MEA), this work focuses on understanding the limiting mechanisms of mass transfer in the aerosol growth and how aerosol can be captured. This work also simulates integrated absorber configurations and operating conditions that have been proposed to mitigate amine emissions. The absorber was modeled with rate-based mass transfer in Aspen Plus[®] RateSep[™] and aerosol growth was calculated by gPROMS[®] ModelBuilder. Multiple variables were evaluated, including aerosol number concentration, variable amine volatility, operating conditions, and process configurations.

In the absorber, amine aerosol growth is driven by amine-limited diffusion. As aerosol concentration increases, aerosol growth decreases due to the depletion of the amine driving force in the gas phase, and the limiting driving force for aerosol growth shifts from gas-to-drop to liquid-to-gas. Understanding aerosol growth mechanisms will help control

¹Part of this chapter has been published in Zhang, Y., Kang, J., Fulk, S., Rochelle, G., 2017. Modeling Amine Aerosol Growth at Realistic Pilot Plant Conditions. Energy Procedia 114, 1045 – 1060. Kang and Fulk helped build the aerosol growth model. Rochelle supervised this work and helped interpret the results.

emissions by selecting appropriate packing types, solvents, and operating conditions. The effect of initial aerosol diameter on aerosol growth is insignificant. At high aerosol concentration, aerosol will remain small and therefore hard to collect. At low aerosol concentration, it is more likely to grow to the point where it is large enough to be collected (3 μm with common types of mist eliminators). Greater amine volatility, higher temperature, and lower solvent loading increase gas phase amine driving force, resulting in faster growth. This work also considers MEA aerosol modeling results for comparison. The differences in volatility, packing types, and aerosol residence time could result in the calculated difference in growth between PZ aerosol and MEA aerosol.

For emissions control, it is not necessary to eliminate all nuclei in the flue gas. The techniques that can reduce the nuclei count to the point where aerosol can grow enough to be collected are sufficient. Aerosol growth can be increased by enhancing the gas-film mass transfer coefficient of packing, e.g., selecting finer packing or operating the column with higher gas velocity, which will produce larger aerosol that is easier to capture. A solvent with moderate volatility, like PZ, will produce aerosol that grows to larger size and is easier to collect. Solvents with low volatility should be avoided as they produce aerosol that is hard to collect. Solvents with very high volatility should also be avoided as they emit high gas phase amine. An absorber operated at higher temperature and lower solvent loading will increase aerosol growth. Process configurations that provide greater water partial pressure in the water wash, such as higher operating temperature and pre-humidified empty space, will increase aerosol growth.

2.1 INTRODUCTION

Amine scrubbing is a robust, energy-efficient, and flexible approach for post-combustion CO₂ capture (Rochelle, 2009). Most solvents used for amine scrubbing are volatile. SO₃ or fine fly ash in flue gas serves as nuclei for amine aerosol, which will grow in the amine scrubber. The amine emissions from scrubbers include gas phase emissions due to volatility, entrainment carryover, and amine carried in aerosol. The first two emission mechanisms have been widely studied, but amine aerosol growth mechanisms are not well understood. Reasonable environmental impact limits total amine emissions to less than 1 ppm, but amine carried in aerosol may increase emissions to more than 100 ppm. If aerosol is not captured, aerosol emissions will cause amine loss and environmental harm.

Analytical measurement techniques, such as Fourier Transform Infrared Spectrometry (FTIR) and Phase Doppler Interferometry (PDI), have been used to measure overall emissions and drop size distribution as well as drop number concentration (Beaudry et al., 2017; Beaudry, 2017; Fulk, 2016). Emissions can be reduced by adjusting the operating conditions of the amine scrubber to make aerosol grow to a large size that can be effectively captured by impaction. Drops greater than 3 μm can be removed by mist eliminators (such as knitted wire mesh). Drops larger than 20 μm in diameter can be collected by inertial impaction on packing.

Several process configurations have been tested in the field for emission control. Acid wash was successfully demonstrated by Aker Solutions for reducing amine emissions (Bade et al., 2014; Knudsen et al., 2013). Linde-BASF successfully tested a two-stage water wash advanced emission control system (Stoffregen et al., 2014). A “dry bed” concept was demonstrated to reduce aerosol emissions by an order of magnitude at the

post-combustion capture pilot plant in Niederaussem by BASF, Linde, and RWE Power (Moser et al., 2014, 2013). To define the most effective emissions control techniques, it is important to understand the limiting process of aerosol growth in the amine scrubbing process. Multiple process configurations are modeled in this study.

The first-generation amine solvent for carbon capture, monoethanolamine (MEA), is relatively volatile (Nguyen et al., 2011). Khakharia et al. used a simplified modeling approach in Aspen Plus[®] to simulate aerosol formation in MEA. He divided the absorber into ten small sections with counter-current contact between the liquid and gas phases as well as co-current contact of aerosol with the resulting gas phase (Khakharia et al., 2014). The model predicted that, with increasing temperature of the lean solvent, MEA emissions in the aerosol phase decreased while emissions in the gas phase increased. At high lean solvent temperature (70–80 °C), MEA emissions were caused mainly by volatile MEA in the gas phase (Khakharia et al., 2015).

Majeed et al. simulated MEA aerosol growth using a rate-based aerosol model in MATLAB[®] and found that both volatility and initial composition affected final droplet size: decreased volatility led to smaller droplets (Majeed et al., 2017a). Majeed had the same limitation as the Fulk model: MEA mass transfer from gas phase to aerosol phase was not included in the overall MEA mass balance. Majeed developed an improved MEA aerosol model in MATLAB[®], which accounted for the mass and heat transfer between gas and aerosol phases (Majeed et al., 2017b). With this model, Majeed studied the effect of gas phase component depletion on the drop growth and predicted concentration profiles in the drop. He concluded that gas phase MEA depletion occurred with greater than 10^5 drops/cm³ with 1.5 μm drops and 5 m MEA (Majeed et al., 2017b). These studies did not identify the limiting process for aerosol mass transfer.

Aqueous piperazine (PZ) has been developed as a superior solvent to MEA and is a well-defined second-generation solvent for amine scrubbing (Chen et al., 2014; Freeman et al., 2010; Rochelle et al., 2011). With a fast absorption rate, relatively wide solubility window, and good energy performance (Chen et al., 2014; Li, 2015; Rochelle et al., 2011), 5 molal (m) PZ (30 wt %) has been widely evaluated and tested in pilot plant campaigns (Chen et al., 2017; Lin et al., 2016; Sachde et al., 2013; Zhang et al., 2017b). It is important to understand how PZ aerosol grows in the scrubbers and how it can be captured.

As shown in Figure 2.1, PZ is less volatile than MEA but depends in a more nonlinear way on loading. Estimated amine driving forces for aerosol growth with 30 wt % MEA and 30 wt % PZ at 40 °C are compared in Figure 2.1, and the correlations are from Nguyen (Nguyen, 2013). The x-axis shows CO₂ loading (in mol CO₂/mol alk) and the y-axis shows gas phase amine partial pressure (in Pa). The typical absorber solvent loading range is 0.24–0.38 (mol CO₂/mol alk) for PZ and 0.2–0.5 (mol CO₂/mol alk) for MEA. The CO₂ partial pressure in the gas phase is 1 kPa at the absorber top and 12 kPa at the absorber bottom. The circles in Figure 2.1 represent the equilibrium partial pressures of amine over the aerosol drop; the dots represent the equilibrium partial pressures of amine over the bulk liquid; the differences are the overall amine driving forces that allow aerosol to grow. Based on the understanding that amine aerosol growth is driven by amine-limited diffusion, the difference in amine driving force between PZ and MEA could make a significant difference in aerosol growth.

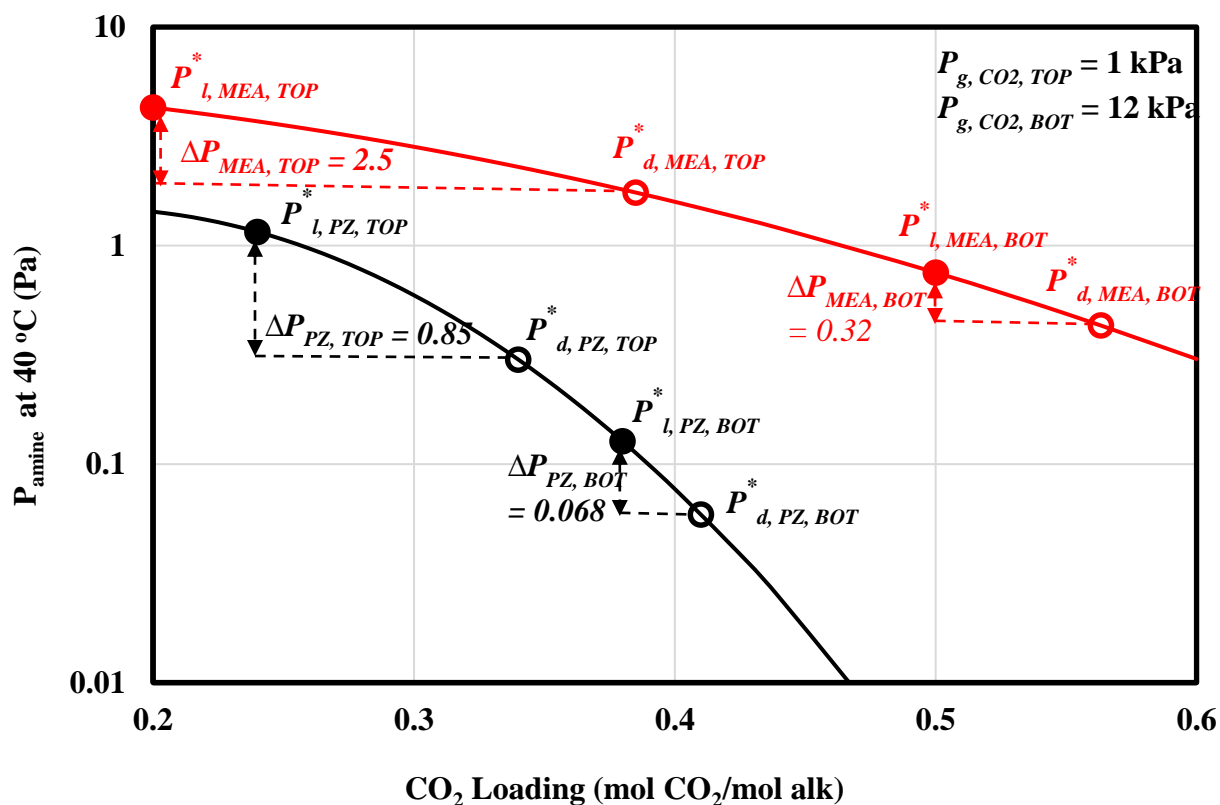


Figure 2.1: Comparison of amine driving forces for aerosol growth between 30 wt % PZ and MEA at 40 °C. Curves predicted from data by Nguyen (Nguyen, 2013). The PZ curve is used in this work. MEA volatility is a linear function of loading. PZ volatility is a non-linear function of loading. The CO_2 partial pressure in the gas phase is assumed to be 1 kPa at the absorber top and 12 kPa at the absorber bottom.

Fulk et al. developed a PZ aerosol growth model in MATLAB[®], but were not able to simulate aerosol smaller than 1 μm and the aerosol mass was not included in the overall mass balance (Fulk, 2016). Improving on Fulk, Zhang et al. developed a new PZ aerosol model in gPROMS[®] ModelBuilder, and simulated a steady-state absorber in Aspen Plus[®] RateSep[™] and calculated PZ aerosol growth in gPROMS[®] (Kang et al., 2017; Zhang et al., 2017a). Small aerosol drops were integrated and gas phase PZ was re-calculated based on PZ mass transfer. Zhang found that aerosol growth was determined by amine

driving force between bulk gas and aerosol, and aerosol was practically at equilibrium with bulk gas CO₂, water, and temperature (Zhang et al., 2017a).

This work models aerosol growth at the unique conditions of PZ and the pilot plant absorber configurations at NCCC. It adds to the previous PZ model the simulation of amine driving force depletion in the bulk gas phase. Compared to the previous work on MEA, this work focuses on understanding the limiting mechanisms of mass transfer on aerosol growth and how aerosol can be captured. This work also simulates integrated absorber configurations and operating conditions that have been proposed to mitigate amine emissions.

2.2 MODELING METHODS

2.2.1 Rate-based Absorber Modeling

The rate-based absorber and water wash using 5 m piperazine (PZ) were modeled using Independence developed by Frailie (Frailie, 2014) in Aspen Plus[®] RateSep[™], with rigorous e-NRTL thermodynamics and rigorous kinetics in the boundary layer. The packing model used in the rate-based column includes models for interfacial area (Tsai, 2010) and gas- and liquid-side physical mass transfer coefficients (Wang, 2015) developed from data collected at the Separations Research Program (SRP) pilot scale air-water column for a variety of packing types. Gas-phase compositions and physical properties calculated using Aspen Plus[®] were input to gPROMS[®] ModelBuilder to calculate aerosol mass and heat transfer.

2.2.2 Aerosol Modeling

Amine aerosol growth was simulated in gPROMS[®], which tracks water, CO₂, and PZ in the bulk gas phase and aerosol phase with mass transfer occurring at the bulk gas-

drop (bulk gas-aerosol) interface and the bulk gas-solvent interface. Concentrations of components are also integrated in the aerosol phase. Aerosol mass transfer fluxes were calculated using Equations 2.1 to 2.4, and heat transfer flux using Equation 2.5. At high drop concentration, mass transfer of PZ from bulk gas to aerosol results in gas phase PZ depletion. Gas phase PZ was re-calculated by PZ mass transfer fluxes at the gas-drop interface and the gas-solvent interface, shown in Equations 2.6 and 2.7. Model details are discussed in Kang et al. (2017) and Zhang et al. (2017a).

2.2.2.1 Aerosol Phase Material and Energy Balance

Material and energy balances are shown in Equations 2.1 to 2.4. Equations 2.1 to 2.2 are the material balance calculations inside the aerosol phase and at the gas-aerosol interface. Equation 2.3 is the aerosol growth calculation as a function of time. Equation 2.4 is the energy balance calculation. The model assumes that there is no convective flux inside the aerosol phase thus the molar density is uniform inside a specific layer. The velocity of the aerosol drops, v_{drop} , is assumed to be the same as the bulk gas velocity, v_{gas} .

When $0 \leq r_D < 1$ (inside the aerosol)

$$\frac{v_{drop}}{H_{col}} C_{tot,drop} \frac{dx_{i,r,drop}}{d\tau_D} = - \frac{C_{tot,drop} x_{i,r,drop}}{R_{ds}} \frac{v_{drop}}{H_{col}} \frac{dR_{ds}}{d\tau_D} - \frac{J_{d,i,r}}{r_D R_{ds}} \quad (2.1)$$

When $r_D = 1$ (at the gas-aerosol interface)

$$\frac{v_{drop}}{H_{col}} C_{tot,drop} \frac{dx_{i,r,drop}}{d\tau_D} = - \frac{C_{tot,drop} x_{i,r,drop}}{R_{ds}} \frac{v_{drop}}{H_{col}} \frac{dR_{ds}}{d\tau_D} + \frac{N_{gd,i}}{R_{ds}} \quad (2.2)$$

$$\frac{v_{drop}}{H_{col}} \frac{dR_{ds}}{d\tau_D} = \frac{\sum N_{gd,i}}{C_{tot,drop}} \quad (2.3)$$

$$\frac{v_{drop}}{H_{col}} \frac{dT_{drop}}{d\tau_D} = -T_{drop} \frac{\sum N_{gd,i} a_{gd}}{C_{tot,drop}} + \frac{Q_{drop} a_{gd}}{C_{tot,drop} C_p} \quad (2.4)$$

where:

r_D = Normalized radius of an aerosol drop;

i = Index of CO₂ and PZ when $0 \leq r_D < 1$; index of H₂O, CO₂, and PZ when $r_D = 1$;

r = Index of layers inside aerosol;

v_{drop} = Velocity of an aerosol drop (m/s);

H_{col} = Total height of the column (m);

$C_{tot,drop}$ = Total concentration of components in an aerosol drop (mol/m³);

$x_{i,r,drop}$ = Mole fraction of the i specie at the r layer in an aerosol drop;

τ_D = Normalized time;

R_{ds} = The radius of an aerosol drop (m);

$J_{d,i,r}$ = Diffusion flux of the i specie in an aerosol drop (mol/m²/s);

$N_{gd,i}$ = Mass transfer flux of the i specie at the bulk gas and aerosol interface (mol/m²/s);

T_{drop} = Temperature of aerosol (K);

a_{gd} = Specific gas and drop contact surface area (1/m);

Q_{drop} = Heat transfer flux at the bulk gas and aerosol interface (J/m²);

C_p = Heat capacity of an aerosol drop (J/mol/K).

At the gas-aerosol interface, the diffusion fluxes are replaced by mass transfer fluxes, shown in Equations 2.5 and 2.6. The Fuchs-Sutugin correction factor is used to correct the mass transfer for small aerosol, and Knudsen number calculation is shown in Equation 2.7. Multi-component diffusion is calculated by Maxwell-Stefan Equation (Equation 2.8), where the diagonal $B_{i,i}$ is calculated by Equation 2.9 and the non-diagonal $B_{i,j}$ is calculated by Equation 2.10.

$$N_{gd,i} = k_{g,i} \frac{(P_{g,i} - P_{d,i}^*)}{RT_g} \varphi(Kn) \quad (2.5)$$

$$N_{gd,CO_2} = k'_g (P_{g,CO_2} - P_{d,CO_2}^*) \quad (2.6)$$

$$Kn = \frac{2\lambda}{d_{drop}} \quad (2.7)$$

$$\begin{pmatrix} J_{d,1,r} \\ \vdots \\ J_{d,i,r} \end{pmatrix} = -C_{tot,drop} \begin{bmatrix} B_{1,1} & \cdots & B_{1,j} \\ \vdots & \ddots & \vdots \\ B_{i,1} & \cdots & B_{i,j} \end{bmatrix}^{-1} \begin{pmatrix} \frac{\partial x_1}{\partial r} \\ \vdots \\ \frac{\partial x_n}{\partial r} \end{pmatrix} \quad (2.8)$$

$$B_{i,i} = \frac{x_i}{D_{i,n}} + \sum_{j \neq i}^n \frac{x_j}{D_{i,j}} \quad (2.9)$$

$$B_{i,j} = -x_i \left(\frac{1}{D_{i,j}} - \frac{1}{D_{i,n}} \right) \quad (2.10)$$

where:

$k_{g,i}$ = Mass transfer coefficient of component i (m/s);

φ = Fuchs-Sutugin correction factor;

Kn = Knudsen number;

k'_g = Liquid side mass transfer coefficient of CO₂ (mol/Pa·m²·s);

$P_{g,i}$ = Partial pressures of i specie in the bulk gas phase (Pa);

$P_{d,i}^*$ = Equilibrium partial pressures of i specie over the aerosol phase (Pa);

λ = Mean free path of a gas molecule;

d_{drop} = Diameter of an aerosol drop (m);

$B_{i,i}$ = Maxwell-Stefan Matrix on diagonal;

$B_{i,j}$ = Maxwell-Stefan Matrix on non-diagonal;

x_i = Mole fraction of i specie;

$D_{i,j}$ = Binary diffusion coefficient of i and j species (m²/s);

$J_{d,i,r}$ = Diffusion flux of i specie (mol/m²/s).

Inside the aerosol, the binary diffusion coefficients between all components are assumed to be the same and represented by the binary diffusion coefficient between PZ and water. This is overestimated in Aspen Plus[®] and is assumed to be half of the diffusivity between CO₂ and solvent. As a result, the diffusion flux $J_{d,i,r}$ calculation in Equation 2.8 can be simplified to Equation 2.11.

$$\begin{pmatrix} J_{d,H_2O,r} \\ J_{d,CO_2,r} \\ J_{d,PZ,r} \end{pmatrix} = -C_{tot,drop} \begin{bmatrix} \frac{D_{CO_2/solvent}}{2} & 0 & 0 \\ 0 & \frac{D_{CO_2/solvent}}{2} & 0 \\ 0 & 0 & \frac{D_{CO_2/solvent}}{2} \end{bmatrix} \begin{pmatrix} \frac{\partial x_{H_2O}}{\partial r} \\ \frac{\partial x_{CO_2}}{\partial r} \\ \frac{\partial x_{PZ}}{\partial r} \end{pmatrix} \quad (2.11)$$

At the gas-aerosol interface, in Equation 2.5, the equilibrium partial pressure of component *i* over the aerosol phase is a function of mole fractions. The gas phase mass transfer coefficients are calculated using Equation 2.12. The gas film diffusion coefficients are from Aspen Plus[®]. The aerosol velocity is assumed to be the same as the bulk gas velocity, thus the Sherwood numbers are assumed to be 2. The liquid side mass transfer coefficient of CO₂ is calculated using Equation 2.13.

$$k_{g,i} = \frac{Sh_i D_{g,i}}{d_{drop}} \quad (2.12)$$

$$k'_g = \frac{\sqrt{k_2 [PZ]^{free} D_{CO_2,mx}}}{H_{CO_2}} \quad (2.13)$$

where:

$k_{g,i}$ = Gas film mass transfer coefficient of component *i* (m/s);

k'_g = Liquid film mass transfer coefficient of CO₂ (mol/Pa/m²/s);

Sh_i = Sherwood number of component *i*;

$D_{g,i}$ = Gas film diffusion coefficient of component *i* (m²/s);

d_{drop} = Diameter of an aerosol drop (μm);

k_2 = Reaction rate of CO₂ (m³/mol/s);

$[PZ]^{free}$ = Free PZ concentration (mol/m³);

$D_{CO_2,mx}$ = CO₂ diffusion coefficient of mixture (m²/s);

H_{CO_2} = Henry's law constant of CO₂ (Pa·m³/mol).

At the bulk gas-aerosol interface, the heat transfer flux Q_{drop} (In Equation 2.4) is calculated by Equation 2.14.

$$Q_{drop} = N_{gd,H_2O}\Delta H_{H_2O} - N_{gd,PZ}\Delta H_{PZ} + N_{gd,CO_2}\Delta H_{CO_2} + h_g(T_g - T_d) \quad (2.14)$$

where:

Q_{drop} = Heat transfer flux at the bulk gas and aerosol interface (J/m²);

ΔH_i = Heat of vaporization for water and PZ, and the heat of absorption for CO₂ (J/mol);

h_g = Heat transfer coefficient (J/m²/K/s);

T_g = Temperature of bulk gas (K).

2.2.2.2 Bulk Gas Phase Material and Energy Balance

In the bulk gas phase, the mole concentration of PZ is much lower than that of N₂, H₂O, and CO₂. The PZ mass transfer from the bulk gas phase to the aerosol phase decreases gas phase PZ. As a result, the model recalculates gas phase PZ while gas phase N₂, CO₂, and H₂O remain constant. The material balance of PZ is shown in Equation 2.15. The mass transfer flux of PZ at the bulk gas and the bulk liquid interface, $N_{gl,PZ}$, is calculated in Equation 2.16.

$$\frac{v_{drop}}{H_{col}} \frac{dP_{g,PZ}}{d\tau_D} = -(N_{gl,PZ}a_{gl} + N_{gd,PZ}A_d N_p)RT_g \quad (2.15)$$

$$N_{gl,PZ} = k_{g,PZ} \frac{(P_{g,PZ} - P_{l,PZ}^*)}{RT_g} \quad (2.16)$$

where:

v_{drop} = Velocity of an aerosol drop (m/s);

H_{col} = Total height of the column (m);

$P_{g,PZ}$ = Partial pressure of PZ in the bulk gas phase (Pa);

τ_D = Normalized time;

$N_{gl,PZ}$ = Mass transfer flux of PZ at the bulk gas and the bulk liquid interface (mol/m²/s);

a_{gl} = Gas-liquid interfacial area (m²/m³);

$N_{gd,PZ}$ = Mass transfer flux of PZ at the bulk gas and aerosol interface (mol/m²/s);

A_d = Surface area of an aerosol drop (m²/m³);

N_p = Aerosol number concentration;

T_g = Temperature of bulk gas (K);

$k_{g,PZ}$ = Gas film mass transfer coefficient of PZ (m/s);

$P_{l,PZ}^*$ = Equilibrium partial pressure of PZ over the bulk liquid phase (Pa).

2.3 AMINE AEROSOL GROWTH MODELING RESULTS

2.3.1 Modeling Conditions – NCCC Pilot Plant

The National Carbon Capture Center (NCCC) provides opportunities to test carbon capture technologies for coal-fired power generation. A test campaign has been planned using the Pilot Solvent Test Unit (PSTU) with 5 m PZ. The absorber inlet flue gas composition, flow rate, temperature, and pressure that will be used in this study are shown in Table 2.1. Figure 2.2 shows the absorber column configuration. The column system has 5 sections of packing: an absorber with two 20-ft sections, a 20-ft absorber extension, a 10-ft empty bed, and a 10-ft water wash. The lean solvent was fed above the 20-ft

absorber and below the 20-ft absorber extension, as a result of which the absorber extension and empty bed were treated as a 30-ft dry bed. The column diameter is 26 inches. The gas phase composition in the dry bed is assumed to be the same as the absorber outlet gas composition. The absorber was simulated at 90% CO₂ removal with a total of 40 ft of packing. Lean solvent at 0.22 mol CO₂/mol alk was fed above the absorber top at 40 °C. Rich solvent loading was at 0.36 mol CO₂/mol alk. The NCCC absorber was modeled with Mellapak 250Y packing. An in-and-out intercooler at 40 °C was applied 20 ft from the bottom of the absorber to reduce the temperature bulge and improve mass transfer driving force (Sachde and Rochelle, 2014). The water wash and DCC were operated at the same temperature to maintain the water balance in the absorber (Zhang et al., 2016).

Table 2.1: NCCC absorber inlet flue gas specifications.

Nominal throughput	MWe	0.5
CO ₂	vol %	12.2
O ₂	vol %	5.7
N ₂	vol %	74.8
H ₂ O	vol %	7.4
Temperature	°C	40
Pressure	kPa	101.3
Volumetric flow rate	ACFM	1028
Mass flow rate	lb/hr	4069

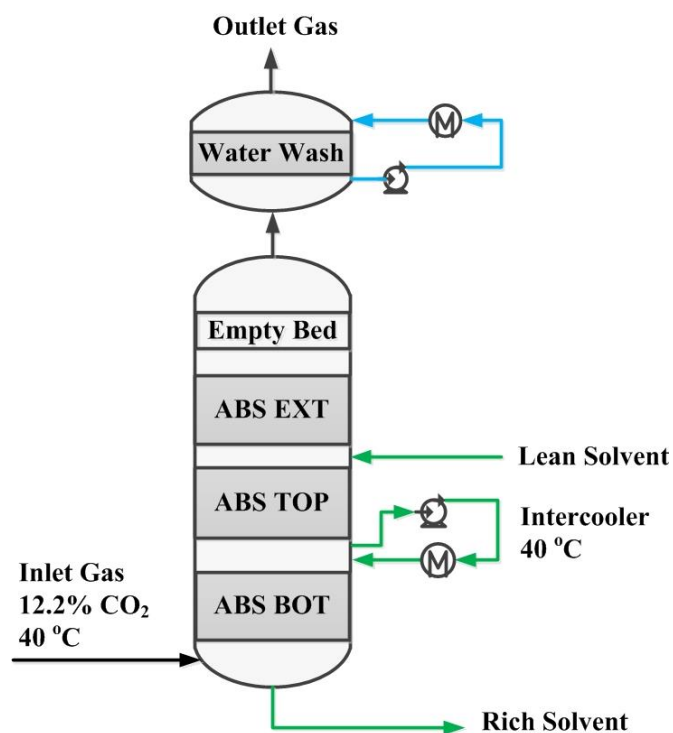


Figure 2.2: NCCC absorber column configuration (40' absorber, 30' dry bed, 10' water wash, 0.22 lean loading, 90% CO₂ removal, water wash at 40 °C, lean solvent at 40 °C, intercooling at 40 °C).

2.3.2 Amine Aerosol Growth Profiles

In this work, each aerosol drop was modeled as a well-mixed liquid with PZ, H₂O, and CO₂. Aerosol was initially assumed to be at the same composition as the rich solvent: 0.36 mol CO₂/alk and 5 m PZ. The initial diameter was assumed to be 0.1 μm, typical of that assumed at multiple pilot plant sites (Beaudry et al., 2017; Fulk, 2016). This work evaluated a wide range of aerosol concentration. 1 drop/cm³ represented a low aerosol concentration. 10⁷ drops/cm³ represented the base case, typical of that assumed or measured at pilot plants with aerosol emissions (Beaudry et al., 2017; Fulk, 2016). 10⁸ drops/cm³ was assumed to be the higher limit of aerosol concentration due to coalescence.

Figure 2.3 shows that aerosol growth decreases with increasing aerosol concentration. At 1 drop/cm³, aerosol grows from 0.1 μm at the absorber bottom to 5.4 μm at the absorber top. Gas is cooled by the liquid near the intercooling ($Z/Z_{\text{tot}} = 0.25$) and absorber top ($Z/Z_{\text{tot}} = 0.48$), which reduces driving force and slows down aerosol growth. Aerosol growth in the dry bed and water wash is not included in the graph due to its sensitivity to the gas phase water. Most types of mist eliminators (such as knitted wire mesh) can collect aerosol of diameter 3 μm and greater. Aerosol with 10⁷ drops/cm³ can grow from 0.1 μm to 4.4 μm in the absorber and up to 10 μm in the water wash; aerosol at 4.4 μm and 10 μm would probably be collected by the packing. Aerosol with 10⁸ drops/cm³ grows from 0.1 μm to 2.6 μm in the absorber and is not collectable without a water wash to allow extended growth. In the dry bed, the gas phase composition is assumed to be at the same composition of the absorber outlet gas thus aerosol does not grow. At high concentration, aerosol will not grow as much and therefore will be hard to collect. Aerosol is more likely to grow more and be collected at low concentration. For emissions control, it is not necessary to eliminate all nuclei in the flue gas. The techniques that can reduce the nuclei count to the point where aerosol can grow enough to be collected are sufficient. In the dry bed, the gas phase composition is assumed to be at the same composition of the absorber outlet gas, thus aerosol does not grow. At high concentration, aerosol will not grow as much and therefore will be hard to collect. Aerosol is more likely to grow more and be collected at low concentration. For emissions control, it is not necessary to eliminate all nuclei in the flue gas. The techniques that can reduce the nuclei count to the point where aerosol can grow enough to be collected are sufficient.

Majeed simulated MEA aerosol growth in a 15-meter absorber column with similar gas phase composition and solvent loading, and found that that MEA aerosol grew from

1.5 μm to 2.7 μm at 1 drop/ cm^3 and 1.6 μm at 10^7 drops/ cm^3 (Majeed et al., 2017b). However, in Majeed there was not enough information about aerosol residence time, packing types, and amine driving force, which are important factors that can affect aerosol growth. Compared with Majeed results for MEA at different conditions, PZ aerosol grows to a larger size at these conditions. The differences in volatility, packing types, and aerosol residence time could result in the calculated difference in growth between PZ aerosol and MEA aerosol.

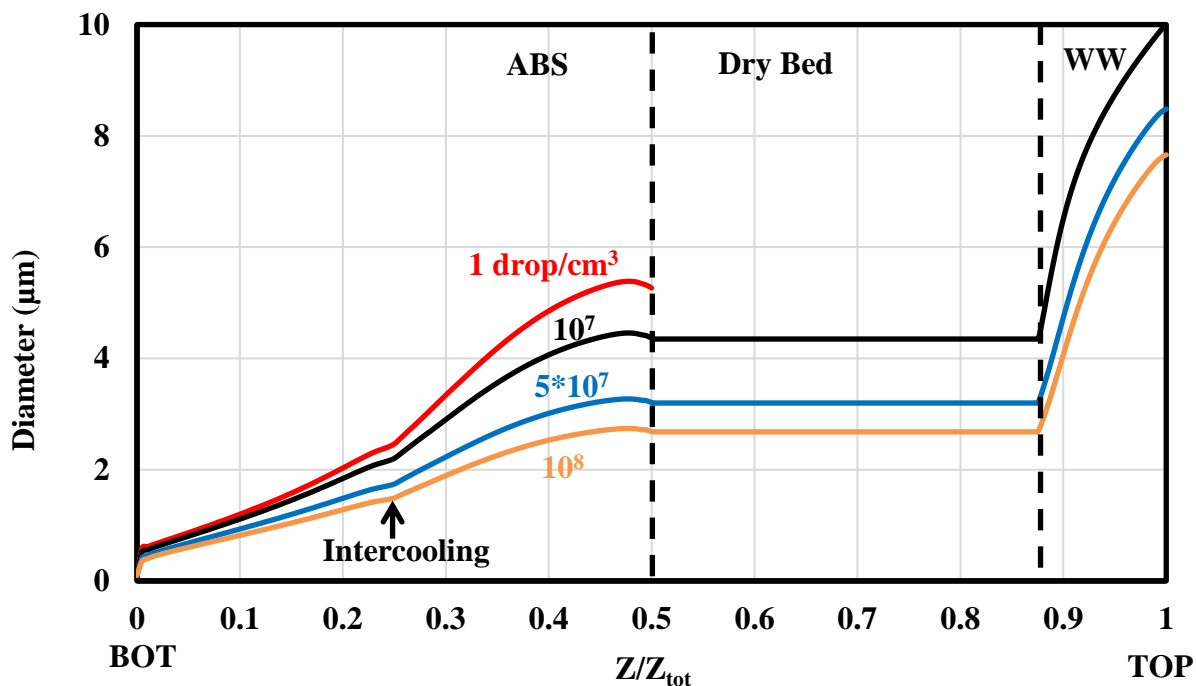


Figure 2.3: Aerosol growth profiles in the column at 1– 10^8 drops/ cm^3 (40' absorber, 30' dry bed, 10' water wash, 0.22 lean loading, 90% CO_2 removal, water wash at 40 °C, lean solvent at 40 °C, intercooling at 40 °C). High aerosol concentration reduces growth.

Column temperature profiles at 10^7 drops/ cm^3 are plotted in Figure 2.4. The in-and-out intercooling at 40 °C effectively reduces the temperature in the absorber. It was

also observed that, in the absorber and water wash, there is a small temperature driving force between the bulk gas and the bulk liquid, while aerosol closely tracks the bulk gas temperature. There is no liquid in the dry bed, and aerosol is practically at equilibrium with gas. The moles of PZ, H₂O, and CO₂ carried in each aerosol drop are shown in Figure 2.5. Aerosol picks up PZ, H₂O, and CO₂ in the absorber. Aerosol picks up a larger amount of H₂O in the water wash.

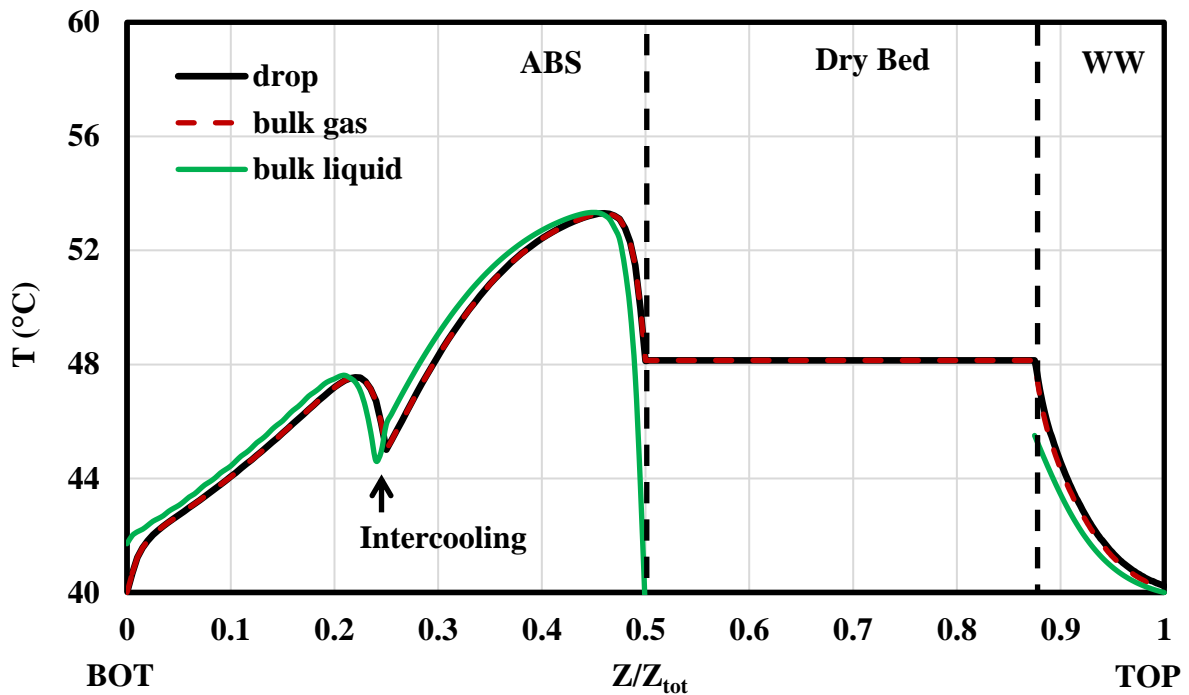


Figure 2.4: Column temperature profiles at 10^7 drops/cm³ (40' absorber, 30' dry bed, 10' water wash, 0.22 lean loading, 0.36 rich loading, 90% CO₂ removal, water wash at 40 °C, lean solvent at 40 °C, intercooling at 40 °C).

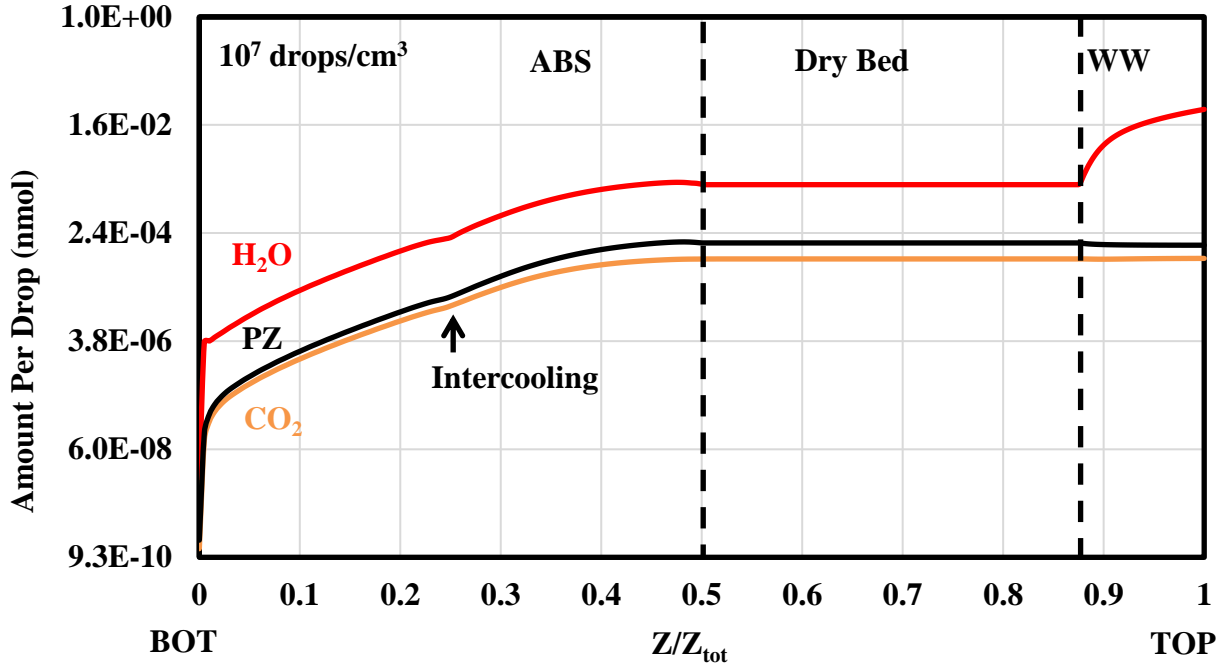


Figure 2.5: The moles of PZ, H₂O, and CO₂ per drop at 10⁷ drops/cm³ (40' absorber, 30' dry bed, 10' water wash, 0.22 lean loading, 0.36 rich loading, 90% CO₂ removal, water wash at 40 °C, lean solvent at 40 °C, intercooling at 40 °C).

Aerosol growth was also modeled without intercooling at the same lean solvent rate and lean loading. Figure 2.6 plots the aerosol growth profiles with and without intercooling. Intercooling reduces gas temperature, which results in lower amine driving force and decreases aerosol growth. Additionally, aerosol growth with two different initial PZ composition was studied. Figures 2.7 through 2.8 present the aerosol growth with initial composition at 0.36 CO₂ loading with 5 m PZ and 0.5 m PZ. Aerosol number concentration was modeled at 10⁷ drops/cm³. In Figure 2.7, aerosol with initial composition at 0.5 m PZ (the red solid line) grows to the same size of that with initial composition at 5 m PZ (the dashed black line). Figure 2.8 suggests that, for aerosol initially at 5 m PZ, PZ in the aerosol initially decreases to 1 m and then comes back to 5 m as aerosol moves up the column. Figure 2.9 presents the moles of PZ, H₂O, and CO₂ per

drop with aerosol initial composition at 5 m PZ and 0.5 m PZ. Aerosol starting at 0.5 m PZ picks up less water at the beginning. The effect of initial amine composition on ultimate aerosol growth is insignificant.

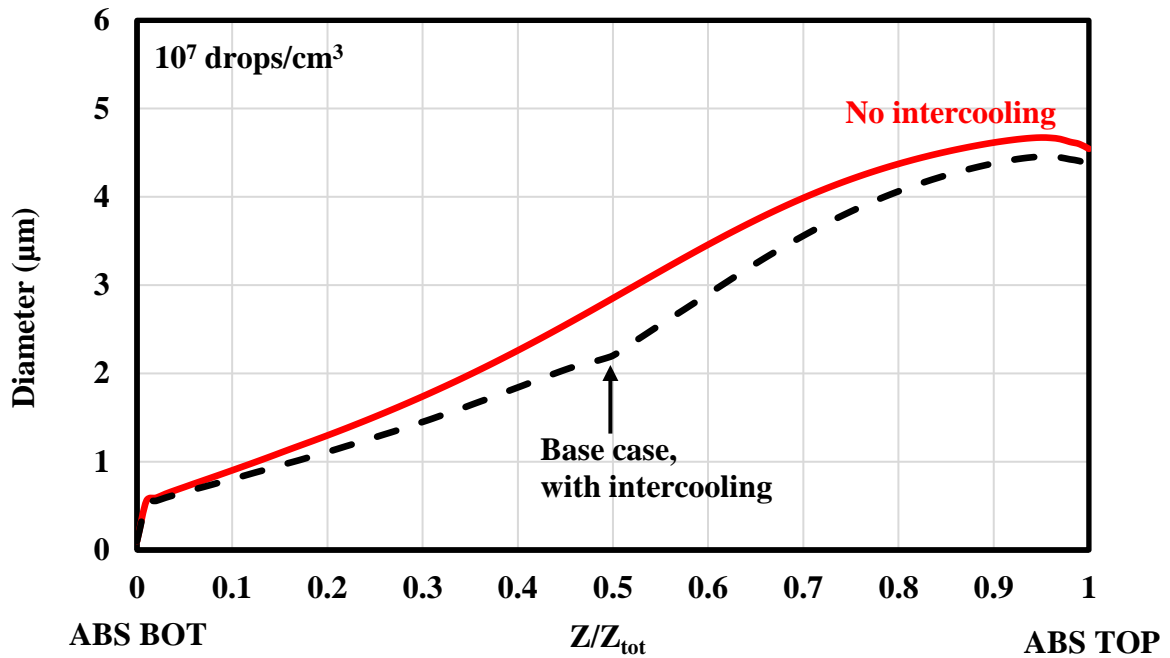


Figure 2.6: Aerosol growth profile without intercooling (10^7 drops/cm³, 40' absorber, 30' dry bed, 10' water wash, same lean solvent rate, 0.22 lean loading, 0.367 rich loading, 87% CO₂ removal, water wash at 40 °C, lean solvent at 40 °C). Intercooling slows down aerosol growth.

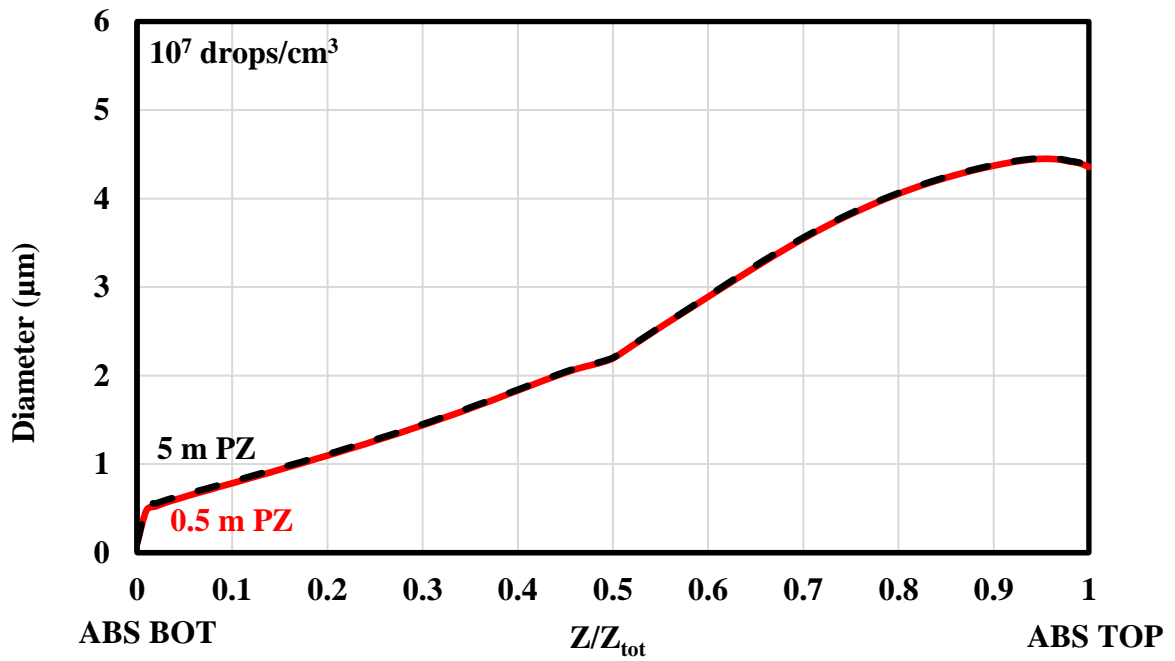


Figure 2.7: Aerosol growth profiles in the absorber column with aerosol initial composition at 5 m PZ and 0.5 m PZ (10^7 drops/cm³, 40' absorber, 30' dry bed, 10' water wash, 0.22 lean loading, 0.36 rich loading, 90% CO₂ removal, water wash at 40 °C, lean solvent at 40 °C, intercooling at 40 °C).

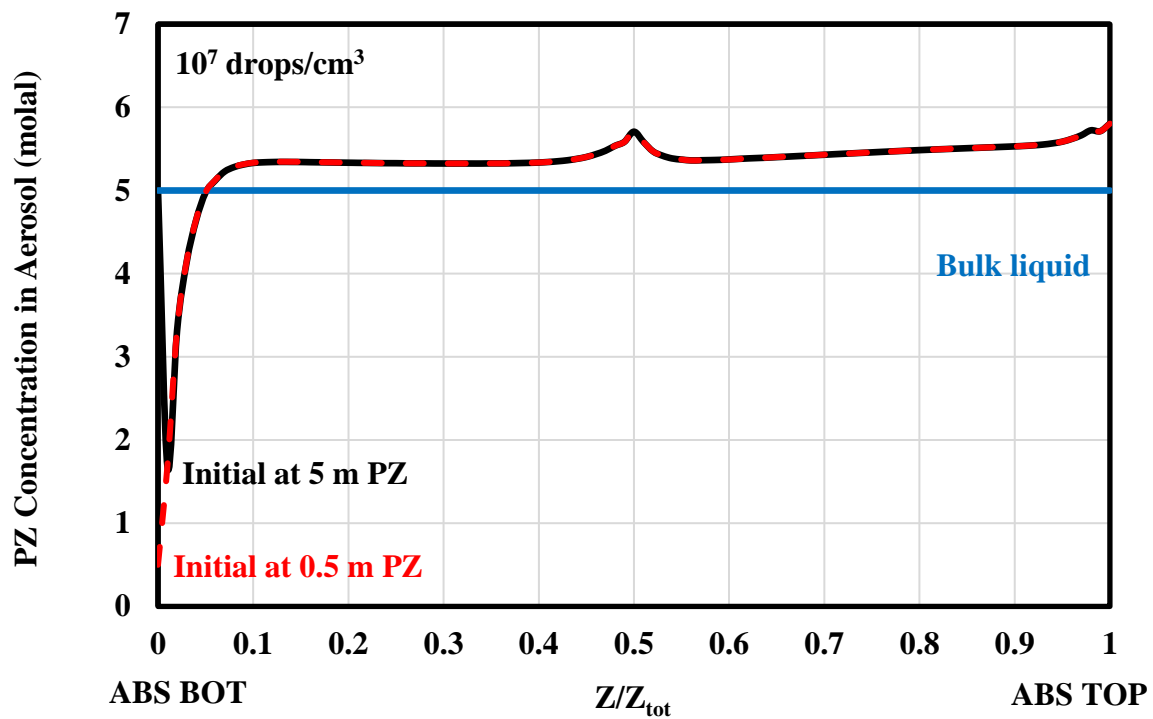


Figure 2.8: PZ concentration in aerosol with initial composition at 5 m PZ and 0.5 m PZ (10^7 drops/cm³, 40' absorber, 30' dry bed, 10' water wash, 0.22 lean loading, 0.36 rich loading, 90% CO₂ removal, water wash at 40 °C, lean solvent at 40 °C, intercooling at 40 °C).

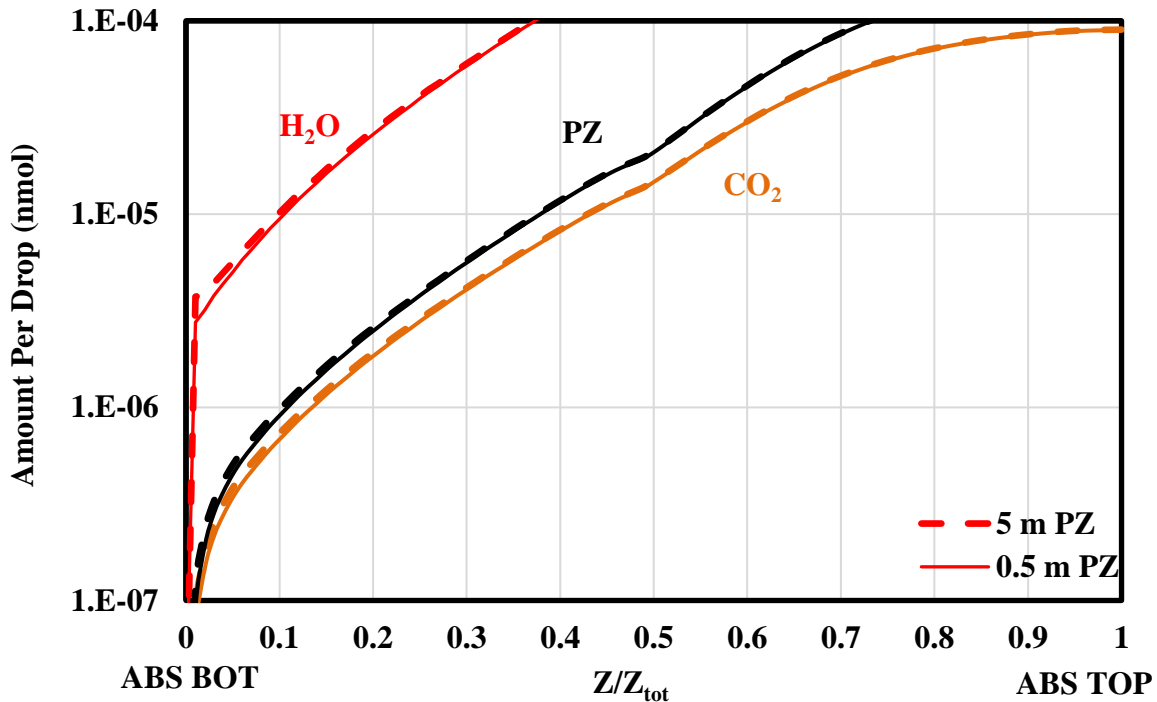


Figure 2.9: The moles of PZ, H₂O, and CO₂ per drop with aerosol initial composition at 5 m PZ and 0.5 m PZ (10^7 drops/cm³, 40' absorber, 30' dry bed, 10' water wash, 0.22 lean loading, 0.36 rich loading, 90% CO₂ removal, water wash at 40 °C, lean solvent at 40 °C, intercooling at 40 °C).

2.3.3 Limiting Mechanisms for Aerosol Growth

The PZ driving force for aerosol growth in absorber is defined in Equation 2.17.

$$\Delta P_{PZ} = P_{g,PZ} - P_{d,PZ}^* \quad (2.17)$$

where

ΔP_{PZ} = Driving force for PZ mass transfer from bulk gas phase to aerosol phase (Pa);

$P_{g,PZ}$ = Gas phase PZ pressure (Pa);

$P_{d,PZ}^*$ = Equilibrium partial pressure of PZ over the aerosol drop phase (Pa).

Majeed et al. had the observation in their recently published work that gas phase amine decreased with aerosol concentration (Majeed et al., 2017b), but the amine partial pressures over the aerosol phase were not compared. What limits aerosol growth is not the gas phase amine, but the amine driving force between the gas phase and the aerosol phase. Figure 2.10 shows the PZ partial pressures in the gas phase over the liquid phase, and over the aerosol phase at $1-10^8$ drops/cm³. The three colored solid lines Figure 2.10 plot the gas phase PZ ($P_{g,PZ}$) with aerosol concentration at 1, 10^7 , and 10^8 drops/cm³; the three colored dashed lines represent the equilibrium PZ over the aerosol drop ($P_{d,PZ}^*$) at 1, 10^7 , and 10^8 drops/cm³. The equilibrium PZ over the bulk liquid ($P_{l,PZ}^*$) does not vary much from 1 to 10^8 drops/cm³. As a result, only $P_{l,PZ}^*$ at 1 drop/cm³ is plotted as the top black dashed line in Figure 2.10. At 1 drop/cm³, the difference between $P_{g,PZ}$ and $P_{l,PZ}^*$ is small and the difference between $P_{g,PZ}$ and $P_{d,PZ}^*$ is quite large, suggesting a small PZ driving force between gas phase and liquid phase and a relatively large PZ driving force between gas phase and aerosol phase. As aerosol concentration increases, PZ driving force for aerosol growth decreases. At high aerosol concentration, PZ mass transfer from bulk liquid phase to bulk gas phase cannot keep up with that from bulk gas phase to aerosol phase, resulting in depletion of PZ driving force for aerosol growth. Majeed also observed that gas phase amine depletion occurred at high aerosol concentration (Majeed et al., 2017b). Figure 2.10 further suggests that PZ driving force for aerosol growth increases as aerosol moves from absorber bottom to absorber top, as a result of higher gas phase free PZ at lower solvent loading. As gas is cooled by the liquid near the intercooling and absorber top, PZ driving force decreases ($Z/Z_{tot} = 0.5$ in Figure 2.10) and even becomes negative ($Z/Z_{tot} = 0.96$ in Figure 2.10), resulting in slower aerosol growth and shrinkage.

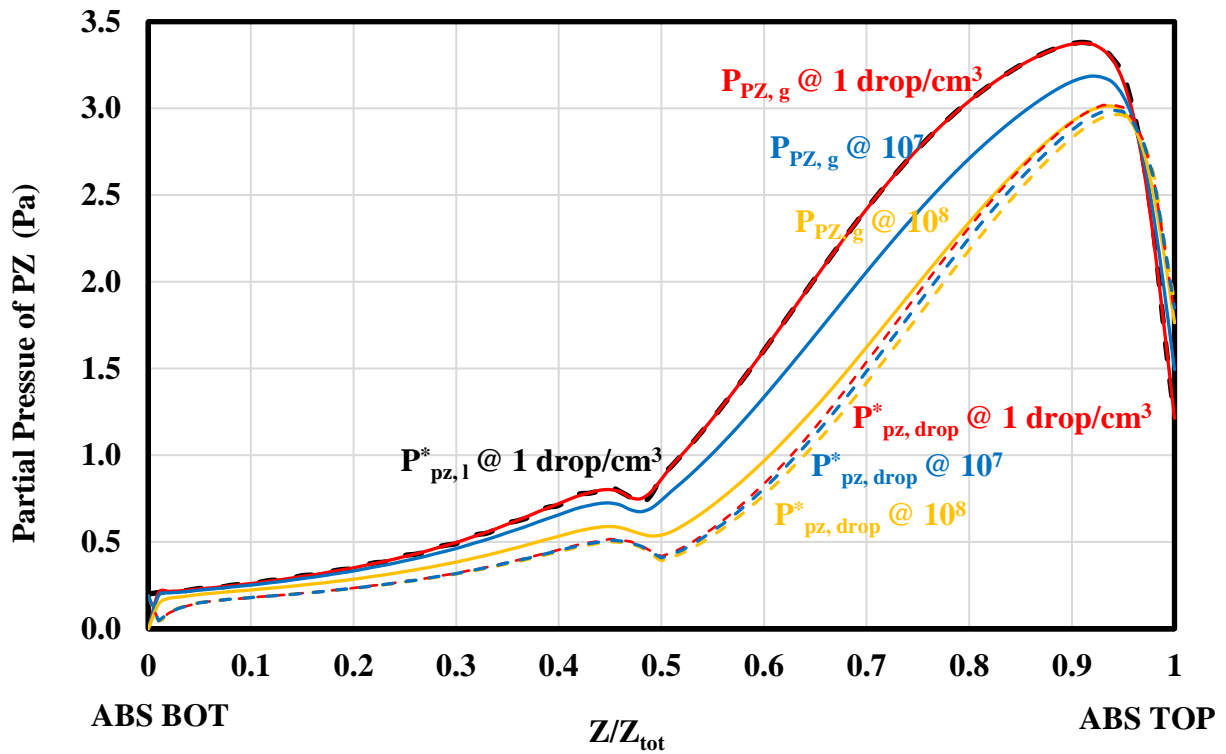


Figure 2.10: PZ partial pressures in the gas phase, over the liquid phase, and over the aerosol phase at $1-10^8$ drops/cm³ (40' absorber, 30' dry bed, 10' water wash, 0.22 lean loading, 0.36 rich loading, 90% CO₂ removal, water wash at 40 °C, lean solvent at 40 °C, intercooling at 40 °C). As aerosol concentration increases, aerosol growth decreases due to depletion of the gas phase amine driving force.

To explain the mechanism that limits aerosol growth, relative driving forces of PZ and water are defined in Equations 2.18 and 2.19. Figure 2.11 shows the relative driving force of PZ (ϕ_{PZ}) in the absorber over a wide range of aerosol concentration. Table 2.2 shows the average ϕ_{PZ} and ϕ_{H_2O} . A 100% relative driving force suggests that bulk gas phase and bulk liquid phase are in equilibrium. The absolute driving force from bulk gas to aerosol is small compared with the absolute driving force from bulk liquid to bulk gas.

A 0% relative driving force means the aerosol is in equilibrium with the bulk gas. Figure 2.11 and Table 2.2 show that aerosol growth is a function of aerosol concentration. As aerosol increases from 1 drop/cm³ to 10⁸ drops/cm³, Φ_{PZ} decreases from 100% to 32%, which suggests PZ driving force depletion. In addition, the average Φ_{H_2O} at all aerosol concentrations is always near zero, suggesting that aerosol is in equilibrium with water in the bulk gas phase. Φ_{PZ} is always greater than Φ_{H_2O} , which suggests that aerosol growth in the absorber is driven by amine-limited diffusion. As aerosol concentration increases, aerosol growth decreases due to depletion of the amine driving force in the gas phase, and the limiting driving force shifts from gas-to-drop to liquid-to-gas.

Understanding this will help control aerosol emissions by selecting appropriate packing types, solvents, and operating conditions. Aerosol growth can be increased by enhancing the gas-film mass transfer coefficient of packing, e.g., selecting finer packing or operating the column with higher gas velocity, which will produce larger aerosol that is easier to capture.

$$\Phi_{PZ} = 100\% * \frac{P_{g,PZ} - P_{d,PZ}^*}{P_{l,PZ}^* - P_{d,PZ}^*} \quad (2.18)$$

$$\Phi_{H_2O} = 100\% * \frac{P_{g,H_2O} - P_{d,H_2O}^*}{P_{l,H_2O}^* - P_{d,H_2O}^*} \quad (2.19)$$

where:

Φ_{PZ} = Relative driving force of PZ;

Φ_{H_2O} = Relative driving force of water;

$P_{l,PZ}^*$ = Equilibrium partial pressure of PZ over the bulk liquid phase (Pa).

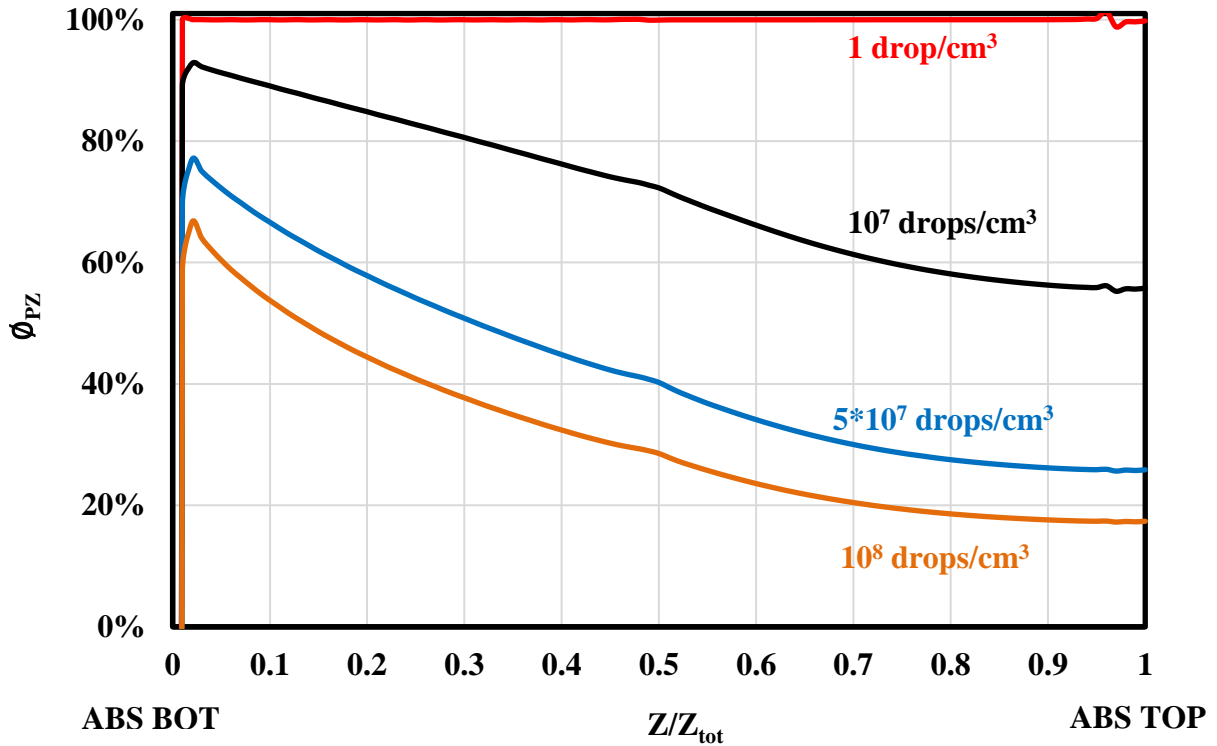


Figure 2.11: ϕ_{PZ} in the absorber at $1-10^8$ drops/cm³ (40' absorber, 30' dry bed, 10' water wash, 0.22 lean loading, 0.36 rich loading, 90% CO₂ removal, water wash at 40 °C, lean solvent at 40 °C, intercooling at 40 °C). Gas phase amine driving force decreases as aerosol concentration increases.

Table 2.2: Average relative driving force of PZ (Avg ϕ_{PZ}) and H₂O (Avg ϕ_{H_2O}) in the absorber at $1-10^8$ drops/cm³.

Aerosol Conc.	1 drop/cm ³	10 ⁷ drops/cm ³	5*10 ⁷ drops/cm ³	10 ⁸ drops/cm ³
Avg ϕ_{PZ}	100%	72%	43%	32%
Avg ϕ_{H_2O}	0%	0%	0%	0%

Greater amine volatility can also increase gas phase amine driving force and aerosol growth. Figure 2.12 compares aerosol growth with amine volatility set at 10 and 0.1 times PZ volatility, suggesting that greater amine volatility increases aerosol growth. Majeed also predicted that the aerosol size grows less with lower amine volatility (Majeed et al.,

2017b). A solvent with moderate volatility, like PZ, will produce aerosol that grows to larger size and is easier to collect. Solvents with very high volatility should be avoided as they emit high gas phase amine. Solvents with low volatility should also be avoided as they produce aerosol that is hard to collect.

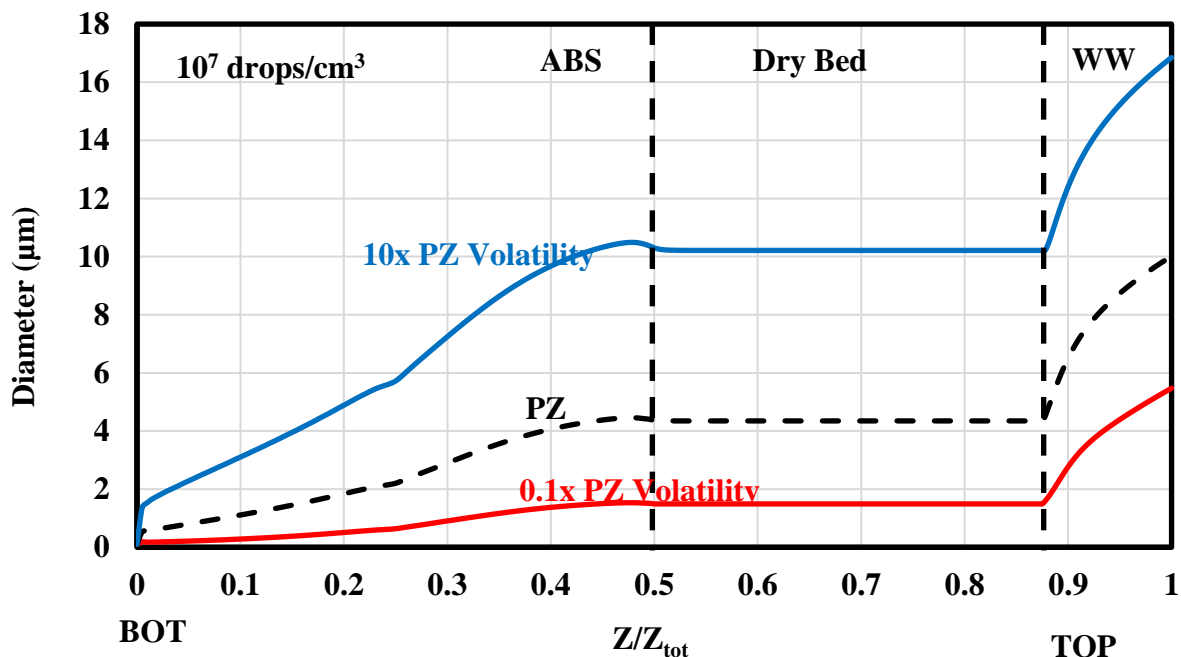


Figure 2.12: Aerosol growth with different amine volatility at 10^7 drops/cm³ (40' absorber, 30' dry bed, 10' water wash, 0.22 lean loading, 0.36 rich loading, 90% CO₂ removal, water wash at 40 °C, lean solvent at 40 °C, intercooling at 40 °C). Greater amine volatility increases aerosol growth with the caveat about high gas phase amine emissions.

Aerosol grows faster at higher temperature. Lean solvent and water wash operating temperatures were increased from 40 °C to 60 °C. Figure 2.13 shows that higher absorber top temperature increases gas phase amine driving force, and thus increases aerosol growth. Lower solvent loading also gives higher gas phase free amine and helps aerosol grow. In the water wash, aerosol approaches equilibrium with water in the gas

phase. As a result, process configurations that provide greater water partial pressure in the water wash will help aerosol grow, such as water wash with a higher operating temperature and pre-humidified empty space. The dry bed and other empty spaces in the column can be humidified by a spray nozzle with water recycle.

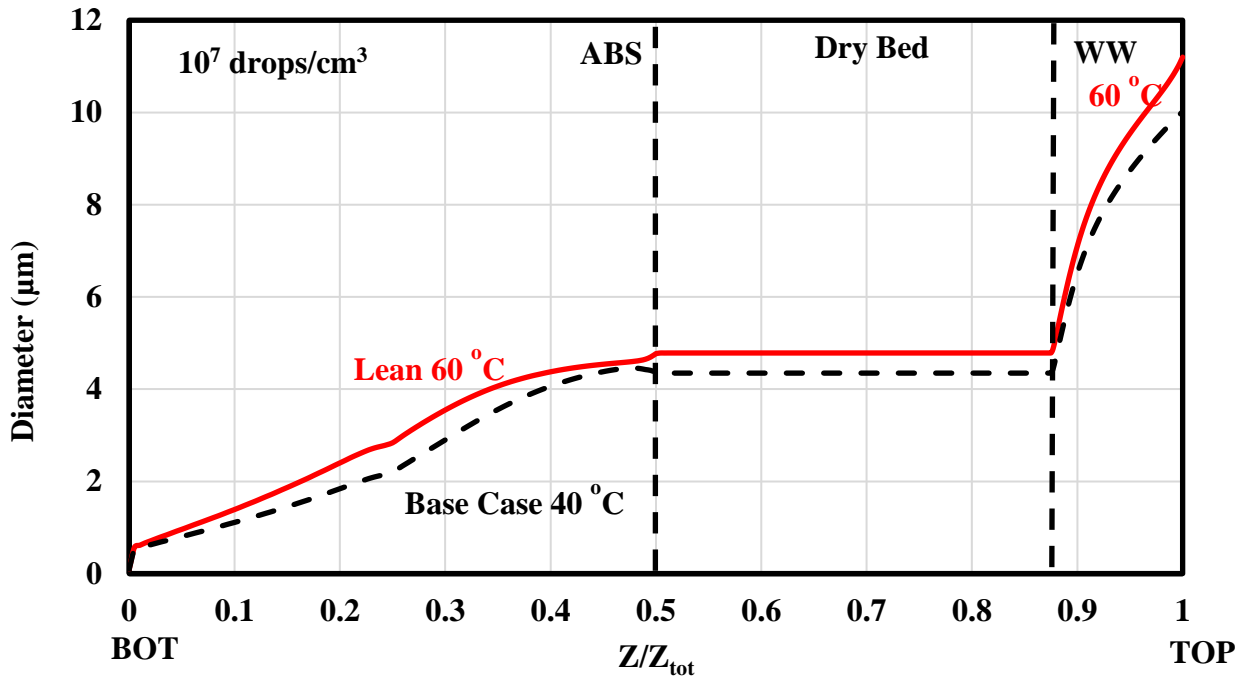


Figure 2.13: Aerosol growth along the column with greater absorber top temperature (10^7 drops/cm³, 40' absorber, 30' dry bed, 10' water wash, 0.22 lean loading, 90% CO₂ removal, lean solvent at 60 °C and water wash at 60 °C, intercooling at 40 °C). Greater absorber top temperature gives higher PZ driving force, resulting in faster aerosol growth.

2.4 CONCLUSIONS AND RECOMMENDATIONS FOR EMISSIONS CONTROL

Aerosol growth is a function of aerosol concentration. At high concentration, aerosol will not grow as much and therefore will be hard to collect. Aerosol is more likely to grow to the point where it can be collected (3 µm with common types of mist eliminators) with low aerosol concentration. For emissions control, removing all nuclei in the flue gas

is expensive and it is not necessary to eliminate all nuclei. The techniques that can reduce the nuclei count to the point where aerosol can grow enough to be collected are sufficient.

In the absorber, amine aerosol growth is driven by amine-limited diffusion. As aerosol concentration increases, aerosol growth decreases due to the depletion of the amine driving force in the gas phase, and the limiting driving force for aerosol growth shifts from gas-to-drop to liquid-to-gas.

Understanding aerosol growth mechanisms will help control emissions by selecting appropriate packing types, solvents, and operating conditions. Aerosol growth can be increased by enhancing the gas-film mass transfer coefficient of packing, e.g., selecting finer packing or operating the column with higher gas velocity, which will produce larger aerosol that is easier to capture.

Greater amine volatility increases aerosol growth. A solvent with moderate volatility, like PZ, will produce aerosol that grows to larger size and is easier to collect. Solvents with low volatility should be avoided as they produce aerosol that is hard to collect. Solvents with very high volatility should also be avoided as they emit high gas phase amine.

An absorber operated at higher temperature and lower solvent loading will increase gas phase amine pressure and driving force, which helps aerosol grow.

The effects of initial aerosol diameter and amine composition on aerosol growth are insignificant.

In the water wash, aerosol approaches equilibrium with water in the gas phase. Process configurations that provide greater water partial pressure in the water wash, such as higher operating temperature and pre-humidified empty space, will help aerosol grow.

2.5 ACKNOWLEDGEMENTS

Financial support was provided by the U.S. Department of Energy, Office of Fossil Energy through the CCSI² project (Carbon Capture Simulation for Industry Impact) (subcontract 318779 with Los Alamos National Laboratory). Aspen Plus[®] proprietary software was provided by an academic license from AspenTech[®]. AspenTech[®] and Aspen Plus[®] are trademarks of Aspen Technology, Inc. All rights reserved.

Chapter 3 : Modeling Absorber Performance at March 2015 UT-SRP Pilot Plant Campaign with 5 m PZ²

A CO₂ capture pilot plant with the advanced flash stripper was operated with aqueous piperazine (PZ) at The University of Texas Separations Research Program (UT-SRP) in March 2015. A wide range of absorber operating conditions (solvent concentration, lean loading, flue gas CO₂, gas rate, liquid-to-gas ratio) and intercooling configurations was tested in the pilot plant campaign.

The pilot plant measurements closed the material balance (+/- 2%) around the absorber. 5 m PZ was tested for the first time and outperformed 8 m PZ at comparable absorber conditions due to enhanced mass transfer rates in the absorber. Operating with 5 m PZ increased the number of transfer units (NTU) by ~20% for each of 3 tests even though 8 m PZ was operated with greater solvent capacity and greater driving force. Operation with full spray intercooling doubled the NTU compared to operation without spray or intercooling at identical absorber conditions.

The pilot plant data were used for further validation of the rigorous rate-based absorber model in Aspen Plus[®]. The pilot plant absorber model has been developed over several pilot plant campaigns, and a consistent method for absorber model validation and correction utilizing a rigorous data reconciliation method with the Independence PZ model was used to predict pilot plant performance for the March 2015 campaign. Pilot plant data suggested that interfacial area correction and CO₂ correction provided similar predictions of pilot plant absorber performance and could be used interchangeably to

²Part of this chapter has been published in Zhang, Y., Sachde, D., Chen, E., Rochelle, G., 2017. Modeling of absorber pilot plant performance for CO₂ capture with aqueous piperazine. *Int. J. Greenh. Gas Control* 64, 300–313. doi:10.1016/j.ijggc.2017.08.004. Chen managed the pilot plant and helped obtain the pilot plant absorber data. Sachde and Rochelle supervised this work and helped the analysis and interpretation of the data.

correct the model. The inhibitor correction to density-predicted loadings was consistent with model-predicted correction to titration data and might provide an explanation for pilot-model offsets. Pilot plant data also suggested a possible time dependence, and absorber NTU values were slightly over-predicted (mean ratio of model-predicted NTU to pilot plant-measured NTU = 1.08). A possible explanation is that several high CO₂ removal cases in the March 2015 campaign were outside the range where the previous model corrections were developed, where the controlling mass transfer resistance in the absorber differed. This observation provides an opportunity to investigate future model corrections at different column mass transfer limiting mechanisms. The column temperature profiles of different intercooling configurations were matched within 2% mean absolute percentage error.

3.1 INTRODUCTION

Amine scrubbing is a robust, energy-efficient, and flexible approach for post-combustion CO₂ capture (Rochelle, 2009; Rochelle et al., 2011). Aqueous piperazine (PZ) has been demonstrated as a new standard solvent for amine scrubbing technology (Chen et al., 2014; Freeman et al., 2010; Rochelle et al., 2011). Details of pilot plant results have been published with 30 wt % monoethanolamine (MEA) and 8 m (40 wt %) PZ (Kay et al., 2014; Knudsen et al., 2011; Rezazadeh et al., 2016; Sachde et al., 2013; Tait et al., 2016; von Harbou et al., 2014). With fast absorption rate, relatively wide solubility window, and good energy performance (Chen et al., 2014; Li, 2015; Rochelle et al., 2011), 5 m PZ (30 wt %) was tested for the first time in the March 2015 pilot plant campaign, while 8 m PZ was evaluated as base case. When operated with 5 m PZ at low

CO₂ loading, careful plant operation and shutdown procedures were followed to avoid solid precipitation.

The pilot plant at the University of Texas Separations Research Program (UT-SRP) has been operated as a carbon capture facility since 2002, and equipment has been upgraded in the intervening years to demonstrate novel configurations and solvents. In a previous simulation of novel capture processes, the advanced flash stripper with cold and warm rich solvent bypass was shown to have superior energy performance over other stripper configurations (Lin et al., 2016; Y. J. Lin and Rochelle, 2016), and was tested in the 21 runs of the March 2015 UT-SRP campaign to validate experimental and simulated results. Plant data revealed that 17 runs with optimized rich solvent bypass achieved process heat duties from 2.1–2.5 GJ/tonne CO₂, which demonstrated that using the advanced flash stripper would reduce the energy requirement by 25% compared with the two-stage flash stripper used in two previous UT-SRP campaigns (Chen et al., 2017; Lin et al., 2016).

Amine aerosol was also characterized in the March 2015 campaign. Aerosol was created by directly injecting either SO₂ gas or vaporized sulfuric acid into the UT-SRP synthetic flue gas, and FTIR and PDI measurements were used to observe amine aerosol growth and emission rates at different absorber operating conditions (Beaudry et al., 2016; Fulk, 2016).

The operating conditions and campaign-specific equipment specifications are summarized in Table 3.1 for five previous PZ campaigns and the March 2015 campaign. The previous UT-SRP campaigns evaluated pilot plant absorber performance with different column internals and intercooling configurations, but a parametric test of conditions relevant to absorber performance was not performed. The initial campaigns were designed as proof of concept for the solvent and equipment configurations. A consistent

method for absorber model validation and correction utilizing a rigorous data reconciliation method with the Independence PZ model was developed over a limited range of conditions by Plaza and Sachde (Plaza, 2011; Sachde et al., 2013). During the first three campaigns, pilot plant data collection and the PZ and absorber model were improved and developed by Plaza (Plaza, 2011). Sachde utilized the October 2011 and November 2013 campaigns to develop a consistent method for absorber model validation and correction by utilizing a rigorous data reconciliation method (Sachde et al., 2013). The rate-based absorber model was simulated by the Independence PZ model developed in Aspen Plus® RateSep™ with a rigorous e-NRTL thermodynamic framework and rigorous kinetics with reactions in the boundary layer (Frailie, 2014). To evaluate the absorber performance within a wider range of operating conditions, the March 2015 campaign systematically varied PZ concentration, CO₂ flue gas concentration, gas rate, lean loading (LLDG), solvent to gas ratio (L/G), and intercooling methods. This paper mainly focuses on pilot plant absorber performance over a wide range of operating conditions with aqueous PZ, and evaluation of the model correction method developed in the previous two campaigns (October 2011 and November 2013) using the absorber data from the March 2015 campaign.

Table 3.1: Previous piperazine pilot plant absorber specifications.

	Nov-08	Sep-10	Dec-10	Oct-11	Nov-13	Mar-15
Solvent	5 - 9 m PZ	8 m PZ	8 m PZ	8 m PZ	3.6 - 3.8 m PZ	5, 8 m PZ
Packing Type & Specific Area(m²/m³)	Structured 205X	Hybrid 250	Hybrid 250	Structured 350Z	Hybrid 250	Hybrid 250
Gas Rate (ACFM)	350	250 - 750	350 - 650	350 - 675	350	350 - 500
Gas Rate (kg/hr)	710	500 - 1550	720 - 1350	710 - 1400	710	710 - 1050
Liquid Rate (GPM)	12 - 18	8 - 26	8 - 26	11 - 22	12	7 - 14
Liquid Rate (kg/hr)	3000 - 4500	2000 - 6500	2000 - 6500	2700 - 5500	3000	1720 - 3540
Intercooling	No	Yes/No	Yes	Yes (with Spray)	Yes (with Spray)/No	Yes (with Spray)/No

3.2 MARCH 2015 PILOT PLANT CAMPAIGN OVERVIEW

Figure 3.1 shows a simplified process flow diagram of the March 2015 UT-SRP pilot plant configuration (Lin et al., 2016; Seibert et al., 2011). The synthetic flue gas was achieved by mixing dry air, pure stripper overhead CO₂ recycle, and pure make-up CO₂. CO₂ was adjusted by varying the pure make-up CO₂. The pilot plant absorber had 2 3.05 m sections of Raschig Super-Pak (RSP-250) structured packing. Solvent intercooling with a spray nozzle return was applied between the packed beds. A chiller and knockout drum were used to remove amine from the absorber outlet gas. The rich solvent was preheated by two exchangers and a steam heater, and fed into the flash tank for solvent regeneration. The pilot plant stripper had 2 meters of Raschig Super-Ring No. 0.3 (RSR no. 0.3) random packing. The lean solvent was fed back to the absorber after two exchangers and a trim cooler.

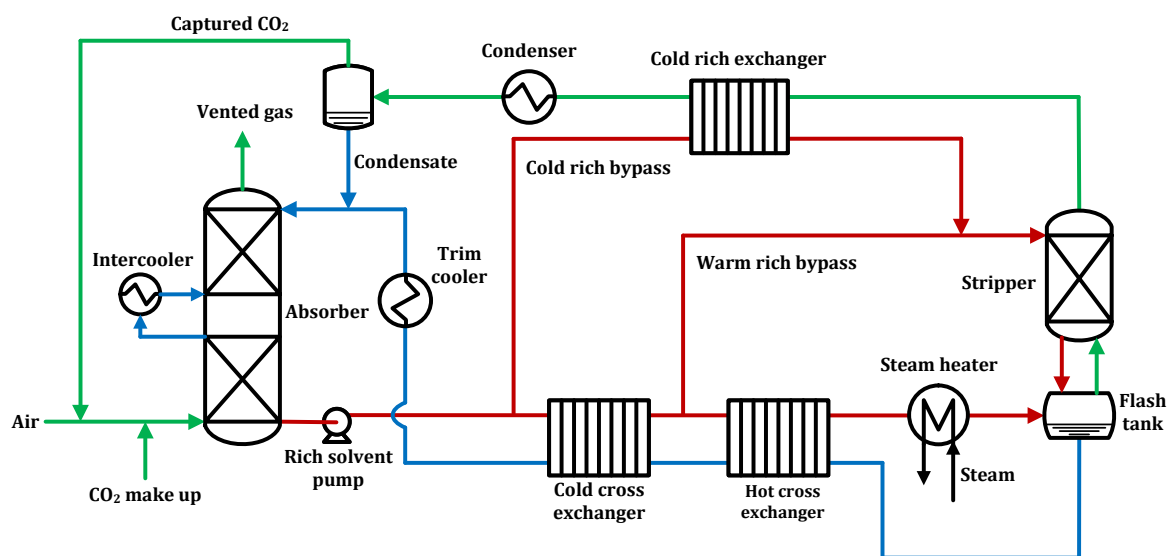


Figure 3.1: Pilot plant absorber configuration in March 2015 (Lin et al., 2016).

Table 3.2 summarizes operating conditions and select equipment design choices implemented for the absorber during the pilot plant campaign. The March 2015 campaign was designed as a parametric test of system performance at a wide range of operating conditions, which allowed for further validation of the absorber and solvent models. Details of the individual runs and parameters will be discussed with the performance results from the campaign.

Table 3.2: Summary of pilot plant operating conditions.

Equipment Specifications		
Column	<i>Inner Diameter (m)</i>	0.43
Packing	<i>Height (m)</i>	6.1 (2 beds x 3.05)
	<i>Specific Area (m²/m³)</i>	250
	<i>Corrugation Angle (°)</i>	Hybrid Packing
	<i>Material</i>	Stainless
Operating Specifications		
Solvent (PZ)	<i>Concentration (m)</i>	5 , 8
	<i>Liquid Rate (gpm)</i>	7 - 14
	<i>Liquid Rate (kg/hr)</i>	1720 - 3540
	<i>Lean Loading (mol CO₂/mol alkalinity)</i>	0.18 - 0.26
Feed Gas	<i>CO₂ (mol %)</i>	6 , 12
	<i>H₂O (mol %)</i>	1 - 2
	<i>T (°C)</i>	30
	<i>Gas Rate (acfm)</i>	350 - 500
	<i>Gas Rate (kg/hr)</i>	710 - 1050

3.3 MATERIAL BALANCE CLOSURE

CO₂ material balance around the absorber requires measurements of gas and liquid flow and CO₂ concentration. Figure 3.2 and Table 3.3 summarize measurement locations and methods used during the campaign.

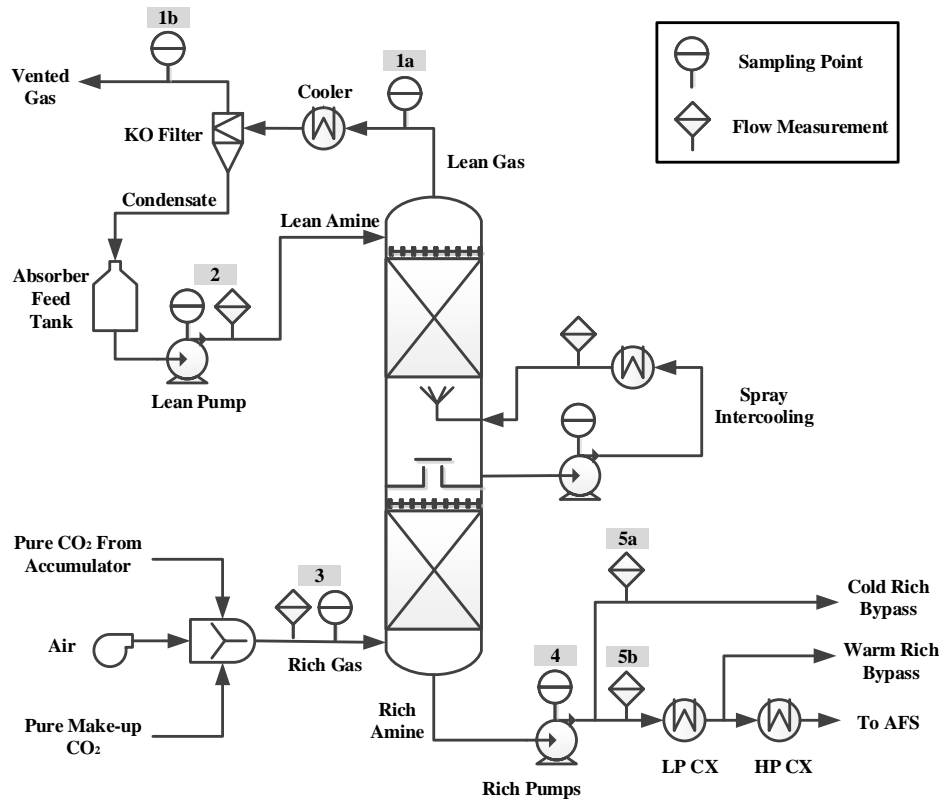


Figure 3.2: Simplified absorber PFD with indications for sampling and measurement points used in the mass balance in this paper. Points 1 through 5 are summarized with corresponding descriptions in Table 3.3.

Table 3.3: Flow and analytical measurements available for absorber mass balance.

Stream and ID	CO ₂		PZ	
	Flow/Density	Analytical	Flow	Analytical
<u>Lean Amine</u> (Point 2 in Figure 3.2)	Micro Motion [®] Coriolis Flow Meters	Manual Titration /TIC	Micro Motion [®] Coriolis Flow Meters	Manual Titration
<u>Rich Amine</u> (Points 4, 5a, and 5b in Figure 3.2)	Micro Motion [®] Coriolis Flow Meter	Manual Titration /TIC	Micro Motion [®] Coriolis Flow Meter	N/A
<u>Lean Gas</u> (Points 1a and 1b in Figure 3.2)	Rosemount [®] Annubar (Differential Pressure) Meter	Vaisala [®] GMT220 CO ₂ Sensor (NDIR Sensor, 1b) & FTIR Sampling (1a & 1b)	N/A	N/A
<u>Rich Gas</u> (Point 3 in Figure 3.2)	Inferred from Inlet	Vaisala [®] GMT220 CO ₂ Sensor (NDIR Sensor) & FTIR Sampling	N/A	N/A

Two methods were evaluated for liquid-side CO₂ concentration. The first approach averaged data from pilot plant titrations conducted during the campaign and total inorganic carbon (TIC) analysis performed in the laboratory after the campaign. The second approach used a modified density correlation to predict loading, which includes an original density correlation developed by Freeman (Equation 3.1) and an additional correction for the presence of a thermally stable free-radical scavenger inhibitor A in the solvent (Equation 3.2) (Freeman, 2011). Water density calculation is based on Tilton (Equation 3.3) (Tilton and Taylor, 1937). The inhibitor has shown promise as an oxidation inhibitor in previous bench-scale oxidation experiments and pilot plant

campaigns (Nielsen et al., 2013; Voice, 2013), and was also used in the March 2015 campaign. The density of the solvent was measured online in the pilot plant. The CO₂ and PZ concentrations were measured by titration. The Inhibitor A concentration used in March 2015 was 1 wt % and 1.3 wt % respectively for 5 m PZ and 8 m PZ, which was measured after the campaign.

$$\rho_{PZ} = \rho_{H_2O} \cdot (0.0407 \cdot C_{CO_2} + 0.008 \cdot C_{PZ} + 0.991) \quad (3.1)$$

$$\frac{\rho_{Pilot}}{\rho_{PZ}} = \frac{\rho_{InhA}}{\rho_{H_2O}} = 0.00741 * Inhibitor(wt\%) + 1.0018 \quad (3.2)$$

$$\rho_{H_2O} = 1000 * \left[1 - \frac{(T-3.9863)^2 * (T+288.9414)}{508929.2 * (T+68.12963)} \right] \quad (3.3)$$

where:

ρ = Liquid density (kg/m³);

ρ_{H_2O} = Water density calculated from Tilton-Taylor formula (kg/m³);

C_{CO_2} = CO₂ concentration in the solution (mol/kg);

C_{PZ} = PZ concentration (mol/kg);

T = Temperature (°C).

The change in loadings (rich - lean) was consistent between the two methods so either approach is suitable for mass balance closure. However, Table 3.4 indicates that the density-predicted loadings exhibit a systematic offset of approximately 7% from the measured titration data.

Table 3.4: Titration-measured LLDGs and density-predicted LLDGs.

Run	Titration LLDG (mol CO ₂ /mol alk)	Density-predicted LLDG (mol CO ₂ /mol alk)	Density-predicted LLDG/ Titration LLDG
1	0.215	0.230	1.07
2	0.217	0.231	1.06
3	0.221	0.233	1.06
4	0.216	0.233	1.08
5	0.214	0.229	1.07
6	0.255	0.272	1.07
7	0.246	0.260	1.06
8	0.236	0.254	1.08
9	0.235	0.252	1.07
10	0.204	0.219	1.07
11	0.201	0.215	1.07
12	0.237	0.255	1.08
13	0.243	0.253	1.04
14	0.241	0.254	1.05
15	0.242	0.254	1.05
16	0.231	0.247	1.07
17	0.200	0.213	1.06
18	0.200	0.222	1.11
19	0.235	0.251	1.07
20	0.184	0.199	1.08
21	0.235	0.257	1.09
Average Ratio			1.07

The 7% offset is consistent with corrections required to titration measurements in previous campaigns to reconcile pilot plant measured absorber performance with model-predicted performance (Sachde et al., 2013). Further investigation of analytical methods is required to understand the source of the offset, but the density-predicted loadings will be discussed in the subsequent modeling section.

Gas-side CO₂ concentrations could be derived from 3 methods:

- NDIR continuous inline CO₂ measurements;
- FTIR discrete sampling;

- CO₂ flow rate calculation from recycle CO₂ and CO₂ make-up rate. At steady state, the CO₂ flow rate in the absorber outlet gas stream should be equal to the pure make-up CO₂ flow rate – referred to as material balance method.

The inlet and outlet CO₂ are compared and summarized in Figure 3.3 and Figure 3.4.

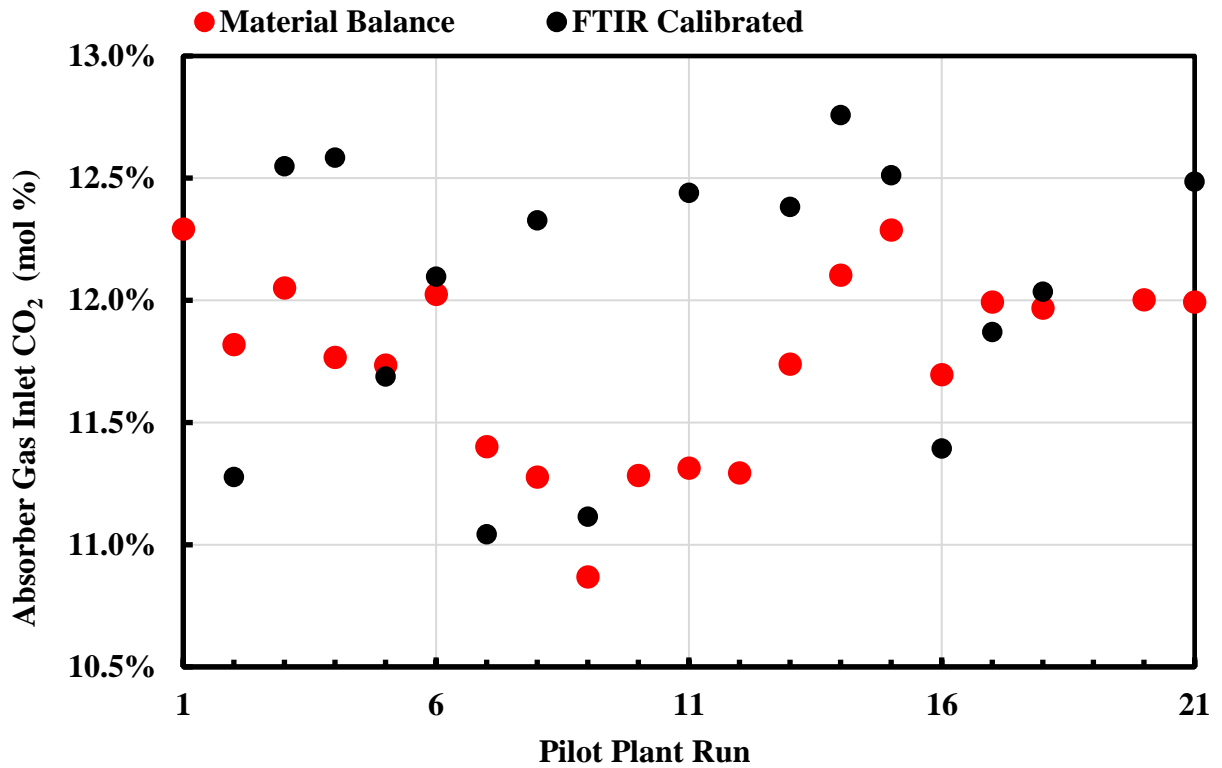


Figure 3.3: Pilot plant inlet CO₂ measurements (Point 3 in Figure 3.2). NDIR measurements not depicted due to large offset from other measurements.

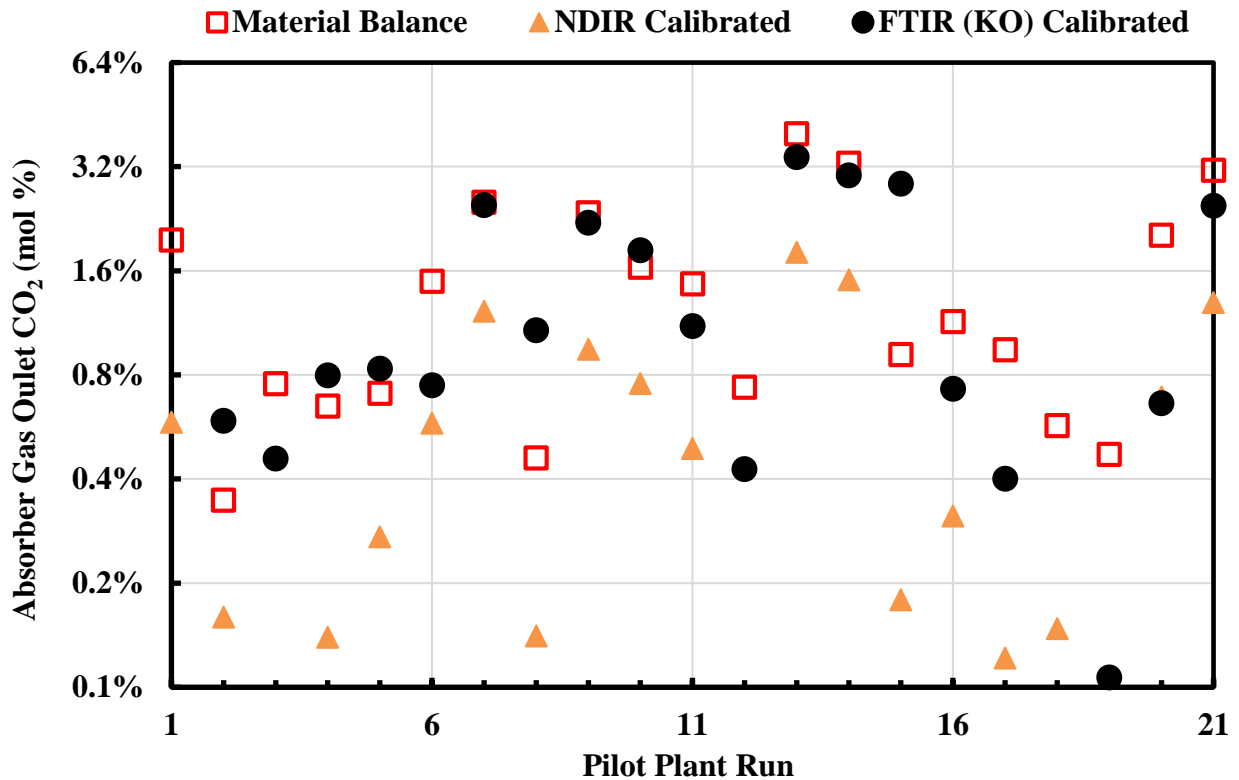


Figure 3.4: Pilot plant outlet CO₂ measurements. FTIR (KO), NDIR located at Point 1b in Figure 3.2. Material balance from CO₂ make-up (CO₂ from bulk in Figure 3.2).

The gas-side data shows some scatter between methods, but the FTIR and material balance methods appeared to be internally consistent, while the NDIR measurements exhibited an offset from the other methods. To determine which gas phase measurements to use in analysis, each measurement method was used in an overall CO₂ material balance around the absorber. A combination of FTIR and material balance measurements was ultimately determined to provide the best mass balance closure with the liquid-side data in the pilot plant. Figure 3.5 summarizes the material balance closure with the final pilot plant data set.

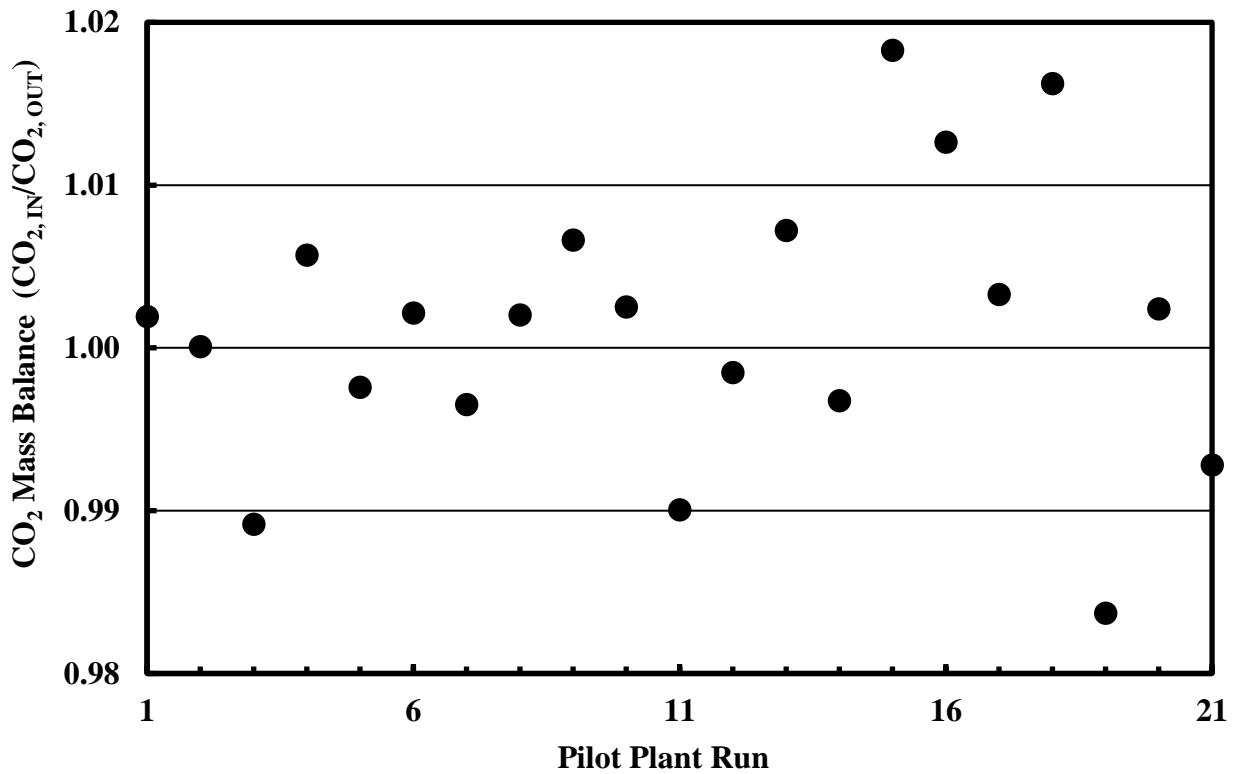


Figure 3.5: CO₂ Material balance around the absorber. Density-predicted loading and FTIR/CO₂ flow data used for liquid and gas composition, respectively.

3.4 PERFORMANCE RESULTS

Table 3.5 provides detailed operating conditions by run and corresponding rich loading (RLDG), CO₂ removal, and number of transfer units (NTU) achieved as calculated from measurements used in the preceding material balance analysis. Equation 3.4 defines NTU.

$$NTU = -\ln(100\% - CO_2 \text{ Removal}\%) \quad (3.4)$$

Table 3.5: Summary of pilot plant absorber performance results for March 2015 Campaign. Parametric testing of absorber operating or equipment conditions is outlined in the table.

Run	Solvent Rate	Gas Rate	PZ	LLDG	Rich Gas	RLDG	Intercooling	Spray	CO ₂ Removal (%)	NTU
	gpm	acfm	m	mol CO ₂ /mol alk.	mol %	mol CO ₂ /mol alk.	Y/N	Y/N	FTIR/ CO ₂ Flow Rates	
1	9.3	350	5	0.215	12.0	0.388	Y	Y	85.7	1.94
2	10.2	350	5	0.217	11.9	0.381	Y	Y	97.4	3.65
3	10.2	350	5	0.221	12.0	0.395	Y	Y	94.5	2.90
4	10.2	350	5	0.216	12.0	0.387	Y	N	94.2	2.85
5	10.2	350	5	0.214	12.0	0.381	Y	N	93.7	2.76
6	12	350	5	0.255	12.1	0.381	Y	Y	88.9	2.20
7	14	350	5	0.244	12.0	0.331	N	N	79.6	1.59
8	14	350	5	0.238	12.0	0.352	Y	Y	96.4	3.32
9	14	500	5	0.235	12.0	0.361	Y	Y	82.1	1.72
10	14	500	5	0.203	12.0	0.360	Y	Y	86.7	2.02
11	9.3	350	5	0.201	12.0	0.365	Y	Y	91.5	2.47
12	14	350	5	0.238	12.0	0.352	Y	Y	94.1	2.83
13	14	500	8	0.242	11.6	0.333	N	Y	68.6	1.16
14	14	500	8	0.236	12.0	0.342	Y	Y	75.2	1.39
15	14	350	8	0.239	11.9	0.328	Y	Y	93.4	2.72
16	10.2	350	8	0.225	12.0	0.344	Y	Y	91.2	2.43
17	10.2	350	5	0.197	11.9	0.360	Y	Y	93.0	2.66
18	10.2	350	5		11.9		Y	Y	95.6	3.12
19	7	350	5	0.232	6.0	0.351	Y	Y	92.1	2.54
20	8.6	350	5	0.183	12.0	0.358	N	N	84.6	1.87
21	10.2	350	5	0.234	12.0	0.372	Y	Y	76.2	1.44

3.4.1 Absorber Intercooling

Cases outlined in bold in Table 3.5 represent runs where the different intercooling configurations in the pilot plant were evaluated at constant operating conditions to isolate

the effects of intercooling methods. Intercooling evaluation was not the primary objective of the current campaign as several previous experiments demonstrated performance improvement due to intercooling and mass transfer enhancement via the spray nozzle in the intercooling loop (Sachde et al., 2013). However, the parametric testing of intercooling yielded further insight into the spray intercooling method employed in the pilot plant:

- Test 1 (Runs 7 and 8): Intercooling with spray vs. no intercooling and no spray to evaluate the full benefit of the pilot plant intercooling system.

Results: Intercooling with spray = 96% CO₂ removal (~3.3 NTU); no intercooling, no spray = 80% CO₂ removal (~1.6 NTU).

- Test 2 (Runs 13 and 14): Intercooling with spray vs. no intercooling with spray to separate the benefit of cooling the solvent from the enhanced mass transfer of the spray.

Results: Intercooling with spray = 75% CO₂ removal (~1.4 NTU); no intercooling with spray = 69% CO₂ removal (1.2 NTU).

In addition, Run 20 evaluated the concept of operating an absorber at “over-stripped” conditions without any intercooling. Previous modeling work indicated that intercooling was not required to achieve maximum solvent capacity if the solvent was operated at a sufficiently low LLDG (Sachde and Rochelle, 2014). Concerns regarding solid solubility at lean conditions limited the operating LLDG in the pilot plant and likely led to some capacity constraint (i.e., not sufficiently lean). However, approximately 85% CO₂ removal was achieved with a low solvent circulation rate and Lin’s evaluation of stripper energy performance in Figure 3.6 indicated that it was not substantially worse than

other runs in the campaign (Lin et al., 2016). Further investigation of the lean operating conditions may be warranted.

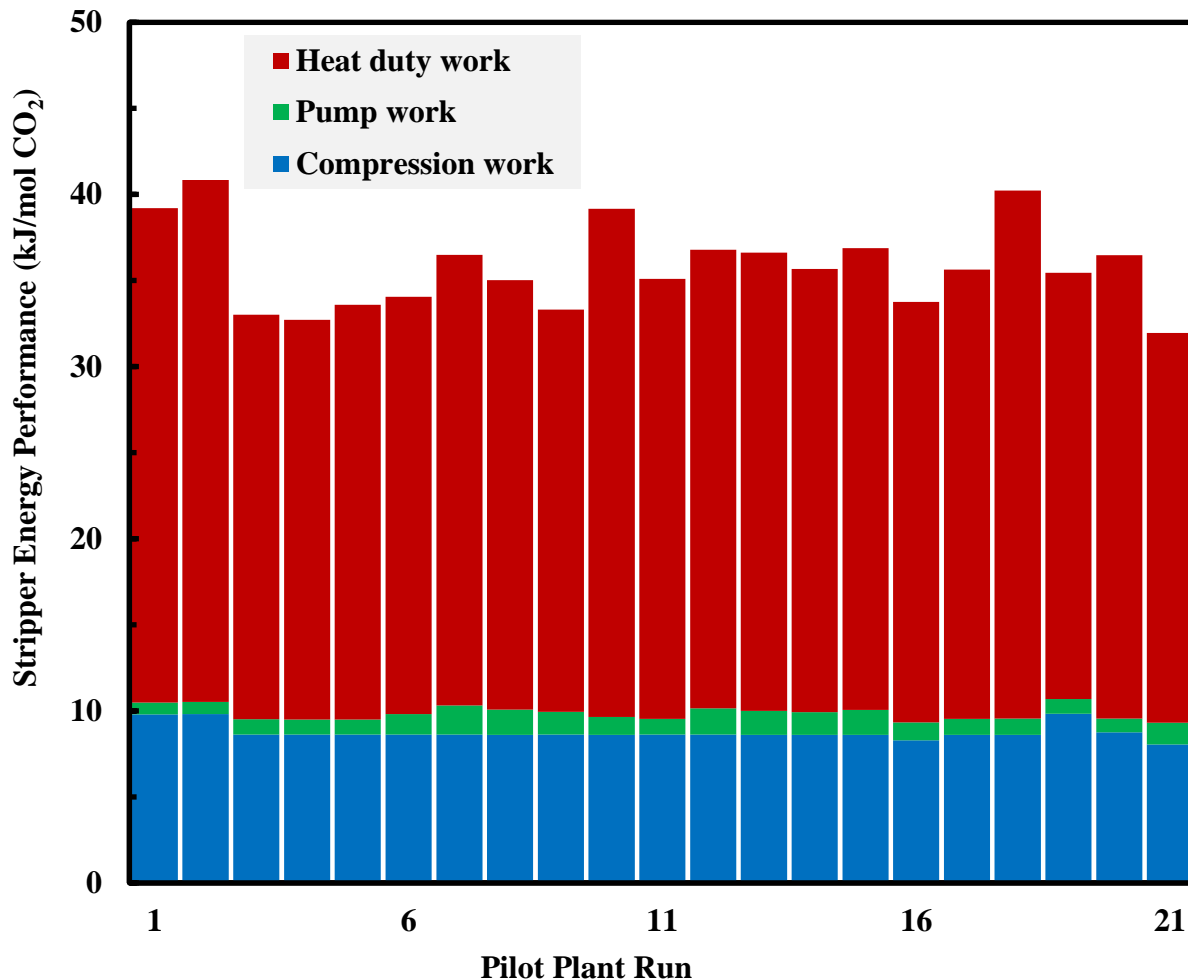


Figure 3.6: Stripper energy performance analysis for March 2015 pilot plant campaign (Lin et al., 2016).

3.4.2 Absorber Performance: 5 m vs. 8 m PZ

4 of the 21 runs of the pilot plant campaign used 8 m PZ rather than 5 m PZ. Table 3.6 compares 3 runs with 8 m PZ to runs with 5 m PZ at practically identical solvent rate, gas rate, and lean loading.

Table 3.6: Effect of solvent concentration on absorber performance – results of parametric testing at pilot plant. All cases with intercooling with spray.

Test	Run	PZ (m)	Solvent Rate (gpm)	Gas Rate (acfm)	LLDG (mol CO ₂ /mol alk.)	P*CO ₂ @ 40 °C	RLDG (mol CO ₂ /mol alk.)	CO ₂ Removal (%)	NTU
1	9	5	14	500	0.235	107	0.347	80	1.72
	14	8			0.236	85	0.329	75	1.39
2	8	5	14	350	0.238	114	0.340	96	3.32
	15	8			0.239	91	0.320	93	2.72
3	3	5	10.2	350	0.221	83	0.374	94	2.90
	16	8			0.225	68	0.333	91	2.43

The volumetric solvent rates were constant for each test, corresponding to a comparatively larger mass flow rate for 8 m PZ in each case. When coupled with the inherently larger solvent capacity of 8 m PZ and the lower equilibrium partial pressure of CO₂ for 8 m PZ in each test, 8 m PZ would be expected to outperform 5 m PZ based on solvent capacity/driving forces available for mass transfer. However, in all tests, 5 m PZ outperformed 8 m PZ despite the favorable operating conditions for 8 m PZ. The enhanced performance is evident in the higher capture rate achieved by 5 m PZ in each test. Additionally, capturing more CO₂ at the same solvent rate results in significantly higher RLDG for 5 m PZ – this corresponds to improved energy performance in the stripping section (reduced H₂O loss and compression work per mole of CO₂ captured) regardless of the specific stripper design and before accounting for potential benefits of reduced viscosity in the heat exchange process. The improved absorber performance can be attributed to enhanced absorption rates due to the lower solvent viscosity (enhanced diffusion and turbulence). The pilot plant results provide preliminary validation of previous modeling work that predicted significant enhancement of mass transfer performance in absorbers when using 5 m PZ.

3.5 MODEL DETAILS

A data reconciliation method and absorber model correction were developed from previous campaign data (October 2011 and November 2013). The reconciliation method is discussed in detail in previous work (Sachde et al., 2013) and will not be reviewed here; instead the results of previous reconciliation approach will be used to predict the performance of the pilot plant in the March 2015 campaign.

3.5.1 Modeling Methods

The process model used in this work was developed in Aspen Plus[®] and is comprised of a solvent model (thermodynamics, kinetics, and physical properties) and rigorous unit operation models for the absorber and stripper.

The PZ solvent model (“Independence” model) was developed by Frailie (2014). The thermodynamic framework represents experimental amine pK_a, CO₂ solubility, heat capacity, speciation, and amine volatility data for the PZ-H₂O-CO₂ system by regression of Gibbs free energy, enthalpy, heat capacity and activity coefficient parameters within the electrolyte non-random two liquid (e-NRTL) framework. Rate expressions for kinetic reactions and diffusion coefficients were regressed from wetted wall column data collected over a range of temperature, solvent concentration, and loading relevant for capture applications considered in this work. Finally, physical property models (e.g., viscosity and density) were regressed as a function of amine concentration, loading, and temperature.

The absorber was modeled rigorously with the Aspen Plus[®] RateSep[™] unit operation, which solves multi-component mass transfer with chemical reaction coupled with heat transfer. The rate-based column requires detailed information on packing mass transfer performance represented by transport sub-models. Separate models for interfacial area (Tsai, 2010) and gas- and liquid-side physical mass transfer coefficients

(Wang, 2015) were developed from data collected at the Separations Research Program (SRP) pilot scale air-water column for a variety of packing types.

3.5.2 Spray Nozzle Impact

Spray intercooling was applied between the packed beds of the absorber. The solvent was pumped out of the column from a chimney tray between the two beds, cooled to approximately 40 °C by an intercooling exchanger, and returned to the column through a spray nozzle which is oriented to spray the solvent upwards into the underside of the top packed section. The spray nozzle generated mass transfer area via pressure drop across the nozzle (breaks the solvent into small drops). Additional interfacial area was developed when liquid drops impact the packing and column internals.

The spray section was modeled as an additional section of well-mixed packing with a pump-around in Aspen Plus[®]. The mass transfer area of the spray was calculated as an equivalent area of packing required to generate the mass transfer enhancement of the spray. A correlation for the mass transfer area generated by the spray nozzle as a function of the solvent rate (proxy for kinetic energy) was developed based on the data reconciliation of the October 2011 campaign (Sachde et al., 2013): the baseline model was first corrected without a spray nozzle for systematic bias, and a full data reconciliation was performed with the adjustable area of the spray nozzle. The results of the spray nozzle equivalent interfacial area correlation are reproduced in Figure 3.7 (Sachde et al., 2013).

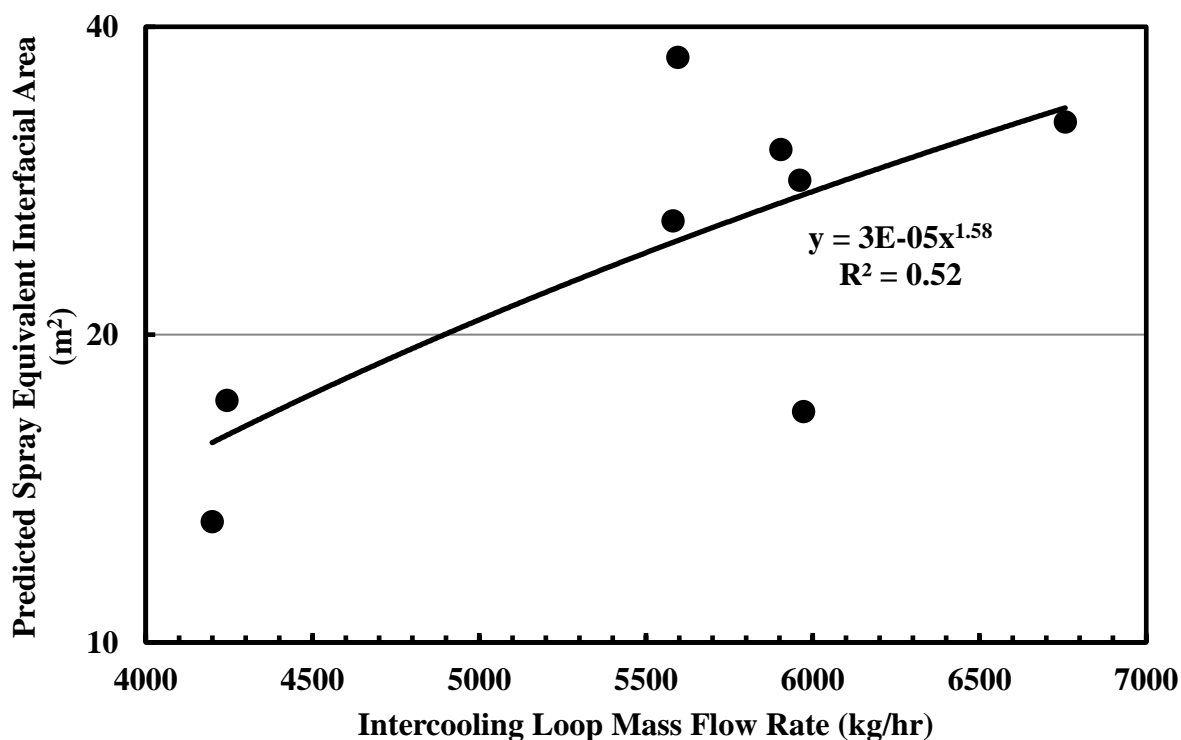


Figure 3.7: Spray nozzle equivalent interfacial area model used in March 2015 pilot plant campaign analysis (Sachde et al., 2013).

3.5.3 Model Correction

The data reconciliation for the October 2011 pilot plant campaign resulted in four independent global corrections to match the pilot plant measured results: interfacial area correction, liquid side mass transfer coefficient correction, CO₂ correction, and PZ correction, shown in Table 3.7 (Sachde et al., 2013). Only one of the four global corrections could be applied to the model, and they provide consistent model prediction. The data reconciliation was performed using Aspen Plus[®] Data-fit tool to minimize the objective function described by Equation 3.5 to perform a maximum likelihood estimation on the pilot plant data.

$$Obj = \text{Min}_{\emptyset, Input} \sum_{i=1}^N \left(\frac{X_{measured,i} - X_{reconciled,i}}{\sigma_{Measured,i}} \right)^2 \quad (3.5)$$

where:

$X_{measured,i}$ = Measured value input or result parameter;

$X_{reconciled,i}$ = Reconciled value of input or result parameter;

$\sigma_{Measured,i}$ = Variance of measured values from plant or experiment;

\emptyset = Adjustable or varied parameters;

$Input$ = Reconciled input parameters.

Table 3.7: Independent global parameter sensitivity analysis with 95% confidence intervals for 2011 October pilot plant campaign (Sachde et al., 2013).

Parameter	Correction Factor	Upper 95%	Lower 95%
Interfacial Area	0.74	0.79	0.68
Liquid Side Mass Transfer Coefficient (k_L)	0.65	0.71	0.59
CO ₂ Correction	1.075	1.1	1.05
PZ Correction	0.93	0.95	0.91

The same data reconciliation approach was applied to the November 2013 campaign which utilized a different range of operating conditions than the October 2011 campaign (Sachde et al., 2013). The resulting model corrections are compared to the corrections for the October 2011 campaign in Table 3.8.

Table 3.8: Model corrections required for November 2013 and October 2011 PZ pilot plant campaigns.

Parameter	Correction Factor: November 2013	Correction Factor: October 2011
CO ₂ Correction	1.073 ± 0.013	1.075 ± 0.011
Interfacial Area	0.61 ± 0.01	0.74 ± 0.03
Interfacial Area (Adjusted)**	0.74 ± 0.01	0.74 ± 0.03

** The adjustment to the area adjustment is required because the different packing types used in each campaign have different fractional or wetted areas available for mass transfer as predicted by the interfacial area model used. The adjustment normalizes the packing types to operate with the same fractional wetted area available for mass transfer when operated at the same conditions. The result of the normalization is that both campaigns require an identical reduction (percentage or relative basis) in packing area to match the CO₂ transfer rates measured in the pilot plant.

The results indicate that a 7.3% increase in the lean CO₂ concentration (or LLDG) will result in the best fit of the model to the pilot data. Alternatively, a 39% reduction in mass transfer area available would yield a similar fit of model to pilot data. The CO₂ correction for November 2013 is nearly identical to the October 2011 correction. This indicates that a systematic bias exists between the model and the pilot plant and that the bias appears to be independent of operating conditions and equipment specifications such as packing. This is further corroborated when the interfacial area adjustments are compared. The adjustment applied in the November 2013 campaign (when corrected to account for a higher mass transfer area generated per unit of packing area with the hybrid 250 series packing compared to the structured 350 series packing used in the October 2011 campaign) is also identical to the correction required in the October 2011 campaign. This result seems to reduce the likelihood that factors such as gas and liquid distribution, which would vary with the different gas and liquid rates and type of packing used in each

campaign, are responsible for the model-to-pilot-plant discrepancy. A discrepancy such as bias in loading measurements could remain consistent regardless of operating and equipment conditions in the plant and have similar impacts on the model deviation.

In this work, both interfacial area correction and CO₂ correction have been applied independently to the model. In the first method, interfacial area correction (interfacial area factor = 0.612) was applied to the model; average TIC and titration-measured LLDG was used for Runs 1 through 6, and titration-measured LLDG was used for Runs 7 through 21. The second method used density-predicted LLDG for all runs (Equation 3.1). As shown in Table 3.4, the density-predicted LLDG results in an increase of 7% in CO₂ content compared to the titration-measured loadings. This deviation is consistent with 1.075 CO₂ correction in the two previous pilot plant campaigns and thus the density-predicted loadings were used in lieu of correction titration data.

3.6 MODEL VALIDATION

Foaming in the pilot plant absorber was observed in Run 4 during the campaign and was omitted from the modeling analysis. All other runs were modeled in Aspen Plus[®] using the interfacial area correction and the CO₂ correction. Model corrections were applied proactively to predict performance in contrast to the data reconciliation in previous campaigns. Model predictions of absorber outlet CO₂ and column temperature profiles were compared with the pilot plant measurements in the model validation section.

3.6.1 Model-predicted Absorber Outlet CO₂

Table 3.9, Figure 3.8, and Figure 3.9 show the model-predicted NTU using both methods as well as the pilot plant-measured NTU for each run in the March 2015 campaign.

Table 3.9: Model-predicted NTU and pilot plant-measured NTU in the March 2015 campaign.

Run	NTU Predicted by Interfacial Area Correction	NTU Predicted by CO₂ Correction	Measured NTU
1	1.8	1.6	1.9
2	2.9	2.4	3.7
3	2.8	2.4	2.9
4	-	-	-
5	2.3	2.1	2.8
6	2.3	1.8	2.2
7	1.4	1.2	1.6
8	4.1	4.0	3.3
9	2.0	1.7	1.7
10	2.5	2.3	2.0
11	2.7	2.3	2.5
12	4.5	4.6	3.2
13	1.2	1.3	1.3
14	2.1	2.1	1.5
15	4.2	4.5	3.1
16	3.6	4.0	2.9
17	4.5	4.8	3.5
18	-	3.3	3.2
19	3.3	3.0	2.6
20	1.9	1.9	1.9
21	1.9	1.4	1.4

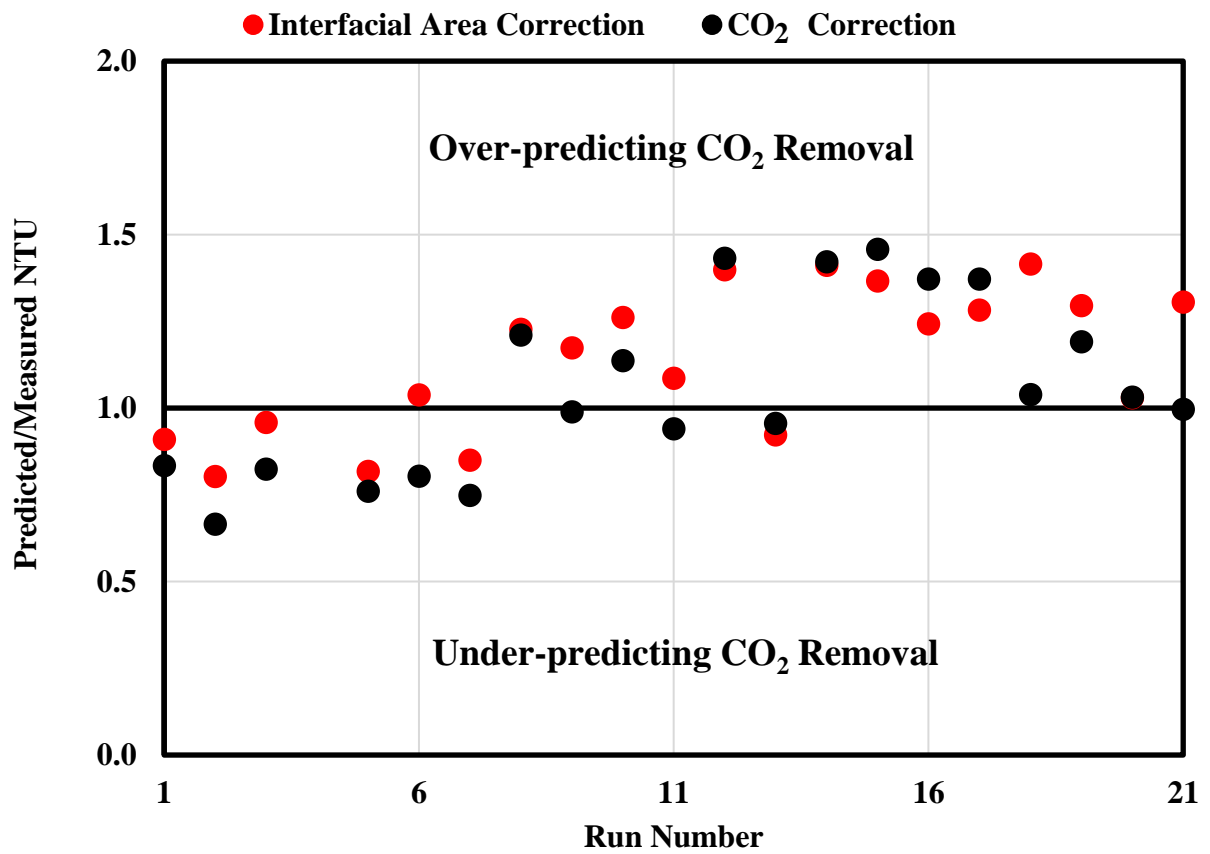


Figure 3.8: Ratio of model-predicted NTU to pilot plant-measured NTU for each run by applying interfacial area correction and CO₂ correction (no data for Run 4).

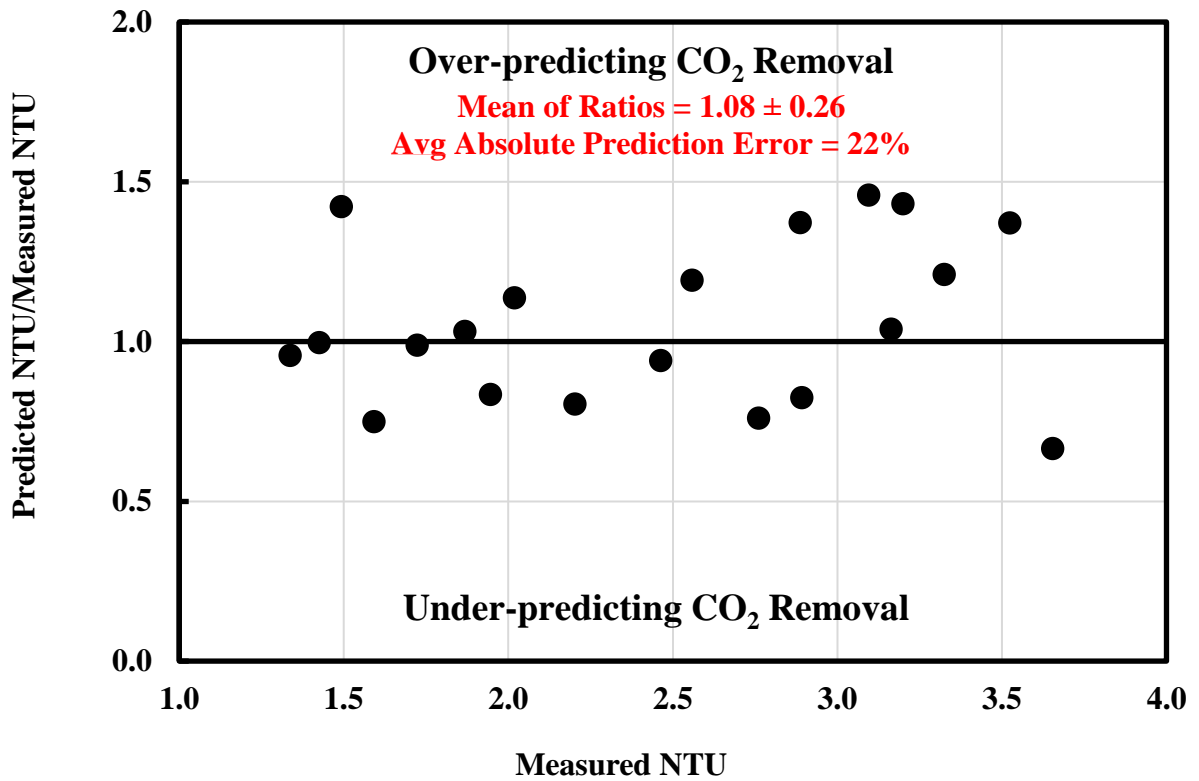


Figure 3.9: Ratio of model-predicted NTU to pilot plant-measured NTU by applying CO₂ correction.

Figure 3.8 shows the ratio of model-predicted NTU to pilot plant-measured NTU as a function of run numbers. For most of the runs, interfacial area correction and CO₂ correction provide consistent prediction. Figure 3.8 also suggests a possible time dependence in the pilot plant data. Figure 3.9 shows the NTU ratio as a function of measured NTU by applying CO₂ correction without a systematic bias. Both figures show that the model is able to match the NTU within a factor of 1.5, and the model is slightly over-predicting NTU (mean NTU ratio = 1.08). A possible explanation is that several high CO₂ removal cases in the March 2015 campaign were outside the region where the

previous model corrections were developed or the previous pilot plant campaigns were operated, and the absorber has different controlling mass transfer resistance at different operating conditions. Liquid-film diffusion resistance increases from the lean to rich end of the column, thus the liquid-film mass transfer coefficient model is critical in a wide range of removal cases (Sachde, 2016). This observation provides an opportunity to investigate future model corrections using different column mass transfer limiting mechanisms. Nevertheless, analytical measurements near detection limits might also result in possible model uncertainty and systematic deviations.

3.6.2 Model-predicted Absorber Temperature Profiles

Twelve temperature transmitters (RTD 40710, RTD 4079, RTD 407W, RTD 4076W, RTD 4072W, RTD 4077, RTD 4076, RTD 4075, RTD 4074, RTD 4073, RTD 4072, RTD 4071) were located along the pilot plant absorber column to provide a temperature profile for each run (Figure 3.10). Combined with the data from temperature transmitters on the inlet gas stream, outlet gas stream, and inlet solvent stream, pilot plant-measured profiles have been compared with the model-predicted profiles with interfacial area correction for all runs (except for Run 4). Figures 3.11 through 3.14 depict four representative column temperature profiles for four different intercooling (IC) configurations: No IC No Spray, No IC With Spray, In-and-out IC, and Full Spray IC. The profiles include a distance of 1 meter between the top and bottom packing sections where the T should be constant. Inlet gas and inlet solvent temperatures were model inputs. The pilot plant measurements can be compared to both gas and liquid temperatures from the model as the pilot plant RTDs likely see a mix of phases in the column.

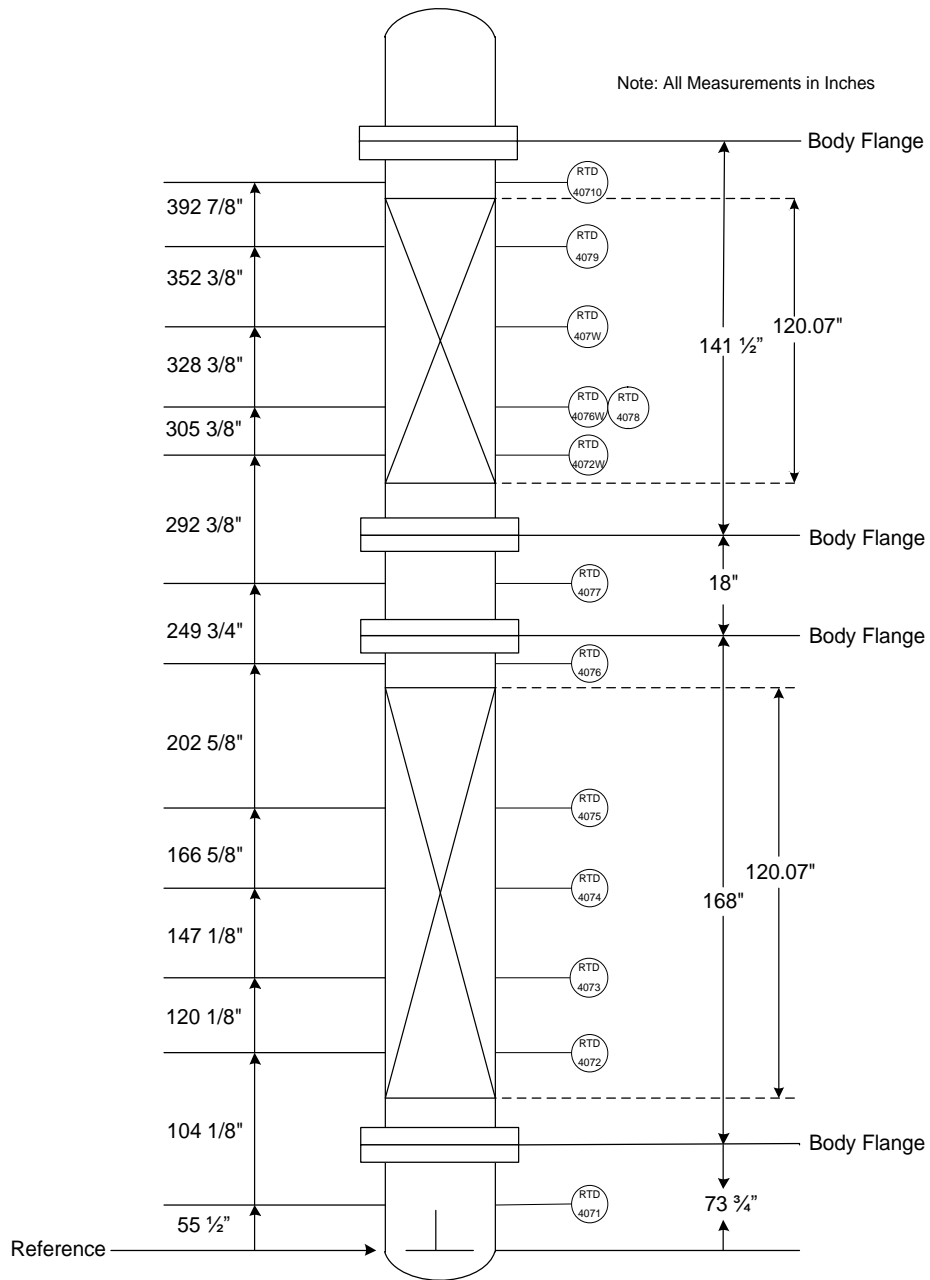


Figure 3.10: Absorber RTD elevations in March 2015 pilot plant campaign.

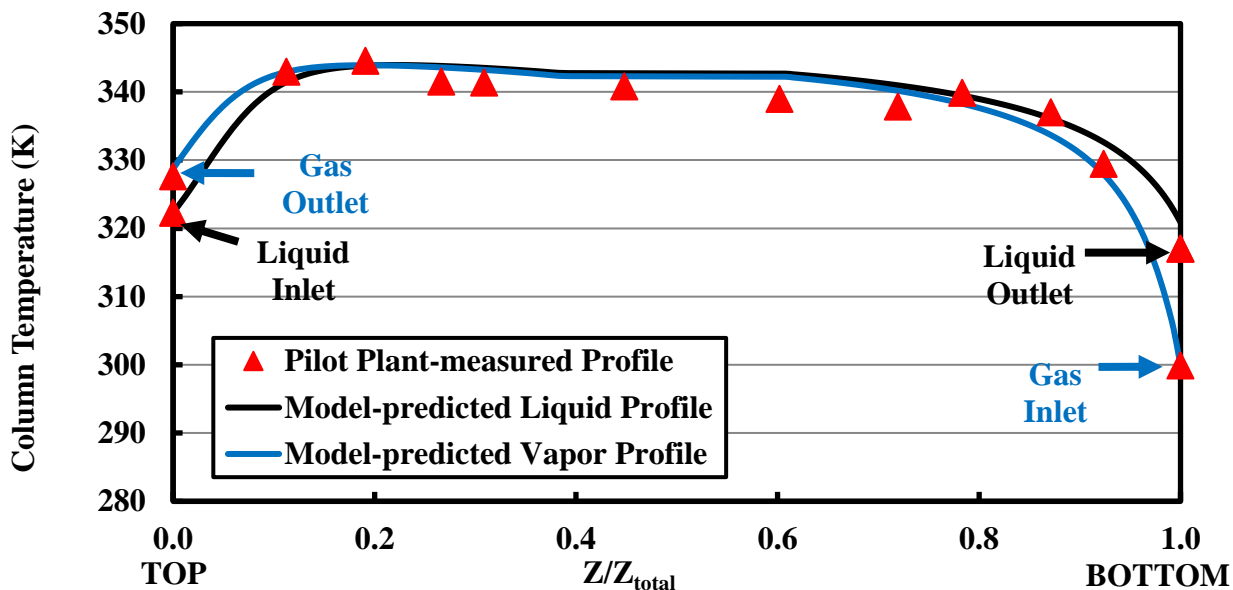


Figure 3.11: Model-predicted temperature profile compared with pilot plant-measured temperature profile for Case 7 (LLDG = 0.246, No IC No Spray, Removal = 80%).

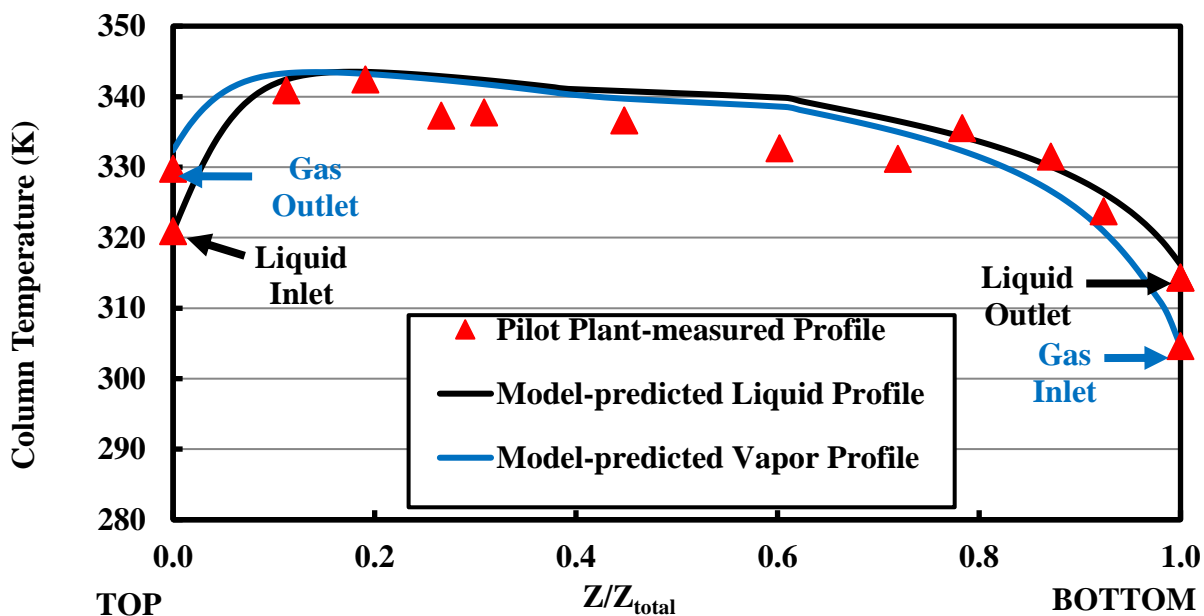


Figure 3.12: Model-predicted temperature profile compared with pilot plant-measured temperature profile for Case 13 (LLDG = 0.243, No IC With Spray, Removal = 68%).

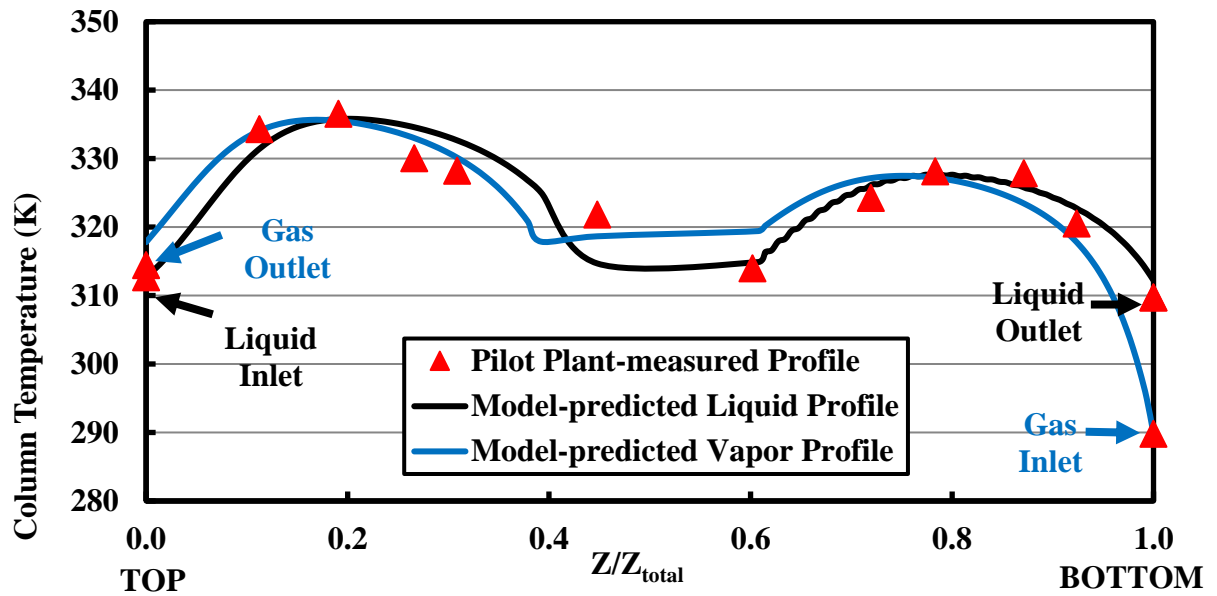


Figure 3.13: Model-predicted temperature profile compared with pilot plant-measured temperature profile for Case 5 (LLDG = 0.214, In-and-out IC, Removal = 94%).

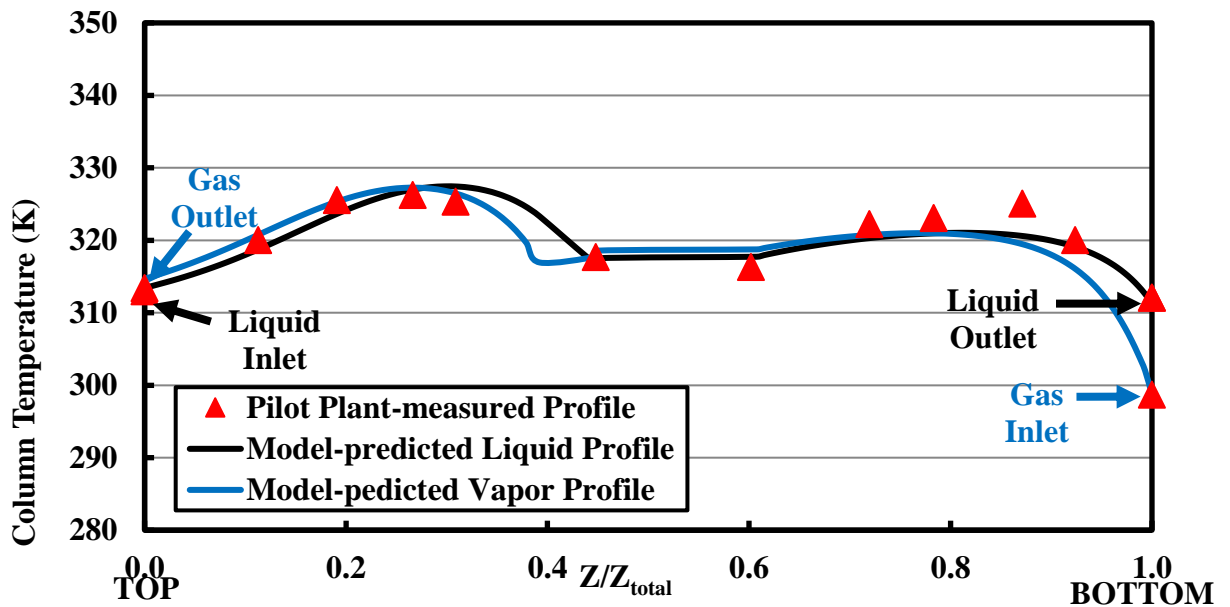


Figure 3.14: Model-predicted temperature profile compared with pilot plant-measured temperature profile for Case 6 (LLDG = 0.255, Full Spray IC, Removal = 89%).

Figure 3.13 shows that after applying in-and-out IC to the absorber, the maximum temperature of the column decreases from 345 K to 335 K. By applying full spray IC to the absorber, the maximum temperature further decreases to 325 K. The model is reasonably able to capture the trend of the temperature profiles for in-and-out IC (Figure 3.13) and No IC No Spray (Figure 3.11). However, with spray nozzle on and IC off (Figure 3.12) the model is not able to capture the mid-column temperature profile, and with full spray IC (Figure 3.14) the model is slightly off in predicting the temperature profile below the spray section. The spray nozzle performance model was developed with limited data in the previous campaigns, and this reflects potential inaccuracy of spray nozzle modeling.

Model-predicted vapor-liquid interface temperature profiles have been compared with measurements of 11 selected RTDs along the column. TT410 is gas outlet temperature and TT4071 is liquid outlet temperature. Average error and mean absolute percentage error are defined in Equations 3.6 and 3.7. Average errors of each RTD for 11 runs are listed in

Table 3.10. The pilot plant absorber model is able to capture column temperature profiles of different intercooling configurations within 2% mean absolute percentage error.

$$\text{Average Error (K)} = \frac{1}{11} \sum_{i=1}^{11} (T_{\text{predicted},i} - T_{\text{measured},i}) \quad (3.6)$$

$$\text{Mean Absolute Percentage Error (\%)} = \frac{1}{11} \sum_{i=1}^{11} \left| \frac{T_{\text{predicted},i} - T_{\text{measured},i}}{T_{\text{measured},i}} \right| \times 100\% \quad (3.7)$$

Table 3.10: Average Error (K) and Mean Absolute Percentage Error (%) of temperature measurements for each run.

Z/Z_{total}	RTDs	1	2	3	5	6	7	8	9	10	11
1 (Bottom)	TT4071	0.5	-1.1	-0.3	2.5	-0.8	3.9	3.3	-0.4	-0.2	5.4
0.92	TT4072	-0.8	-1.4	0.9	1.8	-1.3	2.5	6.7	-1.1	-1.2	12.0
0.87	TT4073	-4.0	-5.4	-3.7	-2.2	-4.6	-1.3	3.7	-3.1	-3.2	6.8
0.78	TT4074	-2.7	-6.5	-6.0	-0.5	-2.1	-0.7	5.0	-0.7	-1.3	2.4
0.72	TT4075	0.8	-2.6	-2.6	2.3	-1.8	2.9	4.3	1.3	1.9	5.7
0.45	TT4077	0.2	-1.1	-1.2	-6.1	-0.5	1.8	0.3	-0.3	0.5	-0.3
0.31	TT4072W	0.5	-1.5	-0.3	4.3	2.1	2.2	-1.2	2.5	1.2	8.3
0.27	TT4076W	5.2	1.8	4.2	4.5	0.8	2.3	-1.9	6.8	4.9	8.9
0.19	TT407W	-0.8	-4.1	0.1	-0.7	-1.7	-0.7	-1.5	-0.3	-5.1	2.2
0.11	TT4079	0.8	-5.0	0.7	-2.6	-1.1	-1.3	0.6	-2.2	-7.7	-0.8
0 (Top)	TT410	3.3	2.4	2.8	3.3	1.7	1.1	1.3	2.0	-1.3	2.0
Average Error (K)		0.3	-2.2	-0.5	0.6	-0.8	1.2	1.9	0.4	-1.0	4.8
Mean Absolute Percentage Error (%)		1%	1%	1%	1%	1%	1%	1%	1%	1%	2%
Z/Z_{total}	RTDs	12	13	14	15	16	17	18	19	20	21
1 (Bottom)	TT4071	5.9	1.9	1.3	4.9	3.3	4.2	4.3	7.4	4.9	6.7
0.92	TT4072	11.2	1.7	1.3	7.5	12.6	6.5	5.9	12.7	8.4	13.7
0.87	TT4073	8.8	-1.9	-2.9	3.7	5.5	2.8	2.2	7.7	3.6	6.8
0.78	TT4074	8.1	-1.5	-2.3	4.1	4.2	2.0	2.1	6.4	4.1	2.3
0.72	TT4075	6.7	5.1	-0.5	3.1	6.6	4.9	4.5	11.7	9.0	5.5
0.45	TT4077	3.3	3.8	0.6	0.1	-0.2	-1.3	-0.7	1.4	6.2	0.1
0.31	TT4072W	-1.6	4.5	0.3	-1.6	-0.8	-7.8	-7.7	4.7	10.5	10.1
0.27	TT4076W	-1.7	5.6	1.4	-2.1	-2.0	-10.8	-10.7	3.1	10.6	11.2
0.19	TT407W	-1.4	1.1	-5.8	-2.0	-6.1	-14.4	-13.9	-1.3	3.6	5.4
0.11	TT4079	-0.2	1.8	-7.1	0.0	-3.9	-7.7	-7.2	1.7	5.9	4.0
0 (Top)	TT410	0.8	2.6	0.4	1.2	1.7	0.8	1.1	2.6	7.2	4.0
Average Error (K)		3.6	2.2	-1.2	1.7	1.9	-1.9	-1.8	5.3	6.7	6.3
Mean Absolute Percentage Error (%)		1%	1%	1%	1%	1%	2%	2%	2%	2%	2%

3.7 CONCLUSIONS

The pilot plant CO₂ material balance around the absorber closed within +/- 2% when using density-predicted (corrected for Inhibitor A) loadings on the liquid side and re-calibrated FTIR data on the gas side.

5 m PZ provided significant absorber performance benefits over 8 m PZ due to enhanced mass transfer rates from lower solvent viscosity.

The pilot plant absorber model was validated over a wide variety of operating conditions: 5 m PZ and 8 m PZ, 6% and 12% inlet CO₂, different intercooling configurations, as well as “over-stripped LLDG” and normal LLDG.

Interfacial area correction and CO₂ correction provided similar predictions of pilot plant absorber performance and could be used interchangeably to correct the model.

The inhibitor correction to density-predicted loadings was consistent with model-predicted correction to titration data and might provide an explanation for pilot-model offsets.

Pilot plant data suggested a possible time dependence, and absorber NTU values were slightly over-predicted (mean ratio of model-predicted NTU to pilot plant-measured NTU = 1.08). A possible explanation is that several high CO₂ removal cases in the March 2015 campaign were outside the region where the previous model corrections were developed, where the controlling mass transfer resistance in the absorber differed. This observation provides an opportunity to investigate future model corrections at different column mass transfer limiting mechanisms.

The pilot plant absorber model was reasonably able to capture pilot plant-measured column temperature profile behaviors of different intercooling configurations within 2% mean absolute percentage error.

3.8 ACKNOWLEDGEMENTS

The author would like to acknowledge Paul Nielsen for TIC data and Di Song for density correction. The author gratefully acknowledges financial support from the Texas Carbon Management Program and the CO₂ Capture Pilot Plant Project in the preparation of this work. Aspen Plus[®] proprietary software was provided by an academic license from AspenTech[®]. AspenTech[®] and Aspen Plus[®] are trademarks of Aspen Technology, Inc. All rights reserved. This work is supported by the Department of Energy under Award Number DE-FE0005654.

Disclaimer: This report was prepared as an account of work sponsored by an agency of the United States Government. Neither the United States Government nor any agency thereof, nor any of their employees, makes any warranty, express or implied, or assumes any legal liability or responsibility for the accuracy, completeness, or usefulness of any information, apparatus, product, or process disclosed, or represents that its use would not infringe privately owned rights. Reference herein to any specific commercial product, process, or service by trade name, trademark, manufacturer, or otherwise does not necessarily constitute or imply its endorsement, recommendation, or favoring by the United States Government or any agency thereof. The views and opinions of authors expressed herein do not necessarily state or reflect those of the United States Government or any agency thereof.

Chapter 4 : Absorber Data Reconciliation for April 2017 UT-SRP Pilot Plant Campaign

4.1 APRIL 2017 PILOT PLANT CAMPAIGN OVERVIEW

The previous University of Texas Separations Research Program (UT-SRP) campaigns evaluated the pilot plant absorber with different internals and intercooling configurations. A consistent method for absorber model validation utilizing a rigorous data reconciliation method with the Independence PZ model was developed over a range of conditions (Frailie, 2014; Plaza, 2011; Sachde et al., 2013). The rate-based absorber model was simulated by the Independence PZ model developed in Aspen Plus[®] RateSep[™] with rigorous thermodynamics and kinetics (Frailie, 2014). To evaluate the absorber performance with a wider range of operating conditions, the April 2017 campaign systematically varied absorber packing height, CO₂ flue gas concentration, gas rate, lean loading, solvent to gas ratio, and intercooling.

Figure 3.1 shows a simplified process flow diagram of the April 2017 UT-SRP pilot plant configuration. The pilot plant absorber had 3 10-ft sections of Raschig Super-Pak (RSP-250) structured packing. An in-and-out intercooler was applied between the bottom two packed beds. A pump-around cooler was applied to the top packed bed. The column was operated in two modes during the campaign: 30-ft absorber; 20-ft absorber and 10-ft water wash. A chiller and a knockout drum were used to remove amine from the absorber outlet gas. The rich solvent was preheated by two exchangers and a steam heater, and fed into the flash tank for solvent regeneration. The lean solvent was fed back to the absorber after two exchangers and a trim cooler.

Table 4.1: Summary of pilot plant operating conditions

Equipment Specifications	
Column	
<i>Inner Diameter (m)</i>	0.43
Packing	
<i>Height (m)</i>	6.1 (3 beds x 3.05)
<i>Specific Area (m²/m³)</i>	250
<i>Corrugation Angle (°)</i>	RSP
<i>Material</i>	Stainless
Operating Specifications	
Solvent (PZ)	
<i>Concentration (m)</i>	5
<i>Liquid Rate (gpm)</i>	4.4 - 24
<i>Lean Loading (mol CO₂/mol alkalinity)</i>	0.18 - 0.27
Feed Gas	
<i>CO₂ (mol %)</i>	4, 12, 20
<i>H₂O (mol %)</i>	1 - 2
<i>T (°C)</i>	30
<i>Gas Rate (acfm)</i>	350, 550, 600

The operating conditions and campaign-specific equipment specifications are summarized in Table 4.2 for six previous PZ campaigns. Pilot plant data collection and the absorber model were improved and developed during the first three campaigns (Plaza, 2011). The Oct. 2011 and Nov. 2013 campaigns were utilized to develop a consistent method for absorber model validation and correction by utilizing a rigorous data reconciliation method with the Independence PZ model in Aspen Plus® (Frailie, 2014; Sachde et al., 2013). The pilot plant absorber performance analysis for the Mar. 2015 campaign showed the corrected pilot plant absorber model was reasonably able to capture pilot plant-measured column performance (Zhang et al., 2017b). In the April 2017 campaign, a wider range of absorber operating conditions has been tested, and the findings of six previous campaigns are used to predict absorber performance.

Table 4.2: Previous piperazine pilot plant absorber specifications

	8-Nov	10-Sep	10-Dec	11-Oct	13-Nov	15-Mar	17-Apr
Solvent	5–9 m PZ	8 m PZ	8 m PZ	8 m PZ	3.6–3.8 m PZ	5, 8 m PZ	5 m PZ
Packing Type & Specific Area(m²/m³)	Structured 205X	Hybrid 250	Hybrid 250	Structured 350Z	Hybrid 250	Hybrid 250	Hybrid 250
Gas Rate (ACFM)	350	250–750	350–650	350–675	350	350–500	350–600
Liquid Rate (GPM)	12–18	8–26	8–26	11–22	12	7–14	4–24
Intercooling	No	Yes/No	Yes	Yes (with Spray)	Yes (with Spray)/No	Yes (with Spray)/No	Yes/No

4.2 MATERIAL BALANCE CLOSURE

CO₂ material balance around the absorber requires measurements of gas and liquid flow and CO₂ concentration. Figure 4.2 and Table 4.3 summarize measurement locations and methods used during the campaign.

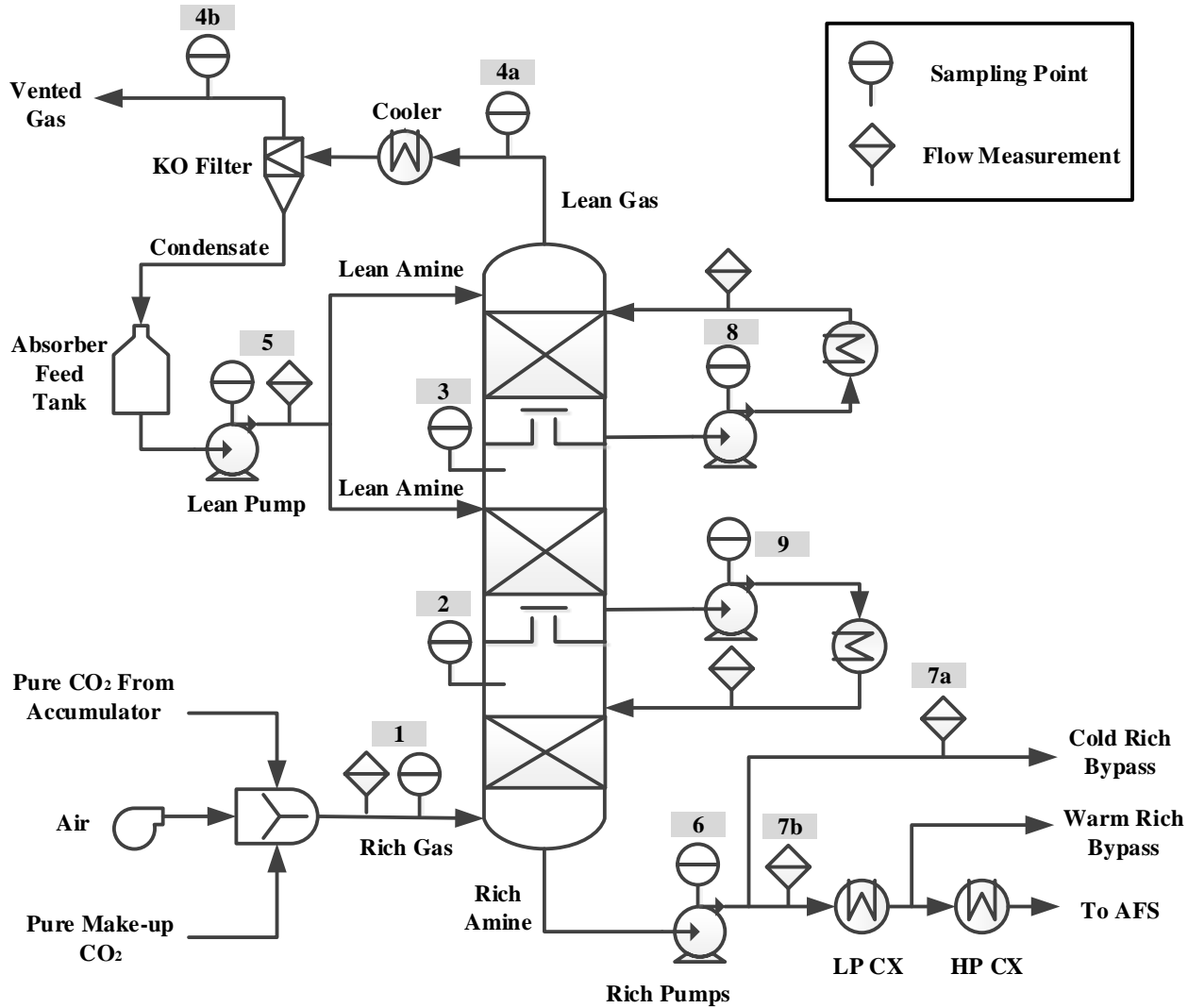


Figure 4.2: Simplified absorber PFD with indications for sampling and measurement points used in the mass balance in this paper. Points 1 through 9 are summarized with corresponding descriptions in Table 4.3.

Table 4.3: Flow and analytical measurements available for absorber mass balance

Stream and ID	CO ₂		PZ	
	Flow/Density	Analytical	Flow	Analytical
<u>Rich Gas</u> (Point 1 in Figure 4.2)	Inferred from Inlet	Vaisala® GMT220 CO ₂ Sensor (NDIR Sensor) & FTIR Sampling	N/A	N/A
<u>Bot Bed Outlet Gas</u> (Point 2 in Figure 4.2)	N/A	FTIR Sampling	N/A	N/A
<u>Mid Bed Outlet Gas</u> (Point 3 in Figure 4.2)	N/A	FTIR Sampling	N/A	N/A
<u>Lean Gas</u> (Points 4a and 4b in Figure 4.2)	Rosemount® Annubar (Differential Pressure) Meter	Vaisala® GMT220 CO ₂ Sensor (NDIR Sensor, 4b) & FTIR Sampling (4a & 4b)	N/A	N/A
<u>Lean Amine</u> (Point 5 in Figure 4.2)	Micro Motion® Coriolis Flow Meters	Manual Titration	Micro Motion® Coriolis Flow Meters	Manual Titration
<u>Rich Amine</u> (Points 6, 7a, and 7b in Figure 4.2)	Micro Motion® Coriolis Flow Meter	Manual Titration	Micro Motion® Coriolis Flow Meter	N/A
<u>Water Wash Process Amine</u> (Point 8 in Figure 4.2)	Micro Motion® Coriolis Flow Meter	N/A	Micro Motion® Coriolis Flow Meter	N/A
<u>Intercooling Amine</u> (Point 9 in Figure 4.2)	Micro Motion® Coriolis Flow Meter	N/A	Micro Motion® Coriolis Flow Meter	N/A

A modified density correlation was used in this work to predict loading, which includes an original density correlation developed by Freeman (Equation 4.1) and an additional correction for the presence of a thermally stable free-radical scavenger, Inhibitor A, in the solvent (Equation 4.2) (Zhang et al., 2017b). Water density calculation is based

on Tilton (Equation 4.3) (Tilton and Taylor, 1937). The density of the solvent was measured online in the pilot plant. The CO₂ and PZ concentrations were measured by titration. The Inhibitor A concentration used in April 2017 was 1 wt %.

$$\rho_{PZ} = \rho_{H_2O} \cdot (0.0407 \cdot C_{CO_2} + 0.008 \cdot C_{PZ} + 0.991) \quad (4.1)$$

$$\frac{\rho_{Pilot}}{\rho_{PZ}} = \frac{\rho_{InhA}}{\rho_{H_2O}} = 0.00741 * Inhibitor(wt\%) + 1.0018 \quad (4.2)$$

$$\rho_{H_2O} = 1000 * \left[1 - \frac{(T-3.9863)^2 * (T+288.9414)}{508929.2 * (T+68.12963)} \right] \quad (4.3)$$

where

ρ = Liquid density (kg/m³);

ρ_{H_2O} = Water density calculated from Tilton-Taylor formula (kg/m³);

C_{CO_2} = CO₂ concentration in the solution (mol/kg);

C_{PZ} = PZ concentration (mol/kg);

T = Temperature (°C).

The data analysis procedure in this work follows:

- A data consistency check to select solvent loading and gas analyzer by CO₂ material balance;
- Gross error detection to identify the variables that require statistically larger changes;
- Data reconciliation with parameter adjustment: if model cannot be reconciled within the measured uncertainty, an adjustable parameter “interfacial area correction” is added.

4.2.1 Overall CO₂ Material Balance

Overall CO₂ material balance has been evaluated to perform data consistency check around the entire pilot plant. Table 4.4 and Table 4.5 compare titration-measured lean loadings with two density-predicted lean loadings (FT403 and FT201 at Point 5 in Figure 4.2) and titration-measured rich loadings with four density-predicted rich loadings (DT200 and DT520 at Point 6, FT515 at Point 7a, and FT518 at 7b in Figure 4.2). For both FT403 and FT201, the average ratios of density-predicted loadings to titration-measured loadings are 1.05. FT403 has smaller standard deviation and is less scattered than FT201.

Table 4.4 indicates that the density-predicted lean loadings exhibit a systematic offset of approximately 5% from the measured titration data. Table 4.5 shows that, for density-predicted rich loadings, DT520 was less scattered than DT200. DT520 was not working functionally in several runs at the first half of the campaign; it was re-configured throughout the campaign and gave reliable density measurements. All four density-predicted rich loadings are relatively consistent with the titration rich loadings. As a result, based on titration, density-predicted lean loadings measured by FT403 were corrected by 5% and density-predicted rich loadings measured by DT520 (DT200 was used when DT520 was out of service) were corrected by 3%; these titration-corrected density-predicted lean and rich loadings are used in the following model analysis, summarized in Table 4.6.

Table 4.4: Titration-measured lean loadings with two density-predicted lean loadings (FT403 and FT201 at Point 5 in Figure 4.2).

Run	Lean						
	Titration mol CO ₂ /mol alk	Density-predicted					
		FT403			FT201		
	Density lb/ft ³	LLDG mol CO ₂ /mol alk	Ratio to Titration	Density lb/ft ³	LLDG mol CO ₂ /mol alk	Ratio to Titration	
1	0.23	67.666	0.245	1.07	67.657	0.244	1.07
2	0.23	67.466	0.239	1.03	67.465	0.239	1.03
3	0.23	67.973	0.243	1.08	67.949	0.241	1.07
4	0.22	67.626	0.229	1.05	67.661	0.234	1.07
5	0.23	67.883	0.243	1.05	67.971	0.251	1.09
6	0.26	68.021	0.274	1.04	68.008	0.273	1.04
7	0.26	67.904	0.265	1.04	67.845	0.261	1.02
8	0.26	67.914	0.267	1.04	67.867	0.264	1.03
9	0.22	67.939	0.238	1.07	68.024	0.247	1.11
10	0.21	67.467	0.221	1.05	67.544	0.229	1.09
11	0.21	67.636	0.217	1.06	67.626	0.217	1.06
12	0.21	67.835	0.225	1.07	67.838	0.225	1.07
13	0.20	67.312	0.211	1.05	67.293	0.211	1.05
14	0.19	67.460	0.204	1.05	67.502	0.208	1.07
15	0.17	67.143	0.179	1.07	67.556	0.205	1.23
16	0.22	67.674	0.236	1.07	67.542	0.229	1.04
17	0.23	68.055	0.241	1.04	68.038	0.241	1.04
18	0.23	67.529	0.245	1.06	67.432	0.239	1.03
19	0.22	67.527	0.229	1.03	67.385	0.221	0.99
20	0.22	67.772	0.235	1.05	67.671	0.229	1.02
21	0.23	67.980	0.235	1.03	67.877	0.232	1.02
22	0.20	67.070	0.207	1.03	67.015	0.206	1.02
23	0.19	67.664	0.200	1.05	67.604	0.199	1.05
24	0.18	66.849	0.184	1.03	66.765	0.180	1.01
25	0.17	66.651	0.177	1.04	66.579	0.174	1.02
26	0.18	66.845	0.188	1.03	66.747	0.182	1.00
27	0.19	67.216	0.203	1.04	67.264	0.207	1.07
28	0.23	67.518	0.236	1.04	67.629	0.245	1.07
29	0.23	67.508	0.242	1.04	67.438	0.239	1.03
Average			1.05			1.05	
Standard deviation			0.02			0.04	

Table 4.5: Titration-measured rich loadings with four density-predicted rich loadings (DT200 and DT520 at Point 6, FT515 at Point 7a, and FT518 at 7b in Figure 4.2).

Run	Rich												
	Titration	Density-predicted											
		DT200			DT520			FT515 Cold Rich Bypass			FT518 Warm Rich Bypass		
		Density	RLDG	Ratio to Titration	Density	RLDG	Ratio to Titration	Density	RLDG	Ratio to Titration	Density	RLDG	Ratio to Titration
mol CO ₂ /mol alk	lb/ft ³	mol CO ₂ /mol alk	lb/ft ³	mol CO ₂ /mol alk	lb/ft ³	mol CO ₂ /mol alk	lb/ft ³	mol CO ₂ /mol alk	lb/ft ³	mol CO ₂ /mol alk	lb/ft ³	mol CO ₂ /mol alk	
1	0.37	69.746	0.371	1.02				69.678	0.366	1.00	66.689	0.386	1.06
2	0.38	69.827	0.383	1.00	69.713	0.375	0.98	69.826	0.382	0.99	66.557	0.403	1.05
3	0.38	70.256	0.385	1.01	70.127	0.376	0.99	70.444	0.390	1.03	67.431	0.402	1.06
4	0.33	69.667	0.337	1.02				69.363	0.320	0.97	66.241	0.341	1.03
5	0.34	69.711	0.346	1.03				69.397	0.328	0.98	66.763	0.342	1.02
6	0.36	69.188	0.351	0.98	69.088	0.344	0.96	69.243	0.353	0.99	66.110	0.371	1.04
7	0.37	69.647	0.376	1.00	69.489	0.365	0.98	69.558	0.369	0.99	66.533	0.388	1.04
8	0.37	69.641	0.378	1.01	69.476	0.367	0.99	69.502	0.368	0.99	66.420	0.390	1.05
9	0.38	70.661	0.385	1.03				70.486	0.375	1.00	67.345	0.398	1.06
10	0.38	70.240	0.381	1.01				70.151	0.374	0.99			
11	0.35	69.603	0.349	1.01				70.074	0.365	1.06	66.883	0.372	1.08
12	0.37	70.180	0.368	1.00				70.292	0.369	1.01	67.303	0.385	1.05
13	0.37	70.019	0.375	1.01				69.890	0.366	0.99	65.533	0.307	0.83
14	0.37	70.254	0.369	1.00	70.090	0.358	0.98	70.023	0.355	0.97			
15	0.34	70.185	0.342	1.01	70.071	0.335	0.99	70.051	0.335	0.99	66.886	0.345	1.02
16	0.34	69.600	0.347	1.02	69.449	0.337	0.99	69.384	0.334	0.98	66.516	0.362	1.06

Table 4.5: Continued.

17	0.36	69.843	0.355	0.99	69.786	0.351	0.97	70.414	0.379	1.05	66.935	0.378	1.05
18	0.34	69.068	0.348	1.02	68.941	0.339	1.00	68.989	0.342	1.01	65.739	0.371	1.09
19	0.34	69.134	0.334	0.98	68.959	0.322	0.95	68.935	0.321	0.94	65.821	0.351	1.03
20	0.33	69.343	0.332	1.01	69.222	0.324	0.98	69.401	0.334	1.01	66.128	0.361	1.09
21	0.30	69.125	0.293	0.99	69.022	0.287	0.96	68.985	0.285	0.96	65.911	0.298	1.00
22	0.32	69.114	0.318	0.99	68.981	0.310	0.96	68.849	0.303	0.94	65.697	0.329	1.02
23	0.33	70.206	0.331	0.99	70.066	0.323	0.97	70.019	0.321	0.96	66.899	0.337	1.01
24	0.33	69.041	0.321	0.98	68.913	0.313	0.96	68.912	0.313	0.96	65.660	0.343	1.05
25	0.33	69.097	0.318	0.97	69.035	0.313	0.96	68.946	0.309	0.95	65.621	0.346	1.06
26	0.32	68.863	0.317	0.98	68.717	0.307	0.95	68.668	0.304	0.95	65.174	0.332	1.03
27	0.33	69.431	0.329	0.99	69.392	0.325	0.98	69.373	0.325	0.98	66.289	0.341	1.03
28	0.38	70.074	0.387	1.01	69.994	0.381	0.99	69.959	0.380	0.99	66.903	0.393	1.02
29	0.38	69.568	0.373	0.99	69.450	0.365	0.97	69.529	0.369	0.98	66.279	0.396	1.05
Average		1.00			0.97			0.99			1.04		
Standard deviation		0.02			0.01			0.03			0.05		

Table 4.6: Titration-measured lean/rich loadings and titration-corrected density-predicted lean loadings (FT403 corrected by 5%) and rich loadings (DT520 corrected by 3%). These loadings are used in the following model analysis.

Run	Titration LLDG (mol CO ₂ /mol alk)	Titration-corrected density-predicted LLDG (mol CO ₂ /mol alk)	Titration RLDG (mol CO ₂ /mol alk)	Titration-corrected density-predicted RLDG (mol CO ₂ /mol alk)
1	0.229	0.233	0.365	0.372
2	0.232	0.228	0.384	0.385
3	0.225	0.232	0.379	0.386
4	0.218	0.219	0.330	0.338
5	0.231	0.232	0.336	0.347
6	0.263	0.261	0.357	0.353
7	0.255	0.253	0.374	0.375
8	0.256	0.255	0.372	0.376
9	0.223	0.227	0.375	0.386
10	0.211	0.211	0.378	0.381
11	0.205	0.207	0.345	0.350
12	0.21	0.214	0.366	0.369
13	0.201	0.201	0.370	0.376
14	0.194	0.195	0.367	0.368
15	0.167	0.171	0.339	0.344
16	0.22	0.225	0.340	0.346
17	0.232	0.23	0.360	0.360
18	0.232	0.234	0.340	0.348
19	0.223	0.219	0.340	0.331
20	0.224	0.224	0.330	0.333
21	0.228	0.224	0.297	0.294
22	0.201	0.197	0.323	0.318
23	0.19	0.191	0.333	0.332
24	0.179	0.176	0.327	0.321
25	0.17	0.169	0.326	0.321
26	0.182	0.179	0.322	0.315
27	0.194	0.193	0.331	0.334
28	0.228	0.225	0.384	0.391
29	0.233	0.231	0.376	0.374

At steady state, the CO₂ removed/captured in the absorber should be equal to the pure stripper overhead CO₂ flow rate. CO₂ removed in the absorber gas phase was calculated from absorber inlet and outlet CO₂ concentrations and flow rates. Flow rates were obtained from flowmeters. Absorber inlet and outlet CO₂ were compared using NDIR continuous inline CO₂ measurements and FTIR discrete online sampling, compared in Table 4.7 and plotted in Figures 4.3 and 4.4. In the operation of April 2017 campaign, the test plan was implemented by watching NDIR inlet CO₂. Figures 4.3 and 4.4 show that FTIR gives higher readings than NDIR at both high CO₂ (higher than 8 mol%) and low CO₂ (lower than 1 mol%).

Table 4.7: Measured absorber inlet and outlet CO₂ by NDIR continuous inline CO₂ measurements and FTIR discrete online sampling.

Run	Absorber Inlet CO ₂			Absorber Outlet CO ₂		
	NDIR	FTIR	NDIR and FTIR Averages	NDIR	FTIR	NDIR and FTIR Averages
	mol%			mol%		
1	12.00		12.00	1.32	1.54	1.43
2	12.00	14.64	13.32	1.34	1.47	1.40
3	19.50	20.78	20.14	3.76	3.42	3.59
4	3.95		3.95	0.10	0.27	0.18
5	3.77	3.51	3.64	0.06	0.21	0.13
6	12.61	14.40	13.50	0.09	0.30	0.19
7	20.43	29.09	24.76	0.86		0.86
8	20.37	28.46	24.41	0.87		0.87
9	4.15	3.82	3.98	0.36	0.48	0.42
10	12.01	13.47	12.74	1.32	1.44	1.38
11	19.97	27.11	23.54	0.99	1.10	1.04
12	21.94	30.88	26.41	0.44		0.44
13	19.52	25.43	22.48	2.08	2.09	2.09
14	20.03	27.31	23.67	0.52	0.82	0.67
15	4.14	3.84	3.99	0.00	0.11	0.06
16	12.00	12.84	12.42	1.65		1.65
17	19.48	28.30	23.89	2.35	2.35	2.35
18	19.52	21.12	20.32	2.87	2.74	2.80
19	19.61	24.66	22.13	1.11		1.11
20	12.01	14.61	13.31	0.65	0.74	0.70
21	3.10	3.01	3.05	0.00	0.09	0.04
22	4.39	3.94	4.17	0.16	0.34	0.25
23	4.31	4.47	4.39	0.10	0.27	0.18
24	19.51	21.29	20.40	2.83	2.81	2.82
25	8.80	12.17	10.49	0.39	0.54	0.47
26	18.99	23.31	21.15	1.49	1.65	1.57
27	3.57	3.53	3.55	0.12		0.12
28	3.80	3.85	3.83	0.37	0.49	0.43
29	16.13	19.35	17.74	0.48	0.55	0.52

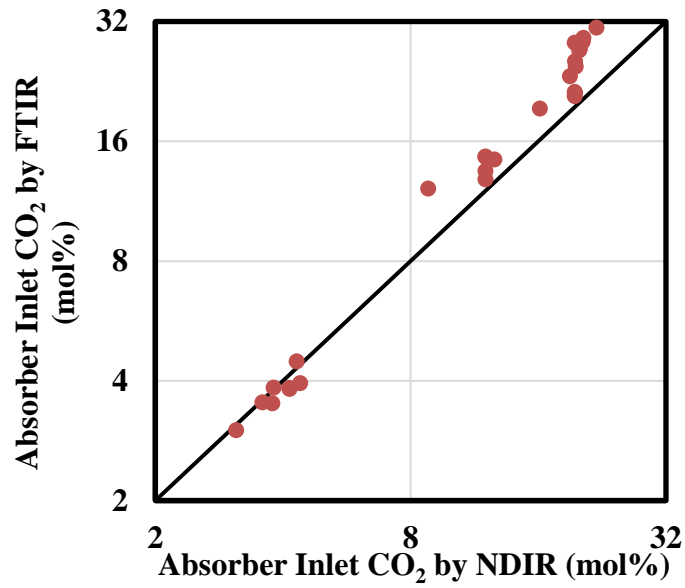


Figure 4.3: Measured absorber inlet CO₂ by NDIR continuous inline CO₂ measurements and FTIR discrete online sampling.

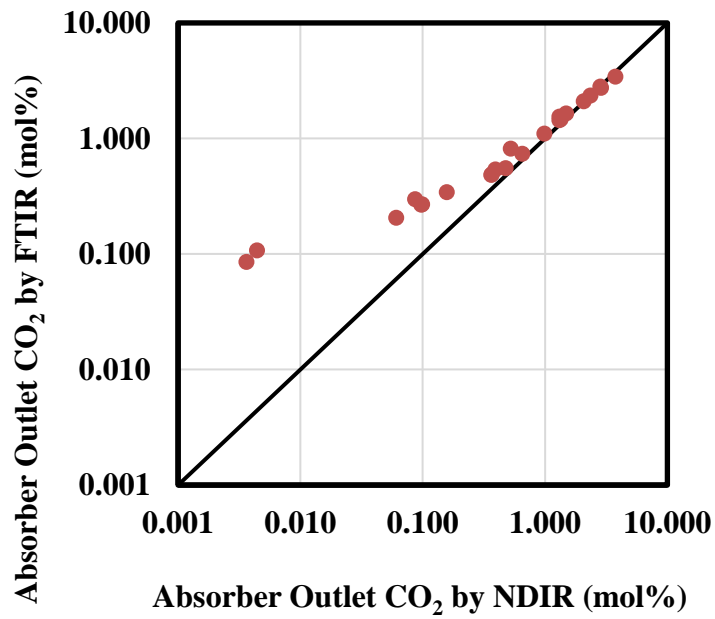


Figure 4.4: Measured absorber outlet CO₂ by NDIR continuous inline CO₂ measurements and FTIR discrete online sampling.

CO₂ lean and rich loadings and flow rates are used to calculate CO₂ captured in the absorber liquid phase. Two methods for lean and rich loadings are used in the material balance analysis.

- Immediate manual titration of samples at the pilot plant;
- Titration-corrected density-predicted loadings.

CO₂ captured in the absorber liquid phase was calculated from titration-corrected density-predicted lean loadings (FT403 corrected by 5% based on titration) and rich loadings (DT520 corrected by 3% based on titration) as well as flow rates. Pure stripper overhead CO₂ flow rate was measured by FT550. CO₂ removed calculated by absorber gas-side measurements and CO₂ captured by absorber liquid-side measurements have been compared with stripper overhead CO₂ flow in Table 4.8. The average ratios of CO₂ removed/captured in the absorber to stripper overhead CO₂ reflect the closure of overall CO₂ material balance around the amine scrubbing system. Table 4.8 also shows that measured absorber CO₂ removed/captured rates are close to the pure stripper overhead CO₂ flow rate, suggesting a reasonably good overall CO₂ material balance. Figure 4.5 and Figure 4.6 compare ratios of absorber gas-side CO₂ removed (inlet and outlet CO₂ measured by both NDIR and FTIR) to stripper overhead CO₂. Figure 4.5 shows that FTIR measurements predict higher gas side CO₂ removal rates than NDIR measurements. In Figure 4.6, NDIR measurements systematically over-predict CO₂ removal rates at 3.5% inlet CO₂ and under-predict CO₂ removal rates at 20% inlet CO₂; FTIR measurements are more scattered and systematically over-predict CO₂ removal rates at 8-20% inlet CO₂. These findings suggest possible errors of NDIR measurements at low outlet CO₂ and high inlet CO₂ as well as systematic bias of FTIR measurements.

Table 4.8: Comparison between CO₂ removed calculated by absorber gas-side measurements, CO₂ captured by absorber liquid-side measurements, and stripper overhead CO₂ flow.

Run	Absorber Liquid Side Total CO ₂ captured				Absorber Gas Side Total CO ₂ removed					Stripper Overhead	
	Density-predicted		Titration		NDIR		FTIR		NDIR and FTIR average		
	lb/hr	Ratio to Stripper Overhead	lb/hr	Ratio to Stripper Overhead	lb/hr	Ratio to Stripper Overhead	lb/hr	Ratio to Stripper Overhead	lb/hr	Ratio to Stripper Overhead	lb/hr
1	450	1.05	441	1.03	410	0.96			410	0.96	427
2	440	1.01	426	0.98	396	0.91	484	1.11	440	1.01	436
3	407	0.98	407	0.98	375	0.9	410	0.99	393	0.94	416
4	161	1.22	151	1.14	147	1.11			147	1.11	132
5	79	1.11	73	1.02	85	1.2	76	1.07	81	1.13	71
6	336	1.15	344	1.18	296	1.02	331	1.14	314	1.08	292
7	495	0.99	484	0.97	449	0.9			449	0.9	499
8	489	0.99	468	0.95	446	0.9			446	0.9	493
9	165	1.18	158	1.13	146	1.04	129	0.92	138	0.98	140
10	226	0.86	221	0.84	253	0.96	283	1.08	268	1.02	262
11	474	0.96	463	0.94	442	0.9	586	1.19	514	1.05	491
12	514	0.95	517	0.96	490	0.91			490	0.91	540
13	497	1.15	481	1.11	405	0.94	527	1.22	466	1.08	432
14	463	0.98	463	0.98	446	0.94	587	1.24	516	1.09	474
15	157	1.1	155	1.09	160	1.13	145	1.02	153	1.07	142
16	249	1.02	245	1.01	236	0.97			236	0.97	243
17	471	0.98	467	0.97	414	0.86	603	1.25	509	1.05	482
18	439	1	417	0.95	395	0.9	433	0.99	414	0.94	439
19	424	0.99	440	1.03	417	0.98			417	0.98	427
20	420	1	411	0.98	420	1	507	1.21	463	1.11	419
21	76	1.16	74	1.13	72	1.1	68	1.04	70	1.07	66
22	160	1.11	163	1.13	161	1.12	138	0.96	150	1.04	144
23	97	1.13	98	1.14	99	1.15	99	1.16	99	1.16	86
24	414	0.97	423	1	397	0.93	436	1.03	417	0.98	425
25	352	1.02	360	1.04	321	0.93	438	1.27	380	1.1	345
26	411	0.99	424	1.02	403	0.97	490	1.18	447	1.08	415
27	146	1.13	143	1.1	135	1.04			135	1.04	130

Table 4.8: Continued.

28	158	1.06	148	0.99	133	0.9	131	0.88	132	0.89	149
29	407	1	407	1	366	0.89	433	1.06	399	0.98	409
Average	1.04		1.03		0.98		1.09		1.02		
Standard Deviation	0.08		0.08		0.09		0.11		0.08		

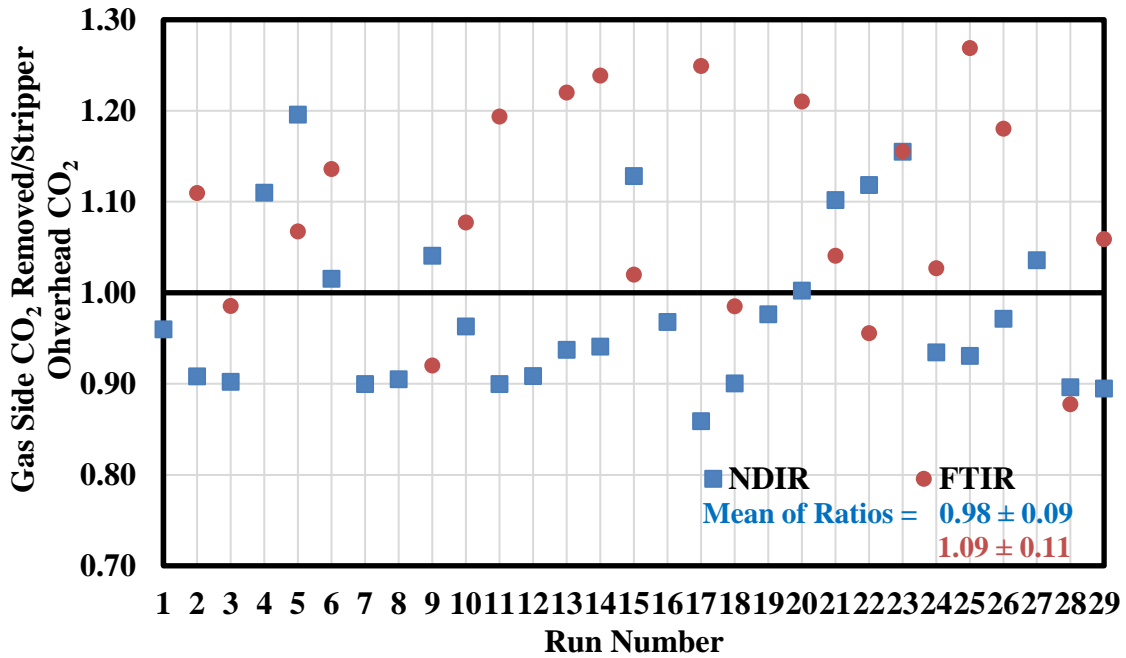


Figure 4.5: Ratios of absorber gas-side CO₂ removed to stripper overhead CO₂ plotted against run number. Absorber inlet and outlet CO₂ measured by NDIR and FTIR.

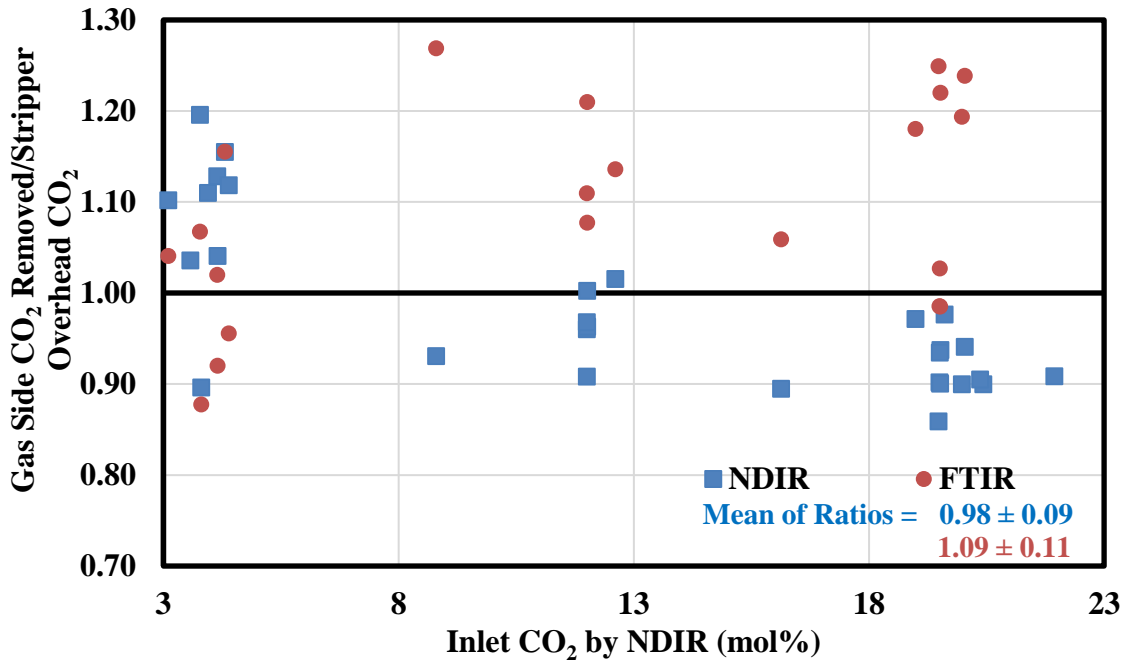


Figure 4.6: Ratios of absorber gas-side CO₂ removed to stripper overhead CO₂ plotted against NDIR inlet CO₂. Absorber inlet and outlet CO₂ measured by NDIR and FTIR.

NDIR and FTIR averages are evaluated (NDIR measurements used for the runs when FTIR was out of service) and are found to give better overall CO₂ material balance closure, as shown in Figure 4.7. As a result, NDIR and FTIR averages are used in the following model analysis. Figure 4.8 compares ratios of absorber liquid-side CO₂ captured to stripper overhead CO₂ and shows that absorber liquid-side CO₂ agrees well with stripper overhead CO₂. The CO₂ material balance closure around the absorber is shown in Figure 4.9. The pilot plant absorber CO₂ material balance closes within +/- 20% when using titration-corrected density-predicted loadings on the liquid side and NDIR and FTIR average data on the gas side. No systematic trends are observed.

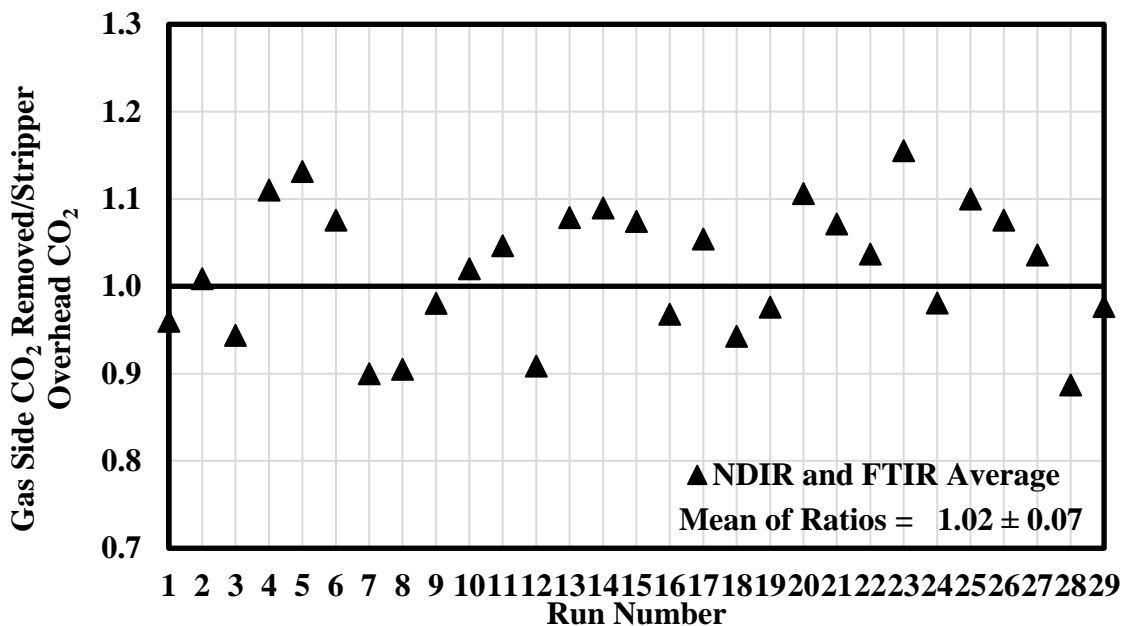


Figure 4.7: Ratios of absorber gas-side CO₂ removed to stripper overhead CO₂. Absorber inlet and outlet CO₂ calculated from NDIR and FTIR averages.

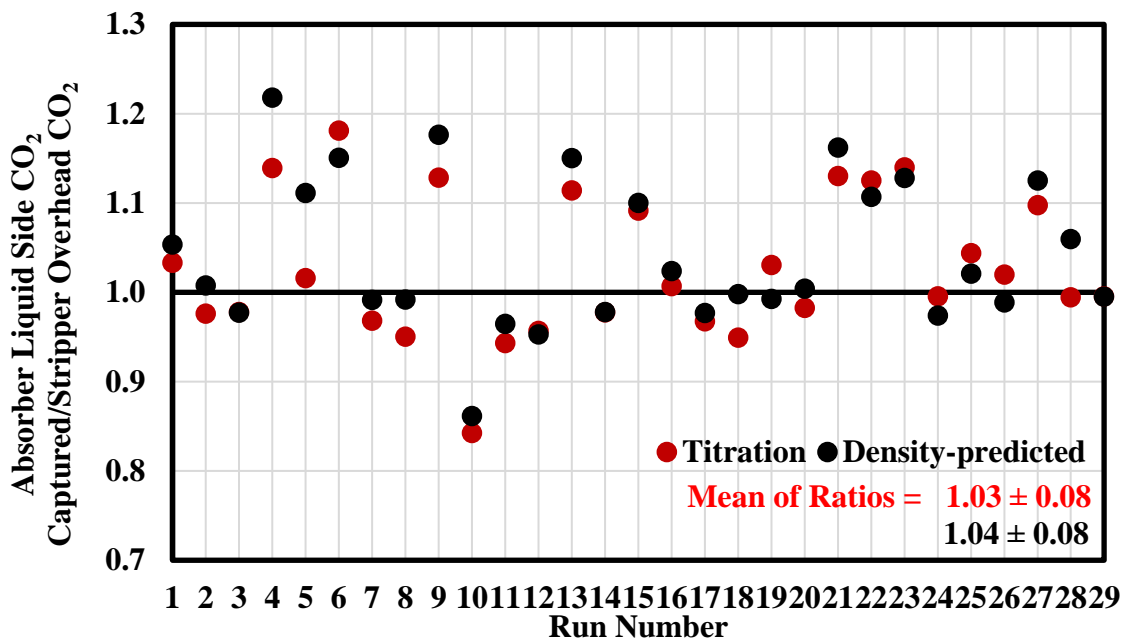


Figure 4.8: Ratios of absorber liquid-side CO₂ captured to stripper overhead CO₂. Titration loadings and titration-corrected density-predicted loadings are compared.

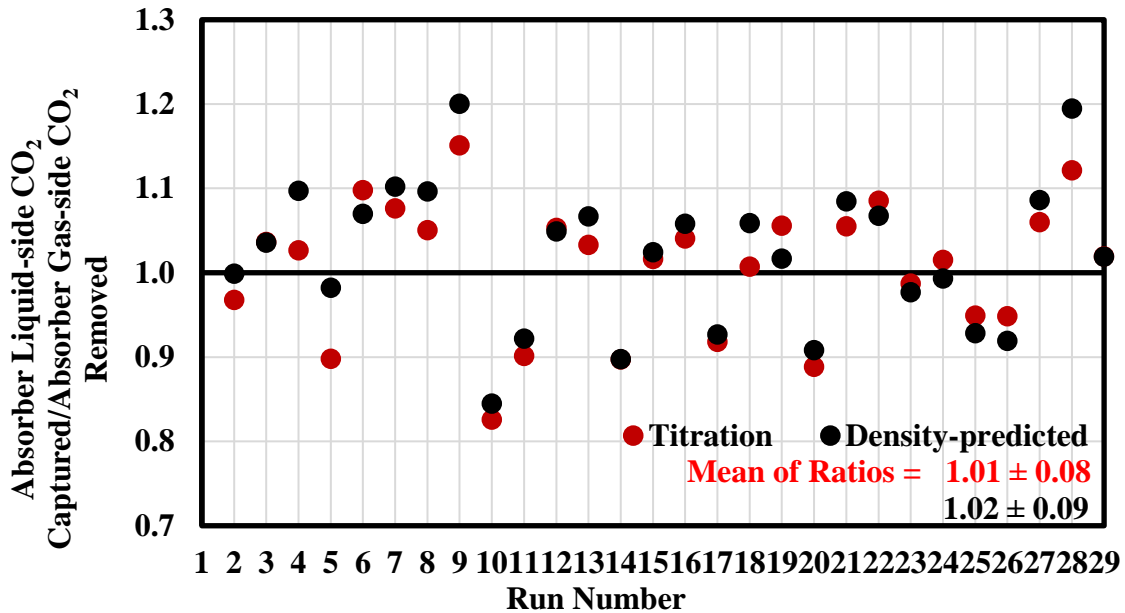


Figure 4.9: The CO₂ material balance closure around absorber. Absorber CO₂ material balance closes within +/- 20% when using titration-corrected density-predicted loadings on the liquid side and NDIR and FTIR average data on the gas side.

4.2.2 Mid CO₂ Material Balance

The absorber top (top 10-ft section for 20-ft absorber and top 10-ft section for 30-ft absorber) can be treated as an independent column for data consistency check. Mid CO₂ data were obtained using FTIR discrete online sampling. Mid loadings (CO₂ loadings of top absorber outlet solvent, at Point 9 in Figure 4.2) were obtained from two following measurements:

- Laboratory analysis by total inorganic carbon (TIC) after the campaign;
- Online density measurements.

The TIC measurements were conducted for 8 runs after the campaign. Densities were obtained from DT430 (at Point 9 in Figure 4.2) for most runs during the campaign.

Table 4.9 compares TIC-measured mid loadings and density-predicted mid loadings and suggests that there is a 4% offset.

Table 4.9: TIC-measured mid loadings and density-predicted mid loadings (DT430 at Point 9 in Figure 4.2).

Run	Mid			
	TIC mol CO ₂ /mol alk	Density-predicted		
		Density lb/ft ³	Mid LDG DT430 mol CO ₂ /mol alk	Ratio to TIC
1		68.7	0.31	
2		68.8	0.32	
3		68.0	0.25	
4	0.29	68.2	0.27	0.94
5	0.31	68.0	0.27	0.87
6		66.4	0.17	
7		68.4	0.29	
8		68.7	0.32	
9	0.30	69.3	0.32	1.07
10	0.26	69.2	0.33	1.28
11		68.0	0.29	
12		69.3	0.32	
13	0.31	69.1	0.32	1.03
14	0.30	69.3	0.31	1.03
15	0.23	68.5	0.24	1.07
16		68.5	0.28	
17		68.8	0.29	
18	0.28	68.2	0.29	1.03
19		66.9	0.19	
20		68.1	0.25	
21		67.8	0.23	
22		67.3	0.23	
23		67.8	0.23	
24		68.0	0.25	
25		67.2	0.21	
26		67.7	0.24	
27		67.4	0.22	
28		68.8	0.33	
29		68.8	0.32	
Average		1.04		
Standard deviation		0.12		

At steady state, in the top section of absorber, the CO₂ removed in the gas phase should be equal to the CO₂ captured in the liquid phase. CO₂ removed in the gas phase was calculated from outlet CO₂ and mid CO₂ (top absorber inlet CO₂, at Point 2 in Figure 4.2) as well as gas flow rates. NDIR and FTIR averages are used for outlet CO₂ and FTIR was used for mid CO₂. Density-predicted and TIC-measured mid loadings, titration-corrected density-predicted lean loadings, and flow rates are used to calculate total CO₂ captured in the liquid phase. Measured gas-side CO₂ removed and liquid-side CO₂ captured in absorber top have been compared in Table 4.10 and Figure 4.10. Density-predicted mid loadings give much better CO₂ material balance than TIC-measured mid loadings. As a result, density-predicted mid loadings are used in the following model analysis.

Table 4.10: Comparison between measured gas-side CO₂ removed and measured liquid-side CO₂ captured in absorber top.

Run	Absorber Liquid Side Total CO ₂ Captured				Absorber Gas Side Total CO ₂ Removed
	Titration-corrected density-predicted lean loadings and density-predicted mid loadings		Titration-corrected density-predicted lean loadings and TIC-measured mid loadings		NDIR and FTIR averages for outlet CO ₂ and FTIR for mid CO ₂
	lb/hr	Ratio to Gas Side	lb/hr	Ratio to Gas Side	
1	250	1.1			286
2	264	1.2			314
3	70	5.3			373
4	63	1.2	85	0.9	73
5	30	1.3	60	0.7	40
6					96
7	167				
8	250				
9	91	1.1	72	1.3	97
10	184	1.1	77	2.8	211

Table 4.10: Continued.

11	314	1.4			429
12	337				
13	284	1.1	265	1.2	317
14	304	1.1	283	1.2	340
15	68	1.3	54	1.6	85
16	121				
17	209	1.0			214
18	184	1.2	159	1.4	228
19					
20	109	1.2			131
21	9	1.5			14
22	38	1.8			69
23	24	2.0			49
24	194	1.4			265
25	93	1.3			117
26	168	1.4			234
27	33				
28	100	1.1			107
29	252	1.1			285
Average		1.47		1.38	
Standard Deviation		0.89		0.63	

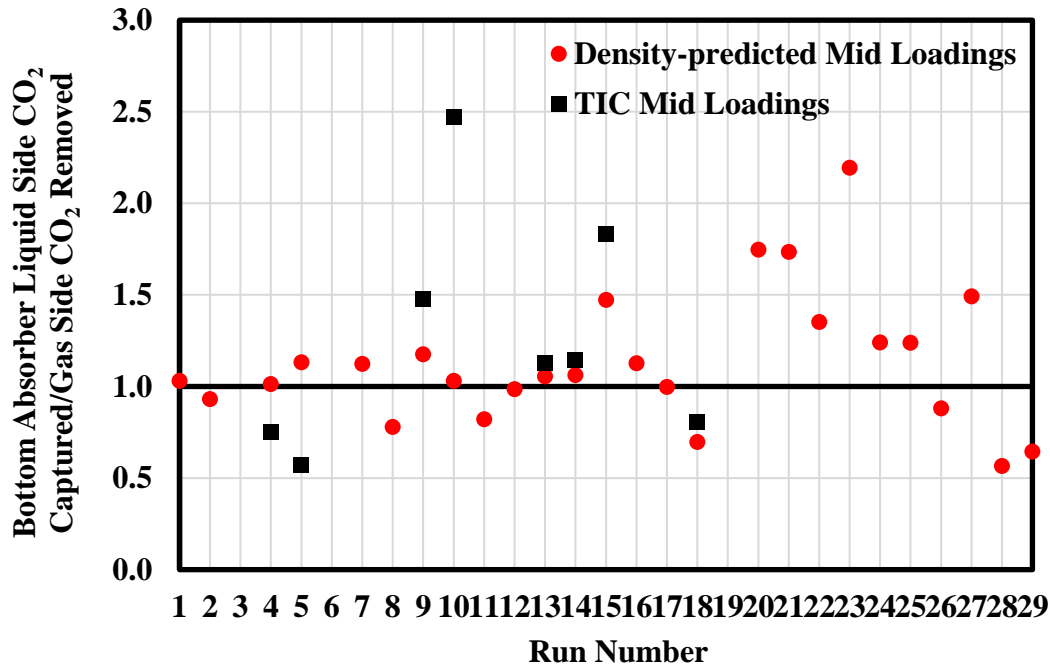


Figure 4.10: Comparison between measured gas-side CO₂ removed and measured liquid-side CO₂ captured in the absorber top (top 10-ft section for 20-ft absorber or top 10-ft section for 30-ft absorber). Liquid-side CO₂ captured is calculated from density-predicted lean and mid loadings as well as density-predicted lean loadings and TIC-measured mid loadings.

4.3 PERFORMANCE RESULTS

4.3.1 Pilot Plant Absorber Performance Results

The column was operated in two modes during the campaign: 30-ft absorber for Runs 1 to 15; 20-ft absorber and 10-ft water wash for Runs 16 to 29. Table 4.11 provides detailed operating conditions by run numbers and corresponding conditions as calculated from measurements used in the preceding material balance analysis:

- Liquid rates, gas rates, and liquid to gas ratio (L/G);
- Intercooling (IC) configurations and temperatures;
- Density-predicted lean loading (LLDG) and rich loading (RLDG);

- Inlet and outlet CO₂ by NDIR and FTIR averages;
- CO₂ removal and number of transfer units (NTU).

Number of transfer units (NTU) is defined by Equation 4.4.

$$NTU = \ln(1 - f_{removed}) \quad (4.4)$$

where

$f_{removed}$ = CO₂ removal fraction;

NTU = Number of transfer units.

Table 4.11: Summary of pilot plant absorber performance results for April 2017 pilot plant campaign.

Run	Liquid Rate	Gas Rate	L/G	IC/W	I	Liquid Side			Gas Side			
						PZ	LLDG	RLDG	Inlet CO ₂	Outlet CO ₂	Removal	NTU
	gpm	acfm	lb/lb	Y or N	°C	wt %	mol CO ₂ /mol alk	mol CO ₂ /mol alk	mol %	mol %		
1	18	600	3.8	Y/N	4	28.	0.23	0.37	12.0	1.43	89.1%	2.2
2	17	550	3.6	Y/N	4	27.	0.23	0.39	13.3	1.40	91.0%	2.4
3	15	350	4.8	Y/N	4	29.	0.23	0.39	20.1	3.59	85.4%	1.9
4	7	600	1.6	Y/N	4	29.	0.22	0.34	3.9	0.18	95.5%	3.1
5	4	350	1.6	N/N	4	28.	0.23	0.35	3.6	0.13	96.4%	3.3
6	22	350	7.3	Y/N	4	27.	0.26	0.35	13.5	0.19	98.8%	4.4
7	24	350	7.9	Y/N	4	27.	0.25	0.37	24.8	0.86	97.6%	3.7
8	24	350	8	Y/N	4	27.	0.26	0.38	24.4	0.87	97.5%	3.7
9	5	600	1.1	N/N	3	29.	0.23	0.39	4.0	0.42	89.6%	2.3
10	9	350	3	Y/N	4	28.	0.21	0.38	12.7	1.38	90.5%	2.4
11	18	350	5.8	N/N	6	30.	0.21	0.35	23.5	1.04	96.9%	3.5
12	18	350	5.9	Y/N	4	30.	0.21	0.37	26.4	0.44	98.9%	4.5
13	14	350	4.5	Y/N	4	29.	0.20	0.38	22.5	2.09	93.1%	2.7
14	14	350	4.6	Y/N	4	30.	0.20	0.37	23.7	0.67	98.0%	3.9
15	5	600	1.1	N/N	1	30.	0.17	0.34	4.0	0.06	98.6%	4.3
16	12	350	4	Y/Y	4	29.	0.23	0.35	12.4	1.65	88.0%	2.1
17	20	350	6.4	Y/Y	3	29.	0.23	0.36	23.9	2.35	93.1%	2.7
18	22	350	7.3	Y/Y	4	27.	0.23	0.35	20.3	2.80	89.0%	2.2
19	21	349	7.1	Y/Y	3	28.	0.22	0.33	22.1	1.11	96.2%	3.3
20	21	550	4.5	Y/Y	4	29.	0.22	0.33	13.3	0.70	95.6%	3.1
21	6	350	2.1	Y/Y	4	30.	0.22	0.29	3.1	0.04	98.6%	4.3
22	8	600	1.6	Y/Y	4	28.	0.20	0.32	4.2	0.25	94.2%	2.8
23	3	350	1.1	N/Y	4	31.	0.19	0.33	4.4	0.18	96.0%	3.2
24	15	350	4.8	Y/Y	4	29.	0.18	0.32	20.4	2.82	89.1%	2.2
25	12	600	2.6	Y/Y	4	28.	0.17	0.32	10.5	0.47	96.1%	3.3
26	16	350	5.3	Y/Y	4	29.	0.18	0.31	21.2	1.57	94.4%	2.9
27	6	600	1.2	Y/Y	4	28.	0.19	0.33	3.6	0.12	96.7%	3.4
28	6	600	1.3	N/Y	4	27.	0.23	0.39	3.8	0.43	89.2%	2.2
29	17	350	5.6	Y/Y	4	27.	0.23	0.37	17.7	0.52	97.7%	3.8

4.3.2 Absorber Intercooling

Absorber intercooling was tested at constant operating conditions in Runs 11 and 12 to isolate the benefits of the intercooling. In Run 11 the absorber achieved 96.9% CO₂ removal (~3.5 NTU) without intercooling; In Run 12 the absorber achieved 98.9% CO₂ removal (~4.5 NTU) with intercooling at 40 °C.

Darshan et al. found that intercooling was not required if the solvent was operated at a sufficiently low LLDG (Sachde, 2016). Pilot plant absorber performance at over-stripping lean loading and without intercooling was tested in the March 2015 campaign (Zhang et al., 2017b) and has been tested again in the April 2017 campaign. In Run 15 the absorber was operated at over-stripping lean loading (= 0.17 mol CO₂/mol alk) without any intercooling and achieved 98.6% CO₂ removal (~4.3 NTU). During the operation of Run 15, cooling water to the intercooling heat exchanger was not shut off and it resulted in precipitation of stagnant PZ in the intercooling heat exchanger by 55 °F cooling water. The intercooling heat exchanger was unplugged by heating it up to 90 °F using a heat gun. Absorber operation with PZ at extremely lean conditions requires careful operation and concerns regarding solid precipitation may limit the operating range of solvent loadings.

4.4 MODEL-PREDICTED ABSORBER PERFORMANCE

A consistent method for absorber model validation utilizing a rigorous data reconciliation method with the Independence PZ model was developed over a range of conditions for the October 2011 and November 2013 campaigns (Frailie, 2014; Plaza, 2011; Sachde et al., 2013). Based on the data reconciliation for previous campaigns, one of the two independent global corrections can be applied to the absorber model to match the pilot plant performance: interfacial area correction on packing model and CO₂ correction on loadings (Sachde et al., 2013). Only one of the two corrections can be

applied to the model and they should provide a consistent model prediction. In the March 2015 campaign, interfacial area correction and CO₂ correction (using density-predicted loadings) were applied independently to the pilot plant absorber model and the model was reasonably able to capture pilot plant-measured NTU and column temperature profiles with either correction (Zhang et al., 2017b). For the April 2017 campaign, the absorber was operated with a wider range of operating conditions and the existing pilot plant absorber model has been evaluated. In this section, the measured NTU has been compared with the predicted NTU using the existing pilot plant absorber model with and without interfacial area correction. The following measurements have been used in this analysis:

- Titration-corrected density-predicted lean loadings (Point 5 in Figure 4.2);
- Lean solvent flow rates by FT403 (Point 5 in Figure 4.2);
- Absorber inlet CO₂ by NDIR and FTIR averages (Point 1 in Figure 4.2);
- Inlet gas flow rates by FT900 (Point 1 in Figure 4.2);

4.4.1 Model-predicted NTU with and without Interfacial Area Correction

NTU has been defined in previous sections (Equation 4.4). The measured NTU was compared with the predicted NTU using the existing pilot plant absorber model with and without interfacial area correction. The specific solvent rate is defined by Equation 4.5. Column cross sectional area is 1.5 ft². Model-predicted NTU and measured NTU are compared in Table 4.12 and Figures 4.11 and 4.12. FTIR data was not available during aerosol tests: Runs 12, 16, 19, and 27; FTIR was down in Runs 7 and 8. NDIR measurements were used to calculate measured NTU for Runs 7, 8, 12, 16, 19, and 27. NDIR and FTIR averages were used to calculate measured NTU for the rest of the runs.

$$\text{Specific } L = \frac{L}{A} \tag{4.5}$$

where

L = lean solvent rate (lb/hr);

A = column cross sectional area (ft²).

Table 4.12: Comparison between measured NTU and predicted NTU using pilot plant absorber model with and without interfacial area correction.

Run	Solvent Rate (L)		Specific L lb/hr/ ft ²	Predicted NTU*		Measured NTU*	NTU* Ratio	
	lb/hr	gpm		With Area Correction	No Area Correction		With Area Correction	No Area Correction
1	10042	18	6525	2.0	2.2	2.2	0.9	1.0
2	9052	17	5882	1.8	2.0	2.4	0.7	0.8
3	8014	15	5207	1.9	2.0	1.9	1.0	1.0
4	4067	7	2643	2.5	2.8	3.1	0.8	0.9
5	2394	4	1555	2.4	2.6	3.3	0.7	0.8
6	12005	22	7800	4.3	4.4	4.4	1.0	1.0
7	13073	24	8495	5.0	5.3	3.6	1.3	1.4
8	13090	24	8506	4.9	5.2	3.6	1.3	1.4
9	2941	5	1911	1.8	2.2	2.3	0.8	1.0
10	4869	9	3164	2.0	2.1	2.3	0.8	0.9
11	9662	18	6278	1.7	1.8	3.3	0.5	0.5
12	9693	18	6298	2.5	2.7	4.3	0.5	0.6
13	7396	14	4806	1.9	2.1	2.6	0.7	0.8
14	7634	14	4960	2.1	2.2	3.8	0.5	0.6
15	2748	5	1785	3.0	3.4	4.3	0.7	0.8
16	6245	12	4058	2.6	2.9	2.1	1.2	1.4
17	10926	20	7099	2.9	4.9	2.5	1.1	1.8
18	12045	22	7826	4.4	5.4	2.2	2.0	2.4
19	11373	21	7390	4.9	5.8	3.2	1.5	1.8
20	11418	21	7419	2.5	3.8	3.1	0.8	1.2
21	3327	6	2162	3.2	3.8	4.3	0.8	0.9
22	4142	8	2691	2.4	3.1	2.9	0.9	1.1
23	1729	3	1123	2.1	2.8	3.2	0.7	0.9
24	7937	15	5157	3.6	5.2	2.2	1.6	2.3
25	6682	12	4342	2.4	3.2	3.2	0.7	1.0
26	8688	16	5645	4.7	6.2	2.8	1.6	2.2
27	3181	6	2067	2.3	3.2	3.4	0.7	0.9
28	3252	6	2113	1.6	2.1	2.2	0.7	1.0
29	9174	17	5961	3.3	4.9	3.7	0.9	1.3

* $NTU = \ln(1 - f_{removed})$

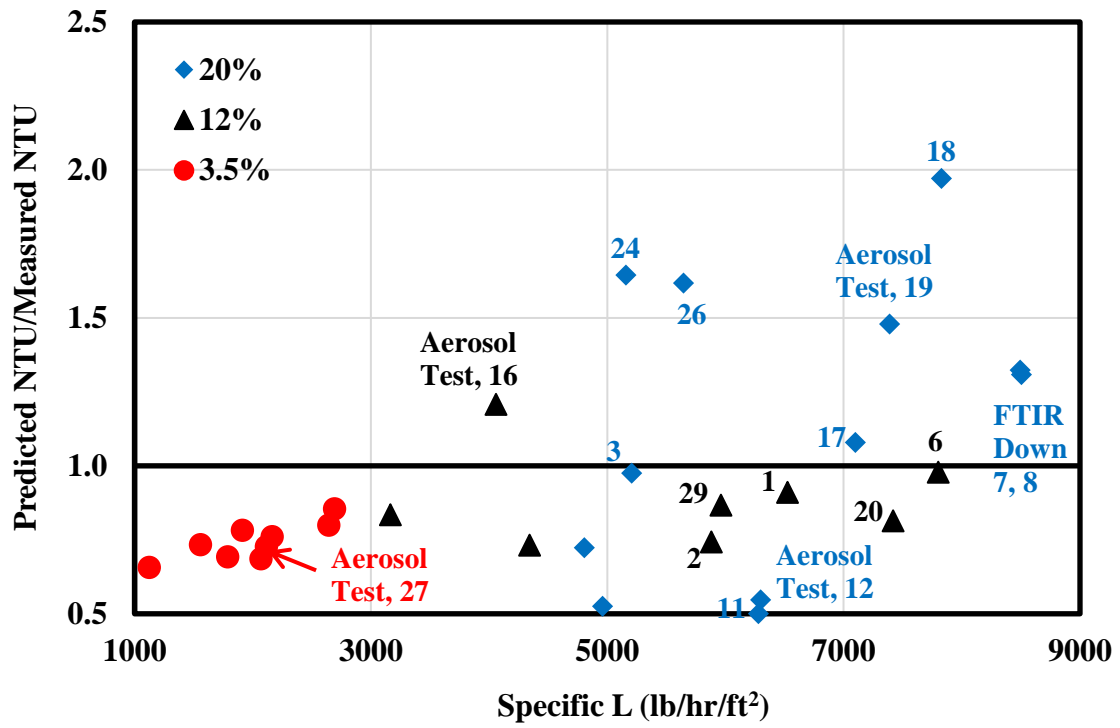


Figure 4.11: Comparison between measured NTU and predicted NTU using pilot plant absorber model with interfacial area correction.

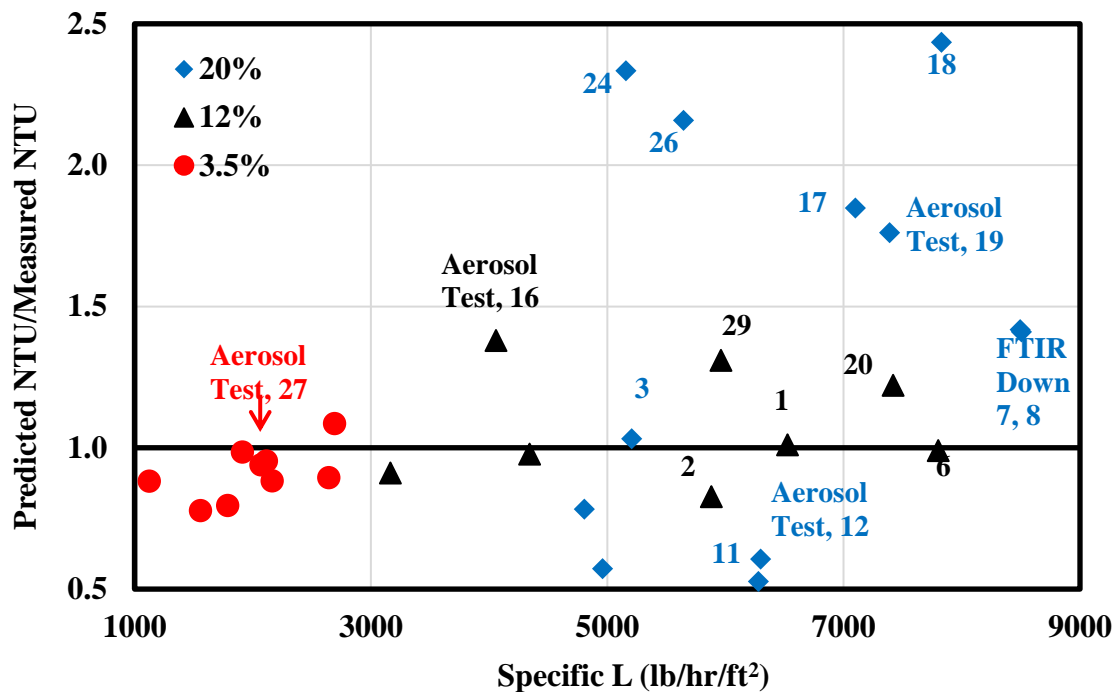


Figure 4.12: Comparison between measured NTU and predicted NTU using pilot plant absorber model without interfacial area correction.

Three Raschig DTS Trough distributors were installed on top of the three absorber packing beds to provide even wetting of the packing. After the campaign, the distributors were found to be undersized: all distributors were sized for 7 to 17 GPM but the absorber in several runs was operated at solvent rates up to 24 GPM. In these runs, the distributors may not perform well and NTU will be over-predicted by the model. All runs with solvent rate greater than 15 GPM have been marked in Figures 4.11 and 4.12: Runs 1, 2, 3, 6, 7, 8, 11, 12, 16, 17, 18, 19, 20, 24, 26, and 29. Table 4.13 summarizes predicted NTU for runs with solvent rate greater than 15 GPM and calculated percentage change of predicted NTU after taking interfacial area correction out from the pilot plant absorber model. Table 4.13 shows that the percentage changes of predicted NTU for Runs 1, 2, 3, 6, 7, 8, 11, and 12 are significantly smaller than that for Runs 16, 17, 18, 19, 20, 24, 26,

and 29. For Runs 1, 2, 3, 6, 7, 8, 11, and 12, the absorber was operated with excessive packing (30-ft packing) and was more likely to approach a pinch; the small relative changes of NTU also confirm that the absorber was operated near pinched conditions. When a pinch occurs in the column, the NTU is less sensitive to solvent distribution. For Runs 16, 17, 18, 19, 20, 24, 26, and 29, the absorber was away from pinch and the contacting problem (resulting from underperformance of distributors) could have a more significant impact on reducing NTU. Figure 4.13 and Figure 4.14 compare measured NTU and predicted NTU without Runs 16, 17, 18, 19, 20, 24, 26, and 29. Figure 4.13 shows that the model with interfacial area correction systematically under-predicts NTU except for Runs 7 and 8. Figure 4.14 compares the measured NTU with the predicted NTU using the absorber model without interfacial area correction and exhibits better fit than Figure 4.13. The pilot plant absorber model without interfacial area correction is better at capturing pilot plant-measured NTU than the model with interfacial area correction. At 3.5-12% CO₂, the model without interfacial area correction can capture the pilot plant absorber NTU within 20% error. At 20% CO₂, the model is able to capture the measured absorber NTU within 50% error. The distributors will be re-sized and the contacting problem will be fixed for future campaigns.

Table 4.13: Predicted NTU for runs with solvent rate greater than 15 GPM and calculated percentage change of predicted NTU.

Run	L gpm	Specific L lb/hr/ft ²	Predicted NTU		% Change
			With Area Correction	No Area Correction	
1	18	6525	2.0	2.2	11%
2	17	5882	1.8	2.0	11%
3	15	5207	1.9	2.0	6%
6	22	7800	4.3	4.4	1%
7	24	8495	5.0	5.3	7%
8	24	8506	4.9	5.2	8%
11	18	6278	1.7	1.8	5%
12	18	6298	2.5	2.7	11%
17	20	7099	2.9	4.9	71%
18	22	7826	4.4	5.4	23%
19	21	7390	4.9	5.8	19%
20	21	7419	2.5	3.8	50%
24	15	5157	3.6	5.2	42%
26	16	5645	4.7	6.2	33%
29	17	5961	3.3	4.9	51%

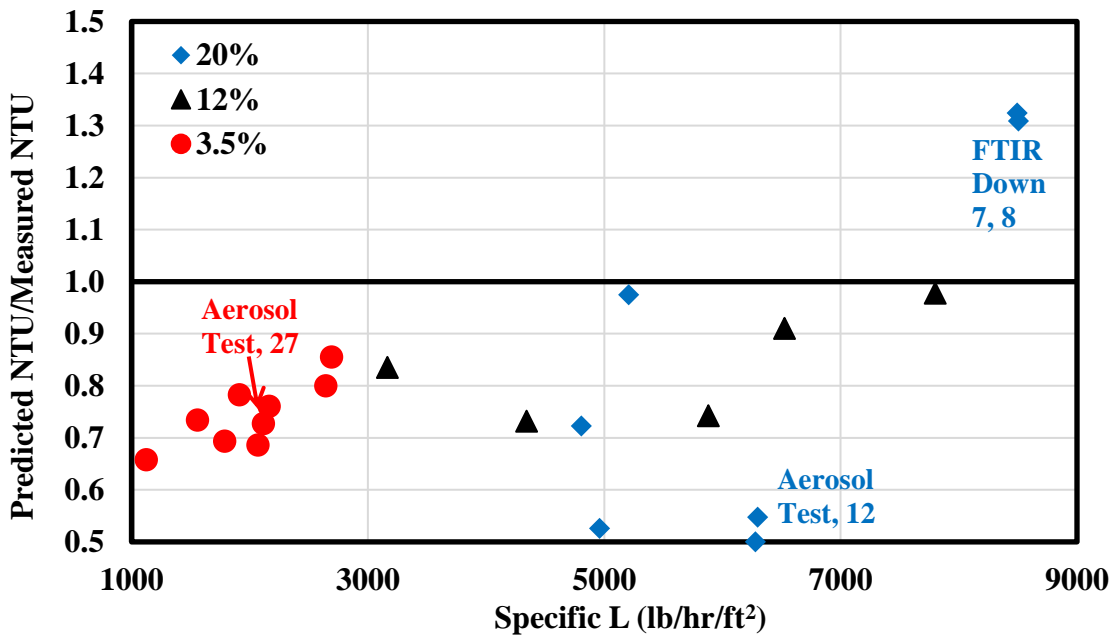


Figure 4.13: Comparison between measured NTU and predicted NTU using pilot plant absorber model with interfacial area correction. The model with interfacial area correction systematically under-predicts NTU except for Runs 7 and 8.

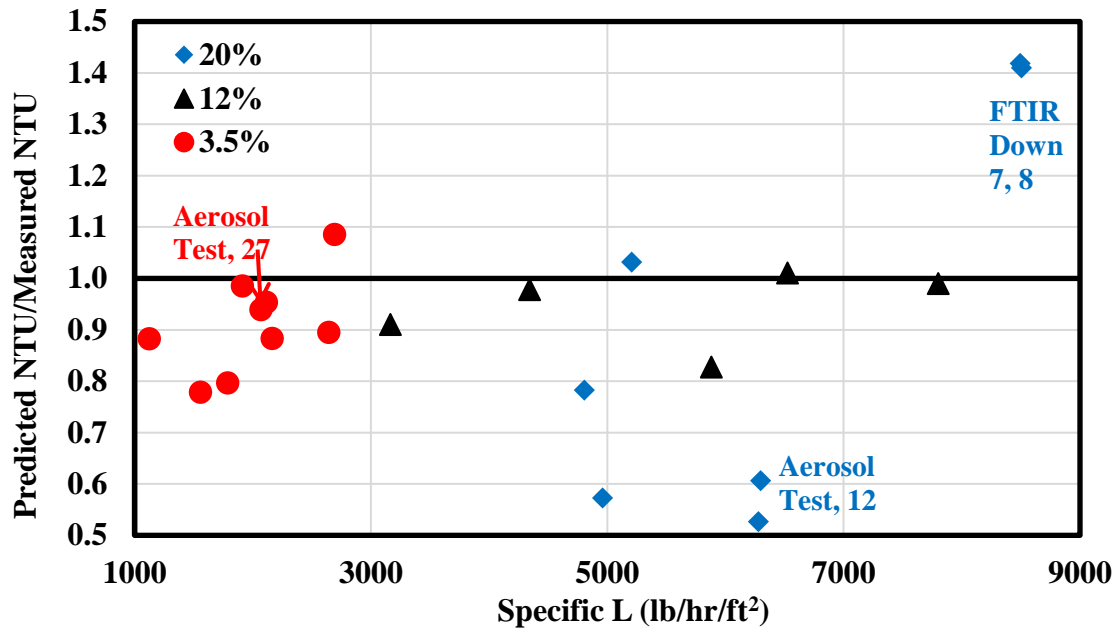


Figure 4.14: Comparison between measured NTU and predicted NTU using pilot plant absorber model without interfacial area correction. At 3.5-12% CO₂, the model without interfacial area correction can capture the measured absorber NTU within 20% error. At 20% CO₂, the model is able to capture the measured absorber NTU within 50% error.

4.4.2 Model-predicted NTU in Absorber Top and Bottom

Predicted and measured NTU in absorber top (top 10-ft section for 20-ft absorber or top 10-ft section for 30-ft absorber) and absorber bottom (bottom 10-ft section) have been compared in this work. An interfacial area correction (= 0.6) was applied to the model. Based on the CO₂ material balance check, the following measurements have been used in this analysis:

- Titration-corrected density-predicted lean and rich loadings;
- Density-predicted mid loadings;
- Absorber inlet and outlet CO₂ by NDIR and FTIR averages;
- Mid CO₂ by FTIR.

Table 4.14 compares NTU in absorber top and absorber bottom with interfacial area correction. FTIR data was not available during aerosol tests: Runs 12, 16, 19, and 27; FTIR was down in Runs 7 and 8. Table 4.14 exhibits large standard deviation between model prediction and pilot plant measurements. Figure 4.15 plots predicted and measured NTU in absorber top and Figure 4.16 plots predicted and measured NTU in absorber bottom. Runs 17, 18, 20, 24, 26, and 29 have been left out from Figures Figure 4.15 and Figure 4.16 due to contacting problem. Figure 4.15 shows that the model with interfacial area correction systematically under-predicts measured absorber top NTU for all runs, exhibiting similar trend as model-predicted absorber overall NTU in Figure 4.13. Figure 4.16 compares measured absorber bottom NTU and predicted absorber bottom NTU using pilot plant absorber model with interfacial area correction. The model can capture the measured absorber bottom NTU for most runs within 50% error. Errors of Runs 3, 11, and 28 exceed 300%, suggesting possible bias in mid CO₂ and mid loading measurements in these runs.

Table 4.14: Comparison of measured and predicted NTU of absorber top and absorber bottom with 0.6 interfacial area correction in April 2017 pilot plant campaign.

Run	Absorber Top			Absorber Bottom		
	Measured NTU	Predicted NTU	Predicted/Measured	Measured NTU	Predicted NTU	Predicted/Measured
1	1.9	1.6	0.8	0.3	0.4	1.4
2	2.1	1.5	0.7	0.3	0.5	1.7
3	1.9	1.7	0.9	0.0	0.3	6.3
4	2.5	1.7	0.7	0.6	0.8	1.2
5	2.7	1.6	0.6	0.7	0.8	1.2
6	3.2	2.8	0.9	1.2	1.5	1.3
7		3.8			1.2	
8		3.8			1.1	
9	2.0	1.5	0.8	0.3	0.2	0.6
10	2.1	1.8	0.8	0.2	0.4	1.8
11	3.2	1.3	0.4	0.2	0.8	4.0
12		5.4			0.8	
13	2.2	2.0	0.9	0.4	0.5	1.5
14	3.4	2.4	0.7	0.4	0.6	1.4
15	3.7	2.4	0.6	0.6	0.5	0.8
16		1.9			0.7	
17	1.7	2.9	1.6	0.8	1.1	1.4
18	1.7	3.1	1.8	0.5	1.3	2.6
19		3.2			1.8	
20	1.9	1.8	0.9	1.2	0.9	0.8
21	2.7	1.7	0.6	1.5	1.6	1.0
22	2.1	1.4	0.7	0.7	0.9	1.3
23	2.6	1.6	0.6	0.7	0.6	0.9
24	1.8	3.2	1.8	0.4	0.8	1.9
25	2.1	1.6	0.8	1.1	1.2	1.1
26	2.2	3.7	1.7	0.6	1.3	2.1
27		1.4			0.9	
28	2.0	1.0	0.5	0.2	0.6	3.3
29	3.4	2.7	0.8	0.3	0.9	2.8
Average			0.9			1.8
Standard Deviation			0.41			1.29

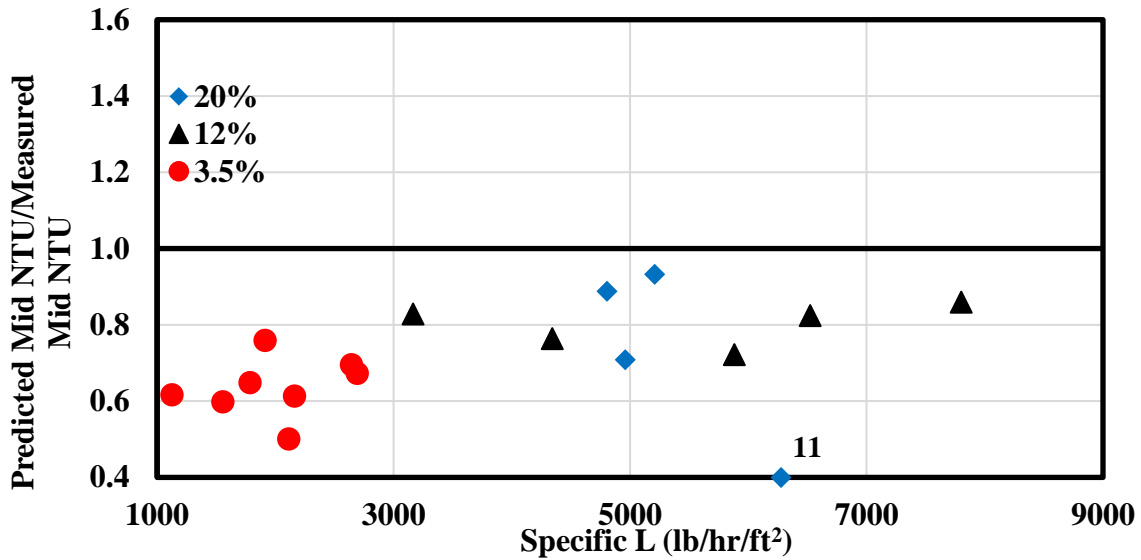


Figure 4.15: Comparison between measured absorber top NTU and predicted absorber top NTU using pilot plant absorber model with interfacial area correction. The model with interfacial area correction systematically under-predicts measured absorber top NTU for all runs. This exhibits similar trend as absorber overall NTU prediction in Figure 4.13.

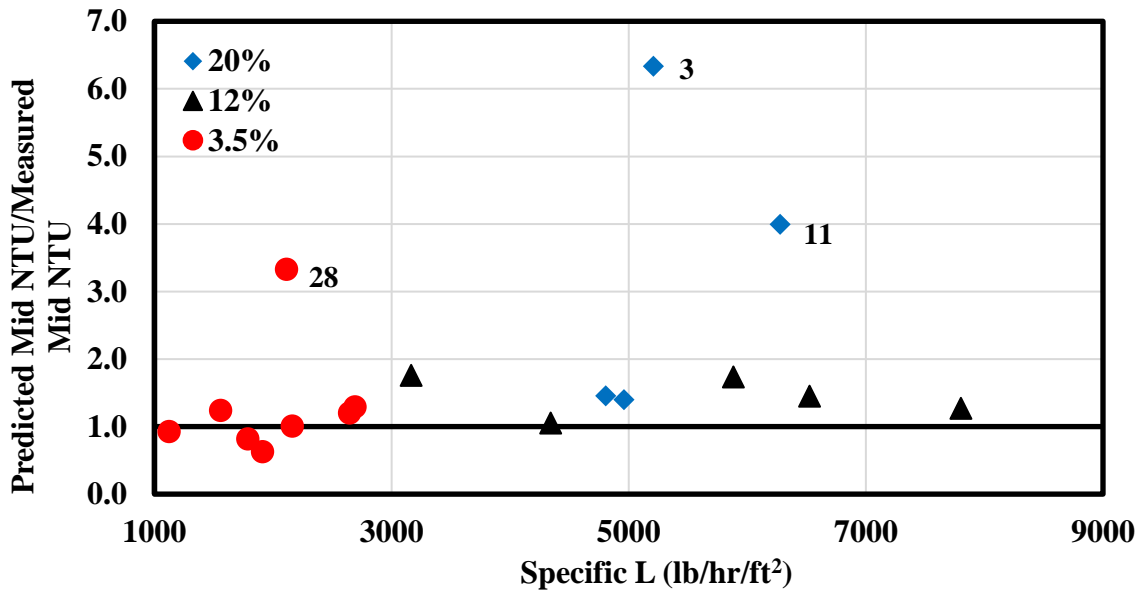


Figure 4.16: Comparison between measured absorber bottom NTU and predicted absorber bottom NTU using pilot plant absorber model with interfacial area correction. The model can capture the measured absorber bottom NTU for most runs within 50% error.

4.5 CONCLUSIONS AND RECOMMENDATIONS

4.5.1 Conclusions

UT-SRP absorber has excessive packing.

NDIR measurements systematically over-predicted removal at 3.5% inlet CO₂ and under-predicted removal at 20% inlet CO₂; FTIR measurements were more scattered and systematically over-predicted removal at 8-20% inlet CO₂. These findings suggested possible errors of NDIR measurements at low outlet CO₂ and high inlet CO₂ as well as systematic bias of FTIR measurements. The averages of NDIR and FTIR were found to give the best overall CO₂ material balance closure.

The pilot plant absorber CO₂ material balance closed within +/- 20% when using titration-corrected density-predicted loadings on the liquid side and NDIR and FTIR average data on the gas side. No systematic trends were observed.

After the campaign, the three Raschig DTS Trough distributors were found to be undersized: all distributors were sized for 7 to 17 GPM but the absorber in several runs was operated at solvent rates up to 24 GPM. In these runs, NTU was over-predicted by the model.

The pilot plant absorber model without interfacial area correction was better at capturing pilot plant-measured NTU than the model with interfacial area correction. At 3.5-12% CO₂, the model without interfacial area correction could capture the pilot plant absorber NTU within 20% error. At 20% CO₂, the model captured the measured absorber NTU within 50% error.

4.5.2 Recommendations for Future Campaigns

The pilot plant absorber should be operated at pinched and not pinched conditions. Equilibrium data can be obtained when absorber is pinched and packing data can be obtained when absorber is not pinched.

In the data reconciliation of all previous campaigns, one global correction factor was applied to the pilot plant absorber to cover all underlying factors. For the data reconciliation of future campaigns, two corrections should be applied to the model at the same time: equilibrium correction (correct for errors in solvent loading measurements and effects of degradation) and packing correction (correct for effects of rivulets and drop and additional mass transfer caused by distributors and chimney trays). In this way, better understandings of equilibrium and packing performance can be obtained.

If the absorber is running with excessive packing and high removal, gas and liquid measurements should be obtained between the packing sections. The outlet CO₂ might be below the detection limit of gas analyzers in some packing sections.

NDIR and FITR should be calibrated carefully in future campaigns.

The liquid distributors have been found to be under-sized in the April 2017 campaign. The distributors will be re-sized and the contacting problem will be fixed for future campaigns.

Viscosity data should be collected to account for solvent degradation effects.

4.6 ACKNOWLEDGEMENTS

The author would like to acknowledge Paul Nielsen for titration data. The author gratefully acknowledges financial support from the Texas Carbon Management Program and the CO₂ Capture Pilot Plant Project in the preparation of this work. Aspen Plus[®] proprietary software was provided by an academic license from AspenTech[®].

AspenTech® and Aspen Plus® are trademarks of Aspen Technology, Inc. All rights reserved.

Chapter 5 : Absorber Modeling for Carbon Capture from Natural Gas Applications³

A hybrid system combining amine scrubbing with membrane technology for carbon capture from natural gas combined cycle (NGCC) power plants is proposed in this paper. In this process, the CO₂ in the flue gas can be enriched from 4% to 18% by the membrane, and the amine scrubbing system will have lower capture costs. Aqueous piperazine (PZ) is chosen as the solvent. Different direct contact cooler (DCC) options, multiple absorber operating conditions, optimal intercooling designs, and different cooling options have been evaluated across a wide range of inlet CO₂. Amine scrubbing without DCC is a superior design for NGCC carbon capture. Pump-around cooling at the bottom of the absorber can effectively manage the temperature of the hot flue gas, and still be effective for CO₂ absorption. The absorber gas inlet must be designed to avoid excessive localized temperature and solvent evaporation. When the inlet CO₂ increases from 4% to 18%, the total absorption costs decrease by 60% and the total regeneration costs remain the same. For hybrid capture, as the inlet CO₂ increases from 12% to 18%, the total membrane costs increase by 108%. Another 10% of the total absorber CAPEX can be saved by eliminating the DCC. In-and-out intercooling works well for high CO₂, while pump-around intercooling is more effective for low CO₂. Dry cooling requires more packing and energy but appears to be technically and economically feasible if cooling water availability is limited.

³Part of this chapter has been published in Zhang, Y., Freeman, B., Hao, P., Rochelle, G., 2016. Absorber Modeling for NGCC Carbon Capture with Aqueous Piperazine. *Faraday Discuss.* 192, 459–477. doi:10.1039/C6FD00030D. In Chapter 5.6.2, Ding calculated the regeneration CAPEX and OPEX; Hao calculated the membrane CAPEX and OPEX. Freeman and Rochelle supervised the project and contributed to the interpretation of the results.

5.1 INTRODUCTION

Amine scrubbing system optimization usually concerns the trade-off between capital expenses (CAPEX) and operating expenses (OPEX). CAPEX can be approximated as absorber packing volume and OPEX can be approximated as stripper equivalent work (Frailie, 2014). Membrane Technology and Research (MTR) previously proposed a hybrid system combining amine scrubbing with membrane technology for carbon capture from coal-fired power plants (Freeman et al., 2014; Merkel et al., 2013; Johannes G Wijmans et al., 2011). Maintaining the same overall CO₂ removal rate, flue gas CO₂ could be enriched by the membrane from 12% to 23%, and the flue gas volume entering the amine scrubbing system could be reduced by 47% (Freeman et al., 2014). With higher CO₂ driving force across the column and treating less amount of gas, the absorber requires less packing while stripper equivalent work still remains the same (Freeman et al., 2014; Wilcox, 2012).

As electricity generation fueled by natural gas grows fast in the U.S., compared with coal-fired power plants, natural gas-fired power plants are relatively easier to construct and emit fewer pollutants (Center for Climate and Energy Solutions, 2013). However, compared with applications with high CO₂, amine scrubbing is less attractive for natural gas combined cycle (NGCC) plants with 4% CO₂ (Rochelle, 2009). In this chapter, a membrane-amine hybrid carbon capture system for the natural gas combined cycle (NGCC) power plants has been discussed. Simple NGCC includes a combustion turbine and a heat recovery steam generator (HRSG) to capture waste heat and improve energy efficiency (DOE/NETL, 2011, 2010), with flue gas containing 4% CO₂. Figure 5.1 shows a simplified process flow diagram of an NGCC plant with amine scrubbing carbon capture. As an improvement of simple NGCC plants, an exhaust gas recycle (EGR) from downstream of the HRSG is applied to decrease the gas volume and increase

the CO₂ in the absorber inlet flue gas stream, as shown in Figure 5.2. With 35% EGR, CO₂ in the flue gas will be enriched to 6%. However, in the proposed membrane-amine hybrid capture process, the CO₂ in the flue gas can be enriched to 18% (Zhang and Rochelle, 2014), as shown in Figure 5.3.

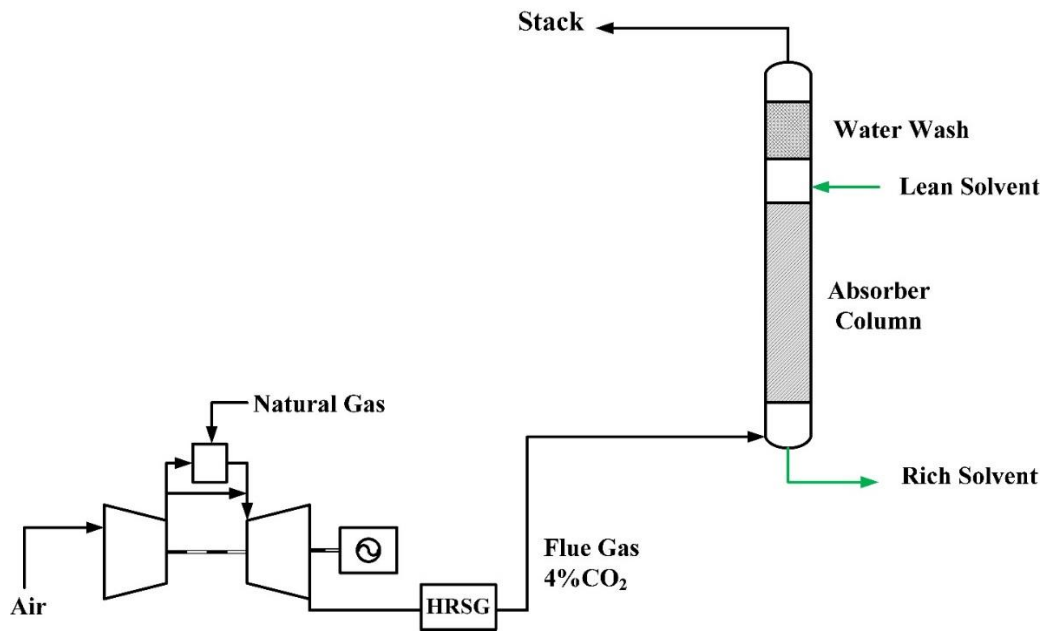


Figure 5.1: Process flow diagram of a simple natural gas combined cycle (NGCC) plant with amine scrubbing.

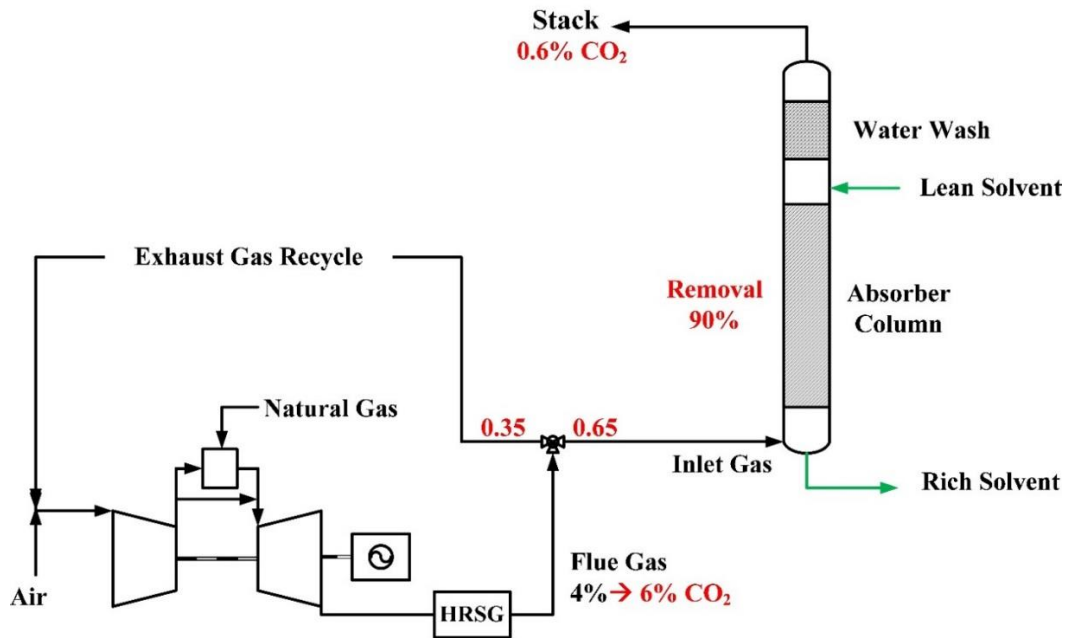


Figure 5.2: Process flow diagram of an NGCC plant with 35% exhaust gas recycle (EGR) with amine scrubbing.

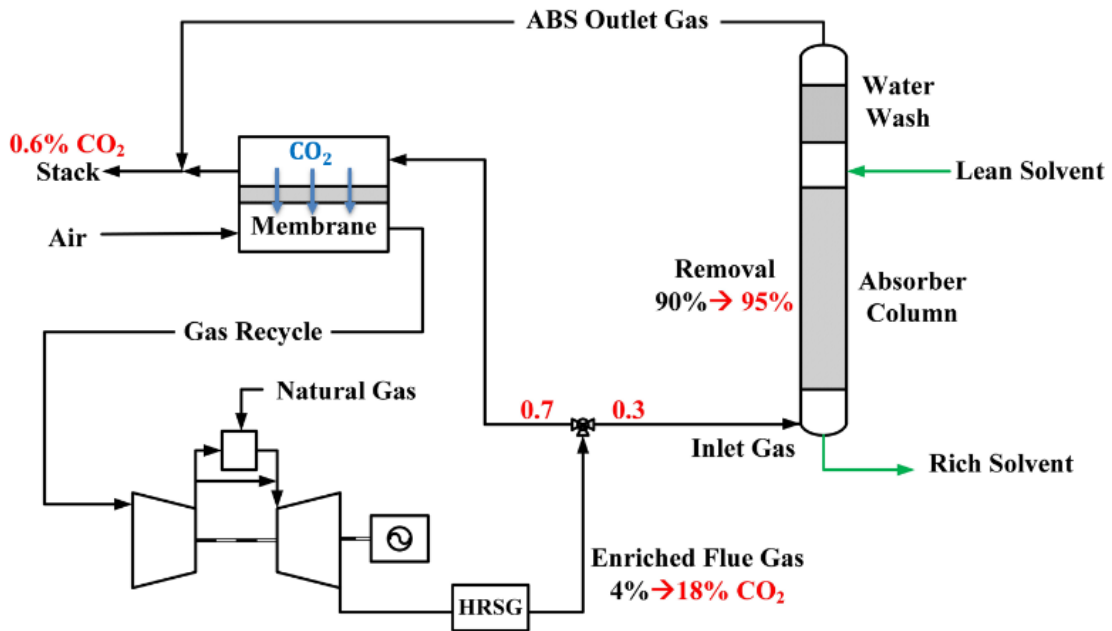


Figure 5.3: Process flow diagram of an NGCC plant with membrane-amine hybrid carbon capture.

Previous study on NGCC capture mainly utilized 30 wt% monoethanolamine (MEA) and 8 molal (8 m, 40 wt%) PZ (Berstad et al., 2011; Gaspar et al., 2016; Rongrong et al., 2008; Sachde and Rochelle, 2014; Sipöcz and Tobiesen, 2012; Ystad et al., 2012). With fast absorption rate, low viscosity, relatively wide solubility window, and good energy performance, 5 m (30 wt %) PZ is evaluated as the solvent for NGCC carbon capture in this study (Chen et al., 2014; Li, 2015; Rochelle et al., 2011). The solid solubility window for 5 m PZ is shown in Figure 5.4 (Chen et al., 2014). When operated at low CO₂ loading, careful plant operation and shutdown procedures should be followed to avoid solid precipitation. HMPD (3-hydroxy-1-methyl-piperidine) is a cyclic and tertiary amine (Du et al., 2016). The solvent blend of 2 m PZ/3 m HMPD has larger CO₂ capacity and greater thermal stability (Du et al., 2016) thus it is also evaluated in this work.

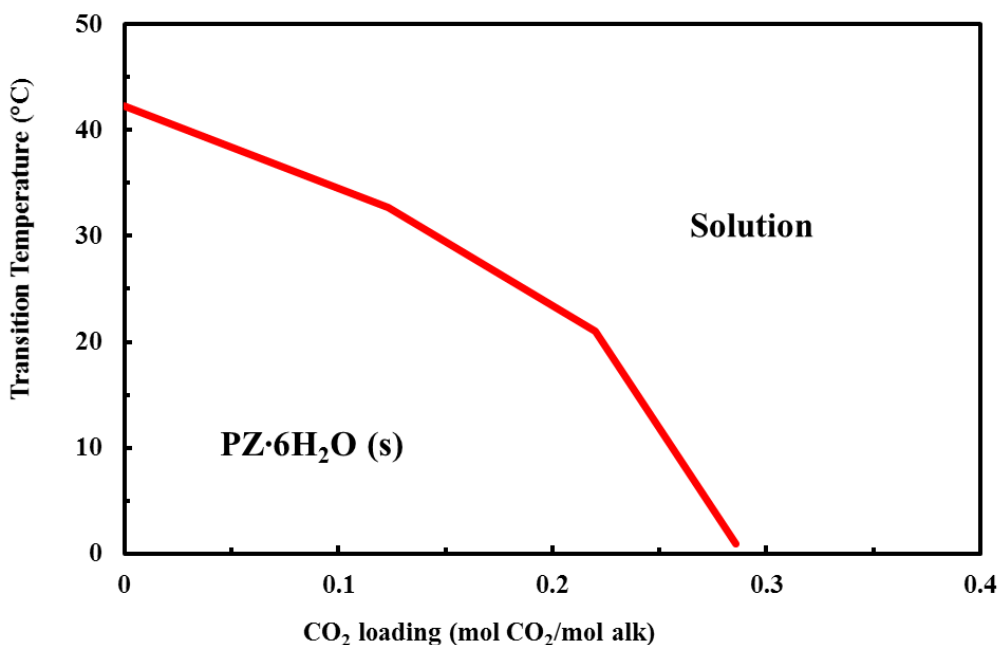


Figure 5.4: Solid solubility of 5 m PZ (Chen et al., 2014).

Previous absorber modeling work for NGCC amine scrubbing carbon capture mainly focused on absorbers without intercooling or with simple intercooling, and none of

them have utilized optimal cooling options or evaluated absorber with a wide range of operating conditions (Berstad et al., 2011; Gaspar et al., 2016; Plaza, 2011; Sachde and Rochelle, 2014; Sachde, 2016; Sipöcz and Tobiesen, 2012; Ystad et al., 2012). This study evaluates the absorber with different direct contact cooler (DCC) options, multiple intercooling designs, different cooling options, and a wide range of lean loadings (LLDG) at 4% to 18% inlet CO₂.

5.2 MODELING METHODS

The absorber is modeled as rate-based in Aspen Plus[®] RateSep[™], which includes solvent model (thermodynamics, kinetics, and physical properties) and rigorous unit operation. The PZ solvent model used in this work was developed by Frailie (Frailie, 2014) and the PZ/HMPD model was developed by Sherman (Sherman, 2016).

The thermodynamic framework represents experimental amine pK_a, CO₂ solubility, heat capacity, speciation, and amine volatility data for the amine-H₂O-CO₂ system by regression of Gibbs free energy, enthalpy, heat capacity and activity coefficient parameters within the electrolyte non-random two liquid (e-NRTL) framework. Rate expressions for kinetic reactions and diffusion coefficients were regressed from wetted wall column data collected over a range of temperature, solvent concentration, and loading relevant for capture applications considered in this work. Finally, physical property models (e.g., viscosity and density) were regressed as a function of amine concentration, loading, and temperature.

The absorber was modeled rigorously with the Aspen Plus[®] RateSep[™] unit operation, which solves multi-component mass transfer with chemical reaction coupled with heat transfer. The rate-based absorber calculation requires detailed information on packing mass transfer performance represented by transport sub-models. Separate

models for interfacial area (Tsai, 2010) and gas- and liquid-side physical mass transfer coefficients (Wang, 2015) were developed from data collected at the Separations Research Program (SRP) pilot scale air-water column for a variety of packing types.

5.3 SIMPLE NGCC, SCRUBBING WITH 5 M PZ

5.3.1 Absorber Configurations and Design Conditions

For an NGCC plant, amine scrubbing designs were based on the flue gas information shown in Table 5.1 (DOE/NETL, 2011).

Table 5.1: Flue gas information for NGCC.

Flow rate (kmol/hr)	113,831
T (°C)	143
P (bar)	1
Composition (mol%)	
CO ₂	4.0%
H ₂ O	8.7%
N ₂	74.3%
Ar	0.9%
O ₂	12.1%

*Flue Gas Info is before the DCC

The absorber is designed to achieve 90% removal. Multiple lean loadings (LLDG) have been evaluated. An intermediate LLDG of 0.182 (mol CO₂/mol alk) has been chosen for the final design. The intermediate lean loading is established by setting the 0.1 ratio of the equilibrium partial pressure of CO₂ over the lean solvent and the partial

pressure of the absorber outlet CO₂. Three cooling options are available (DOE/NETL, 2010). Parallel cooling and wet cooling have been evaluated for simple NGCC capture.

Dry Cooling: Water wash water is cooled in air coolers. The solvent is cooled by ambient air in absorber air-intercoolers.

Parallel Cooling: Water wash water is cooled in air coolers. Absorber intercoolers use available cooling water at the site.

Wet Cooling: Both water wash and absorber intercoolers use available cooling water at the site.

Absorber intercooling (IC) can reduce the column temperature bulge to improve the mass transfer rate, and has been proposed and evaluated by several previous researchers (Karimi et al., 2011; Kvamsdal et al., 2011; Kvamsdal and Rochelle, 2008; Plaza, 2011; Sachde and Rochelle, 2014). The direct contact cooler (DCC) can cool the hot flue gas by contact with cooling water before entering the absorber. Absorber designs have been evaluated with IC/no DCC (Figure 5.5), with DCC and IC (Figure 5.6), and with DCC/no IC (Figure 5.7). The intercooling solvent recycle rate (L_R) was set at five times the gas rate (G) without DCC and three times the gas rate with DCC. A brief description of the absorber configurations and cooling options evaluated follows.

With IC and no DCC (Figure 5.5)

Parallel Cooling: 3 absorber beds; middle (Mid) pump-around (PA) intercooling (IC), and bottom (Bot) pump-around (PA) intercooling (IC); water wash (WW) at 48 °C, IC at 40 °C; $L_R/G = 5$.

With DCC and IC (Figure 5.6)

Wet Cooling: 3 absorber beds; Mid Advanced PA IC; WW and IC at 40 °C; $L_R/G = 3$.

With DCC and no IC (Figure 5.7)

Wet Cooling: 1 absorber bed; No IC; WW at 40 °C.

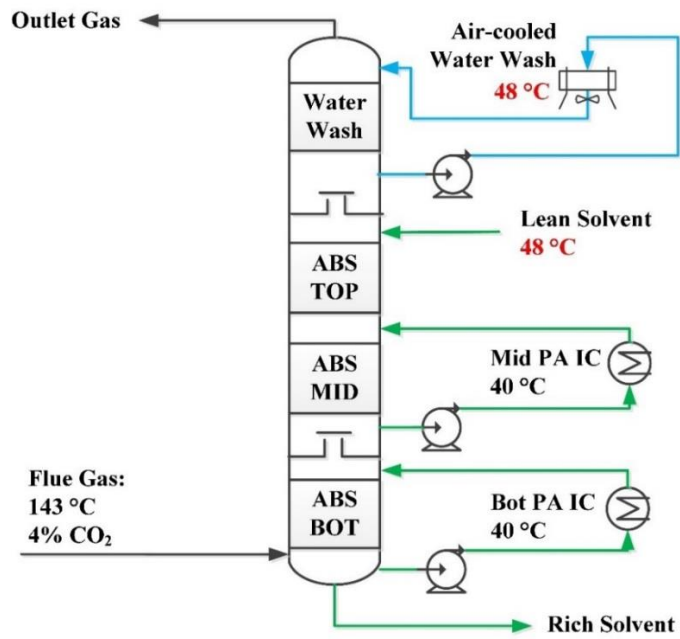


Figure 5.5: Absorber configuration with IC and no DCC.

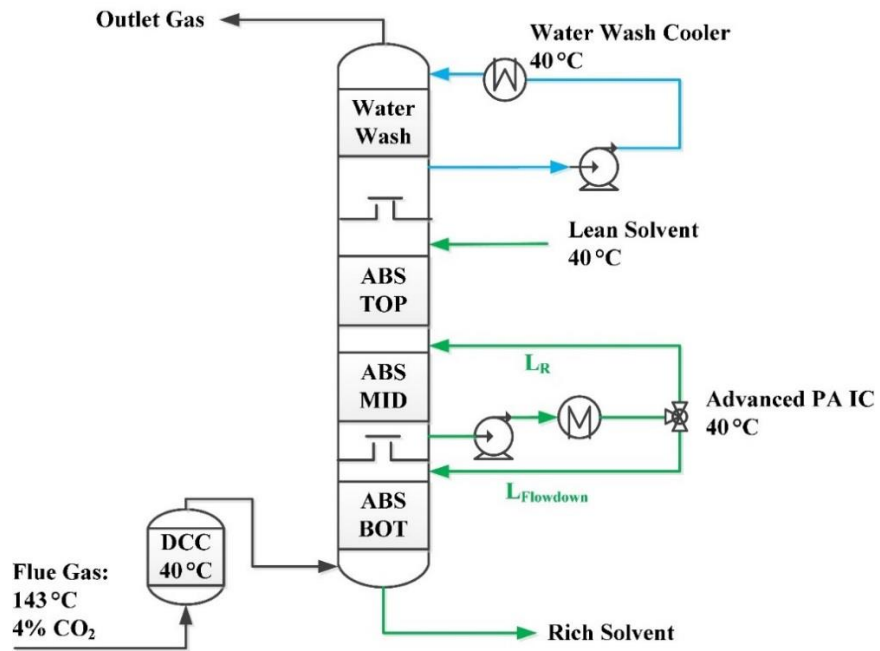


Figure 5.6: Absorber configuration with DCC and IC.

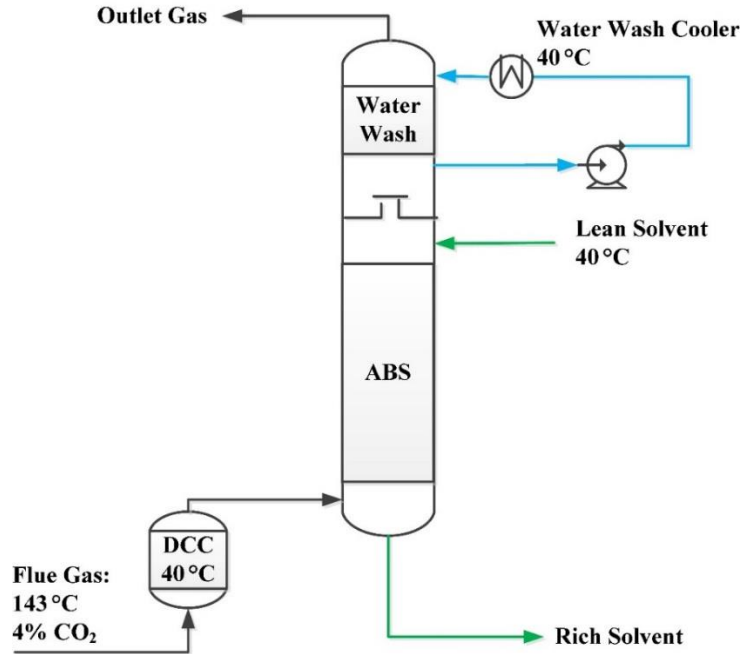


Figure 5.7: Absorber configuration with DCC and no IC.

For absorber without DCC, the hot flue gas will be sent directly to the bottom of the absorber. The absorber gas inlet must be designed to avoid excessive localized temperature and solvent evaporation. The water wash section was operated at 48 °C to maintain the water balance in the absorber. Any water picked up by the gas stream from the solvent in the absorber needs to be condensed in the water wash section. As a result of operating a hot water wash section, amine volatility might become a problem but this issue is not in the scope of this paper. Since the cooling water temperature achieved in the air cooler would be higher than that achieved with wet cooling, this design demonstrates the potential feasibility of applying air coolers to the water wash. Two intercoolers at 40 °C were applied to the absorber: a pump-around intercooling (PA IC) applied to the bottom of the column to cool down the hot flue gas, and another PA IC applied to the middle of the column to reduce the temperature bulge. Mellapak 250X structured packing was used for the packed sections without solvent recycle, and coarse structured packing Mellapak

2X was used for the pump-around recycle sections to minimize pressure drop and match flooding fractions along the absorber column (Sachde and Rochelle, 2014), as shown in Figure 5.5.

For the absorber with DCC, advanced pump-around (PA) intercooling (IC) at 40 °C has been applied. The advanced PA IC recycles the cooled solvent back to the upper bed and still allows for a stream flowing to the next stage, as depicted in Figure 5.6 (Sachde and Rochelle, 2014). The absorber has been tested with and without IC to evaluate the potential benefits of intercooling at 0.182 (mol CO₂/mol alk) LLDG.

5.3.2 Absorber Performance

The absorber packing distribution has been optimized to get the minimum total packing interfacial area using the Aspen Plus[®] Independence Model (Frailie, 2014). For each design, L/L_{min} was set at 1.2 (mol/mol). The model calculates solvent rate, rich loading, optimal packing distribution, and normalized packing for each design. The normalized packing area (NP) reflects the absorber efficiency. A lower value for NP indicates better absorber performance. The NP is also the reciprocal of the average CO₂ flux, shown in Equation 5.1. Normalized flux is the CO₂ vapor flux divided by the CO₂ vapor mole fraction (Equation 5.2).

Table 5.2 compares the absorber performance. Figures 5.8 to 5.10 show the column temperature and flux profiles.

$$NP = \frac{\text{Total surface area}}{\text{Total Gas flow rate} * CO_2 * \text{Removal}} \quad (5.1)$$

$$\text{Normalized Flux} = \frac{CO_2 \text{ Vapor Flux}}{CO_2 \text{ vapor mol fraction}} \quad (5.2)$$

Table 5.2: Absorber performance with/without DCC and with/without IC at intermediate LLDG = 0.182 (mol CO₂/mol alk) for simple NGCC with 5 m PZ.

RLDG mol CO ₂ /mol alk	ΔLDG		L _R /G mol/mol	L/G TOP	Packing Area Fraction		NP m ² /(mol/sec)
	mol CO ₂ /mol alk	mol/mol			MID	BOT	
Parallel Cooling, With IC and no DCC							
0.353	0.171	5	1.3	42%	31%	27%	399
Wet Cooling, With DCC and IC							
0.353	0.171	3	1.3	39%	25%	36%	410
Wet Cooling, With DCC and no IC							
0.353	0.171		3	1.3	100%		514

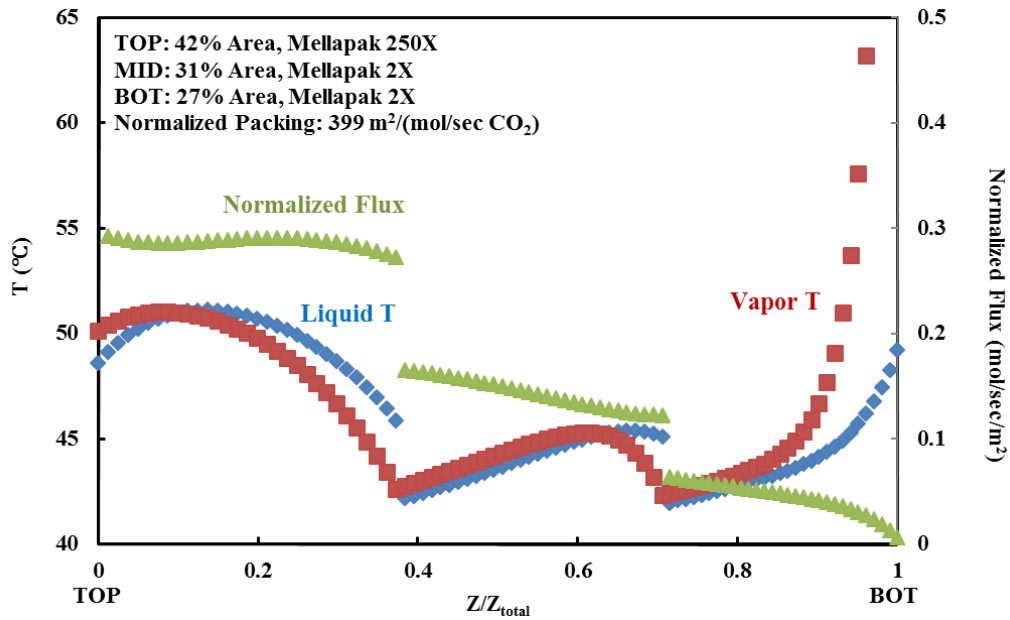


Figure 5.8: Temperature and flux profiles with IC and no DCC with 5 m PZ. Inlet CO₂ at 4%; Water wash at 48 °C; Mid PA IC and Bot PA IC at 40 °C; L_R/G = 5; Intermediate LLDG = 0.182 (mol CO₂/mol alk); L = 1.2*L_{min}.

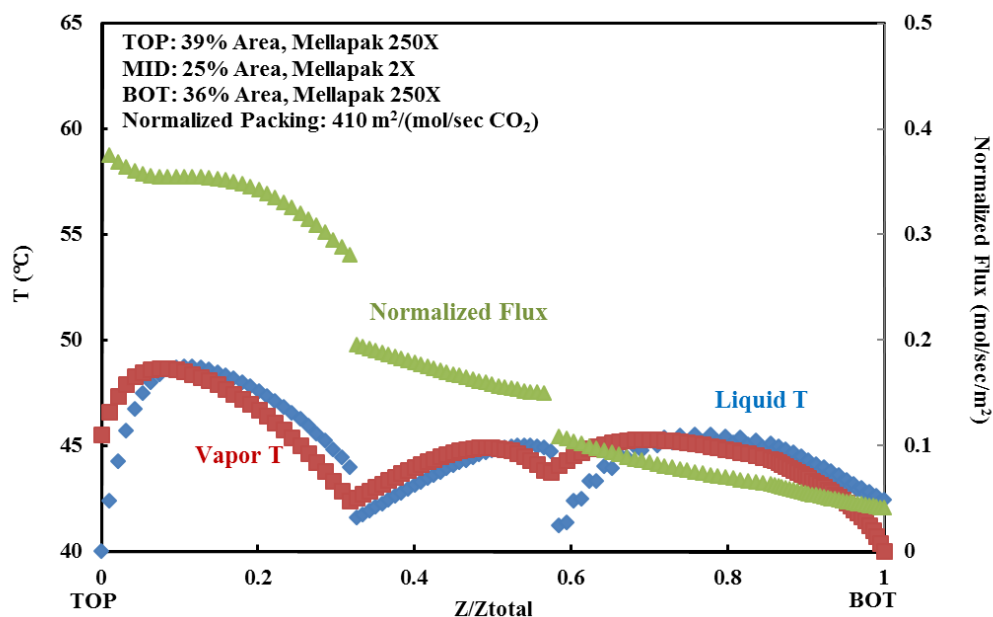


Figure 5.9: Temperature and flux profiles with DCC and IC with 5 m PZ. Inlet CO₂ at 4%; Mid Advanced PA IC at 40 °C; L_R/G = 3; Intermediate LLDG = 0.182 (mol CO₂/mol alk); L = 1.2*L_{min}.

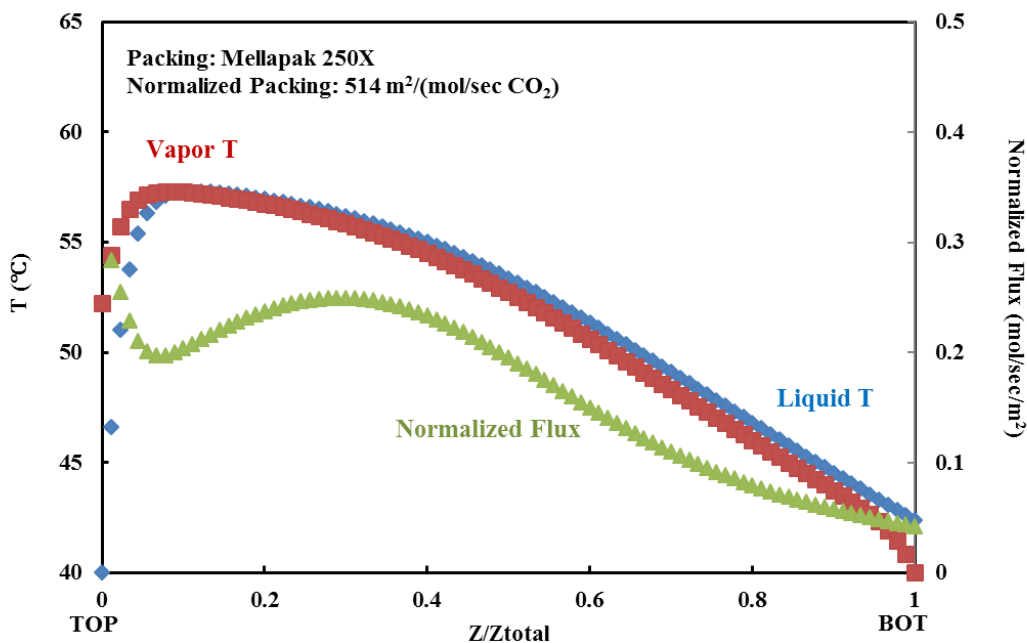


Figure 5.10: Temperature and flux profiles with DCC and no IC with 5 m PZ. Inlet CO₂ at 4%; Intermediate LLDG = 0.182 (mol CO₂/mol alk); L = 1.2*L_{min}.

Table 5.2 shows that the design without DCC gives minimum absorber packing volume with same energy (as shown by same Δ LDG and L/G (Y.-J. Lin and Rochelle, 2016)). With IC and no DCC, Figure 8 shows that the absorber bottom pump-around intercooling can effectively cool the inlet hot flue gas from 143 °C to 43 °C, and give a reasonable model predicted rich solvent outlet temperature (less than 50 °C), with no solvent degradation issue. Absorber gas inlet must be designed to avoid excessive localized temperature and solvent evaporation. The flux profile in Figure 8 also shows that the bottom pump-around cooling loop is still effective for CO₂ absorption while replicating the cooling effect of a DCC. With IC, both Figure 5.8 and Figure 5.9 show relatively uniform temperature profiles across the column, suggesting that adequate absorber performance can be achieved. However, with DCC and no IC, Figure 5.10 shows that a temperature bulge develops at the lean end of the column. At low L/G, gas carries the heat released by absorption, and pushes the temperature bulge to the top of the column. The temperature bulge reduces CO₂ driving force at the lean end, but the large driving force brought by the 0.182 (mol CO₂/mol alk) LLDG compensates for that, so the temperature bulge does not result in a mass transfer pinch. The potential benefits of intercooling at extremely low LLDG are not as evident as those at high LLDG.

5.4 NGCC WITH 35% EGR, SCRUBBING WITH 5 M PZ

5.4.1 Absorber Configurations and Design Conditions

For an NGCC plant with 35% EGR, amine scrubbing designs were based on the flue gas information shown in Table 5.3 (DOE/NETL, 2011).

Table 5.3: Flue gas information for NGCC with 35% EGR.

Flow rate (kmol/hr)	72,164
T (°C)	135
P (bar)	1
Composition (mol %)	
CO ₂	6.3%
H ₂ O	10.1%
N ₂	74.9%
Ar	0.9%
O ₂	7.8%

*Flue Gas Info is before the DCC

The absorber is operated at 90% removal with intercooling. An intermediate LLDG of 0.21 (mol CO₂/mol alk) has been evaluated, which is established by 0.1 ratio of the equilibrium partial pressure of CO₂ over the lean solvent and the partial pressure of the absorber outlet CO₂. Absorber configurations and cooling options for simple NGCC capture have been discussed in the previous section, and similar designs have been evaluated for NGCC with EGR. A brief description follows:

With IC and no DCC (Figure 5)

Parallel Cooling: 3 absorber beds; middle (Mid) pump-around (PA) intercooling (IC), and bottom (Bot) pump-around (PA) intercooling (IC); water wash (WW) at 48 °C, IC at 40 °C; L_R/G = 5.

With DCC and IC (Figure 6)

Wet Cooling: 3 absorber beds; Mid Advanced PA IC; WW and IC at 40 °C; L_R/G = 3.

5.4.2 Absorber Performance

L/L_{\min} was also set at 1.2 (mol/mol), and the absorber packing distribution has been optimized. Table 5.4 compares model-calculated absorber performance and normalized packing with and without DCC. Figure 5.11 and Figure 5.12 show the corresponding column temperature and flux profiles.

Table 5.4: Absorber performance with and without DCC at intermediate LLDG = 0.210 (mol CO₂/mol alk) with 5 m PZ.

RLDG mol CO ₂ /mol alk	Δ LDG mol CO ₂ /mol alk	L_R/G mol/mol	L/G mol/mol	Packing Area Fraction			NP m ² /(mol/sec)
				TOP	MID	BOT	
Parallel Cooling, With IC and no DCC							
0.368	0.158	5	2.3	30%	34%	35%	302
Wet Cooling, With DCC and IC							
0.369	0.159	3	2.2	32%	34%	34%	310

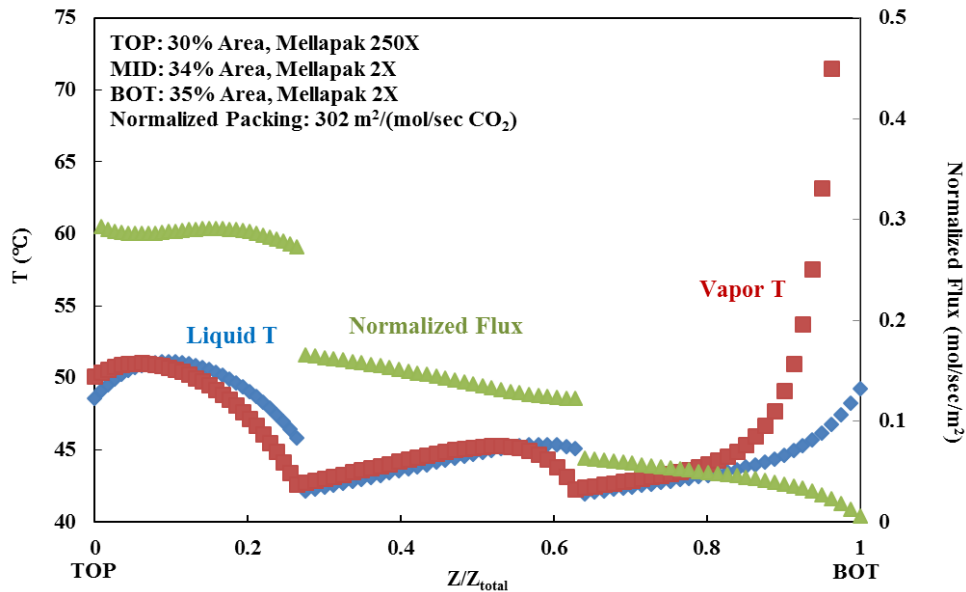


Figure 5.11: Temperature and flux profiles with IC and no DCC with 5 m PZ. Inlet CO₂ at 6.3%; Water wash at 48 °C; Mid PA IC and Bot PA IC at 40 °C; $L_R/G = 5$; Intermediate LLDG = 0.21 (mol CO₂/mol alk); $L = 1.2 * L_{\min}$.

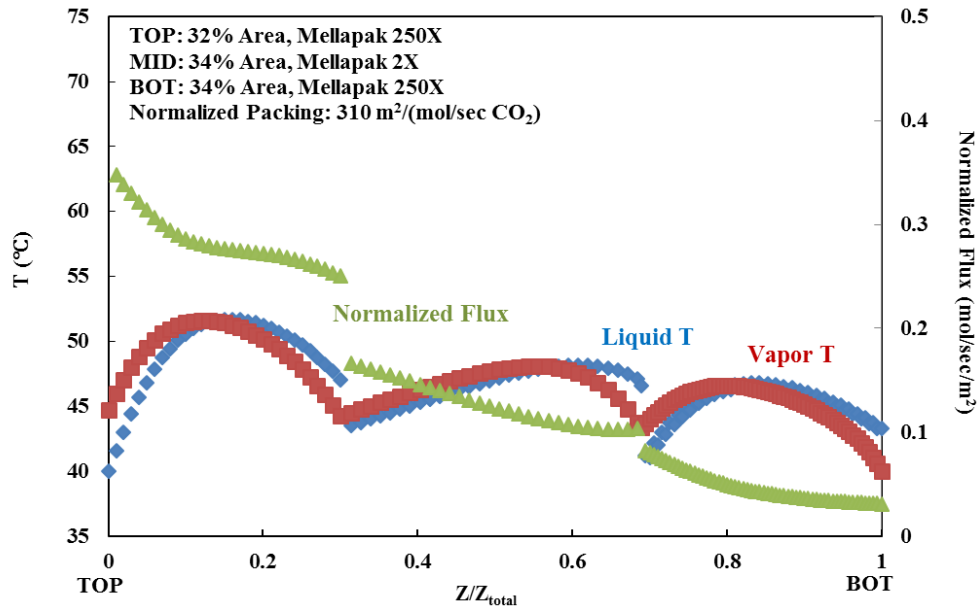


Figure 5.12: Temperature and flux profiles with DCC and IC with 5 m PZ. Inlet CO₂ at 6.3%; Mid Advanced PA IC at 40 °C; L_R/G = 3; Intermediate LLDG = 0.21 (mol CO₂/mol alk); L = 1.2*L_{min}.

Table 5.4 shows that the design without DCC has slightly less absorber packing with slightly greater energy (as shown by lower Δ LDG and higher L/G) than with DCC. Both Figure 5.11 and Figure 5.12 exhibit similar temperature and flux profiles as simple NGCC capture.

5.5 NGCC HYBRID CAPTURE WITH 5 M PZ

5.5.1 Absorber Configurations and Design Conditions

For the hybrid carbon capture process, a membrane is used to enrich CO₂ in flue gas, and the amine scrubbing system is expected to have higher energy efficiency (Freeman et al., 2014; Merkel et al., 2013; Johannes G Wijmans et al., 2011; Johannes G. Wijmans et al., 2011). Simplified process flow diagrams are shown in Figure 5.13 and Figure 5.14.

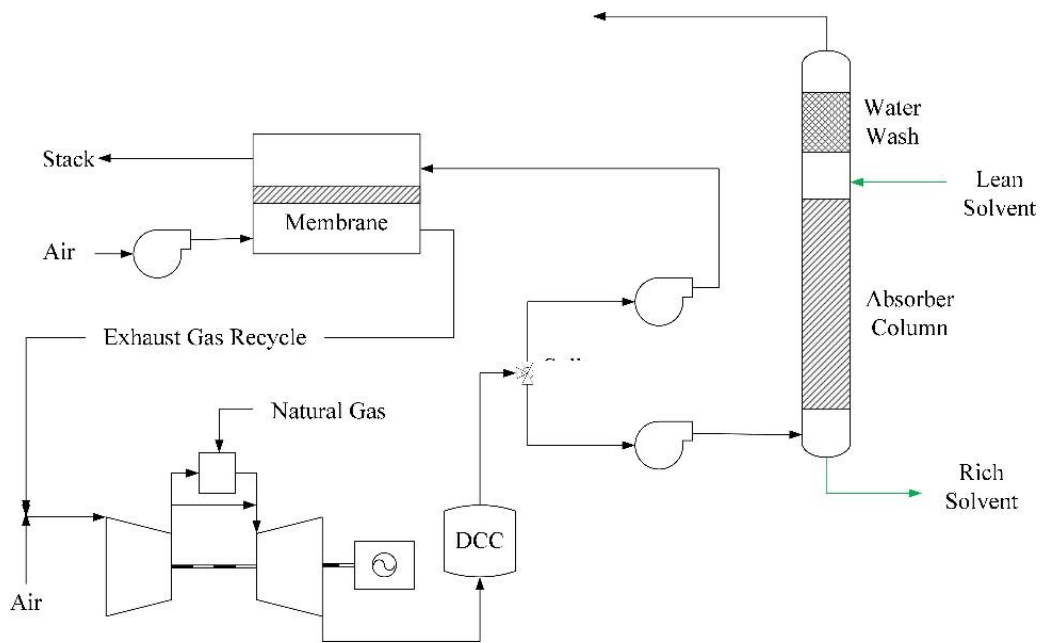


Figure 5.13: NGCC hybrid capture. Amine scrubbing with DCC.

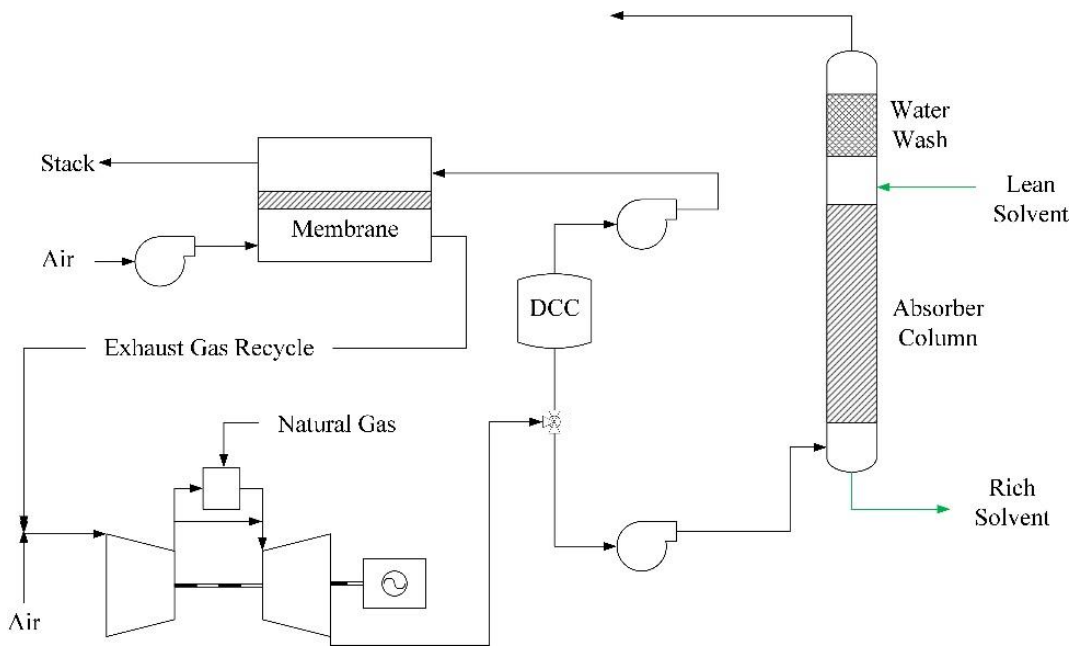


Figure 5.14: NGCC hybrid capture. Amine scrubbing without DCC.

Four hybrid capture cases with and without DCC have been proposed, corresponding to different membrane types and gas splitting ratios. Design with DCC

(Cases 1, 3, & 4) and without DCC (Case 2) are discussed in this section. The overall CO₂ capture rate was kept at 90%, and the absorber was kept at 95% removal (DOE/NETL, 2011, 2010). Absorber inlet gas information for each case is shown in Table 5.5 (DOE/NETL, 2011).

Table 5.5: Absorber inlet flue gas for NGCC hybrid capture.

	Case 1	Case 2	Case 3	Case 4
	Membrane A	Membrane A	Membrane B	Membrane B
	With DCC	No DCC	With DCC	With DCC
Flow rate (kmol/hr)	28,757	30,506	23,894	35,830
T (°C)	30	146	30	30
P (bar)	1.05	1.05	1.05	1.05
Composition (mol %)				
CO ₂	15%	14%	18%	12%
H ₂ O	3%	11%	3%	3%
N ₂	73%	67%	70%	75%
Ar	1%	1%	1%	1%
O ₂	8%	7%	8%	9%

Multiple intercooling configurations and cooling options have been evaluated. In-and-out intercooling works well for high inlet CO₂ (high LLDG, high L/G). A brief description of the most cost-effective absorber configuration and cooling option for each design follows:

With DCC and IC (Figure 5.15)

Wet Cooling: 2 absorber beds; In-and-out IC; DCC, WW, and IC at 25 °C.

With IC and no DCC (Figure 5.16)

Dry Cooling: 2 absorber beds; Bot PA IC; WW at 50 °C, IC at 50 °C; L_R/G = 5.

Parallel Cooling: 2 absorber beds; Bot PA IC; WW at 50 °C, IC at 25 °C; L_R/G =

5.

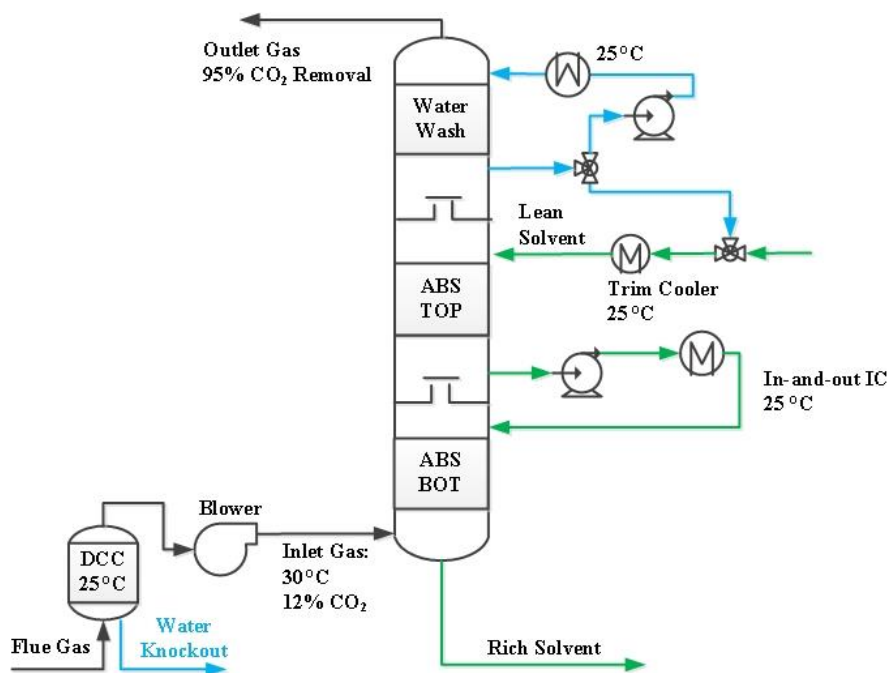


Figure 5.15: Absorber with DCC and IC. Flue gas concentrated by membrane. In-and-out intercooling at 25 °C.

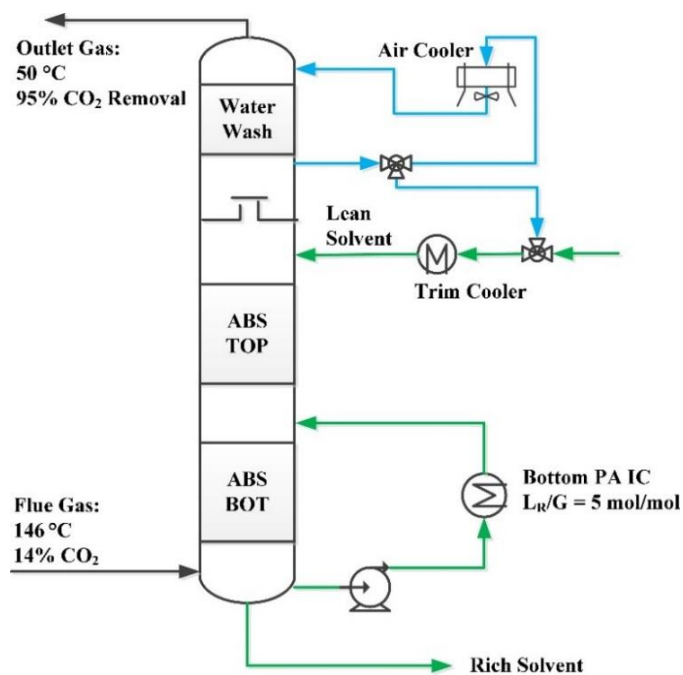


Figure 5.16: Absorber with IC and no DCC. Flue gas concentrated by membrane. Bot PA IC at 25 °C (parallel cooling) or 50 °C (dry cooling).

Structured packing Mellapak 250X was used for the absorber with DCC (Figure 5.15). Based on cooling water availability at the site, the DCC, the WW, and the intercoolers were operated at 25 °C (DOE/NETL, 2011). As a result of high CO₂ in flue gas, the absorber was operated with a high L/G, in which case one single intercooler was able to effectively cool down both liquid and vapor.

For absorber design without DCC, Mellapak 250X was used for the top section and Mellapak 2X was used for the bottom section (Figure 5.16). Dry cooling and parallel cooling have been tested.

Both over-stripping LLDG and intermediate LLDG have been evaluated. The over-stripping LLDG is established by setting the 0.037 ratio of the equilibrium partial pressure of CO₂ over the lean solvent and the partial pressure of the absorber outlet CO₂. Table 5.6 shows the most cost-effective LLDG for each case.

Table 5.6: The most cost-effective LLDGs with 5 m PZ.

	DCC		$P_{CO_2}^*/P_{CO_2,out}$	LLDG (mol CO ₂ /mol alk)
Case 1	with	Over-stripping LLDG	0.037	0.259
Case 2	without	Intermediate LLDG	0.1	0.159
Case 3	with	Over-stripping LLDG	0.037	0.268
Case 4	with	Over-stripping LLDG	0.037	0.247

5.5.2 Absorber Performance with Gas Concentrated by Membrane

5.5.2.1 With DCC and IC (Cases 1, 3, & 4)

For absorber design with DCC and IC, wet cooling has been tested. Absorber configuration is shown as:

Wet Cooling: 2 absorber beds; In-and-out IC; DCC, WW, and IC at 25 °C.

L/L_{\min} was set at 1.2 mol/mol. Table 5.7 summarizes the absorber performance of Cases 1, 3, & 4 at over-stripping LLDG. Figure 5.17 shows the column temperature and flux profiles for Case 3.

Table 5.7: Absorber performance with DCC and IC for Case 1, 3, & 4 at over-stripping LLDGs with 5 m PZ.

Case Number	LLDG	RLDG	Δ LDG	L/G	Packing Area Fraction		NP
	mol CO ₂ /mol alk	mol CO ₂ /mol alk	mol CO ₂ /mol alk	mol/mol	TOP	BOT	m ² /(mol/sec)
1	0.259	0.403	0.144	6.3	64%	36%	197
3	0.268	0.408	0.139	7.8	71%	29%	179
4	0.247	0.396	0.149	4.8	56%	44%	218

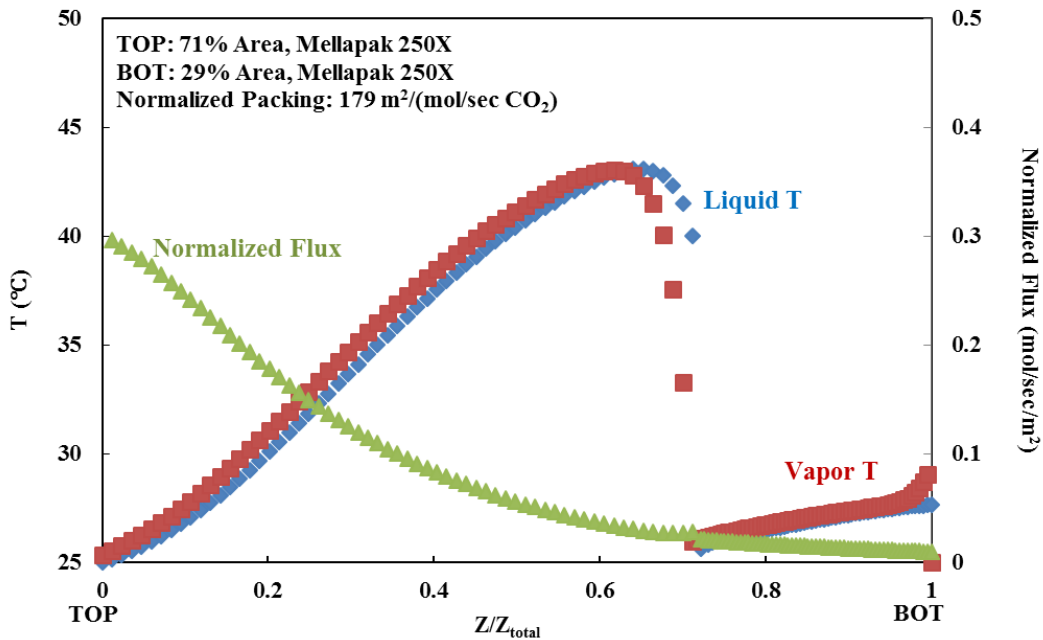


Figure 5.17: Temperature and flux profiles with DCC and IC (Case 3) with 5 m PZ. Inlet CO₂ at 18%; In-and-out IC at 25 °C; Over-stripping LLDG = 0.268 (mol CO₂/mol alk); $L = 1.2 \cdot L_{\min}$.

With increasing inlet CO₂, absorber normalized packing decreases, while L/G increases and Δ LDG decreases. High inlet CO₂ gives lower absorber costs but results in a greater energy requirement. Figure 5.17 shows a minor temperature bulge in the middle of the column that does not result in a mass transfer pinch.

5.5.2.2 With IC and no DCC (Case 2)

For the absorber with IC but no DCC, both dry cooling and parallel cooling have been tested. A brief description follows:

Dry Cooling: 2 absorber beds; Bot PA IC; WW and IC at 50 °C; L_R/G = 5.

Parallel Cooling: 2 absorber beds; Bot PA IC; WW at 50 °C, IC at 25 °C; L_R/G = 5.

L/L_{min} was set at 1.2 mol/mol. The absorber performance of Case 2 at intermediate LLDG = 0.159 (mol CO₂/mol alk) is shown in Table 5.8. Figures 5.18 and 5.19 show the column temperature and flux profiles by using dry cooling and parallel cooling.

Table 5.8: Absorber performance with IC and no DCC for Case 2 at intermediate LLDGs with 5 m PZ.

Cooling Option	RLDG	Δ LDG	L _R /G	L/G	Packing Area Fraction		NP
	mol CO ₂ /mol alk	mol CO ₂ /mol alk	mol/mol	mol/mol	TOP	BOT	m ² /(mol/sec)
Dry Cooling	0.321	0.162	5	5.1	60%	40%	194
Parallel Cooling	0.369	0.21	5	4	48%	52%	144

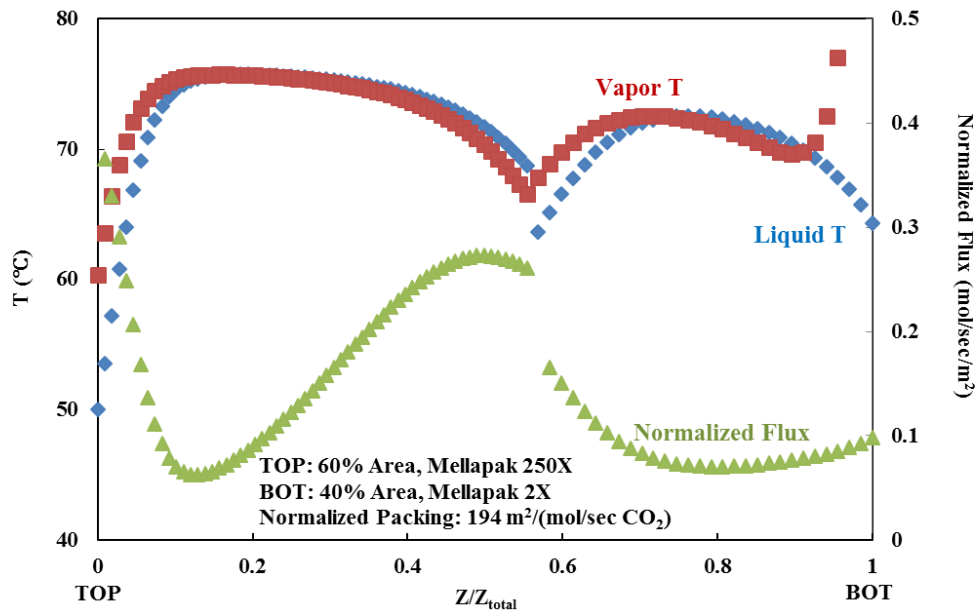


Figure 5.18: Temperature and flux profiles with IC and no DCC (Case 2) with 5 m PZ. Inlet CO₂ at 14%; Dry Cooling, Bot PA IC at 50 °C; L_R/G = 5; Intermediate LLDG = 0.159 (mol CO₂/mol alk); L = 1.2*L_{min}.

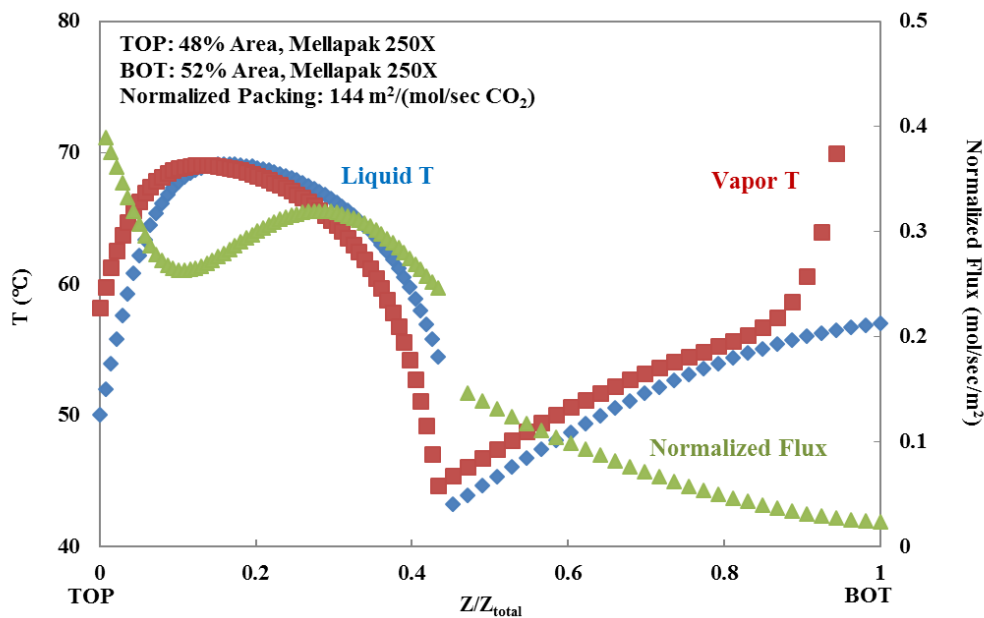


Figure 5.19: Temperature and flux profiles with IC and no DCC (Case 2) with 5 m PZ. Inlet CO₂ at 14%; Parallel Cooling, Bot PA IC at 25 °C; L_R/G = 5; Intermediate LLDG = 0.159 (mol CO₂/mol alk); L = 1.2*L_{min}.

Table 5.8 shows that dry cooling has a slightly higher but still acceptable packing requirement and slightly worse energy performance (as shown by the smaller ΔLDG and higher L/G) than parallel cooling. Dry cooling requires more packing and energy but appears to be technically and economically feasible if cooling water availability is limited. Figures 5.18 and 5.19 show that pump-around cooling at the bottom of the absorber can effectively manage the temperature of the hot flue gas, and still be effective for CO₂ absorption. The columns also exhibit relatively uniform temperature profiles with either dry cooling or parallel cooling.

5.6 ECONOMICS ANALYSIS OF NGCC CAPTURE WITH 5 M PZ

5.6.1 Absorber Economics with 5 m PZ

Purchased Equipment Cost (PEC) for the absorber was calculated by empirical expressions for each column component using the Aspen Plus® modeling results. Annualized capital costs (CAPEX) is expressed in dollars per metric ton of CO₂ captured, and can be converted from PEC using Equation 5.3. α converts the PEC to a total capital requirement and β is factor to annualize the cost. Literature value for α ranges from 2 to 10, depending on different process units. The factor β takes into account return on investment (10%), depreciation (3–10%, depending on plant lifetime), taxes (35% of return on investment), as well as maintenance (2–3%). Typical value of β ranges from 0.1 to 0.3. In this work, α is chosen to be 5 and β is chosen to be 0.2 (Frailie, 2014).

$$CAPEX (\$/TONNE CO_2) = \frac{\alpha * \beta * PEC}{Total\ MT\ captured\ per\ year} \quad (5.3)$$

The absorber CAPEX includes CAPEX for the DCC column, absorber column, absorber intercoolers, absorber intercooler pumps, water wash columns, and possible additional water wash air coolers. The air coolers were modeled and costed using Aspen

Exchanger Design and Rating. Tables 5.9 and 5.10 as well as Figure 5.20 show the absorber CAPEX comparison with and without DCC for simple NGCC amine scrubbing capture, NGCC with EGR amine scrubbing capture, and NGCC hybrid capture with 5 m PZ. All the absorbers are operated with intercooling. All three capture systems were designed for 90% overall CO₂ removal, capturing 1.4 million tonne CO₂ per year.

Table 5.9: Absorber PEC (in Million USD) and CAPEX (in \$/TONNE CO₂) with and without DCC for amine scrubbing with 5 m PZ from simple NGCC and NGCC with 35% EGR.

Application DCC Option Cooling Option	Simple NGCC		NGCC with 35% EGR		
	Without	With	Without	With	
	Parallel Cooling	Wet Cooling at 40 °C	Parallel Cooling	Wet Cooling at 40 °C	
CO ₂ Inlet	4%		6%		
Packing Height (m)	6.1	7	7.1	8.1	
Diameter (m)	20.8	19	16.9	15.3	
PEC (\$M)	DCC Column	--	7.8	--	5.7
	Absorber Column	13	11.2	9.4	8.1
	Absorber Intercoolers	2.5	0.7	2.1	1.1
	Absorber Intercooling Pumps	1.8	0.8	1.2	0.6
	Water Wash Column	8	7	5.7	5
	Water Wash Air Cooler	0.07*	--	0.07*	--
ABS PEC (\$M)	25.5	27.6	18.5	20.5	
ABS CAPEX (\$/TONNE CO ₂)	17.8	19.2	13	14.4	

*Air Cooler Used

Table 5.10: Absorber PEC in Million USD (\$M) of NGCC hybrid carbon capture with 5 m PZ.

Case Number	Case 1	Case 2	Case 3	Case 4
DCC Option	With	Without	With	With
Cooling Option	Wet Cooling at 25 °C	Dry Cooling at 50 °C	Wet Cooling at 25 °C	Wet Cooling at 25 °C
CO ₂ Inlet	15%	14%	18%	12%
Packing Height (m)	10.1	8.9	10.5	9.5
Diameter (m)	10.7	11.7	10	11.6
PEC (\$M)				
DCC Column	3	--	2.9	3.6
Absorber Column	4	4.8	3.7	4.4
Absorber Intercoolers	1.1	1.1*	0.7	0.7
Absorber Intercooling Pumps	0.3	0.1	0.3	0.3
Water Wash Column	2.9	3.3	2.6	3.2
Water Wash Air Cooler	--	0.8*	--	--
ABS PEC (\$M)	11.5	10.1	10.1	12.2
ABS CAPEX (\$/TONNE CO ₂)	8	7	7	8.5

*Air Cooler Used

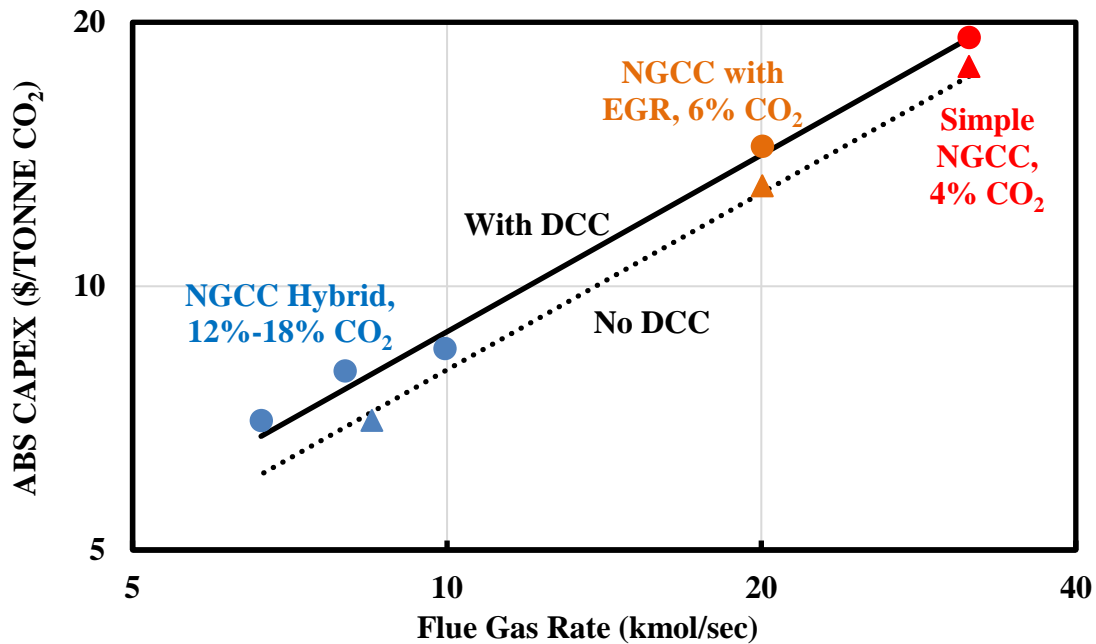


Figure 5.20: Absorber CAPEX (in \$/TONNE CO₂) with and without DCC for simple NGCC amine scrubbing capture, NGCC with EGR amine scrubbing capture, and NGCC hybrid capture with 5 m PZ.

Table 5.9 shows that for amine scrubbing capture from simple NGCC and NGCC with EGR, the design without DCC requires \$5-7 M higher absorber column and intercooling costs as well as \$0.07 M additional air cooler costs but can save \$6-8 M associated with the DCC column and finally gives the minimum total absorber PEC. For hybrid capture, the design without DCC also gives the minimum total absorber PEC, shown in Table 5.10. Figure 5.20 shows that when the inlet CO₂ increases from 4% to 18%, the absorber CAPEX decreases by 60%. Another 10% saving of absorber CAPEX can be achieved by eliminating the DCC.

5.6.2 Total Capture Costs

The total capture costs include annualized capital costs (CAPEX) and annualized operating expenses (OPEX). The total capture costs of the hybrid capture process involve the trade-off between amine scrubbing system costs and membrane costs.

Table 5.11 compares the total capture costs of simple NGCC capture, NGCC with EGR capture, and NGCC hybrid capture processes with 5 m PZ. All absorbers are designed with DCC. The absorption segment includes blower, DCC, absorber, water wash, pumps, intercoolers, and water wash coolers; the regeneration segment involves stripper, flash tank, heat exchangers, pumps, and compressors. The regeneration CAPEX and OPEX were calculated by Junyuan Ding (Ding, 2016), and the membrane CAPEX and OPEX were calculated by Pingjiao Hao. The total capture costs by segments are plotted in Figure 5.21.

$$\text{Total Capture Costs (\$/TONNE CO}_2\text{)} = \text{CAPEX} + \text{OPEX} \quad (5.4)$$

Table 5.11: Total capture costs (\$/TONNE CO₂) comparison of NGCC carbon capture with 5 m PZ.

		Inlet CO ₂	4%	6%	12%	15%	18%
CAPEX (\$/TONNE CO ₂)	Amine Scrubbing	Absorption Regeneration	21.0 18.3	15.1 18.3	10.4 18.5	9.4 18.4	8.6 18.5
	Membrane		-	-	5.0	6.7	14.4
OPEX (\$/TONNE CO ₂)	Amine Scrubbing	Absorption Regeneration	2.8 16.7	2.0 16.7	0.7 15.4	0.6 15.1	0.5 14.9
	Membrane		-	-	3.9	3.9	3.9
Total Capture Costs (\$/TONNE CO ₂)	Amine Scrubbing	Absorption Regeneration	23.8 34.7	17.0 34.7	11.1 33.9	9.9 33.5	9.1 33.4
	Membrane		-	-	8.8	10.6	18.3
	Overall			58.5	51.7	53.8	54.0

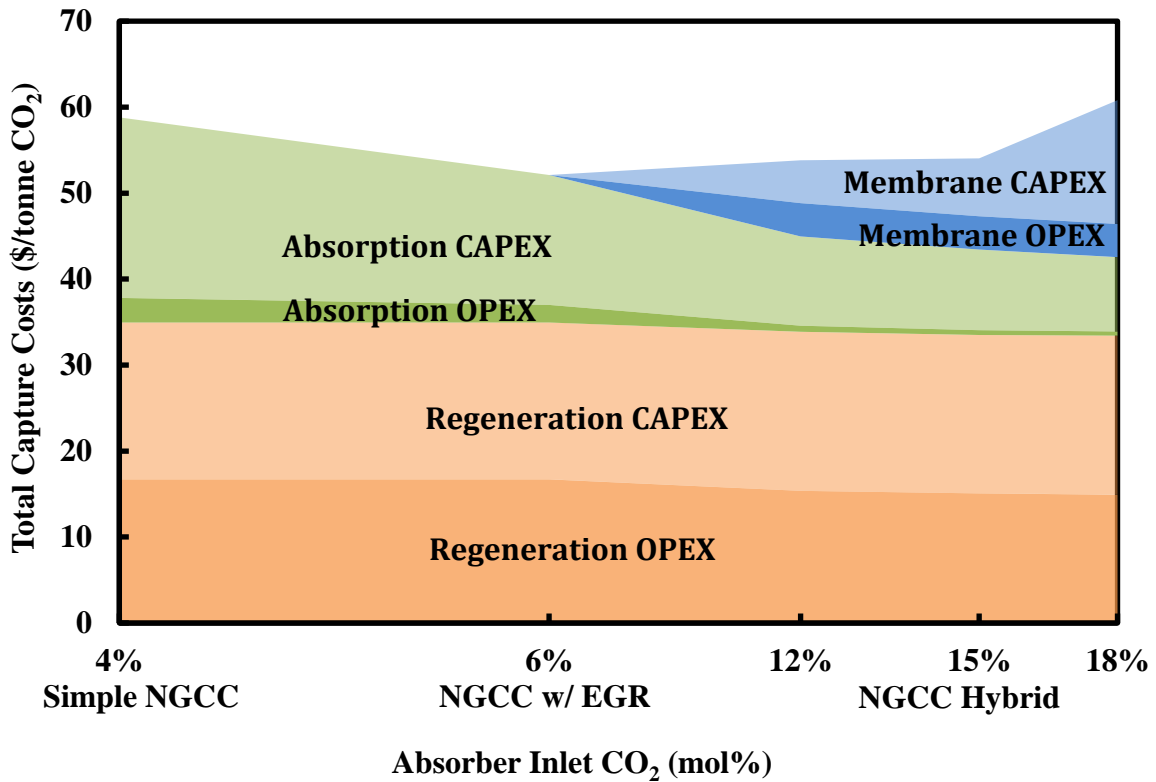


Figure 5.21: Total capture costs (\$/TONNE CO₂) comparison of NGCC carbon capture with 5 m PZ.

Figure 5.21 shows that, as the inlet CO₂ increases from 4% to 18%, the total amine scrubbing system costs decrease by 27% - the total absorption costs decrease by 60% and the total regeneration costs almost remain the same. As the inlet CO₂ increases from 12% to 18%, the membrane area required for air sweeping to enrich the CO₂ increases dramatically and the total membrane costs increase by 108%. At 18% inlet CO₂, the membrane CAPEX is almost the half of the total amine scrubbing system CAPEX. The membrane-amine hybrid capture system would be more economically feasible if it is operated at a lower overall CO₂ removal rate (where less membrane area is required) or if the membrane capital costs can be reduced. To become more cost-effective, this hybrid system still needs further study, such as overall system design, optimization of overall CO₂ capture rate, and solvent selection.

5.7 NGCC HYBRID CAPTURE WITH 2 M PZ/3 M HMPD BLEND

5.7.1 Vapor-liquid-equilibrium Comparison of 5 m PZ and 2 m PZ/3 m HMPD

HMPD (3-hydroxy-1-methyl-piperidine) is a cyclic and tertiary amine (Du et al., 2016). 2 m PZ/3 m HMPD blend has larger CO₂ capacity and greater thermal stability (Du et al., 2016) thus it is also evaluated in this work. CO₂ vapor-liquid-equilibrium (VLE) capacities of 5 m PZ and the blend of 2 m PZ/3 m HMPD are compared in Figure 5.22, plotted using the regressed data from PZ solvent model developed by Frailie (Frailie, 2014) and the PZ/HMPD model developed by Sherman (Sherman, 2016). The equilibrium partial pressure of CO₂ over the solvent is plotting against CO₂ loading (mol CO₂/mol alk). Figure 5.22 shows that the VLE curve of 2 m PZ/3 m HMPD is much flatter than that of 5 m PZ, suggesting that 2 m PZ/3 m HMPD has higher CO₂ equilibrium

capacity, especially at the rich end. With the highest CO₂ (18%) of the four hybrid carbon capture cases (Table 5.5), Case 3 is expected to benefit most from this high capacity solvent. The absorber performance with 2 m PZ/3 m HMPD has been evaluated with DCC and without DCC.

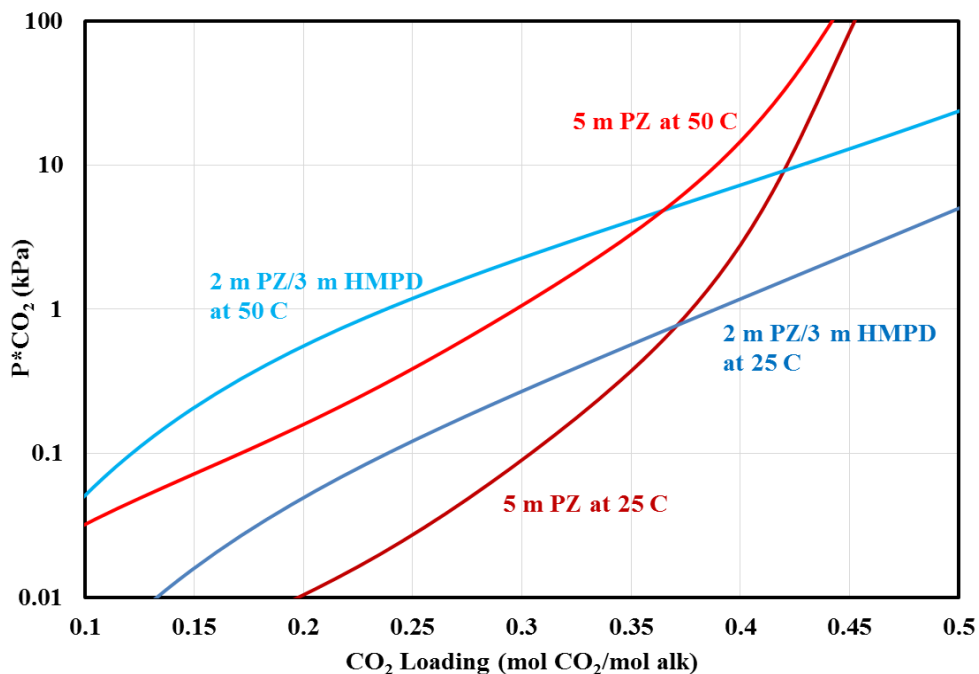


Figure 5.22: CO₂ vapor-liquid-equilibrium (VLE) Comparison between 5 m PZ and 2 m PZ/3 m HMPD. PZ model was developed by Frailie (Frailie, 2014) and PZ/HMPD model was developed by Sherman (Sherman, 2016).

5.7.2 Absorber Configurations

To make a fair comparison, the absorber configurations with 2 m PZ/3 m HMPD have been kept the same as that with 5 m PZ. This work evaluates two DCC options: with DCC and IC (Case 3, Figure 5.15); with IC and no DCC (Case 2, Figure 5.16). A brief description of the absorber configurations follows:

With DCC and IC (Case 3, Figure 5.15)

Wet Cooling: 2 absorber beds; In-and-out IC; DCC, WW, and IC at 25 °C.

With IC and no DCC (Case 2, Figure 5.16)

Dry Cooling: 2 absorber beds; Bot PA IC; WW at 50 °C, IC at 50 °C; $L_R/G = 5$.

In previous sections with 5 m PZ, over-stripping LLDG was found to be more cost-effective for Case 3 and intermediate LLDG was more cost-effective for Case 2. Intermediate LLDG is defined by $P^*_{CO_2}/P_{CO_2,out} = 0.1$; over-stripping LLDG is defined by $P^*_{CO_2}/P_{CO_2,out} = 0.037$. As a result, with 2 m PZ/3 m HMPD, over-stripping LLDG has been evaluated for Case 3 and intermediate LLDG has been evaluated for Case 2, summarized in Table 5.12.

Table 5.12: LLDGs used for Cases 2 and 3. Intermediate LLDG and over-stripping LLDG are defined by $P^*_{CO_2}/P_{CO_2,out}$.

	DCC		$P^*_{CO_2}/P_{CO_2,out}$	LLDG (mol CO ₂ /mol alk)
Case 2	without	Intermediate LLDG	0.1	0.115
Case 3	with	Over-stripping LLDG	0.037	0.191

5.7.3 Absorber Performance with 2 m PZ/3 m HMPD

The rate-based absorber is modeled using the PZ/HMPD solvent model developed in Aspen Plus[®] RateSep[™] by Sherman (Sherman, 2016), with rigorous thermodynamics and kinetics. The data were collected by Du (Du et al., 2016). The interfacial area model used in this work was developed using data collected by Tsai (Tsai, 2010); the gas- and liquid-side physical mass transfer coefficients were collected by Wang (Wang, 2015).

5.7.3.1 Absorber design with DCC and IC (Case 3)

The absorber was operated at 95% CO₂ removal and L/L_{min} was set at 1.2 mol/mol.

Table 5.13 compares the absorber performance with 5 m PZ and 2 m PZ/3 m HMPD at over-stripping LLDGs. Figure 5.23 shows the column profiles with 2 m PZ/3 m HMPD.

Table 5.13: Absorber performance of 5 m PZ and 2 m PZ/3 m HMPD at over-stripping LLDGs.

LLDG	RLDG	Δ LDG	L/G	Packing Area Fraction		NP
				TOP	BOT	
mol CO ₂ /mol alk	mol CO ₂ /mol alk	mol CO ₂ /mol alk	mol/mol			m ² /(mol/sec)
5 m PZ. I&O IC at 25 °C						
0.268	0.408	0.139	7.8	71%	29%	179
2 m PZ/3 m HMPD. I&O IC at 25 °C						
0.191	0.475	0.284	5.4	53%	47%	400

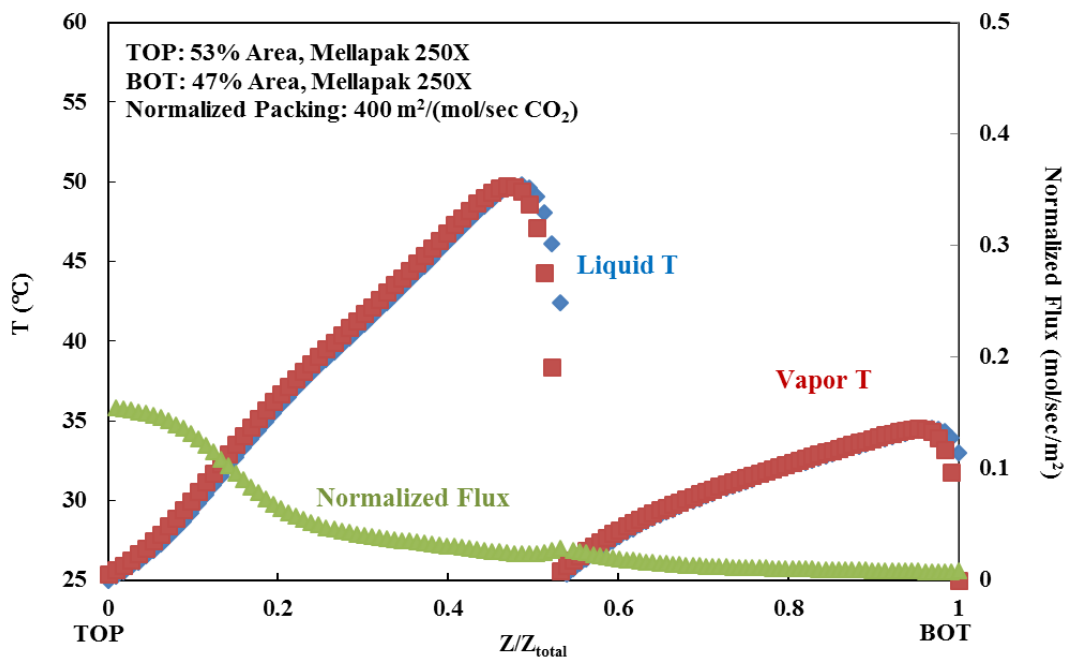


Figure 5.23: Temperature and flux profiles with DCC and IC (Case 3) with 2 m PZ/3 m HMPD. In-and-out IC at 25 °C; Over-stripping LLDG = 0.191 (mol CO₂/mol alk); L = 1.2*L_{min}.

In

Table 5.13, with DCC and IC, 2 m PZ/3 m HMPD results in much greater Δ loading and lower L/G than 5 m PZ, which suggests that 2 m PZ/3 m HMPD has higher CO₂ capacity and better energy performance. Because of slower kinetics, especially at the rich end, 2 m PZ/3 m HMPD requires 123% more packing as 5 m PZ.

5.7.3.2 Absorber design without DCC and with IC (Case 2)

For Case 2, L/L_{min} was set at 1.2 mol/mol and intercooling recycle ratio was set at L_R/G = 5 mol/mol. Table 8 summarizes the absorber performance comparison between 5 m PZ and 2 m PZ/3 m HMPD at intermediate LLDGs. The column temperature and flux profiles are shown in Figure 5.24 and Figure 5.25. Table 5.14 suggests that, without DCC, 2 m PZ/3 m HMPD results in greater Δ loading and almost the same L/G, but the absorber requires 74% more packing area.

Table 5.14: Absorber performance of 5 m PZ and 2 m PZ/3 m HMPD at intermediate LLDGs.

LLDG	RLDG	Δ LDG	L _R /G	L/G	Packing Area Fraction		NP
					TOP	BOT	
mol CO ₂ /mol alk	mol CO ₂ /mol alk	mol CO ₂ /mol alk	mol/mol	mol/mol	m ²		m ² /(mol/sec)
5 m PZ. Dry Cooling. Bot PA IC.							
0.159	0.321	0.162	5	5.1	60%	40%	194
2 m PZ/3 m HMPD. Dry Cooling. Bot PA IC.							
0.115	0.318	0.203	5	5.8	60%	40%	338

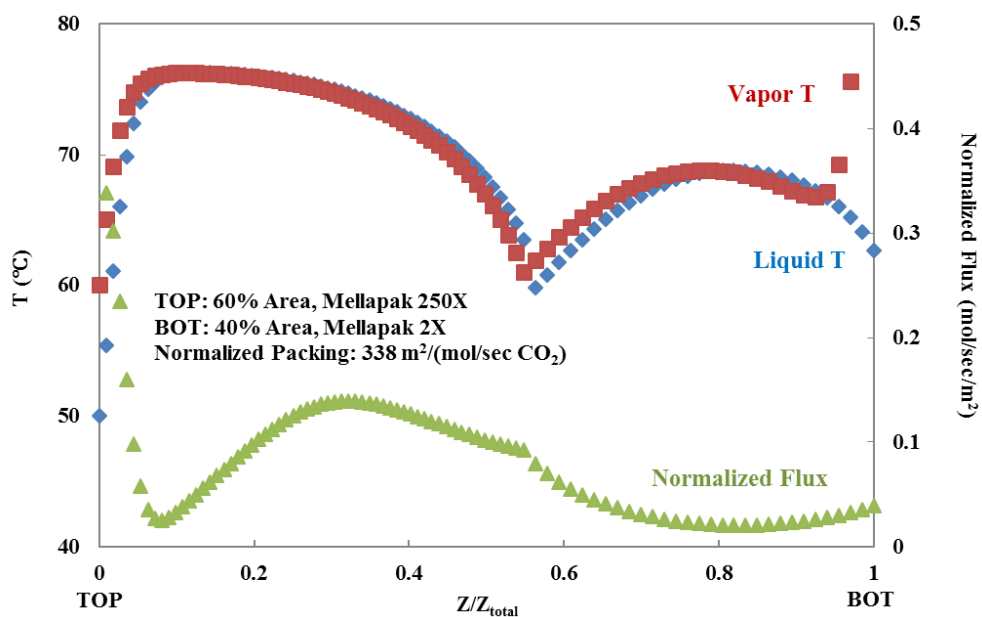


Figure 5.24: Temperature and flux profiles without DCC (Case 2) with 2 m PZ/3 m HMPD. Bot PA IC at 50 $^{\circ}\text{C}$; $L_R/G = 5$; Intermediate LLDG = 0.115 (mol $\text{CO}_2/\text{mol alk}$); $L = 1.2 \cdot L_{min}$.

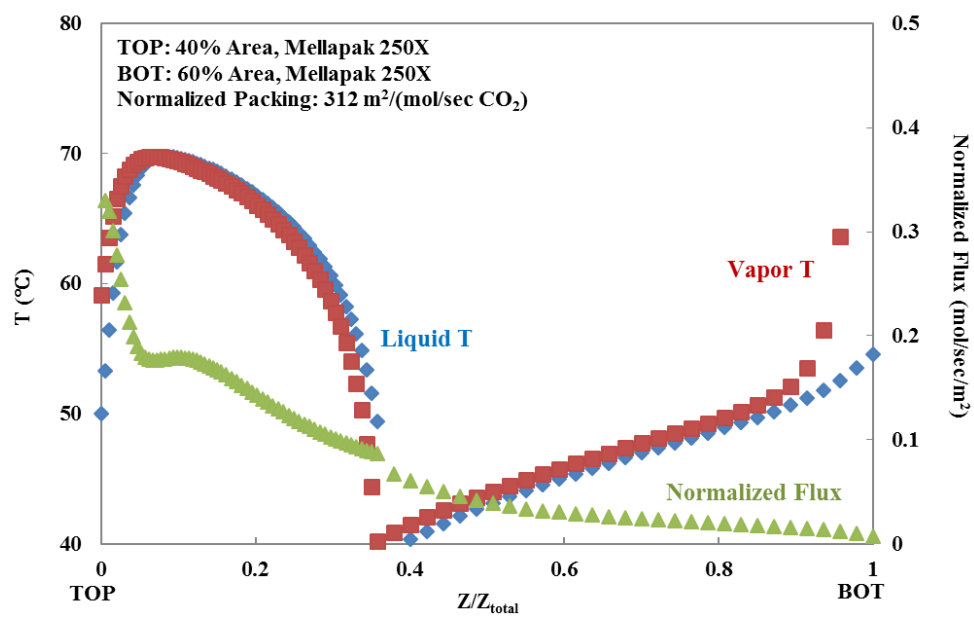


Figure 5.25: Temperature and flux profiles without DCC (Case 2) with 2 m PZ/3 m HMPD. Bot PA IC at 25 $^{\circ}\text{C}$; $L_R/G = 5$; Intermediate LLDG = 0.115 (mol $\text{CO}_2/\text{mol alk}$); $L = 1.2 \cdot L_{min}$.

5.7.4 Absorber Economics

Table 5.15 shows the absorber CAPEX comparison between 5 m PZ and 2 m PZ/3 m HMPD at different DCC options for NGCC hybrid capture. Compared with 5 m PZ, 2 m PZ/3 m HMPD requires \$2 M more in absorber columns costs, suggesting slower kinetics.

Table 5.15: Absorber PEC (in Million USD) and CAPEX (in \$/TONNE CO₂) of 5 m PZ and 2 m PZ/3 m HMPD for NGCC hybrid capture.

Case Number	Case 2	Case 3
DCC Option	Without	With
Cooling Option	Dry Cooling at 50 °C	Wet Cooling at 25 °C
CO ₂ Inlet	14%	18%
Packing Height (m)	8.9	10.5
Diameter (m)	11.7	10
NGCC Hybrid, 5 m PZ		
DCC Column	--	2.9
Absorber Column	4.8	3.7
Absorber Intercoolers	1.1*	0.7
Absorber Intercooling Pumps	0.1	0.3
Water Wash Column	3.3	2.6
Water Wash Air Cooler	0.8*	--
ABS PEC (\$M)	10.1	10.1
ABS CAPEX (\$/TONNE CO ₂)	7	7
NGCC Hybrid, 2 m PZ/3 m HMPD		
DCC Column	--	2.9
Absorber Column	6.7	5.9
Absorber Intercoolers	0.9*	0.7
Absorber Intercooling Pumps	0.2	0.2
Water Wash Column	3.4	2.7
Water Wash Air Cooler	0.8*	--
ABS PEC (\$M)	11.9	12.4
ABS CAPEX (\$/TONNE CO ₂)	8	9

*Air Cooler Used

5.8 CONCLUSIONS

Amine scrubbing without the direct contact cooler is a superior design for NGCC carbon capture. 10% of the absorber CAPEX can be saved by eliminating the DCC.

When DCC is eliminated, pump-around cooling at the bottom of the absorber can effectively manage the temperature of the hot flue gas, and still be effective for CO₂ absorption. Model-predicted temperature of the rich solvent never exceeds 55 °C. The absorber gas inlet must be designed to avoid excessive localized temperature and solvent evaporation.

When the inlet CO₂ increases from 4% to 18%, the total absorption costs decrease by 60% and the total regeneration costs remain the same. For hybrid capture, as the inlet CO₂ increases from 12% to 18%, the total membrane costs increase by 108%. The hybrid system would be more economically feasible if it is operated at a lower overall CO₂ removal rate (where less membrane area is required) or if the membrane capital costs can be reduced.

In-and-out intercooling works well for the hybrid capture system with a membrane and amine scrubbing (high CO₂ in flue gas, high LLDG, high L/G). Pump-around intercooling is more effective for simple NGCC capture (low CO₂ in flue gas, low LLDG, low L/G). The potential benefits of intercooling at extremely low LLDG are not as evident as those at high LLDG.

Dry cooling requires more packing and energy but appears to be technically and economically feasible if cooling water availability is limited.

5.9 ACKNOWLEDGEMENTS

The author gratefully acknowledges financial support from Membrane Technology and Research, Inc. (MTR) and the Texas Carbon Management Program in the preparation

of this work. Aspen Plus[®] proprietary software was provided by an academic license from AspenTech[®]. AspenTech[®] and Aspen Plus[®] are trademarks of Aspen Technology, Inc. All rights reserved.

Chapter 6 : Absorber Test Plan Development for 2018 National Carbon Capture Center Pilot Plant Campaign

A CO₂ capture pilot plant with the advanced flash stripper has been operated with aqueous piperazine (PZ) at the National Carbon Capture Center (NCCC) since March 2018 and will last until December 2018. A test plan was developed before the campaign to evaluate the NCCC absorber packing and solvent performance. The absorber performance was predicted using the rate-based absorber model in Aspen Plus[®] that was developed over several campaigns at The University of Texas Separations Research Program (UT-SRP) pilot plant (Plaza, 2011; Sachde et al., 2013; Zhang et al., 2017b). In this work, the NCCC absorber is found to be over-designed with excessive packing. In order to maximize the value of packing performance data, design of experiments should avoid mass transfer pinches. This chapter focuses on absorber test plan development for the 2018 NCCC pilot plant campaign.

6.1 NCCC PILOT PLANT ABSORBER OVERVIEW

The NCCC pilot plant provides opportunities to test carbon capture technologies for coal-fired power generation. A test campaign was planned using the Pilot Solvent Test Unit (PSTU) with 5 m PZ. The NCCC absorber inlet flue gas composition, flow rate, temperature, and pressure are shown in Table 6.1. Figure 1.1 shows the NCCC absorber column configuration. The column system has 5 sections of packing: an absorber with two 20-ft sections, a 20-ft absorber extension, a 10-ft empty bed, and a 10-ft water wash. The 20-ft absorber extension can be used as an additional section for the absorber. The column can be operated in two modes: 40-ft absorber, 30-ft dry bed, and 10-ft water wash (lean solvent is fed at point 1 in Figure 1.1); 60-ft absorber, 10-ft dry bed, and 10-ft water wash (lean solvent is fed at point 2 in Figure 1.1). The column diameter

is 26 inches. The NCCC absorber has Mellapak 252Y packing and has been modeled as Mellapak 250Y packing. An in-and-out intercooler was applied 20 ft from the bottom of the absorber to reduce the temperature bulge and improve mass transfer driving force. The water wash and DCC should be operated at the same temperature to maintain the water balance in the absorber.

Table 6.1: NCCC absorber inlet flue gas specifications.

Nominal throughput	MWe	0.5	0.8
CO ₂	vol %	12.2	12.2
O ₂	vol %	5.7	5.7
N ₂	vol %	74.8	74.8
H ₂ O	vol %	7.4	7.4
Temperature	°C	40	40
Pressure	kPa	101.3	101.3
Mass flow rate	lb/hr	4069	6510

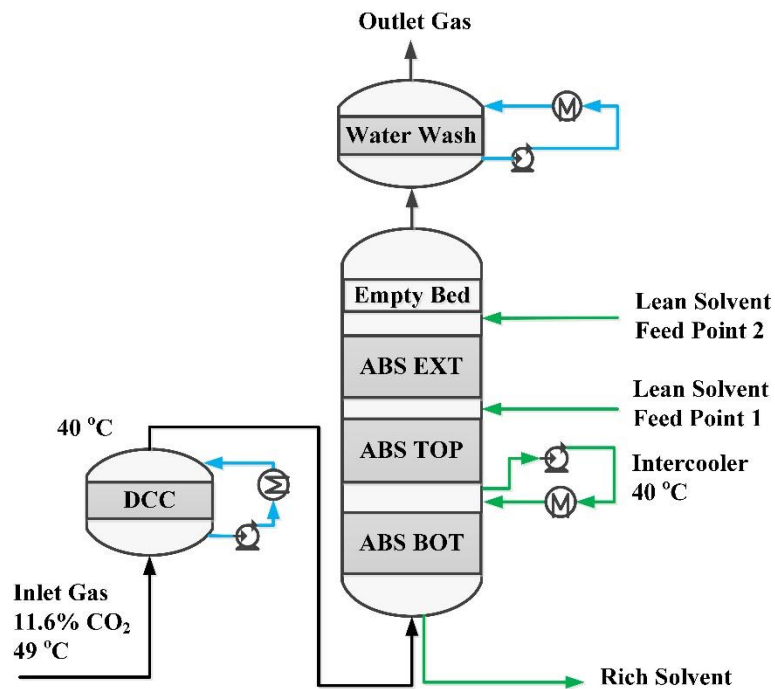


Figure 6.1: NCCC absorber column configuration.

6.2 NCCC PILOT PLANT ABSORBER MODELING ACTIVITIES

Absorber modeling activities with the pilot plant include pre-campaign, in-campaign, and post-campaign activities.

6.2.1 Pre-campaign Absorber Modeling Activities

Pre-campaign absorber modeling consists of three broad steps:

- Absorber factorial design;
- Accurate simulation of absorber test conditions;
- Design of experiments (DoE) using simulation results.

Factorial design is an experiment that consists of two or more factors, each with discrete values. The factors in NCCC absorber testing are flue gas rate, cooling temperature, lean loading, and CO₂ removal rate. Factorial design generates absorber test conditions that take on all possible combinations of all values across these factors, which can help study the effect of each factor on absorber performance, as well as the effects of interactions between factors. The absorber is simulated using the pilot plant absorber model under these test conditions and design of experiments (DoE) is performed using simulation results. In DoE, constraints of experimental variables are taken into account, e.g., capacities of pumps and fans, detection ranges of analyzers and instruments, safety limits, etc.

6.2.2 In-campaign and Post-campaign Absorber Modeling Activities

During the campaign, model-predicted absorber performance is compared with real-time pilot plant absorber data and the test plan is adjusted. Post-campaign absorber modeling activities include material balance check, data reconciliation, and model improvements. More details of in-campaign and post-campaign activities have been

discussed in Chapter 3 for the March 2015 UT-SRP campaign and Chapter 4 for the April 2017 UT-SRP campaign.

6.3 PRE-CAMPAIGN ABSORBER TEST PLAN DEVELOPMENT FOR 2018 NCCC CAMPAIGN

In previous chapters, a pilot plant absorber model was described and it was able to capture UT-SRP pilot plant absorber performance over a wide range of conditions (Plaza, 2011; Sachde et al., 2013; Zhang et al., 2017b). 16.8-inch UT-SRP absorber is filled with Raschig Super-Pak (RSP-250) structured packing and 26-inch NCCC absorber is filled with Mellapak 252Y structured packing. The UT-SRP absorber packing model has been used in this work to predict NCCC absorber performance.

Absorber testing in the 2018 NCCC pilot plant campaign consists of factorial testing and long-term testing. The experiment in factorial testing is designed as a parametric test of absorber performance at different lean loading (LLDG) and rich loading (RLDG). The biggest absorber cost trade-off is between packing area and solvent rate (Plaza, 2011; Sachde, 2016). Minimum solvent rate (L_{\min}) is obtained by adding excessive packing into the column, and mass transfer pinches tend to occur at low L/L_{\min} . In order to maximize the value of packing performance data, design of experiments should avoid mass transfer pinches and L/L_{\min} usually falls between 1.1 to 1.3.

A test plan has been developed before the campaign to evaluate the NCCC absorber packing and solvent performance. Table 6.2 summarizes a total of 15 testing conditions (Run 1 for long-term testing and Runs 2 to 15 for factorial testing) and model-predicted absorber performance. In Run 1, as a base case, the absorber is operated at 0.24 LLDG, 40 °C intercooling T, and 90% removal, resulting in 0.387 RLDG. The reasonable loading difference (rich - lean) indicates good energy performance. In Run 5, intercooling

T is reduced from 40 °C to 30 °C and the column is expected to give a higher rich loading and will result in better energy performance. Absorber operated with a high lean loading will be tested in Run 6. Due to the excessive packing, the NCCC absorber in Runs 1 through 10 exhibits low L/L_{min} . In order to avoid a mass transfer pinch and get reliable packing data, the absorber in Runs 11 to 15 is operated with 99% and 95% removal at relatively higher L/L_{min} .

Table 6.2: Absorber test plan for 2018 NCCC pilot plant campaign.

Run	G lb/hr	Cooling T °C	LLDG mol CO ₂ /mol alk	Removal %	Predicted RLDG mol CO ₂ /mol alk	Predicted L lb/hr	L/L_{min} lb/lb	L/G lb/lb	Comments
1	4069	40	0.24	90	0.387	15900	1.006	3.9	Base Case
2	4069	40	0.24	90	(0.4+)				Stripper optimization at fixed removal
3	4069	40	0.24	90	(0.4+)				
4	4069	40	0.24	90	(0.4+)				
5	4069	30	0.24	90	0.408	13875		3.4	Decrease intercooling T
6	4069	30	0.27	90	0.410	16750		4.1	Increase lean loading
7	4069	30	0.24	90	(0.4+)				Stripper optimization at fixed removal
8	4069	30	0.24	90	(0.4+)				
9	4069	30	0.24	90	(0.4+)				
10	4069	30	0.24	90	(0.4+)				
11	4069	40	0.24	99	0.38	18200	1.16	4.5	Lower rich loading, higher L/L_{min}
12	4069	40	0.24	(95+)	0.38				Stripper optimization at fixed rich loading
13	4069	40	0.27	(95+)	0.38				
14	4069	40	0.21	(95+)	0.38				
15	6510	40	0.24	95	0.38	28215	1.1	4.3	High gas rate

Figures 6.2 and 6.3 show the model-predicted absorber temperature, normalized flux, and CO₂ vapor composition profiles for Run 1 with normal 40-ft packing and 80-ft

packing (at L_{min}). Normalized flux is the CO_2 vapor flux divided by the CO_2 vapor mole fraction (Equation 6.1). In Figure 6.2, the column exhibits two temperature bulges and a relatively low flux rate at the bottom packing section. Mass transfer pinch occurs where flux rate approaches zero. In Figure 6.3, at L_{min} , two mass transfer pinches are observed in both packing sections. It suggests that the NCCC absorber is over-designed with excessive packing.

$$Normalized\ Flux = \frac{CO_2\ Vapor\ Flux}{CO_2\ vapor\ mol\ fraction} \quad (6.1)$$

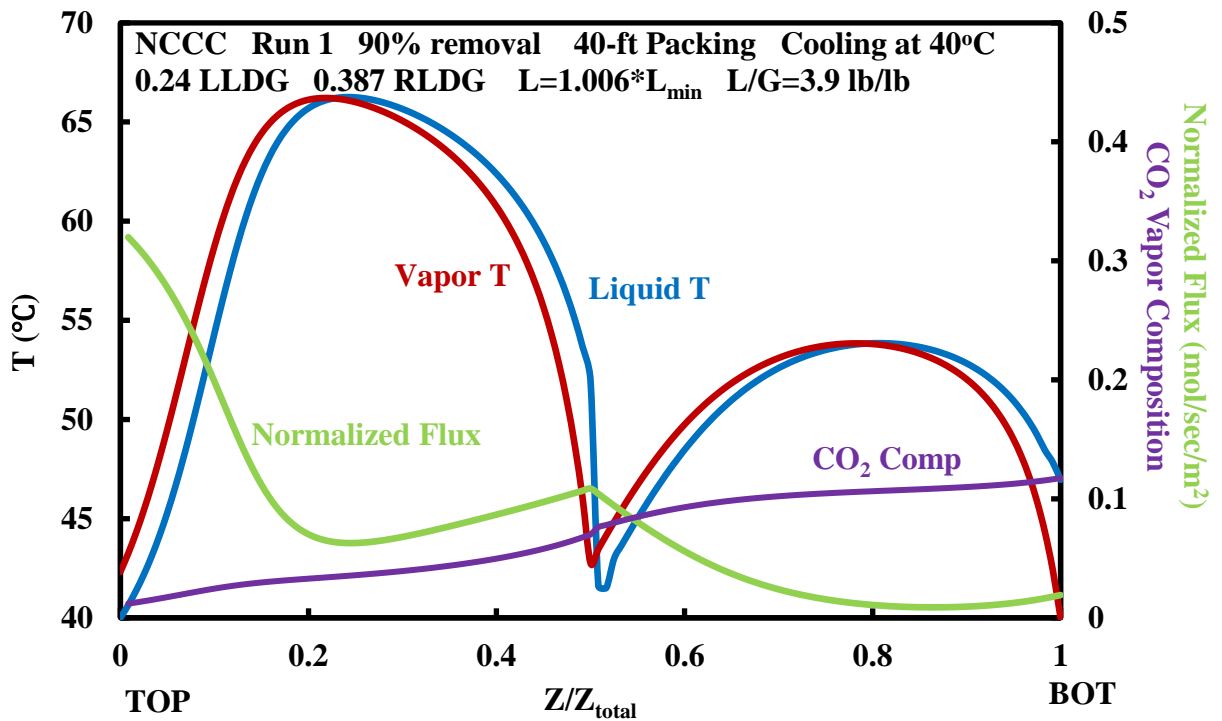


Figure 6.2: Model-predicted NCCC absorber temperature and flux profiles for Run 1.

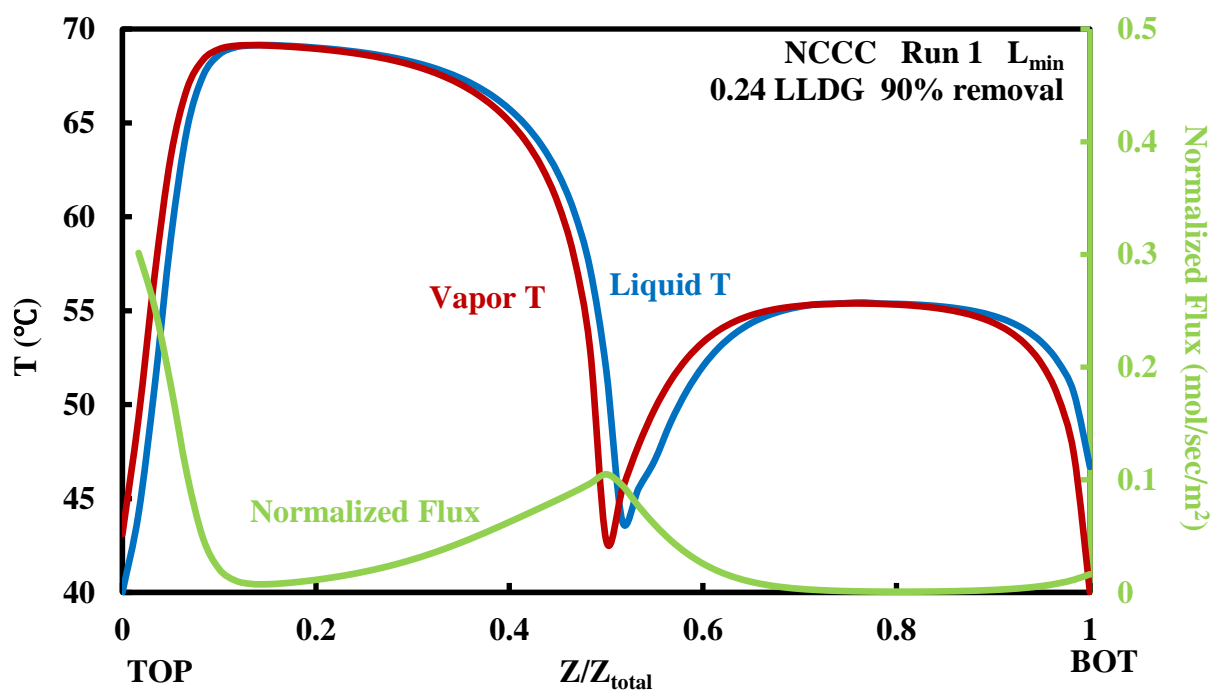


Figure 6.3: Model-predicted NCCC absorber temperature and flux profiles for Run 1 with 80-ft packing (at L_{min}).

Figure 6.4 shows the model-predicted absorber performance for Run 11, with 0.24 LLDG, 0.366 RLDG, 99% removal, and 1.16 L/L_{min} . With a higher L/G , the liquid tends to carry the heat and pushes the temperature bulge to the bottom end of the column. The huge temperature bulge in the bottom packing section is a result of the high CO_2 removal. Figure 6.4 also exhibits higher average flux across column without mass transfer pinch. Run 11 is expected to provide more reliable absorber packing performance data than Run 1.

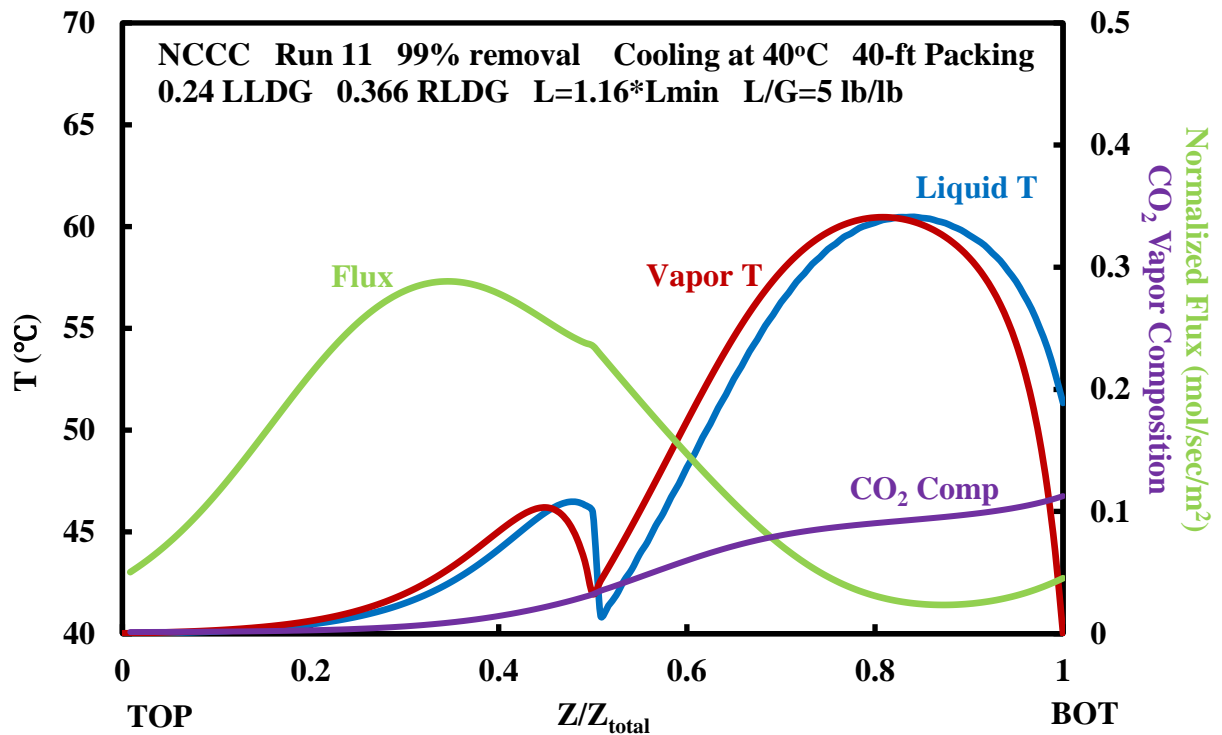


Figure 6.4: Model-predicted NCCC absorber temperature and flux profiles for Run 11.

The absorbers in Runs 5 and 6 are operated with cooling temperature at 30 °C. Run 5 is operated at 0.24 LLDG, and Run 6 is operated at 0.27 LLDG. Figures 6.5 and 6.6 show that, compared with Run 1, less CO₂ is removed in the bottom packing section, resulting in smaller temperature bulge near the bottom end of the column. The solid solubility window for 5 m PZ is shown in Figure 6.7 (Chen et al., 2014). The lean solvent trim cooler is where the solvent is most likely to precipitate. 5 m PZ with 0.24 CO₂ loading precipitates at 16 °C, and that with 0.27 loading precipitates at 5 °C. Careful plant operation and shutdown procedures should be followed to avoid solid precipitation. When the NCCC absorber is operated at a low cooling temperature, 0.27 LLDG is probably a better choice for reliable plant operation. Absorber performance with maximum throughput, 0.8 MWe, has also been evaluated. In Run 15, the absorber is operated with

0.24 LLDG and 0.38 RLDG, giving 95% removal and 1.1 L/L_{min}. The NCCC absorber is able to handle the maximum throughput with good performance.

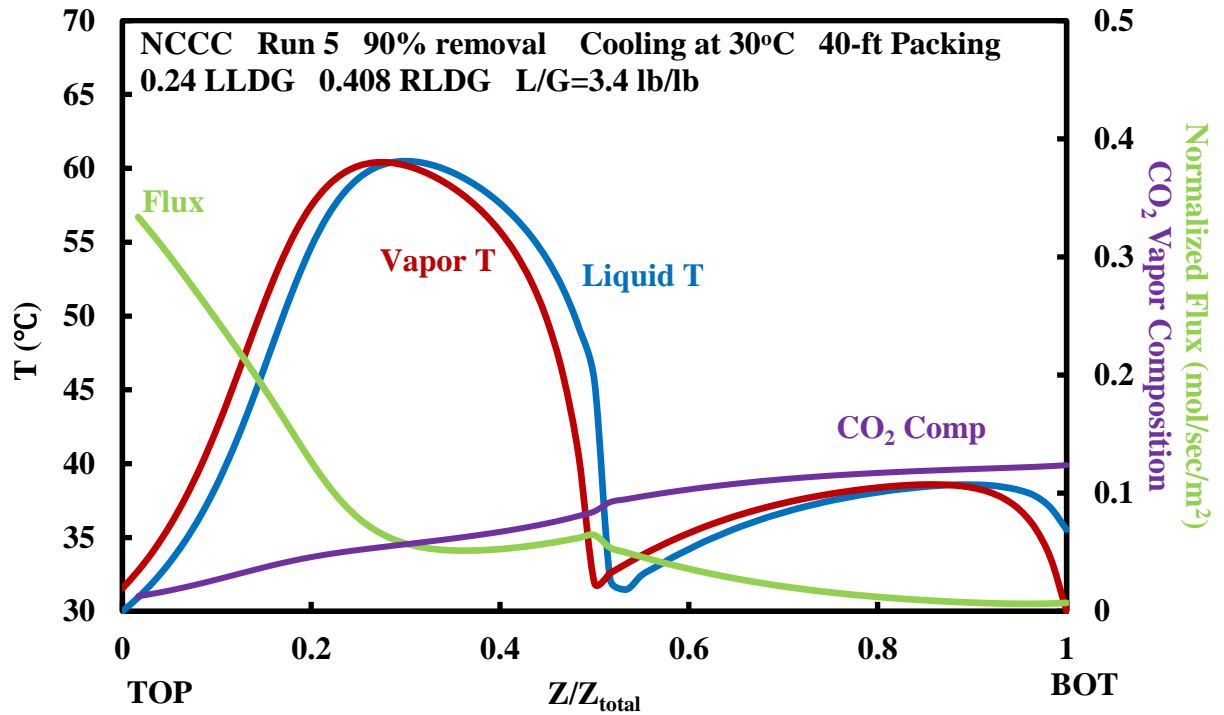


Figure 6.5: Model-predicted NCCC absorber temperature and flux profiles for Run 5.

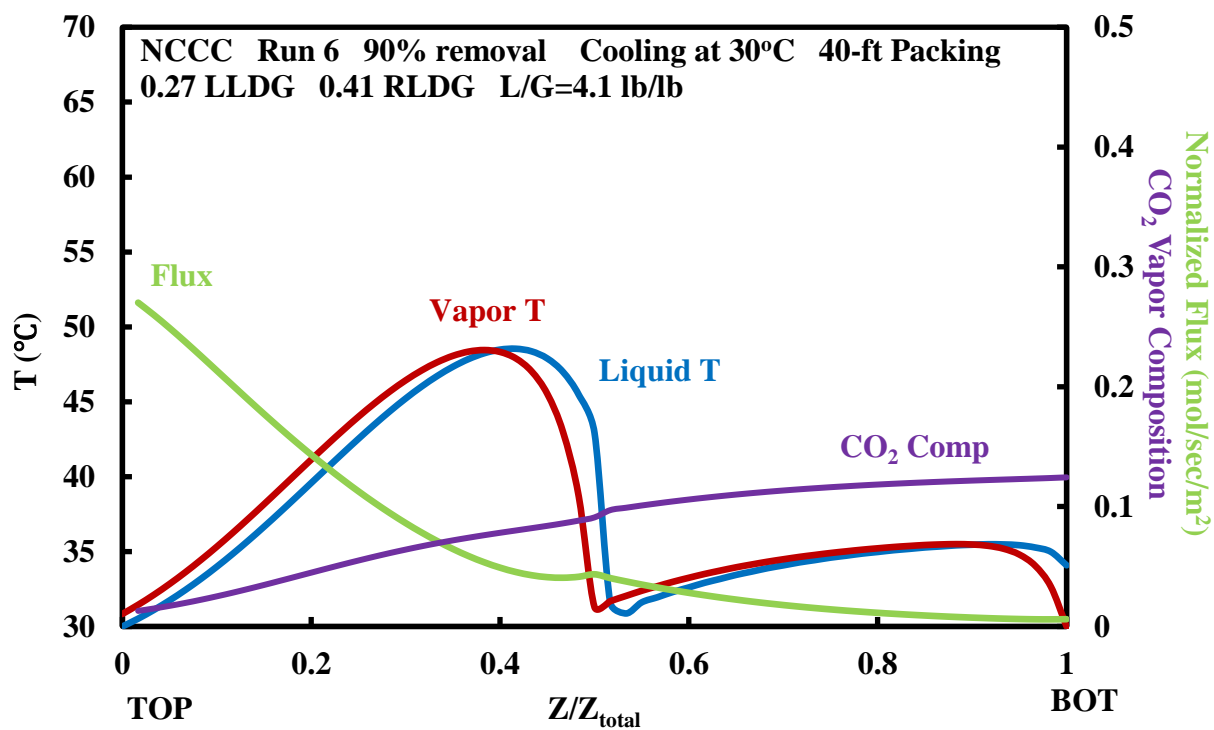


Figure 6.6: Model-predicted NCCC absorber temperature and flux profiles for Run 6.

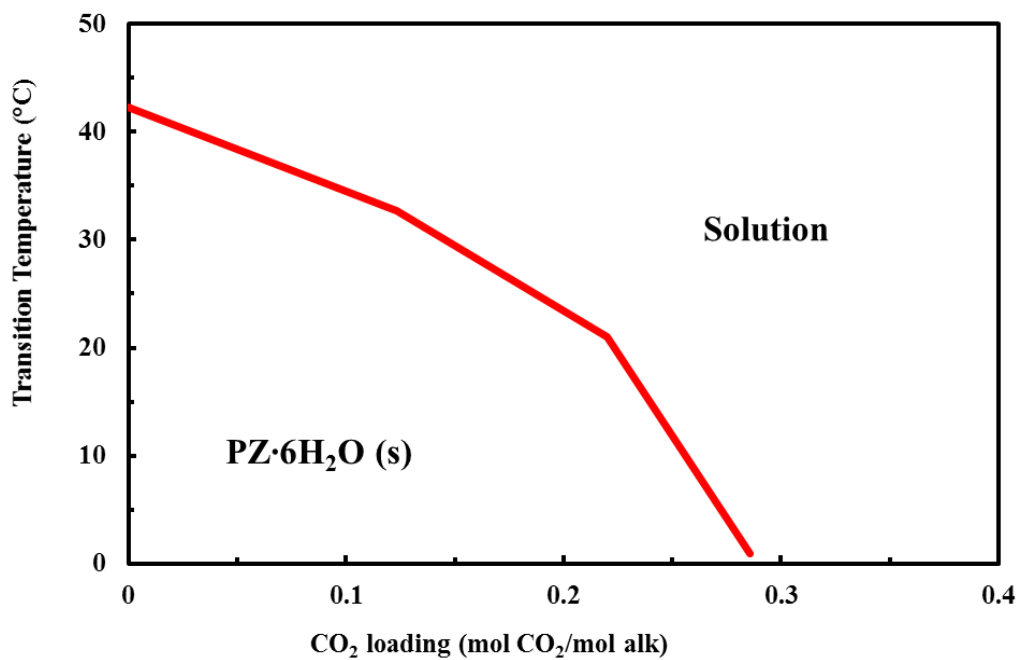


Figure 6.7: Solid solubility of 5 m PZ (Chen et al., 2014).

6.4 LOADING PREDICTION USING ONLINE DENSITY MEASUREMENTS

In the March 2015 UT-SRP campaign, a density correlation was used to predict solvent loadings from online density measurements (Zhang et al., 2017b). The density-predicted loadings were accurate, self-consistent, and can be collected with minimal efforts. The same approach is used to predict solvent loadings in the 2018 NCCC campaign. The density correlation was originally developed by Freeman (Equation 6.2) and water density is estimated from temperature (Equation 6.3) (Freeman, 2011; Tilton and Taylor, 1937). PZ concentration is assumed to be at 5 m throughout the campaign. In Table 6.3 and Figure 6.8, the solvent loadings are predicted as a function of solvent densities at 95 F, 104 F, 110 F, and 115 F. This will provide guidance for operators during the plant operation.

$$\rho_{PZ} = \rho_{H2O} \cdot (0.0407 \cdot C_{CO2} + 0.008 \cdot C_{PZ} + 0.991) \quad (6.2)$$

$$\rho_{H2O} = 1000 * \left[1 - \frac{(T-3.9863)^2 * (T+288.9414)}{508929.2 * (T+68.12963)} \right] \quad (6.3)$$

where:

ρ = Liquid density (kg/m³);

ρ_{H2O} = Water density calculated from Tilton-Taylor formula (kg/m³);

C_{CO2} = CO₂ concentration in the solution (mol/kg);

C_{PZ} = PZ concentration (mol/kg);

T = Temperature (°C).

Table 6.3: Predicted solvent densities as a function of loadings in 2018 NCCC pilot plant campaign.

T F	Loading mol CO ₂ /mol alk	Predicted Density lb/ft ³
95	0.24	67.06
95	0.27	67.50
95	0.35	68.64
95	0.40	69.33
104	0.24	66.94
104	0.27	67.38
104	0.35	68.52
104	0.40	69.21
110	0.24	66.85
110	0.27	67.29
110	0.35	68.43
110	0.40	69.11
115	0.24	66.77
115	0.27	67.21
115	0.38	68.76
115	0.40	69.03
242	0.24	63.77
242	0.27	64.19
242	0.38	65.67
242	0.40	65.93

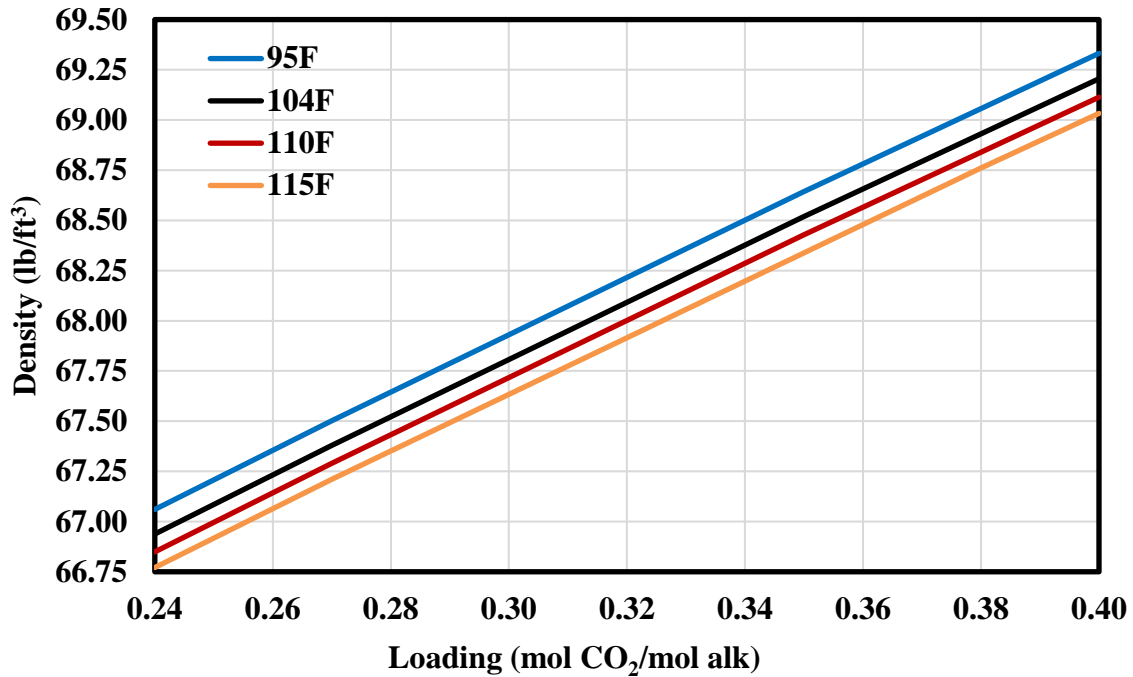


Figure 6.8: Predicted solvent densities as a function of loadings in 2018 NCCC pilot plant campaign.

6.5 CONCLUSIONS

The NCCC absorber is over-designed with excessive packing.

In order to maximize the value of packing performance data, design of experiments should avoid mass transfer pinches and L/L_{\min} should be designed between 1.1 to 1.3.

At 0.5 MWe flue gas, the absorber operated at 0.24 LLDG and 90% removal is close to pinch. The absorber operated with 0.24 LLDG and 99% removal is expected to provide more reliable absorber packing performance data.

At 0.8 MWe flue gas, the absorber operated at 0.24 LLDG and 0.38 RLDG is expected to perform reasonable well, with 95% removal and 1.1 L/L_{\min} .

5 m PZ with 0.24 CO₂ loading precipitates at 16 °C, and that with 0.27 loading precipitates at 5 °C. When the NCCC absorber is operated at a low cooling temperature, 0.27 LLDG is a better choice for reliable plant operation.

Chapter 7 : Conclusions and Recommendations

7.1 SUMMARY

This work developed a rate-based PZ aerosol model with complete overall mass balance in gPROMS[®] ModelBuilder and simulated aerosol growth at the unique conditions of PZ and the pilot plant absorber configurations at the National Carbon Capture Center (NCCC) conditions. Aerosol growth mechanisms were investigated and the limiting mass transfer driving force was identified. This work added to the previous aerosol growth model the simulation of amine driving force depletion in the bulk gas phase. This work simulated integrated absorber configurations and operating conditions that were proposed to mitigate amine emissions and gave recommendations for emissions control.

5 m PZ has become a new standard solvent for amine scrubbing carbon capture. In this work, the UT-SRP pilot plant was operated with 5 m PZ for the first time, and two pilot plant campaigns were designed and conducted. To evaluate the absorber performance within a wider range of operating conditions, a parametric test was performed with systematically varied PZ concentration, inlet CO₂, gas rate, lean loading, solvent to gas ratio, packing sections, and intercooling methods. The existing model correction method developed in previous campaigns was also evaluated using the newly collected absorber data.

This work also proposed and evaluated a membrane-amine hybrid carbon capture system for natural gas combined cycle (NGCC) power plants, where the CO₂ in the flue gas was enriched from 4% to 18% and absorber costs were greatly reduced. Amine scrubbing without the direct contact cooler was found to be a superior design for NGCC carbon capture. The absorber was optimized with different direct contact cooler options, multiple intercooling designs, different cooling options, and a wide range of lean loadings

at 4% to 18% inlet CO₂. Technical economic analysis was performed for the hybrid system to evaluate the economic feasibility.

7.2 CONCLUSIONS AND RECOMMENDATIONS FOR AEROSOL GROWTH MODELING

7.2.1 Mechanisms and Mitigation of Amine Aerosol Growth

Aerosol growth is a function of aerosol concentration. At high concentration, aerosol will not grow as much and therefore will be hard to collect. Aerosol is more likely to grow to the point where it can be collected (3 μm with common types of mist eliminators) with low aerosol concentration. For emissions control, removing all nuclei in the flue gas is expensive and it is not necessary to eliminate all nuclei. The techniques that can reduce the nuclei count to the point where aerosol can grow enough to be collected are sufficient.

In the absorber, amine aerosol growth is driven by amine-limited diffusion. As aerosol concentration increases, aerosol growth decreases due to the depletion of the amine driving force in the gas phase, and the limiting driving force for aerosol growth shifts from gas-to-drop to liquid-to-gas.

Understanding aerosol growth mechanisms will help control emissions by selecting appropriate packing types, solvents, and operating conditions. Aerosol growth can be increased by enhancing the gas-film mass transfer coefficient of packing, e.g., selecting finer packing or operating the column with higher gas velocity, which will produce larger aerosol that is easier to capture.

Greater amine volatility increases aerosol growth. A solvent with moderate volatility, like PZ, will produce aerosol that grows to larger size and is easier to collect. Solvents with low volatility should be avoided as they produce aerosol that is hard to collect. Solvents with very high volatility should also be avoided as they emit high gas phase amine.

An absorber operated at higher temperature and lower solvent loading will increase gas phase amine pressure and driving force, which helps aerosol grow.

The effects of initial aerosol diameter and amine composition on aerosol growth are insignificant.

In the water wash, aerosol approaches equilibrium with water in the gas phase. Process configurations that provide greater water partial pressure in the water wash, such as higher operating temperature and pre-humidified empty space, will help aerosol grow.

7.2.2 Recommendations for Aerosol Growth Model Development

In this work, all aerosol drops are assumed to have the same size. In the future model development, aerosol size distribution can be added to the model. Also, aerosol can be collected by packing if it grows to a size larger than 10 μm , resulting in a different size distribution. As a further improvement, drop collection mechanisms can also be added.

7.3 CONCLUSIONS AND RECOMMENDATIONS FOR PILOT PLANT ABSORBER DATA RECONCILIATION

7.3.1 Conclusions of the March 2015 Campaign with 5 m PZ

In the March 2015 UT-SRP campaign, the pilot plant absorber CO_2 material balance closed within +/- 2% when using density-predicted (corrected for Inhibitor A) loadings on the liquid side and re-calibrated FTIR data on the gas side.

5 m PZ provided significant absorber performance benefits over 8 m PZ due to enhanced mass transfer rates from lower solvent viscosity.

The pilot plant absorber model was validated over a wide variety of operating conditions: 5 m PZ and 8 m PZ, 6% and 12% inlet CO_2 , different intercooling configurations, as well as “over-stripped LLDG” and normal LLDG.

Interfacial area correction and CO₂ correction provided similar predictions of pilot plant absorber performance and could be used interchangeably to correct the model.

The inhibitor correction to density-predicted loadings was consistent with model-predicted correction to titration data and might provide an explanation for pilot-model offsets.

Pilot plant data suggested a possible time dependence, and absorber NTU values were slightly over-predicted (mean ratio of model-predicted NTU to pilot plant-measured NTU = 1.08). A possible explanation is that several high CO₂ removal cases in the March 2015 campaign were outside the region where the previous model corrections were developed, where the controlling mass transfer resistance in the absorber differed. This observation provides an opportunity to investigate future model corrections at different column mass transfer limiting mechanisms.

The pilot plant absorber model was reasonably able to capture pilot plant-measured column temperature profile behaviors of different intercooling configurations within 2% mean absolute percentage error.

7.3.2 Conclusions of the April 2017 Campaign with 5 m PZ

In the April 2017 UT-SRP campaign, NDIR measurements systematically over-predicted removal at 3.5% inlet CO₂ and under-predicted removal at 20% inlet CO₂; FTIR measurements were more scattered and systematically over-predicted removal at 8-20% inlet CO₂. These findings suggested possible errors of NDIR measurements at low outlet CO₂ and high inlet CO₂ as well as systematic bias of FTIR measurements. The averages of NDIR and FTIR were found to give the best overall CO₂ material balance closure.

The pilot plant absorber CO₂ material balance closed within +/- 20% when using titration-corrected density-predicted loadings on the liquid side and NDIR and FTIR average data on the gas side. No systematic trends were observed.

After the campaign, the three Raschig DTS Trough distributors were found to be undersized: all distributors were sized for 7 to 17 GPM but the absorber in several runs was operated at solvent rates up to 24 GPM. In these runs, NTU was over-predicted by the model.

The pilot plant absorber model without interfacial area correction was better at capturing pilot plant-measured NTU than the model with interfacial area correction. At 3.5-12% CO₂, the model without interfacial area correction could capture the pilot plant absorber NTU within 20% error. At 20% CO₂, the model captured the measured absorber NTU within 50% error.

7.3.3 Recommendations for Future Campaigns

The pilot plant absorber should be operated at both pinched and not pinched conditions. Equilibrium data can be obtained when absorber is pinched and packing data can be obtained when absorber is not pinched.

In the data reconciliation of all previous campaigns, one global correction factor was applied to the pilot plant absorber to cover all underlying factors. For the data reconciliation of future campaigns, two corrections should be applied to the model at the same time: an equilibrium correction (correct for errors in solvent loading measurements and effects of degradation) and a packing correction (correct for effects of rivulets and drop and additional mass transfer caused by distributors and chimney trays). In this way, better understanding of equilibrium and packing performance can be obtained.

If the absorber is running with excessive packing and high removal, gas and liquid measurements should be obtained between the packing sections. The outlet CO₂ might be below the detection limit of gas analyzers in some packing sections.

NDIR and FITR should be calibrated carefully in future campaigns.

The liquid distributors have been found to be under-sized in the April 2017 campaign. The distributors will be re-sized and the contacting problem will be fixed for future campaigns.

Viscosity data should be collected to account for solvent degradation effects.

7.4 CONCLUSIONS AND RECOMMENDATIONS FOR ABSORBER DESIGN

Amine scrubbing without the direct contact cooler is a superior design for NGCC carbon capture. 10% of the absorber CAPEX can be saved by eliminating the DCC. When DCC is eliminated, pump-around cooling at the bottom of the absorber can effectively manage the temperature of the hot flue gas, and still be effective for CO₂ absorption. Model-predicted temperature of the rich solvent never exceeds 55 °C. The absorber gas inlet must be designed to avoid excessive localized temperature and solvent evaporation.

When the inlet CO₂ increases from 4% to 18%, the total absorption costs decrease by 60% and the total regeneration costs remain the same. For hybrid membrane-amine scrubbing capture, as the inlet CO₂ increases from 12% to 18%, the total membrane costs increase by 108%. The hybrid system would be more economically feasible if it is operated at a lower overall CO₂ removal rate (where less membrane area is required) or if the membrane capital costs can be reduced.

In-and-out intercooling works well for the hybrid capture system with a membrane and amine scrubbing (high CO₂ in flue gas, high LLDG, high L/G). Pump-around

intercooling is more effective for simple NGCC capture (low CO₂ in flue gas, low LLDG, low L/G). The potential benefits of intercooling at extremely low LLDG are not as evident as those at high LLDG.

Dry cooling requires more packing and energy but appears to be technically and economically feasible if cooling water availability is limited.

Appendix A: Amine Aerosol Growth Model Code

The aerosol growth model was built in gPROMS[®] ModelBuilder. The model details are discussed in Chapter 2 and the code are included in this appendix. The aerosol growth model includes two parts: aerosol integration and physical properties.

A.1 AEROSOL INTEGRATION

```
##Aerosol Growth Model##  
  
#Aerosol Integration  
  
#Last Revised by: Yue Zhang  
  
#Date Modified: 2018/02/01  
  
#-----  
  
PARAMETER  
  
Column_Stages AS INTEGER DEFAULT 30  
  
Stages AS INTEGER DEFAULT 100  
  
Layers AS INTEGER DEFAULT 3  
  
Aspen_Profile AS FOREIGN_OBJECT "ExcelFO"  
  
Comps AS ORDERED_SET DEFAULT ["N2","H2O","CO2","PZ"]  
  
#Const  
  
pi AS REAL DEFAULT 3.14159265359  
  
g AS REAL DEFAULT 9.80665 #[m/s^2]  
  
R_const AS REAL DEFAULT 8.3144621 #m3·Pa·K-1·mol-1  
  
#Column Parameters  
  
H_col AS REAL DEFAULT 1.74625 #m  
  
D_col AS REAL DEFAULT 0.0427228 #m  
  
vfrac AS REAL DEFAULT 0.96
```

initial_Diameter_Drop AS REAL DEFAULT 2.3 #um
Num_Drop AS REAL DEFAULT 1e6 # Num/cm3
MW AS ARRAY(Comps) OF REAL
initial_LDG_Drop AS REAL DEFAULT 0.4 #molCO2/mol alk.
initial_molal_PZ_Drop AS REAL DEFAULT 5 # m
initial_xApp AS ARRAY(COMPS) OF REAL #mol/mol
initial_MW AS REAL #g/mol
initial_Rho AS REAL #kg/m3
initial_Conc_tot AS REAL #mol/m3
initial_Vol_drop AS REAL #m3
initial_T_Drop AS REAL DEFAULT 313 # m

UNIT

Phy_Props AS Phy_Props

VARIABLE

Parameters of Column

T_BulkG AS temperature

T_BulkL AS temperature

#y_BulkG AS ARRAY(Comps) OF molar_fraction

pp_BulkG AS ARRAY(Comps) OF pressure

#MW_BulkG AS molecular_weight

RHO_BulkG AS mass_density

K_BulkG AS thermo_conductivity

#CP_BulkG AS molar_specific_heat_capacity

MU_BulkG AS dynamic_viscosity
 Diff_BulkG AS ARRAY(Comps) OF diffusion_coefficient
 VOLFL_BulkG AS volume_flowrate
 #FN2_BulkG AS molar_flowrate
 #FH2O_BulkG AS molar_flowrate
 #FCO2_BulkG AS molar_flowrate
 #FPZ_BulkG AS molar_flowrate
 Kg_Bulk AS ARRAY(Comps) OF mass_transfer_coefficient
 IA_Bulk AS specific_surface_area
 x_BulkL AS ARRAY(Comps) OF molar_fraction
 C_BulkL AS ARRAY(Comps) OF molar_concentration
 LDG_BulkL AS loading
 HOLDUP_BulkL AS no_type
 #Parameters of Gas Side
 #Conc_BulkG AS ARRAY(Comps) OF molar_concentration
 ppeq_BulkL AS ARRAY(Comps) OF pressure
 N_gl AS ARRAY(Comps) OF no_type
 #Parameters of Aerosol Side
 T_Drop AS temperature #Drop temperature, K
 n AS ARRAY(Comps) OF nanomoles # mole of drop, nano mole
 n_tot AS nanomoles# mole of drop, nano mole
 Conc_Drop AS ARRAY(Comps) OF molar_concentration # concentration of drop, mole/m3
 Conc_Drop_Free AS ARRAY(Comps) OF molar_concentration # concentration of drop,
 mole/m3
 Conc_tot_Drop AS molar_concentration # concentration of drop, mole/m3

```

Rds AS Radius_Drop # Radius of drop, um
Diff_Drop AS ARRAY(Comps) OF diffusion_coefficient # diffusion coefficient of drop, m2/s
Ngd AS ARRAY(Comps) OF no_type #mass transfer flux between gas and drop, mol/m2-s
v_Drop AS velocity #velocity of drop, m/s
v_BulkG AS velocity #velocity of gas, m/s

#If considering relative velocity between drops and the bulk gas, activate the following
equations#

#v_Rel AS no_type # related velocity, m/s

d_drop AS Radius_Drop # diameter pf drop, um
RHO_Drop AS mass_density #density of drop, kg/m3

## activate following equations##

#Cc AS no_type

## activate following equations##

#avgKn AS no_type

Kn AS ARRAY(Comps) OF no_type

## activate following equations##

#avgmfp AS no_type

mfp AS ARRAY(Comps) OF no_type

LDG_Drop AS loading #CO2 loading, mol CO2/mol alk.

Cplmx AS molar_specific_heat_capacity #heat capacity, J/mol-K

xApp AS ARRAY(Comps) OF molar_fraction #apprant mole fractions of drop, mole/mole

Qd AS heat_flux #heat transfer flux, J/m2-s

delHd AS ARRAY(Comps) OF molar_specific_enthalpy #heat of vaporation and absorption,
J/mol

hg AS heat_transfer_coefficient #heat transfer coeff.

```

```

kg AS ARRAY(Comps) OF mass_transfer_coefficient #mass transfer coeff.
kgprime_Drop AS mass_transfer_coefficient #mass transfer coeff.
A_Drop AS area_Drop
agd AS specific_surface_area
Vol_Drop AS volume
Fuchs AS ARRAY(Comps) OF no_type
ppeq_Drop_Outlayer AS ARRAY(Comps) OF pressure
k2d AS no_type
Henry_Drop AS no_type
Nu AS Dimentionless
## activate following equations##
#Re AS Dimentionless
#Pr AS Dimentionless
#Sc AS ARRAY(Comps) OF Dimentionless
Sh AS ARRAY(Comps) OF Dimentionless
v_gmol AS ARRAY(Comps) OF no_type
molal_PZ_Drop AS molal_concentration
h AS length
Thermal_Conductivity_Drop AS thermo_conductivity
MW_Drop AS molecular_weight

SELECTOR

MT_Mode AS (DefaultMode,InitializationMode) DEFAULT DefaultMode
kgprime_Mode AS (DefaultMode,InitializationMode) DEFAULT DefaultMode

```

SET

```
Phy_Props.Stages := Stages;
Phy_Props.Layers := Layers;
Phy_Props.Comps := Comps;
MW := [28.0134, 18.01528, 44.0095, 86.1356]; #g/gmol
initial_xApp('N2') := 0;
initial_xApp('H2O')
(1000/18)/((1000/18)+(2*initial_molal_PZ_Drop*initial_LDG_Drop)+(initial_molal_PZ_Drop));
initial_xApp('CO2')
(2*initial_molal_PZ_Drop*initial_LDG_Drop)/((1000/18)+(2*initial_molal_PZ_Drop*initial_LDG_Drop
)+(initial_molal_PZ_Drop));
initial_xApp('PZ')
(initial_molal_PZ_Drop)/((1000/18)+(2*initial_molal_PZ_Drop*initial_LDG_Drop)+(initial_molal_PZ_
Drop));
initial_MW
initial_xApp('H2O')*MW('H2O')+initial_xApp('CO2')*MW('CO2')+initial_xApp('PZ')*MW('PZ');#g/gm
ol
initial_Rho := 1000*(1.5494 -0.0005728 *initial_T_Drop)*LOG(2.676 *initial_xApp('CO2')-
0.030977 *initial_xApp('PZ')-0.0726176 *initial_LDG_Drop+2.102569 );#kg/m3
initial_Conc_tot := initial_Rho/(initial_MW/1000);#mol/m^3
initial_Vol_drop := 1/6*pi*initial_Diameter_Drop^3; #um^3
```

EQUATION

```
# Model equations #
```

```
# GAS Profiles #
```

```
T_BulkG = Aspen_Profile.TG(h);
```

```
#y_BulkG('N2') = Aspen_Profile.yN2(h);
#y_BulkG('H2O') = Aspen_Profile.yH2O(h);
#y_BulkG('CO2') = Aspen_Profile.yCO2(h);
#y_BulkG('PZ') = Aspen_Profile.yPZ(h);
pp_BulkG('N2') = Aspen_Profile.ppN2(h);
pp_BulkG('H2O') = Aspen_Profile.ppH2O(h);
pp_BulkG('CO2') = Aspen_Profile.ppCO2(h);
#pp_BulkG('PZ') = Aspen_Profile.ppPZ(h);
#MW_BulkG = Aspen_Profile.MW(h);
RHO_BulkG = Aspen_Profile.RHOG(h);
K_BulkG = Aspen_Profile.K(h);
#CP_BulkG = Aspen_Profile.CPG(h);
MU_BulkG = Aspen_Profile.MUG(h);
Diff_BulkG('N2') = Aspen_Profile.DGN2(h);
Diff_BulkG('H2O') = Aspen_Profile.DGH2O(h);
Diff_BulkG('CO2') = Aspen_Profile.DGCO2(h);
Diff_BulkG('PZ') = Aspen_Profile.DGPZ(h);
VOLFL_BulkG = Aspen_Profile.VOLFLG(h);
#FN2_BulkG = Aspen_Profile.FGN2(h);
#FH2O_BulkG = Aspen_Profile.FGH2O(h);
#FCO2_BulkG = Aspen_Profile.FGCO2(h);
#FPZ_BulkG = Aspen_Profile.FGPZ(h);
Kg_Bulk('N2') = Aspen_Profile.KGN2(h);
Kg_Bulk('H2O') = Aspen_Profile.KGH2O(h);
Kg_Bulk('CO2') = Aspen_Profile.KGCO2(h);
```

```

Kg_Bulk('PZ') = Aspen_Profile.KGPZ(h);
IA_Bulk = Aspen_Profile.IA(h)/(pi*D_col^2/4*H_col/Column_Stages);
x_BulkL('N2') = Aspen_Profile.xN2(h);
x_BulkL('H2O') = Aspen_Profile.xH2O(h);
x_BulkL('CO2') = Aspen_Profile.xCO2(h);
x_BulkL('PZ') = Aspen_Profile.xPZ(h);
C_BulkL('N2') = Aspen_Profile.CLN2P(h);
C_BulkL('H2O') = Aspen_Profile.CLH2OP(h);
C_BulkL('CO2') = Aspen_Profile.CLCO2P(h);
C_BulkL('PZ') = Aspen_Profile.CLPZP(h);
LDG_BulkL = Aspen_Profile.LDG(h);
T_BulkL = Aspen_Profile.TL(h);
HOLDUP_BulkL = Aspen_Profile.HOLDUPL(h)/(pi*D_col^2/4*H_col/Column_Stages);
#Physical Properties Input Parameters
Phy_Props.T_BulkG = T_BulkG;
Phy_Props.T_BulkL = T_BulkL;
Phy_Props.T_Drop = T_Drop;
Phy_Props.xApp = xApp;
Phy_Props.x_BulkL = x_BulkL;
Phy_Props.LDG_Drop = LDG_Drop;
Phy_Props.LDG_BulkL = LDG_BulkL;
Phy_Props.d_drop = d_drop;
#Properties of Aerosol side
Diff_Drop = Phy_Props.Diff_Drop;
Cplmx = Phy_Props.Cplmx;

```

```

delHd('N2') = Phy_Props.delHd('N2');
delHd('H2O') = Phy_Props.delHd('H2O');
delHd('CO2') = Phy_Props.delHd('CO2');
delHd('PZ') = Phy_Props.delHd('PZ');
Thermal_Conductivity_Drop = Phy_Props.Thermal_Conductivity_Drop;
ppeq_Drop_Outlayer = Phy_Props.ppeq_Drop_Outlayer;
v_gmol = Phy_Props.v_gmol;
RHO_Drop = Phy_Props.RHO_Drop;
k2d = Phy_Props.k2d;
Henry_Drop = Phy_Props.Henry_Drop;
MW_Drop = xApp('H2O')*MW('H2O')+xApp('CO2')*MW('CO2')+xApp('PZ')*MW('PZ');
#Algebraic Equations of Aerosol
# Calc. CO2 Loading
If xApp('PZ')>0 Then
LDG_Drop = xApp('CO2')/(2*xApp('PZ'));
Else
LDG_Drop = 0;
End
#Calc. Kn
mfp = 3*Diff_BulkG/(v_gmol);
## activate following equations##
#avgmfp = sigma(mfp)/Comps.Card;
d_drop = 2*Rds;
Kn = (2*mfp/(d_drop*(1E-6)));
## activate following equations##

```

```

#avgKn = (2*avgmfp/(d_drop*(1E-6)));

#Calc. Cc

#Cc = 1+avgKn*(1.246+0.418*exp(-0.867/avgKn));#Cunningham slip used to correct Stokes'
Law.

#Calc. Fuchs(i)

Fuchs = (0.75*1*(1+Kn))/(Kn^2+Kn+0.283*Kn*1+0.75*1);#alpha = 1;

# Calc. v_Drop

v_BulkG = 4*VOLFL_BulkG/((vfrac-HOLDUP_BulkL)*pi*(D_col^2));

## activate following equations##

#v_Rel = (d_drop*(1E-6))^2*(RHO_DropMix-RHO_BulkG)*g*Cc/(18*MU_BulkG);

v_Drop = v_BulkG;

##change the following equations##

#v_Drop= v_BulkG -v_Rel;

#Calc. Ngd

Ngd('N2') = 0;

Ngd('H2O') = Fuchs('H2O')*kg('H2O')/(R_const*T_BulkG)*(pp_BulkG('H2O')-
ppeq_Drop_Outlayer('H2O'));

Ngd('CO2') = kgprime_Drop*(pp_BulkG('CO2')-ppeq_Drop_Outlayer('CO2'));

Ngd('PZ') = Fuchs('PZ')*kg('PZ')/(R_const*T_BulkG)*(pp_BulkG('PZ')-
ppeq_Drop_Outlayer('PZ'));

#Calc. Qd

Qd = (Ngd('H2O')*delHd('H2O')-
Ngd('PZ')*delHd('PZ')+Ngd('CO2')*delHd('CO2'))+hg*(T_BulkG-T_Drop);

#Calc. Dimensionless Numbers

## activate following equations##

```

```

#Sc = MU_BulkG/RHO_BulkG/Diff_BulkG;

#Pr = (MU_BulkG*CP_BulkG)/(K_BulkG*MW_BulkG);

#Re = ABS(RHO_BulkG*v_Rel*d_drop*(1E-6)/MU_BulkG);

Sh = 2; #2+0.6*(Re^(1/2))*(Sc^(1/3));

Nu = 2; #+0.6*(Re^(1/2))*(Pr^(1/3));

#Calc. kg

kg = Sh*Diff_BulkG/(d_drop*(1E-6));

#Calc. kg'

If Conc_Drop_Free('PZ')>0 Then

kgprime_Drop = (k2d*Conc_Drop_Free('PZ') *Diff_Drop('CO2'))^(1/2)/Henry_Drop;

Else

kgprime_Drop = 0;

End

#Calc. hg

hg = Nu*K_BulkG/(d_drop*(1E-6));

#Calc. A_Drop

A_Drop = 4*pi*Rds^2; #um^2

agd = 4*pi*Rds^2/(4/3*pi*Rds^3)*(1E-6)^2/(1E-6)^3;

#Calc. Vol_Drop

Vol_Drop = 4/3*pi*Rds^3 = (n_tot*(1E-9)/Conc_tot_Drop)*(1E6)^3; #um^3

molal_PZ_Drop = (1000/18)*xApp('PZ')/xApp('H2O');

Conc_Drop_Free('N2') = 0;

Conc_Drop_Free('H2O') = Conc_Drop('H2O');

Conc_Drop_Free('CO2') = 0;

Conc_Drop_Free('PZ') = Conc_Drop('PZ')-Conc_Drop('CO2');

```

```

# Total Conc.
Conc_tot_Drop = RHO_Drop/(MW_Drop/1000);
#Calc. Conc_Drop
xApp*Conc_tot_Drop = Conc_Drop;
#Calc. xApp
xApp = n/n_tot;
n_tot = SIGMA(n);
#Differential Equations of Aerosol
n('N2') = 0;
For i in ['H2O','CO2','PZ'] Do
    v_Drop/H_col*$n(i)*(1E-9) = Ngd(i)*A_Drop*(1E-6)^2;
End
v_Drop/H_col*$T_Drop
v_Drop/H_col*T_Drop/n_tot*SIGMA($n('H2O':'PZ'))+Qd*A_Drop*(1E-6)^2/(Cplmx*n_tot*(1E-9));
#Properties of Gas
ppeq_BulkL=Phy_Props.ppeq_BulkL;
#Algebraic Equations of Gas
N_gl( Comps - 'PZ') = 0;
N_gl('PZ') = Kg_Bulk('PZ')*(pp_BulkG('PZ')-ppeq_BulkL('PZ'));
#Differential Equations of Gas
v_Drop/H_col*$pp_BulkG('PZ') = (-Ngd('PZ')*A_Drop*(1E-6)^2*Num_Drop*(1E2)^3-
N_gl('PZ')*IA_Bulk)*R_const*T_BulkG;

ASSIGN
h := TIME;

```

INITIAL

#STEADY_STATE

T_Drop = initial_T_Drop;

$n(\text{'CO2'}) \times (1\text{E-}9) = \text{initial_xApp}(\text{'CO2'}) \times \text{initial_Conc_tot} \times \text{initial_Vol_drop} \times (1\text{E-}6)^3$;

$n(\text{'PZ'}) \times (1\text{E-}9) = \text{initial_xApp}(\text{'PZ'}) \times \text{initial_Conc_tot} \times \text{initial_Vol_drop} \times (1\text{E-}6)^3$;

$n(\text{'H2O'}) \times (1\text{E-}9) = \text{initial_xApp}(\text{'H2O'}) \times \text{initial_Conc_tot} \times \text{initial_Vol_drop} \times (1\text{E-}6)^3$;

pp_BulkG('PZ') = Aspen_Profile.ppPZ(0);

A.2 PHYSICAL PROPERTIES

##Aerosol Growth Model##

#Physical Properties

#Last Revised by: Yue Zhang

#Date Modified: 2018/02/01

#-----

PARAMETER

ParameterName AS INTEGER || REAL || LOGICAL || VariableType < DEFAULT Value >

ParameterName AS ARRAY (Size < , ... >) OF INTEGER || REAL || LOGICAL || VariableType

< DEFAULT Value >

ParameterName AS FOREIGN_OBJECT < "ForeignObjectClass" > < DEFAULT

"ForeignObjectValue" >

ParameterName AS ORDERED_SET < DEFAULT ["Name" < , ... >] >

Stages AS INTEGER

Layers AS INTEGER

Comps AS ORDERED_SET DEFAULT ["N2","H2O","CO2","PZ"]

pi AS REAL DEFAULT 3.14159265359

R_const AS REAL DEFAULT 8.3144621 #m3·Pa·K-1·mol-1

MW AS ARRAY(Comps) OF REAL

DISTRIBUTION_DOMAIN

#Height AS [0 : 1]

Radius AS [0 : 1]

VARIABLE

VariableName AS VariableType

VariableName AS ARRAY (Size || OrderedSet < , ... >) OF VariableType

VariableName AS DISTRIBUTION (DomainName < , ... >) OF VariableType

T_Drop AS temperature

T_BulkG AS temperature

T_BulkL AS temperature

LDG_Drop AS loading

LDG_BulkL AS loading

xApp AS ARRAY(Comps) OF molar_fraction

xwApp AS ARRAY(Comps) OF mass_fraction

x_BulkL AS ARRAY(Comps) OF molar_fraction

d_drop AS Radius_Drop

ppeq_BulkL AS ARRAY(Comps) OF pressure

Diff_Drop AS ARRAY(Comps) OF diffusion_coefficient

ppeq_Drop_Outlayer AS ARRAY(Comps) OF pressure

v_gmol AS ARRAY(Comps) OF no_type

RHO_Drop AS mass_density
 k2d AS no_type
 Henry_Drop AS no_type
 MUDH2O AS dynamic_viscosity
 MUDMIX AS dynamic_viscosity
 VmolD AS ARRAY(Comps) OF no_type
 TAUD AS ARRAY(Comps) OF no_type
 Cp_Drop AS ARRAY (Comps) OF molar_specific_heat_capacity
 Cp_Ex_Drop AS molar_specific_heat_capacity
 Cplmx AS molar_specific_heat_capacity
 delHd AS ARRAY(Comps) OF molar_specific_enthalpy
 Thermal_Conductivity_Drop AS thermo_conductivity

SET

#Height := [BFDM,Stages];
 Radius := [OCFEM,2,Layers];
 MW := [28.0134, 18.01528, 44.0095, 86.1356];

EQUATION

Model equations
 #Properties of Aerosol side
 Diff_Drop('N2') = 0;
 Diff_Drop('H2O') = (1/100^2)*0.024*EXP(-2122/T_Drop);#9E-9;
 Diff_Drop('PZ') = Diff_Drop('CO2')/2;
 Diff_Drop('CO2') = (1/100^2)*0.024*EXP(-2122/T_Drop)*(MUDH2O/MUDMIX)^0.72;

$$\text{MUDH2O} = \text{EXP}(-52.843 + (3703.6 / \text{T_Drop}) + 5.866 * \text{LOG}(\text{T_Drop}) - 5.88\text{E-}29 * \text{T_Drop}^10);$$

$$\text{xwApp}(\text{'N2'}) = \frac{\text{MW}(\text{'N2'}) * \text{xApp}(\text{'N2'})}{\text{MW}(\text{'N2'}) * \text{xApp}(\text{'N2'}) + \text{MW}(\text{'H2O'}) * \text{xApp}(\text{'H2O'}) + \text{MW}(\text{'CO2'}) * \text{xApp}(\text{'CO2'}) + \text{MW}(\text{'PZ'}) * \text{xApp}(\text{'PZ'})};$$

$$\text{xwApp}(\text{'H2O'}) = \frac{\text{MW}(\text{'H2O'}) * \text{xApp}(\text{'H2O'})}{\text{MW}(\text{'N2'}) * \text{xApp}(\text{'N2'}) + \text{MW}(\text{'H2O'}) * \text{xApp}(\text{'H2O'}) + \text{MW}(\text{'CO2'}) * \text{xApp}(\text{'CO2'}) + \text{MW}(\text{'PZ'}) * \text{xApp}(\text{'PZ'})};$$

$$\text{xwApp}(\text{'CO2'}) = \frac{\text{MW}(\text{'CO2'}) * \text{xApp}(\text{'CO2'})}{\text{MW}(\text{'N2'}) * \text{xApp}(\text{'N2'}) + \text{MW}(\text{'H2O'}) * \text{xApp}(\text{'H2O'}) + \text{MW}(\text{'CO2'}) * \text{xApp}(\text{'CO2'}) + \text{MW}(\text{'PZ'}) * \text{xApp}(\text{'PZ'})};$$

$$\text{xwApp}(\text{'PZ'}) = \frac{\text{MW}(\text{'PZ'}) * \text{xApp}(\text{'PZ'})}{\text{MW}(\text{'N2'}) * \text{xApp}(\text{'N2'}) + \text{MW}(\text{'H2O'}) * \text{xApp}(\text{'H2O'}) + \text{MW}(\text{'CO2'}) * \text{xApp}(\text{'CO2'}) + \text{MW}(\text{'PZ'}) * \text{xApp}(\text{'PZ'})};$$

$$\text{MUDMIX} = \text{MUDH2O} * \text{EXP}(((487.52 * \text{xwApp}(\text{'PZ'}) + 1389.31 * \text{T_Drop} + (1.58 * \text{xwApp}(\text{'PZ'}) + 4.5)) * (\text{LDG_Drop} * (8.73 * \text{xwApp}(\text{'PZ'}) - 0.0038 * \text{T_Drop} - 0.3) + 1) * \text{xwApp}(\text{'PZ'})) / \text{T_Drop}^2);$$

$$\text{ppeq_Drop_Outlayer}(\text{'N2'}) = 0;$$

$$\text{ppeq_Drop_Outlayer}(\text{'H2O'}) = \frac{\text{xApp}(\text{'H2O'})}{(\text{xApp}(\text{'PZ'}) + \text{xApp}(\text{'H2O'})) * \text{EXP}(73.649 + (-7258.2 / \text{T_Drop}) - 7.3037 * \text{LOG}(\text{T_Drop}) + 4.17\text{E-}06 * \text{T_Drop}^2) * \text{EXP}(4 * \text{SIGMA}(\text{xApp}(\text{'H2O'}) * \text{TAUD}(\text{'H2O'}) + \text{xApp}(\text{'CO2'}) * \text{TAUD}(\text{'CO2'}) + \text{xApp}(\text{'PZ'}) * \text{TAUD}(\text{'PZ'})) * \text{Vmold}(\text{'H2O'}) / (1.38065\text{E-}23 * \text{T_Drop} * \text{d_drop} * 1\text{E-}6))};$$

$$\text{ppeq_Drop_Outlayer}(\text{'CO2'}) = \frac{\text{EXP}(35.5 + (-11082 / \text{T_Drop}) - 22.5 * \text{LDG_Drop}^2 + 4713 * (\text{LDG_Drop} / \text{T_Drop}) + 11722 * (\text{LDG_Drop}^2 / \text{T_Drop})) * \text{EXP}(4 * \text{SIGMA}(\text{xApp}(\text{'H2O'}) * \text{TAUD}(\text{'H2O'}) + \text{xApp}(\text{'CO2'}) * \text{TAUD}(\text{'CO2'}) + \text{xApp}(\text{'PZ'}) * \text{TAUD}(\text{'PZ'})) * \text{Vmold}(\text{'CO2'}) / (1.38065\text{E-}23 * \text{T_Drop} * \text{d_drop} * 1\text{E-}6))};$$

$$\text{ppeq_Drop_Outlayer}(\text{'PZ'}) = \frac{\text{xApp}(\text{'PZ'})}{(\text{xApp}(\text{'H2O'}) + \text{xApp}(\text{'PZ'})) * \text{EXP}(-123 + 21.6 * \text{LOG}(\text{T_Drop}) + 19.9 * \text{LDG_Drop} - 18027$$

$$*(LDG_Drop^2/T_Drop))*EXP(4*SIGMA(xApp('H2O')*TAUD('H2O')+xApp('CO2')*TAUD('CO2')+xApp('PZ')*TAUD('PZ'))*Vmold('PZ'))/(1.38065E-23 *T_Drop*d_drop*1E-6));$$

$$Vmold('N2') = 0;$$

$$Vmold('H2O') = (1/(6.0221415*10^23*1000))*(-13.851 +0.64038 *T_Drop-0.0019124 *T_Drop^2+1.82E-06 *T_Drop^3)^{-1};$$

$$Vmold('CO2') = (1/(6.0221415*10^23*1000))*(2.768 /0.26212 ^{1+(1-(304.21/304.21))^{0.2908}})^{-1};$$

$$Vmold('PZ') = (1/(6.0221415*10^23*1000))*(1.0425 /0.323 ^{1+(1-(T_Drop/638))^{0.28571}})^{-1};$$

$$TAUD('N2') = 0;$$

$$TAUD('H2O') = 0.17766 *(1-T_Drop/647.096)^{2.567 -3.3377 *T_Drop/647.096 +1.9699 *(T_Drop/647.096)^2};$$

$$TAUD('CO2') = 0;$$

$$TAUD('PZ') = 0.024853*(1-T_Drop/638)^{1.1667 +0*T_Drop/638 +0*(T_Drop/638)^2};$$

$$v_gmol('N2') = ((1000*6.0221415*10^23*8*1.3806503*10^{23})*T_BulkG)/(pi*MW('N2'))^{1/2};$$

$$v_gmol('H2O') = ((1000*6.0221415*10^23*8*1.3806503*10^{23})*T_BulkG)/(pi*MW('H2O'))^{1/2};$$

$$v_gmol('CO2') = ((1000*6.0221415*10^23*8*1.3806503*10^{23})*T_BulkG)/(pi*MW('CO2'))^{1/2};$$

$$v_gmol('PZ') = ((1000*6.0221415*10^23*8*1.3806503*10^{23})*T_BulkG)/(pi*MW('PZ'))^{1/2};$$

```

RHO_Drop = 1000*(1.5494 -0.0005728 *T_Drop)*LOG(2.676 *xApp('CO2')-0.030977
*xApp('PZ')-0.0726176 *LDG_Drop+2.102569 );
k2d = 65700000 *EXP(-34100 /(8.3144621*T_Drop));
Henry_Drop = 17107000 *EXP(-1886.1 /T_Drop)*101325/(100^3);

Cp_Drop('N2') = 0;
Cp_Drop('H2O') = 276370 -2090.1 *T_Drop+8.125 *T_Drop^2-0.014116 *T_Drop^3+9.37E-
06 *T_Drop^4;
Cp_Drop('CO2') = 0;
Cp_Drop('PZ') = 46690 +431.5*T_Drop+0*T_Drop^2+0*T_Drop^3+0*T_Drop^4;

Cp_Ex_Drop = (xApp('PZ')*xApp('CO2')*(-8722.163507 +36.220997 *T_Drop)+(40762.0731
-173.383544 *T_Drop)*(xApp('PZ')-xApp('CO2')))+xApp('H2O')*xApp('CO2')*((4604.181038 -
17.76459089 *T_Drop)+(-5368.404949 +20.37895136 *T_Drop)*(xApp('H2O')-xApp('CO2'))))*1000;

Cplmx =
1/1000*((Cp_Drop('N2')*xApp('N2')+Cp_Drop('H2O')*xApp('H2O')+Cp_Drop('CO2')*xApp('CO2')+C
p_Drop('PZ')*xApp('PZ'))+Cp_Ex_Drop);#J/mol K

delHd('N2') = 0;
delHd('H2O') = (1/1000)*51546000 *(1-T_Drop/647.096)^(0.28402 -0.15843
*(T_Drop/647.096)+0.2375 *(T_Drop/647.096)^2);
delHd('CO2') = (1/1000)*(-R_const)*(-11082 +4713 *LDG_Drop+11722 *LDG_Drop^2);
delHd('PZ') = (1/1000)*(-R_const)*(21.6 *T_Drop-18027 *LDG_Drop^2);
Thermal_Conductivity_Drop = 0.6;

```

```

#Properties of Gas

ppeq_BulkL('N2') = 0;

ppeq_BulkL('H2O') = x_BulkL('H2O')/(x_BulkL('PZ')+x_BulkL('H2O'))*EXP(73.649+(-7258.2
/T_BulkL)-7.3037*LOG(T_BulkL)+4.17E-06*T_BulkL^2);

ppeq_BulkL('CO2') = EXP(35.5 +(-11082 /T_BulkL)-22.5 *LDG_BulkL^2+4713
*(LDG_BulkL/T_BulkL)+11722*(LDG_BulkL^2/T_BulkL));

ppeq_BulkL('PZ') = x_BulkL('PZ')/(x_BulkL('H2O')+x_BulkL('PZ'))*EXP(-123 +21.6
*LOG(T_BulkL)+19.9*LDG_BulkL-18027*(LDG_BulkL^2/T_BulkL));

```

Appendix B: Development of DeltaV Graphical Operator Interface for the April 2017 UT-SRP Pilot Plant Campaign

In the April 2017 UT-SRP pilot plant campaign, the DeltaV operator interface graphics for absorber (Figure B.2) have been completely redesigned; the operator interface graphics for absorber gas and stripper (Figure B.1 and Figure B.3) have been greatly improved based on the graphics of the March 2015 UT-SRP pilot plant campaign. Figure B.1 is the operator interface for controlling the gas flow, CO₂ recycle and CO₂ make-up; Figure B.2 is the operator interface for controlling the levels of storage tanks, absorber liquid flow, intercoolers, and pumps; Figure B.3 is the interface for controlling the advanced flash stripper (AFS), including pumps, steam flows, bypass flows, and pressure.

B.1 OPERATOR INTERFACE GRAPHICS

The operator interface graphics for absorber are shown in Figures B.1 and B.2, and the operator interface graphics for the advanced flash stripper are shown in Figure B.3.

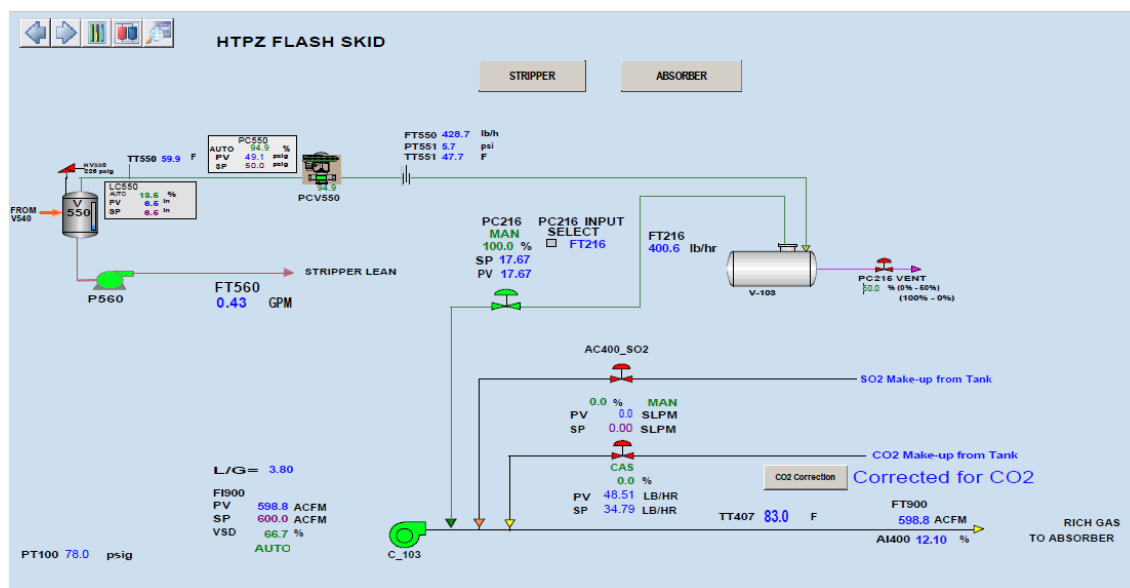


Figure B.1: DeltaV user interface for absorber gas.

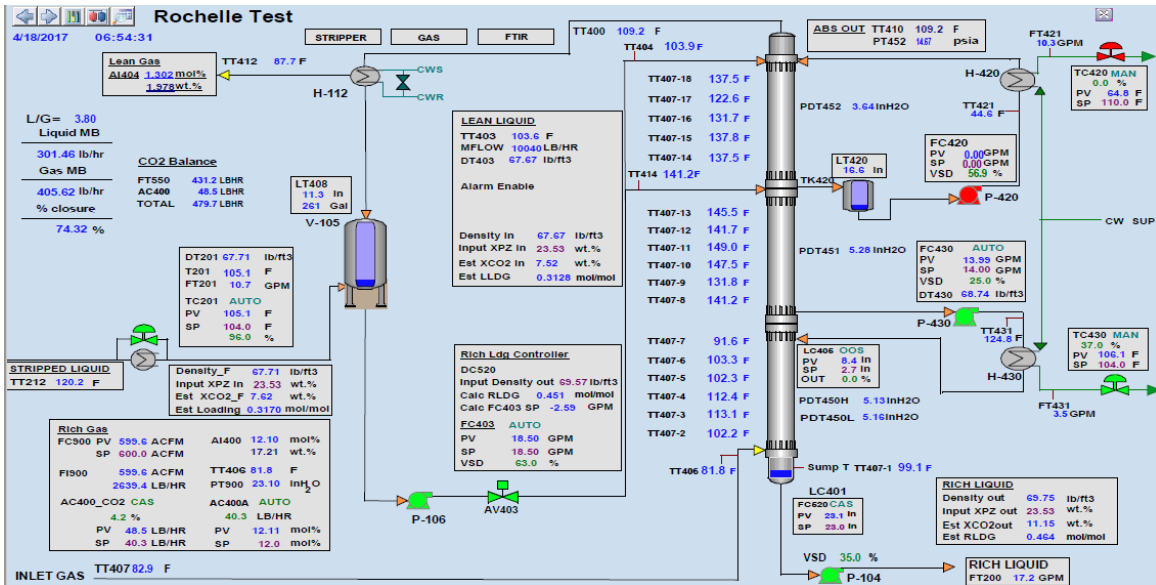


Figure B.2: DeltaV user interface for absorber.

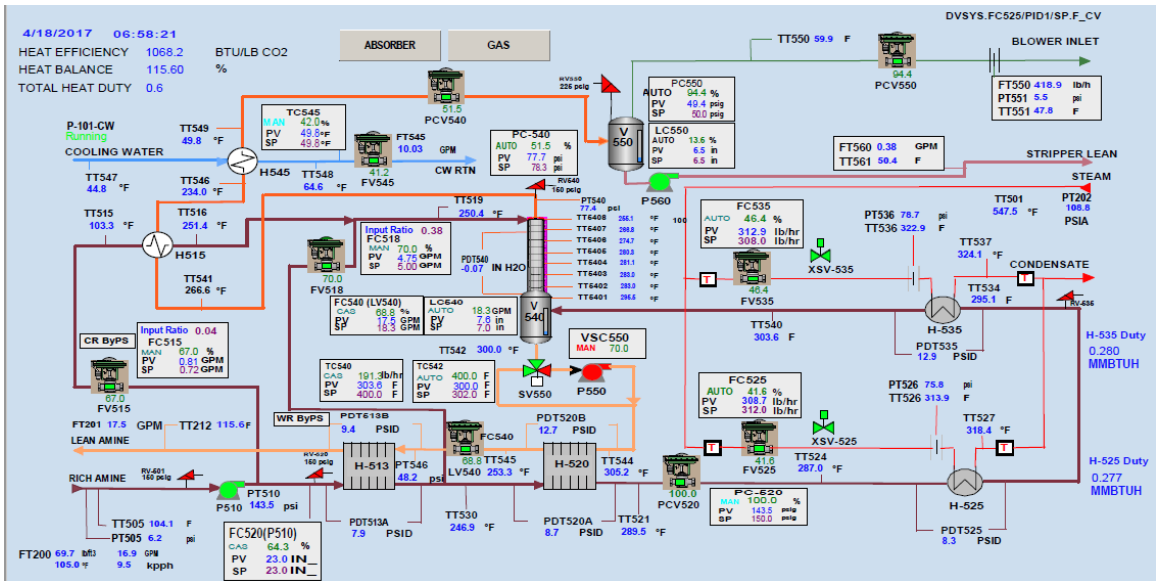


Figure B.3: DeltaV user interface for the advanced flash stripper.

B.2 FTIR AUTO SAMPLING SYSTEM

In the April 2017 pilot plant campaign, real-time and accurate gas composition data was required for process control. A FTIR multi-stream auto sampling switch system has been developed and implemented in DeltaV. Operator interface graphics have been developed to allow the user to easily switch between sampling locations, change sampling times, change heating temperature, and control solenoid valves. This system also allows users to switch from sampling gas to calibration gas. The FTIR auto sampling switch system graphics are shown in Figures Figure B.4 through Figure B.6. There are two operation modes: AUTO mode and MANUAL mode. In the MANUAL mode (Figure B.4), users can choose sampling lines in use, select sampling points (indicated by the green light), and input sampling time. In the AUTO mode (Figure B.5), the system will switch sampling points automatically by the user-specified sampling time. Figure B.6 shows the temperature control interface for seven FTIR heated lines/probes/pads as well as the MSSH box.

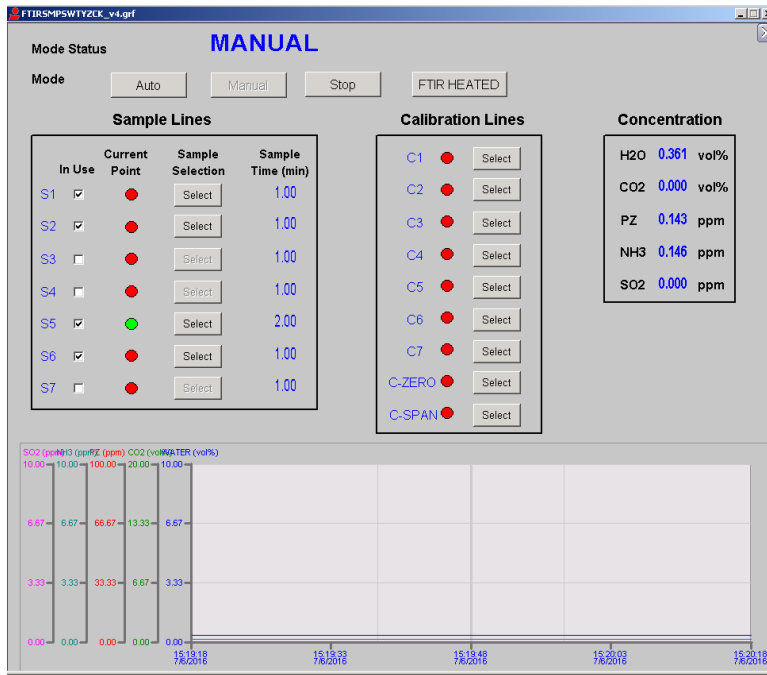


Figure B.4: DeltaV user interface for the FTIR auto sampling switch control (Manual Mode)

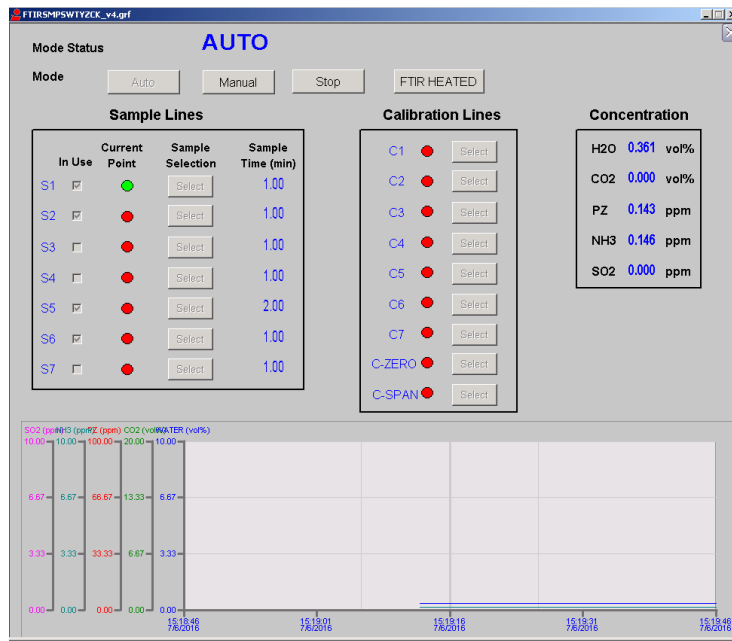


Figure B.5: DeltaV user interface for the FTIR auto sampling switch control (Auto Mode).

Studio screenshots for the cold rich solvent bypass control is shown in Figure B.7. The control variables are:

- FT515: Cold rich bypass flow;
- TT516: Cold rich bypass temperature exiting HX;
- TT541: AFS outlet vapor temperature.

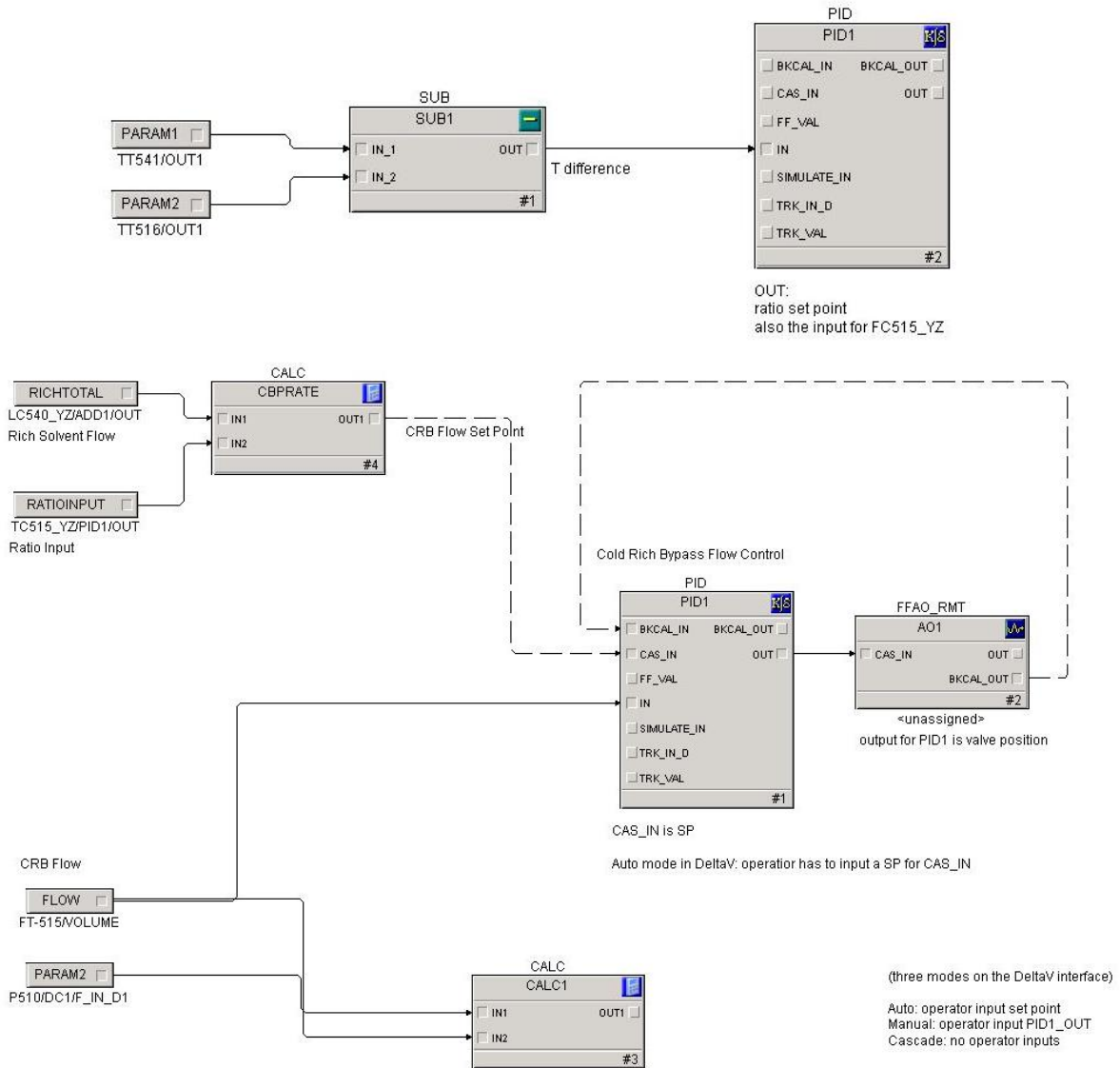
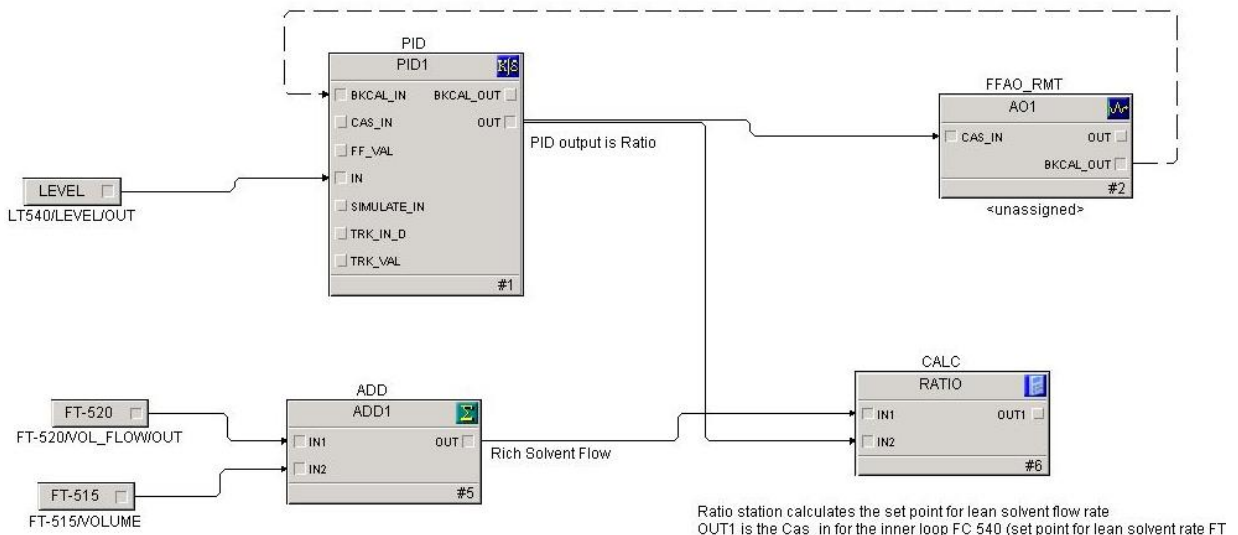


Figure B.7: DeltaV Control Studio screenshots for the cold rich solvent bypass control.

B.1.2 AFS Level Control

AFS sump level indicator transmitter is used to measure the level of the AFS. The offset in level is used to define a new rich-to-lean solvent flow ratio for the process via a level controller. The ratio is defined as the ratio of the measured rich solvent volumetric flow rate leaving the absorber (FT515+FT520) and the measured lean solvent volumetric flow rate leaving the heat exchanger H-513 (FT201). The new rich-to-lean solvent flow ratio defines a new set point for the lean solvent rate. The lean solvent flow rate is controlled via the variable speed drive pump by comparing the measured lean solvent flow to its new set point. DeltaV Control Studio screenshots for the AFS level control is shown in Figure B.8. The control variables are:

- LT540: AFS sump level indicator transmitter;
- LIT-40573: AFS sump radar level indicator transmitter;
- FT520 & FT515: Calculated rich solvent flow rate;
- FT201: AFS lean solvent flow rate.



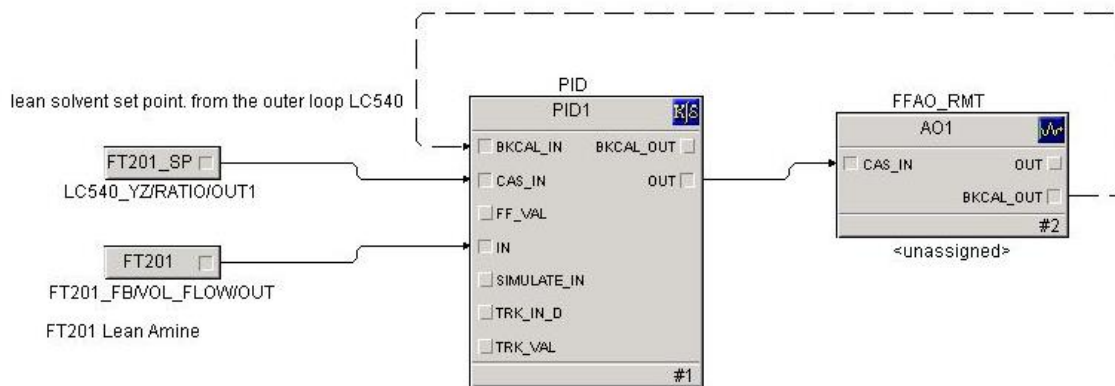


Figure B.8: DeltaV Control Studio screenshots for the AFS level control.

B.1.3 Rich Solvent Density Control

A lean solvent storage tank was installed in SRP. As a result, SRP control loops will maintain the rich solvent density by controlling the lean solvent rate. The first portion of the control scheme compares the measured rich solvent density (FT520) corrected to 40°C (via a calculation block) to the density set point of the process, which defines a new L/G_{CO2} set point for the process. The feedforward portion of the control scheme uses the new L/G_{CO2} set point and measured CO₂ flow rate entering in the flue gas to define a new lean solvent flow rate set point via the ratio station. The new set point for the lean solvent flow rate is compared to the measured lean solvent flow rate (FT201) which is controlled by a variable speed drive lean solvent pump. Figure B.9 shows the DeltaV Control Studio screenshots for the rich solvent density control. The control variables are:

- FT520: Rich solvent density;
- FI900: Inlet flue gas mass flow rate;
- FT201: Lean solvent flow rate after lean solvent tank.

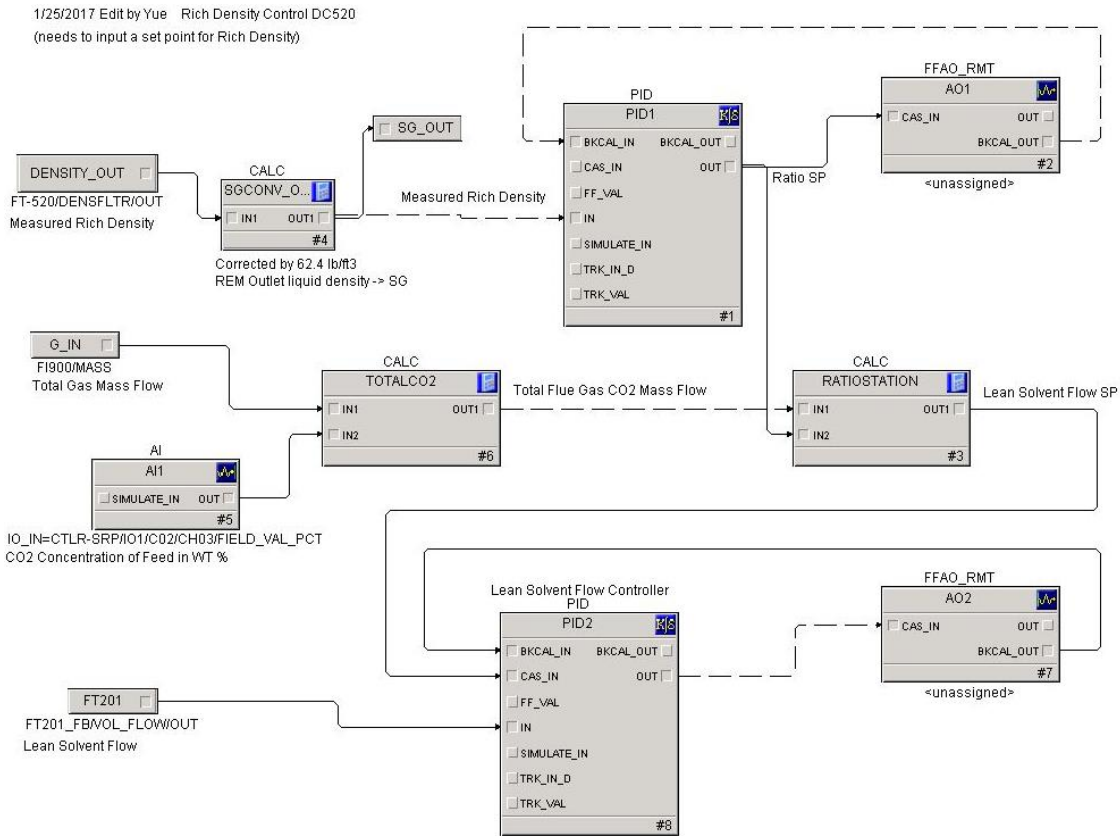


Figure B.9: DeltaV Control Studio screenshots for the rich solvent density control.

B.1.4 AFS Sump Temperature Control

The AFS temperature control approach is a two-level control structure, shown in Figure B.10. The outer layer of the control structure uses the measured AFS sump temperature (TT540) to define a new set point for the steam flow. The inner layer of the control structure controls the steam flow rate (FT535) by changing the steam control valve position. The control variables are:

- FT535: Steam flow indicator transmitter;
- TT540: AFS sump temperature indicator transmitter.

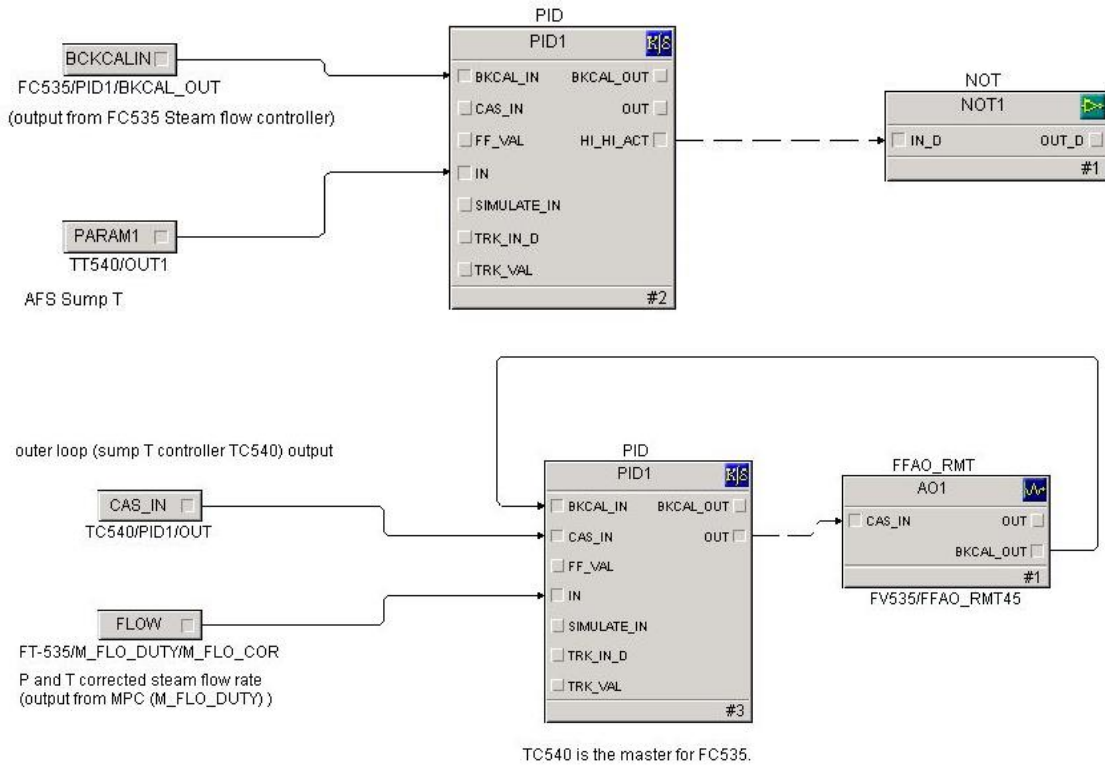


Figure B.10: DeltaV Control Studio screenshots for the AFS sump temperature control.

B.4 ONE-CLICK DATA SPREADSHEET

An “one-click” time-based Excel data spreadsheet has also been constructed using Microsoft Visual Basic in this work. The user interface is shown in Figure B.11. Users should define the following inputs: run number, date, start and end time, and time interval (in minutes). By clicking “Retrieve”, the Excel will search the pilot plant data tags in the DeltaV data log and return the values. The Visual Basic code is included in this appendix and the comments are highlighted in green. The code can be accessed from the Developer Tab in the Excel.

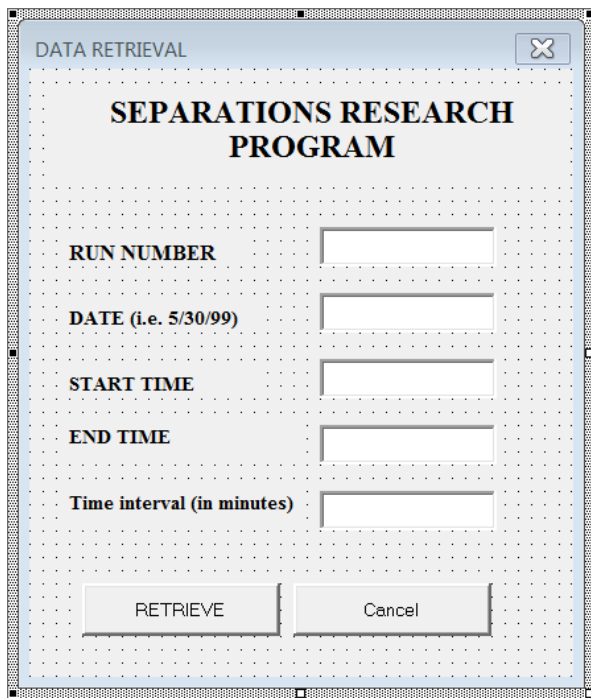


Figure B.11: User interface of “one-click” time-based data log built using Microsoft Visual Basic.

' Coded by Yue Zhang

' Last Modified: 2016/03/08

Private Sub cmdRetrieve_Click()

' First item of Range should be the final column heading, i.e. "KT"

Range("A19:KT99999").Select

Selection.ClearContents

'Range("C2:C4").Select

'Selection.ClearContents

runnum = inRun.Value

Range("F2").Select

ActiveCell.FormulaR1C1 = runnum

firstarg = inDate.Value + " " + inTime.Value

```

Range("C2").Select
ActiveCell.FormulaR1C1 = firstarg
Range("I1").Select
ActiveCell.FormulaR1C1 = inDate.Value
Range("I2").Select
ActiveCell.FormulaR1C1 = inTime.Value
secondarg = inDate.Value + " " + outTime.Value
Range("C3").Select
ActiveCell.FormulaR1C1 = secondarg
Range("I3").Select
ActiveCell.FormulaR1C1 = outTime.Value
thirdarg = inInterval.Value + "minutes"
Range("C4").Select
ActiveCell.FormulaR1C1 = thirdarg
Range("I4").Select
ActiveCell.FormulaR1C1 = inInterval.Value
cellnum = Round(Range("D4").Value)
nmbcells = cellnum + 19
total = nmbcells
Range("F4").Select
ActiveCell.FormulaR1C1 = total
Range("a19:a" & nmbcells).Select
Selection.FormulaArray = _
    "=DvCHInterpolated(A2, $A$18, FALSE, A5, A4, $C$2, $C$3, $C$4)"

```

' A5 is timestamp

```

Range(Cells(19, 1), Cells(nmbcells, 1)).Select
' First item of Range should be the final column heading, i.e. "KT"
For i = 1 To Range("KT" & 1).Column
Range(Cells(19, i), Cells(nmbcells, i)).Select
If Cells(18, i) = "FT202A/AI1/PV.CV" Then
Selection.FormulaArray = _
    "=DvCHInterpolated(A2, " & Cells(18, i).Address(True, False) & ", FALSE, A5, A4,
    $$2, $$3, $$4)"
ElseIf Cells(18, i) = "" Then
Selection = ""
Else
Selection.FormulaArray = _
    "=DvCHInterpolated(A2, " & Cells(18, i).Address(True, False) & ", FALSE, A6, A4,
    $$2, $$3, $$4)"
End Sub

```

B.5 ACKNOWLEDGEMENT

Robert Montgomery, Eric Chen, and Jia-lin Kang provided great help in developing the DeltaV Graphical Operator Interfaces. Matt Walters and Gary Rochelle advised the advanced control for the advanced flash stripper.

References

Bade, O.M., Knudsen, J.N., Gorset, O., Askestad, I., 2014. Controlling amine mist formation in CO₂ capture from Residual Catalytic Cracker (RCC) flue gas. *Energy Procedia* 63, 884–892. doi:10.1016/j.egypro.2014.11.098

Beaudry, M., Fulk, S., Rochelle, G., 2017. Field measurement of amine aerosol by FTIR and Phase Doppler Interferometry. *Energy Procedia* 114, 906–929.

Beaudry, M., Fulk, S., Rochelle, G., 2016. Field measurement of amine aerosol by FTIR and Phase Doppler Interferometry, in: GHGT-13. Lausanne, Switzerland.

Beaudry, M.R., 2017. Aerosol Measurement and Mitigation in CO₂ Capture by Amine Scrubbing. Ph.D. Dissertation, The University of Texas at Austin.

Berstad, D., Arasto, A., Jordal, K., Haugen, G., 2011. Parametric study and benchmarking of NGCC, coal and biomass power cycles integrated with MEA-based post-combustion CO₂ capture. *Energy Procedia* 4, 1737–1744. doi:10.1016/j.egypro.2011.02.048

Center for Climate and Energy Solutions, 2013. Leveraging Natural Gas to Reduce Greenhouse Gas Emissions.

Chen, E., Fulk, S., Sache, D., Lin, Y., Rochelle, G.T., 2014. Pilot plant activities with concentrated piperazine. *Energy Procedia* 63, 1376–1391. doi:10.1016/j.egypro.2014.11.147

Chen, E., Zhang, Y., Lin, Y., Nielsenb, P., Rochelle, G., 2017. Review of Recent Pilot Plant Activities with Concentrated Piperazine. *Energy Procedia* 114, 1110–1127. doi:10.1016/j.egypro.2017.03.1266

Ding, J., 2016. Modeling the Advanced Flash Stripper for CO₂ capture using 5 m Piperazine.

DOE/NETL, 2011. Carbon Capture Approaches for Natural Gas Combined Cycle Systems. U.S. Dep. Energy Rep. No. DOE/NETL-2011/1470.

DOE/NETL, 2010. Cost and performance baseline for fossil energy plants, Volume 1: Bituminous Coal and Natural Gas to Electricity. Natl. Energy Technol. Lab. Rep. No. DOE/NETL-2010/1397 1. doi:DOE/NETL-2010/1397

Du, Y., Wang, Y., Rochelle, G.T., 2016. Thermal Degradation of Piperazine/4-Hydroxy-1-methylpiperidine for CO₂ Capture. *Ind. Eng. Chem. Res.* 55, 10004–10010. doi:10.1021/acs.iecr.6b02568

Frailie, P.T., 2014. Modeling of Carbon Dioxide Absorption/Stripping by Aqueous Methyldiethanolamine / Piperazine. Ph.D. Dissertation, The University of Texas at Austin.

Freeman, B., Hao, P., Baker, R., Kniep, J., Chen, E., Ding, J., Zhang, Y., Rochelle, G.T., 2014. Hybrid Membrane-absorption CO₂ Capture Process. *Energy Procedia* 63, 605–613. doi:10.1016/j.egypro.2014.11.065

Freeman, S.A., 2011. Thermal Degradation and Oxidation of Aqueous Piperazine for Carbon Dioxide Capture. Ph.D. Dissertation, The University of Texas at Austin.

Freeman, S.A., Dugas, R., Van Wagener, D.H., Nguyen, T., Rochelle, G.T., 2010. Carbon dioxide capture with concentrated, aqueous piperazine. *Int. J. Greenh. Gas Control* 4, 119–124. doi:10.1016/j.ijggc.2009.10.008

Fulk, S.M., 2016. Measuring and Modeling Aerosols in Carbon Dioxide Capture by Aqueous Amines. Ph.D. Dissertation, The University of Texas at Austin.

Gaspar, J., von Solms, N., Thomsen, K., Fosbøl, P.L., 2016. Multivariable Optimization of the Piperazine CO₂ Post-Combustion Capture Process. 8th Trondheim Conf. CO₂ Capture, Transp. Storage 86, 229–238. doi:http://dx.doi.org/10.1016/j.egypro.2014.11.115

Kang, J.L., Zhang, Y., Fulk, S., Rochelle, G.T., 2017. Modeling Amine Aerosol Growth in the Absorber and Water Wash. *Energy Procedia* 114, 959–976. doi:10.1016/j.egypro.2017.03.1241

Karimi, M., Hillestad, M., Svendsen, H.F., 2011. Investigation of intercooling effect in CO₂ capture energy consumption. *Energy Procedia* 4, 1601–1607. doi:10.1016/j.egypro.2011.02.030

Kay, J.P., Jensen, M.D., Fiala, N.J., 2014. Pilot-scale evaluations of advanced solvents for postcombustion CO₂ capture. *Energy Procedia* 63, 1903–1910. doi:10.1016/j.egypro.2014.11.199

Khakharia, P., Brachert, L., Mertens, J., Anderlohr, C., Huizinga, A., Fernandez, E.S., Schallert, B., Schaber, K., Vlucht, T.J.H., Goetheer, E., 2015. Understanding aerosol based emissions in a Post Combustion CO₂ Capture process: Parameter testing and mechanisms. *Int. J. Greenh. Gas Control* 34, 63–74. doi:10.1016/j.ijggc.2015.01.001

Khakharia, P., Mertens, J., Vlucht, T.J.H., Goetheer, E., 2014. Predicting aerosol based emissions in a post combustion CO₂ capture process using an aspen plus model. *Energy Procedia* 63, 911–925. doi:10.1016/j.egypro.2014.11.101

Knudsen, J.N., Andersen, J., Jensen, J.N., Biede, O., 2011. Evaluation of process upgrades and novel solvents for the post combustion CO₂ capture process in pilot-scale. *Energy Procedia* 4, 1558–1565. doi:10.1016/j.egypro.2011.02.025

Knudsen, J.N., Bade, O.M., Anheden, M., Bjorklund, R., Gorset, O., Woodhouse, S., 2013. Novel concept for emission control in post combustion capture. *Energy Procedia* 37, 1804–1813. doi:10.1016/j.egypro.2013.06.058

Kvamsdal, H.M., Haugen, G., Svendsen, H.F., 2011. Flue-gas cooling in post-combustion capture plants. *Chem. Eng. Res. Des.* 89, 1544–1552. doi:10.1016/j.cherd.2011.02.029

Kvamsdal, H.M., Rochelle, G.T., 2008. Effects of the temperature bulge in CO₂ absorption from flue gas by aqueous monoethanolamine. *Ind. Eng. Chem. Res.* 47, 867–875. doi:10.1021/ie061651s

Li, L., 2015. Carbon Dioxide Solubility and Mass Transfer in Aqueous Amines for Carbon Capture. Ph.D. Dissertation, The University of Texas at Austin.

Lin, Y.-J., Chen, E., Rochelle, G.T., 2016. Pilot Plant Test of the Advanced Flash Stripper for CO₂ Capture. *Faraday Discuss.* 192, 37–58. doi:10.1039/C6FD00029K

Lin, Y.-J., Rochelle, G.T., 2016. Approaching a reversible stripping process for CO₂ capture. *Chem. Eng. J.* 283, 1033–1043. doi:10.1016/j.cej.2015.08.086

Lin, Y., 2016. Modeling Advanced Flash Stripper for Carbon Dioxide Capture Using Aqueous Amines.

Lin, Y.J., Rochelle, G.T., 2016. Approaching a reversible stripping process for CO₂ capture. *Chem. Eng. J.* 283, 1033–1043.

Majeed, H., Knuutila, H., Hillestad, M., Svendsen, H.F., 2017a. Effect of Amine Volatility on Aerosol Droplet Development in Absorption Columns. *Energy Procedia* 114, 977–986. doi:10.1016/j.egypro.2017.03.1243

Majeed, H., Knuutila, H., Hillestad, M., Svendsen, H.F., 2017b. Gas phase amine depletion created by aerosol formation and growth. *Int. J. Greenh. Gas Control* 64, 212–222. doi:10.1016/j.ijggc.2017.07.001

Merkel, T.C., Wei, X., He, Z., White, L.S., Wijmans, J.G., Baker, R.W., 2013. Selective Exhaust Gas Recycle with Membranes for CO₂ Capture from Natural Gas Combined Cycle Power Plants. *Ind. Eng. Chem. Res.* 52, 1150–1159. doi:10.1021/ie302110z

Moser, P., Schmidt, S., Stahl, K., Vorberg, G., Lozano, G.A., Stoffregen, T., Rösler, F., 2014. Demonstrating emission reduction - Results from the post-combustion capture

pilot plant at niederaussem. *Energy Procedia* 63, 902–910.
doi:10.1016/j.egypro.2014.11.100

Moser, P., Schmidt, S., Wallus, S., Ginsberg, T., Sieder, G., Clausen, I., Palacios, J.G., Stoffregen, T., Mihailowitsch, D., 2013. Enhancement and long-term testing of optimised post-combustion capture technology - Results of the second phase of the testing programme at the Niederaussem pilot plant. *Energy Procedia* 37, 2377–2388.
doi:10.1016/j.egypro.2013.06.119

Nguyen, B.-T.H., 2013. Amine Volatility in CO₂ Capture. Ph.D. Dissertation, The University of Texas at Austin.

Nguyen, T., Hilliard, M., Rochelle, G., 2011. Volatility of aqueous amines in CO₂ capture. *Energy Procedia* 4, 1624–1630. doi:10.1016/j.egypro.2011.02.033

Nielsen, P.T., Li, L., Rochelle, G.T., 2013. Piperazine degradation in pilot plants. *Energy Procedia* 37, 1912–1923. doi:10.1016/j.egypro.2013.06.072

Plaza, J.M., 2011. Modeling of Carbon Dioxide Absorption using Aqueous Monoethanolamine, Piperazine and Promoted Potassium Carbonate. Ph.D. Dissertation, The University of Texas at Austin.

Rezazadeh, F., Gale, W.F., Akram, M., Hughes, K.J., Pourkashanian, M., 2016. Performance evaluation and optimisation of post combustion CO₂ capture processes for natural gas applications at pilot scale via a verified rate-based model. *Int. J. Greenh. Gas Control* 53, 243–253. doi:10.1016/j.ijggc.2016.08.003

Rochelle, G.T., 2015. CO₂ Capture by Aqueous Absorption, First Quarterly Progress Report 2015, Texas Carbon Management Program. The University of Texas at Austin.

Rochelle, G.T., 2009. Amine scrubbing for CO₂ capture. *Science* 325, 1652–1654.
doi:10.1126/science.1176731

Rochelle, G.T., Chen, E., Freeman, S., Van Wagener, D., Xu, Q., Voice, A., 2011. Aqueous piperazine as the new standard for CO₂ capture technology. *Chem. Eng. J.* 171, 725–733. doi:10.1016/j.cej.2011.02.011

Rongrong, Z., Yongping, Y., Liqiang, D., Qin, Y.A.N., 2008. Economical Performance Study for NGCC system with CO₂ removal plant. 2008 IEEE Int. Conf. Sustain. Energy Technol. 178–181. doi:10.1109/ICSET.2008.4746996

Sachde, D., Chen, E., Rochelle, G.T., 2013. Modeling Pilot Plant Performance of an Absorber with Aqueous Piperazine. *Energy Procedia* 37, 1987–2001. doi:10.1016/j.egypro.2013.06.079

Sachde, D., Rochelle, G.T., 2014. Absorber Intercooling Configurations using Aqueous Piperazine for Capture from Sources with 4 to 27% CO₂. *Energy Procedia* 63, 1637–1656. doi:10.1016/j.egypro.2014.11.174

Sachde, D.J., 2016. Absorber Performance and Configurations for CO₂ Capture using Aqueous Piperazine. Ph.D. Dissertation, The University of Texas at Austin.

Seibert, F., Chen, E., Perry, M., Briggs, S., Montgomery, R., Rochelle, G., 2011. UT/SRP CO₂ capture pilot plant - Operating experience and procedures. *Energy Procedia* 4, 1616–1623. doi:10.1016/j.egypro.2011.02.032

Sherman, B., 2016. Thermodynamic and Mass Transfer Modeling of Aqueous Hindered Amines for Carbon Dioxide Capture.

Sipöcz, N., Tobiesen, F.A., 2012. Natural gas combined cycle power plants with CO₂ capture – Opportunities to reduce cost. *Int. J. Greenh. Gas Control* 7, 98–106. doi:10.1016/j.ijggc.2012.01.003

Song, D., 2017. Effect of liquid viscosity on liquid-side mass transfer coefficients for packings. Ph.D. Dissertation, The University of Texas at Austin.

Stoffregen, T., Rigby, S., Jovanovic, S., Krishnamurthy, K.R., 2014. Pilot-scale demonstration of an advanced aqueous amine-based post-combustion capture technology for CO₂ capture from power plant flue gases. *Energy Procedia* 63, 1456–1469. doi:10.1016/j.egypro.2014.11.155

Tait, P., Buschle, B., Ausner, I., Valluri, P., Wehrli, M., Lucquiaud, M., 2016. A pilot-scale study of dynamic response scenarios for the flexible operation of post-combustion CO₂ capture. *Int. J. Greenh. Gas Control* 48, 216–233. doi:10.1016/j.ijggc.2015.12.009

Tilton, L.W., Taylor, J.K., 1937. Accurate representation of the refractivity and density of distilled water as a function of temperature. *J. Res. Natl. Bur. Stand.* (1934). 18, 205–214. doi:10.6028/jres.018.008

Tsai, R., 2010. Mass Transfer Area of Structured Packing. Ph.D. Dissertation, The University of Texas at Austin.

Voice, A.K., 2013. Amine oxidation in carbon dioxide capture by aqueous scrubbing. Ph.D. Dissertation, The University of Texas at Austin.

von Harbou, I., Imle, M., Hasse, H., 2014. Modeling and simulation of reactive absorption of CO₂ with MEA: Results for four different packings on two different scales. *Chem. Eng. Sci.* 105, 179–190. doi:10.1016/j.ces.2013.11.005

Wang, C., 2015. Mass Transfer Coefficients and Effective Area of Packing. Ph.D. Dissertation, The University of Texas at Austin.

Wijmans, J.G., Merkel, T.C., Baker, R.W., 2011. Process for separating carbon dioxide from flue gas using parallel carbon dioxide capture and sweep-based membrane separation steps. United States Pat. 8025715. doi:10.1021/ja8090388.RaZuvaev

Wijmans, J.G., Merkel, T.C., Baker, R.W., 2011. Gas separation process using membranes with permeate sweep to remove CO₂ from gaseous fuel combustion exhaust. United States Pat. 7964020.

Wilcox, J., 2012. Carbon Capture, Carbon Capture. doi:10.1007/978-1-4614-2215-0

Ystad, P.A.M., Bolland, O., Hillestad, M., 2012. NGCC and hard-coal power plant with CO₂ capture based on absorption. Energy Procedia 23, 33–44. doi:10.1016/j.egypro.2012.06.019

Zhang, Y., Freeman, B., Hao, P., Rochelle, G., 2016. Absorber Modeling for NGCC Carbon Capture with Aqueous Piperazine. Faraday Discuss. 192, 459–477. doi:10.1039/C6FD00030D

Zhang, Y., Kang, J., Fulk, S., Rochelle, G., 2017a. Modeling Amine Aerosol Growth at Realistic Pilot Plant Conditions. Energy Procedia 114, 1045 – 1060.

Zhang, Y., Rochelle, G.T., 2014. Absorber Performance with High CO₂. Energy Procedia 63, 1329–1338. doi:10.1016/j.egypro.2014.11.142

Zhang, Y., Sachde, D., Chen, E., Rochelle, G., 2017b. Modeling of absorber pilot plant performance for CO₂ capture with aqueous piperazine. Int. J. Greenh. Gas Control 64, 300–313. doi:10.1016/j.ijggc.2017.08.004

Vita

Yue Zhang was born in China in December 1992. She attended Zhejiang University from 2009 to 2013, where she graduated with a B.S. in Chemical Engineering. In the summer of 2012, she conducted a research internship at McMaster University in Canada and she decided to apply to graduate school. She began her graduate studies in Chemical Engineering at the University of Texas at Austin in the fall of 2013. In the summer of 2015, she performed an R&D internship at Membrane Technology and Research in Newark, CA. She has accepted a full-time position at The Dow Chemical Company in Lake Jackson, TX.

Permanent email: yuezhanguetexas@gmail.com

This dissertation was typed by the author.